

MICROCOPY RESOLUTION TEST CHART
NATIONAL BUREAU OF STANDARDS-1963-A

NONLINEAR BURNING STABILITY OF SOLID PROPELLANTS

AD-A143 573

Final Technical Report
July 1981 - December 1983

by

Luigi De Luca (Principal Investigator)
Giulio Riva (Investigator)
Claudio Zanotti (Investigator)

31 December 1983

EUROPEAN RESEARCH OFFICE

United States Army
London England

S
JUL 25 1984
A

CONTRACT NUMBER DAJA37-81-C-0215

GRANTEE Prof. Corrado Casci, Director
CNPM - Dipartimento di Energetica
Politecnico di Milano
20133 Milano, Italy

Approved for Public Release; distribution unlimited

DC FILE COPY

84 07 24 001

NONLINEAR BURNING STABILITY OF SOLID PROPELLANTS

Final Technical Report
July 1981 - December 1983

by

Luigi/De Luca (Principal Investigator)
Giulio Riva (Investigator)
Claudio Zanotti (Investigator)

31 December 1983

EUROPEAN RESEARCH OFFICE

United States Army
London England

CONTRACT NUMBER DAJA37-81-C-0215

GRANTEE Prof. Corrado Casci, Director
CNPM - Dipartimento di Energetica
Politecnico di Milano
20133 Milano, Italy

Approved for Public Release; distribution unlimited

REPORT DOCUMENTATION PAGE		HEADLINE INFORMATION BEFORE COMPLETING FORM	
1. REPORT NUMBER	2. GOVT ACCESSION NO.	3. RECIPIENT'S CATALOG NUMBER	
	AD-A143 573		
4. TITLE (and Subtitle) Nonlinear Burning Stability of Solid Propellants		5. TYPE OF REPORT & PERIOD COVERED Final Technical Report July 1981 - December 83	
		6. PERFORMING ORG. REPORT NUMBER	
7. AUTHOR(s) Luigi De Luca, Giulio Riva, Claudio Zanotti		8. CONTRACT OR GRANT NUMBER(s) DAJA37-81-C-0215	
9. PERFORMING ORGANIZATION NAME AND ADDRESS Istituto di Macchine Politecnico di Milano		10. PROGRAM ELEMENT, PROJECT, TASK AREA & WORK UNIT NUMBERS 6.11.02A IT161102BH57-06	
11. CONTROLLING OFFICE NAME AND ADDRESS USARDSG-UK Box 65 FPO NY 09510		12. REPORT DATE 31 December 83	
		13. NUMBER OF PAGES 195	
14. MONITORING AGENCY NAME & ADDRESS (if different from Controlling Office)		15. SECURITY CLASS. (of this report) Unclassified	
		15a. DECLASSIFICATION/DOWNGRADING SCHEDULE	
16. DISTRIBUTION STATEMENT (of this Report) Approved for public release; distribution unlimited			
17. DISTRIBUTION STATEMENT (of the abstract entered in Block 20, if different from Report)			
18. SUPPLEMENTARY NOTES			
19. KEY WORDS (Continue on reverse side if necessary and identify by block number) Solid Propellant Combustion; Combustion Stability; Static and Dynamic Stability; Combustion Dynamics; Oscillatory Burning; Pressure Deflagration Limit; Variable Thermal Properties; Condensed Phase Distributed Reactions; Heterogeneous Thin Flames.			
20. ABSTRACT (Continue on reverse side if necessary and identify by block number) The nonlinear burning analysis of solid rocket propellants, under development by this research group, was extended to include in particular variable thermal properties and volumetrically distributed chemical reactions in the condensed phase. The theory is restricted to monodimensional combustion waves and thin (i.e., quasi-steady gas phase) heterogeneous flames of thermal nature. Bifurcation diagrams were obtained, predicting the existence of: time-indepen- dent steady burning, self-sustained oscillatory steady burning, no steady sustained burning. Several bifurcation parameters were recognized. Static			

20. Continued

stability boundaries, dynamic stability boundaries, static burning boundaries, pressure deflagration limits were determined for unmetallized AP-based composite propellants. Several thin flame models, available from literature, were properly modified and extended.

A large amount of computer simulated tests, performed under a wide variety of operating conditions, substantially confirmed the analytical predictions. Moreover excellent agreement was found with experimental results obtained by a depressurization strand burner; reasonable agreement was found with the qualitative experimental results obtained by a piston tube apparatus; good agreement was found with low pressure experimental tests (pressure deflagration limit and associated self-sustained oscillatory burning phenomena).

ACKNOWLEDGMENTS

The authors wish to express their sincere gratitude to the many students who offered a substantial help during the development of this research project: Messrs. R. Dondé, A. Poli, F. Magugliani, C. Grimaldi, V. Lapegna, A. Oleari, A. Portaro, N. Lunghi, D. Marongiu and A. Molinari. Special thanks are due to ing. I. Tanturli (SIAI-Marchetti), prof. A. Reggiori, ing. R. Carlevaro, dr. C. Bruno, and Mr. G. Colombo for their technical cooperation. Messrs. G. Sensolo and G. Zucchetti contributed to the graphical work, Mr. G. Daminelli to the electronics.

The solid rocket propellants used for the experimental part of this research project were courteously provided by SNIA-BPD.



A-1

TABLE OF CONTENTS

	page
Title page	i
ABSTRACT	ii
ACKNOWLEDGMENTS	iv
TABLE OF CONTENTS	v
<u>CHAPTER 1 - SCOPE, BACKGROUND, AND OBJECTIVES</u>	1
1.1 - SCOPE OF THE RESEARCH STUDY	1
1.2 - BACKGROUND OF THE RESEARCH STUDY	2
1.3 - BACKGROUND OF THIS RESEARCH PROJECT	3
1.4 - OBJECTIVES OF THIS RESEARCH PROJECT	6
1.5 - PLAN OF PRESENTATION OF THIS REPORT	7
<u>CHAPTER 2 - LITERATURE SURVEY</u>	8
2.1 - FAST DEPRESSURIZATION	9
2.1.1 - Theoretical results on dynamic extinction by fast depressurization	9
2.1.2 - Experimental results on dynamic extinction by fast depressurization	14
2.2 - NONLINEAR DYNAMIC EXTINCTION BY FAST DERADIATION	20
2.3 - NONLINEAR OSCILLATORY COMBUSTION	24
2.4 - PRESSURE DEFLAGRATION LIMIT	28
2.4.1 - AP monopropellant	29
2.4.2 - AP composite propellants	33
2.5 - VARIABLE THERMAL PROPERTIES	39

	Page
<u>CHAPTER 3 - NONLINEAR UNSTEADY BURNING OF SOLID PROPELLANTS</u>	41
3.1 - FORMULATION OF THE GENERAL HETEROGENEOUS THIN FLAME PROBLEM	41
3.2 - STEADY THERMAL PROFILES IN THE NONREACTING CONDENSED PHASE	48
3.3 - QUASI-STEADY FLAME MODELS	52
3.3.1 - MTS Flame	52
3.3.2 - KTSS flame	55
3.3.3 - KZ flame	57
3.3.4 - LC flame	57
3.4 - WORKING MAP	59
3.5 - CONCLUDING REMARKS	60
<u>CHAPTER 4 - NONLINEAR BURNING STABILITY OF SOLID PROPELLANTS</u>	62
4.1 - BACKGROUND AND NOMENCLATURE	62
4.2 - THE NONLINEAR BURNING STABILITY EQUATION	64
4.3 - THE STATIC RESTORING FUNCTION	71
4.3.1 - Meaning of the algebraic roots	71
4.3.2 - Effect of operating conditions (pressure and diabaticity)	74
4.3.3 - Effect of flame models	75
4.3.4 - Effect of approximating polynomial order	76
4.3.5 - Effect of approximating profile type	76
4.3.6 - Concluding remarks	77
4.4 - NONLINEAR STATIC BURNING STABILITY	77
4.4.1 - Number and nature of the allowed static solutions	78
4.4.2 - Static burning boundary	78
4.4.3 - Measurement of static stability strength	79

	Page
4.5 - NONLINEAR DYNAMIC BURNING STABILITY	80
4.5.1 - Dynamic extinction of solid propellants	81
4.5.2 - Lower and upper dynamic combustion stability	84
4.6 - BIFURCATION PHENOMENA	85
4.6.1 - Morphology of the static restoring function	85
4.6.2 - Bifurcation diagrams	87
4.6.3 - Self-sustained oscillatory burning	88
4.6.4 - Bifurcation parameters	89
4.6.5 - Pressure deflagration limit	90
4.6.6 - A physical interpretation of the bifurcation diagram	91
4.7 - EFFECTS OF THERMAL PROPERTIES	92
4.8 - EFFECTS OF CONDENSED PHASE DISTRIBUTED REACTIONS	93
4.9 - THE BURNING RATE VS PRESSURE PLOT REVISITED	94
4.10- CONCLUDING REMARKS ON COMBUSTION STABILITY	96
<u>CHAPTER 5 - NUMERICAL APPROACH</u>	97
5.1 - THE MATHEMATICAL PROBLEM	97
5.2 - FORMULATION OF THE FINITE DIFFERENCE PROBLEM	98
5.3 - STABILITY AND CONVERGENCE OF THE NUMERICAL SOLUTION	101
5.4 - SOME PROBLEMS RELATED TO THE BOUNDARY CONDITIONS	102
5.5 - THE INITIAL CONDITION	104
5.6 - THE NUMERICAL CODE	105
5.7 - NUMERICAL SIMULATION OF DYNAMIC EXTINCTION	107
5.8 - NUMERICAL VALIDATION OF THE BIFURCATION DIAGRAMS	108
5.9 - NUMERICAL SIMULATION OF RADIATION PULSES	110
5.10- CONCLUDING REMARKS	111

	Page
<u>CHAPTER 6 - EXPERIMENTAL RESULTS</u>	113
6.1 - FAST DEPRESSURIZATION EXPERIMENTS	113
6.2 - SHOCK TUBE EXPERIMENTS	119
6.2.1 - Shock tube configuration	119
6.2.2 - Piston tube configuration	121
6.3 - RESULTS FROM STEADY BURNING EXPERIMENTS	127
6.4 - SUBATMOSPHERIC BURNING EXPERIMENTS	129
6.4.1 - Pressure deflagration limit measurement	129
6.4.2 - Self-sustained oscillatory burning	130
6.5 - CONCLUDING REMARKS	133
<u>CHAPTER 7 - CONCLUSIONS AND FUTURE WORK</u>	135
7.1 - STATE OF THE ART OF THE RESEARCH STUDY	135
7.2 - CONCLUSIONS	138
7.3 - FUTURE WORK	141
REFERENCES	143
NOMENCLATURE	160
LIST OF TABLES	166
LIST OF FIGURES	167
TABLES 1-4	
FIGURES 1-94	

CHAPTER 1 - SCOPE, BACKGROUND AND OBJECTIVES

1.1 - SCOPE OF THE RESEARCH STUDY

General purpose of this research study is to formulate the basic laws governing the nonlinear burning stability of solid rocket propellants. The reader is assumed familiar with the books by Williams (Ref. 1), Williams-Barrère-Huang (Ref.2), and Price-Culick (Ref.3); these are excellent textbooks in the areas respectively of combustion fundamentals, solid propellant rocket motors, and solid propellant burning. The Soviet state-of-the-art in solid propellant burning is well represented by the monographs by Librovich (Ref.4), Novozhilov (Ref.5), and Zeldovich - Leipunskiy-Librovich (Ref.6). A collection of specialized articles on experimental techniques in solid propellant burning was published in 1978 (Ref. 7). An update textbook, collecting specialized contributions on fundamentals of solid propellant burning, is on print (Ref.8).

The research project described in this report is just the continuation of a previous 3 year research project whose Final Technical Report was released in December 1980 (Ref.9). The format of this report is intentionally kept unchanged as much as possible, in order to help the reader who is already familiar with the previous report. The main restriction of this research study is that heterogeneous thin flames only are considered; a solid propellant flame is thin if the gas phase behaves quasi-steadily. On the other hand, considering the general standpoint taken in this study, it is emphasized that:

- (1) Findings are easily extendable to other cases of heterogeneous combustion; in particular, the basic results of this research are not dependent on the specific nature of the solid propellant of interest.
- (2) No proposal is made of new transient flame models; again, the basic results of this research are not dependent on the specific nature of the implemented flame model. Rather a method is offered to evaluate on a quantitative basis how good a transient flame model is.
- (3) Information concerning steady state burning is obtained as a by-product of the overall unsteady combustion analysis.
- (4) Interactions combustion/fluidynamics of the type occurring in a rocket motor combustion chamber are not considered; thermokinetic phenomena mainly are studied within the framework of heterogeneous thin flames.

This Final Technical Report supersedes all previous reports in the area of nonlinear combustion and nonlinear stability of solid propellants. Although efforts were made for this Final Technical Report to be comprehensive too, the amount of material to deal with is so vast that the authors felt obliged to give up. However, for the reader's convenience, the fundamental theoretical results are repeated, while the previous numerical and experimental validations of significance are summarized at the appropriate places. This Final Technical Report, together with the Final Technical Report of the previous grant period (Ref. 9), virtually comprehends all research activities by the research group of Politecnico di Milano in the pertinent area of investigation. The important specialized literature so far published by this research group or the senior author is listed as Refs. 10-40. Remark that: Refs. 28-32 are principally of experimental nature; Refs. 33-36 are theses written by students for completion of their studies at Politecnico di Milano (in particular Ref. 36 is a doctoral thesis); Refs. 37-40 were offered before this research study started, but are listed at this point for future convenience.

1.2 - BACKGROUND OF THE RESEARCH STUDY

The basic topics, included in the nonlinear burning stability of solid rocket propellants as presented in this report, are: dynamic extinction, nonacoustic or intrinsic self-sustained combustion oscillations, low pressure extinction, variable thermal properties in the condensed phase, and distributed chemical reactions in the condensed phase. A list of minor subjects is also dealt with (e.g., radiative heat loss from the burning surface). All of the above phenomena are treated from a unique viewpoint, leading to unifying physical concepts expressed in terms of unique analytical predictions (bifurcation diagrams). Numerical and experimental validations of these analytical predictions are copious, albeit not yet complete.

Contributions from the open literature are scattered. A detailed critical review will be offered in Chapter 2. At this point it is only emphasized that a vast body of literature, about what we consider just one problem, is broken in "segments" often with no connections: dynamic extinction by fast depressurization (Refs. 41-80), dynamic extinction by fast deradiation (Ref. 81-87), oscillatory burning (Refs. 88-107), deflagration and low pressure extinction of ammonium perchlorate (Refs. 108-122), low pressure extinction of composite propellants (Refs. 123-132), variable thermal properties (Refs. 133-135). Please notice that, for future convenience, in each

of the above literature segment, papers are included not directly connected with the mentioned subject.

Several years of efforts at the Politecnico di Milano were dedicated to the question of dynamic extinction driven by fast changes of pressure or external radiant flux (Refs. 10-13, 15-19, 21-23, 25-28, 31). This line of research was motivated by experimental results, on dynamic extinction by fast deradiation collected by the senior author during his stay at Princeton University (Refs. 12, 38-40). An original theoretical approach of nonlinear burning stability of solid propellants was hence developed (Refs. 10-11). This analysis could predict, among other things, the existence of a minimum burning rate (lower dynamic stability limit, or dynamic extinction limit) under which extinction of the burning propellant necessarily occurs, independently on its past history (Ref. 10). The same analysis would also, unexpectedly, suggest the existence of special sets of operating conditions, for which the only allowed steady burning is self-sustained oscillatory (Ref. 11). Moreover, a prediction of pressure deflagration limit comes out when the effects of pressure on the self-sustained oscillatory regime are investigated (Ref. 17).

It can be seen that apparently disconnected facts are tied up all together, with no string attached, by a powerful theoretical tool initially set up in an attempt to explain only experimental extinction by fast deradiation (Ref. 38). The philosophy of this method is illustrated in next section.

1.3 - BACKGROUND OF THIS RESEARCH PROJECT

Consider a monodimensional strand of solid propellant subjected to a radiant flux impinging with instantaneous intensity $(1-\bar{\epsilon}_\lambda) I_0(t)$ on its surface, burning with instantaneous rate $r_b(t)$ in a vessel at instantaneous pressure $p(t)$. See the schematic in Fig. 1. It is assumed that a uniform pressure exists in the vessel, with the instantaneous pressure level exclusively controlled from the exterior. Radiant flux is supposed to be provided by an external source (e.g., a continuous wave laser) of adjustable intensity and known properties. The ambient temperature is taken as constant in time, but it can be changed parametrically. Pressure, radiant flux, and ambient temperature will be called (external) controlling parameters of the burning processes.

For a fixed set of controlling parameters, the strand of the solid propellant is usually observed to burn steadily. If the controlling parameters change in time, the strand will

usually burn with a variable but finite rate. Extinction implies quenching of all chemical activity of the strand: roughly this corresponds to the zero burning rate. Extinction can be achieved statically or dynamically. Static extinction means that, for a given set of controlling parameters, the trivial zero burning rate solution is the only allowed stable steady solution. Dynamic extinction means that extinction occurs following an attempt to perform a combustion transition from some initial to some final set of controlling parameters, for which a final stable steady burning solution exists. Under these circumstances, extinction is due to an excessively fast change of the controlling parameters with respect to the response time of the solid propellant (time required to adjust itself to the new set of operating conditions).

Static extinction is therefore associated with excessively low values of pressure (pressure deflagration limit) and/or ambient temperature and/or large values of heat exchange with the exterior. Dynamic extinction is associated with fast changes of pressure (depressurization or dp/dt extinction) and/or heat exchange (usually deradiation, i.e., radiation input decrease).

In this research project, quantitative criteria for nonlinear static and dynamic burning stability of solid propellants are defined by means of thermal flame models (Refs. 44, 136-138). By making a quite general set of assumptions (see Sec. 3.1), the mathematical problem is essentially reduced to study the stability properties of the nonlinear heat conduction equation in the propellant condensed phase (the Fourier partial differential equation with time-varying boundary conditions). This is done by an approximate analytical technique (an integral method is enforced to transform the partial into an ordinary differential equation), but keeping the nonlinearity of the problem. Thus a nonlinear algebraic function, called static restoring function, is determined defining nonlinear static and dynamic burning stability for finite size disturbances. The associated stability boundaries are valid for any kind of transient burning (e.g., depressurization or deradiation). Bifurcation diagrams can then be constructed from the static restoring functions, putting in evidence the existence of three regions for steady burning: time-independent, self-sustained oscillatory, and extinguished.

The integral method of Goodman (Ref.139) is implemented in order to apply known mathematical methods (Ref.140) to the resulting approximate ODE formulation. The same method has already been applied (Ref.105) to particle burning; somewhat simpler use has been made at Princeton (Refs. 141-142) on solid

propellant rocket engines. The concept of using the simpler ODE formulation of the problem, instead of the PDE one, is relatively common in the Soviet literature. However, the method of transformation is rather different; an interesting review of the mathematical problem was made by Gostintsev (Ref.143). The approach has been applied mainly to ignition, unsteady burning, and stability problems. Remark that the Soviet approach differs not only in the mathematical details, but especially in the structure of the physical model. Instead of using a flame model, the Soviet investigators resort to the Zeldovich method (e.g., see Ref. 58-59), consisting of constructing the instantaneous thermal gradient at the condensed phase side of the burning surface from experimental steady state data. However, this method is useful in establishing intrinsic stability boundaries, but cannot be applied to dynamic burning. Nevertheless, the nonlinear burning stability theory developed in this research study can be extended to the Zeldovich method as well; in this case the Zeldovich method would predict dynamic stability boundaries too.

In principle, both static and dynamic burning stability have to be analyzed by nonlinear equations and finite size disturbances. This is particularly important for dynamic extinction, which is related to the combustion transition between two equilibrium configurations that are usually drastically different. Static stability, being related to an equilibrium configuration stability, can also be analyzed by means of linearized equations and infinitesimal disturbances. But the validity of the results is restricted: if instability is found, the fate of the burning propellant is not predictable (incipient instability); if stability is found, it is limited to infinitesimally small disturbances (linear stability).

No attempt is made to explain the steady flame structure of burning propellants. In fact, the steady state solution is incorporated into the combustion stability analysis by assigning: the burning rate vs pressure (from experimental data under adiabatic combustion and reference ambient temperature) and the flame temperature vs pressure (from thermochemistry computations under adiabatic combustion). Any other steady state configuration can be deduced from these pieces of information.

1.4 - OBJECTIVES OF THIS RESEARCH PROJECT

Within the framework of heterogeneous thin flames of thermal nature, specific objectives of this research project are to:

- (1) Extend the nonlinear burning stability analysis to optically transparent condensed phase.
- (2) Include polychromatic external radiation in the overall approach (nonlinear numerical simulation and burning stability).
- (3) Include temperature dependent thermal conductivity in the overall approach (nonlinear numerical simulation and burning stability).
- (4) Include temperature dependent specific heat in the overall approach (nonlinear numerical simulation and burning stability).
- (5) Include distributed chemical reactions in the overall approach (nonlinear numerical simulation and burning stability).
- (6) Predict nonlinear static burning stability boundaries, dynamic burning stability boundaries, static burning boundaries.
- (7) Obtain bifurcation diagrams.
- (8) Evaluate the influence of the integral method on the analytical predictions.
- (9) Validate numerically and experimentally the analytical predictions.

Remark that the knowledge of bifurcation diagrams implies predicting self-sustained oscillatory regimes, dynamic extinction boundaries, and deflagration limits (in terms of pressure, for example).

This nonlinear burning stability analysis can be applied to any solid propellant composition and flame model. But of course the numerical values do depend on the specific solid propellant composition and flame model implemented, as well as on the enforced set of external controlling parameters (pressure, diabaticity, and ambient temperature).

Two unmetallized, composite, ammonium perchlorate (AP)-based solid rocket propellants are taken as datum case throughout this report. The first, denoted as AP/PBAA No. 941, was in use at Princeton University; the second, denoted as

AP 84/CTPB 16, was manufactured by SNIA-BPD and was used for most experimental tests of this research project. While the choice of these two solid propellants makes more realistic the implementation of some of the currently available thermal flame models, by no means the overall theoretical approach is restricted to this specific class of solid propellants. The physical, chemical, and ballistic properties of the two selected solid propellants are listed in Table 1 (AP/PBAA No. 941) and Table 2 (AP 84/CTPB 16).

1.5 - PLAN OF PRESENTATION OF THIS REPORT

A detailed critical review of theoretical and experimental contributions available in the open literature is offered in Chapter 2 as to: dynamic extinction by fast depressurization (Sec. 2.1) or fast deradiation (Sec. 2.2), self-sustained oscillatory burning (Sec. 2.3), and pressure deflagration limit (Sec. 2.4). A mathematical statement of the problem, based on the PDE describing the temperature field in the solid propellant, is given in Chapter 3. The stability properties of the governing set of equations are analytically deduced in Chapter 4, after reduction of the problem from a PDE into an ODE formulation. Notice that this special formulation will be used not to find actual solutions, but to predict the behavior of solutions under steady or unsteady conditions. The analytical predictions will be validated by numerical integration of the PDE formulation of the problem (Chapter 5) and/or experimental tests (Chapter 6). Conclusions and suggestions for future work are contained in Chapter 7.

CHAPTER 2 - LITERATURE SURVEY

The question of solid propellant burning stability in general and dynamic or low pressure extinction in particular has been much discussed in the relevant literature, but few works have been really constructive. The erroneous application of the quasi-steady gas phase assumption, the strong limitations of linearized theories, and the empirical nature of several of the proposed extinction criteria are the most serious drawbacks in this area. In particular a rather fundamental but subtle error, concerning a conceptual confusion between static and dynamic extinction, is seen to permeate the literature. As mentioned in the previous section, static and dynamic extinction are different in nature. Static extinction received little attention in recent years; a good review can be found in standard textbooks (e.g., see Refs. 1-6). The mechanism usually accepted, but unproved, to explain static extinction invokes radiative heat loss from the burning surface. This is questionable; in any event, there is no doubt that static extinction is not directly related to changes in the externally controlling parameters.

Dynamic extinction may occur under a variety of conditions. However, only dynamic extinction by fast depressurization appears largely analyzed. This is due to both its technological importance and the pioneering work by Ciepluch (Refs. 41-43) in 1961. Unfortunately, the scientific understanding of this phenomenon is still little satisfactory. No criterion whatsoever is found in the literature for the case of dynamic extinction by fast deradiation reported by the Princeton group (Refs. 38-40). As to the low pressure extinction (or PDL extinction), a large amount of experimental and theoretical work was performed on pure AP deflagration but without conclusive results; less work appears to have been done on AP-based composite propellants and even less on other propellants. Oscillatory burning was studied mainly in the USSR; progress in USA appears more casual.

Papers dealing mainly with rocket engine performances, rather than just a semi-closed volume (no tight combustion/fluid-dynamics coupling), are neglected in this review.

2.1 - FAST DEPRESSURIZATION

Dynamic extinction of solid rocket propellant by fast depressurization was largely studied, in the past twenty years, following Ciepluch (Refs. 41-43). The increasing employment of solid propellants in rocket propulsion has emphasized the importance of fast depressurization as precise technique of commanding motor termination, possibly permitting reignition at a later time. Notwithstanding its technical importance, fast depressurization effect on solid propellant flames still is not fully understood from a scientific standpoint.

2.1.1 - Theoretical Results on Dynamic Extinction by Fast Depressurization

Theoretical results are reviewed prior to experimental results because the latter look scattered and may be misleading for unexperienced readers. Although basically experimental in nature, the work of Ciepluch (Refs. 41-43) is recalled first since this was the starting point for all successive works.

Ciepluch, from 1961 to 1964, conducted the first systematic experimental study of depressurization transients in a laboratory combustion chamber closely simulating conditions of an actual motor. Fast depressurization was obtained by suddenly opening a chamber vent hole. Initial chamber pressure in the range of 34-82 atm and ambient pressures down to 3.5 mm of mercury were explored. The burning transient was followed by measuring simultaneously combustion luminosity (primarily in the visible range) and chamber pressure. Several ammonium perchlorate (AP)-based composite propellants were tested; few data on double-base (DB) compositions were also reported. The following conclusions were reached:

- 1) A critical depressurization rate exists below which burning continues and above which extinction occurs.
- 2) The critical depressurization rate increases linearly as the chamber pressure prior to venting increases.
- 3) The critical depressurization rate is substantially affected by the propellant composition.
- 4) Reignition may follow extinction if the depressurization is not too fast and/or nozzle back pressure is not too low.

A large number of papers was offered after this study; an important critical review of these contributions was

given by Merkle, Turk and Summerfield (Ref. 44) in 1969. Since the pressure decay in Ciepluch's experiments was exponential, the maximum depressurization rate occurred at the very beginning of the transient burning. This was erroneously interpreted to suggest a tight dependence of dynamic extinction on the initial depressurization rate. Merkle et al. recognized that dynamic extinction depends on the entire $p(t)$ curve, corrected several mistakes that had crept in the literature, and furnished a new quasi-steady flame model. However, Merkle et al. did not formulate an extinction criterion. For numerical simulation purposes only, a critical value of surface temperature ($T_s=600$ K) was empirically picked up, below which chemical reactions are considered too weak to sustain deflagration waves.

The papers by Von Elbe should be noted; an analytical expression given by this author for the critical depressurization rate has been rather widely accepted. Although later proved wrong by Merkle et al. (Ref. 44) and Krier (Ref. 45) on different arguments, this expression

$$(2.1) \quad r_b(t) = \bar{r}_b \left[1 + \psi \frac{n}{p(t)} \frac{\alpha_c}{\bar{r}_b^2} \frac{dp(t)}{dt} \right]$$

was intended to describe transient burning rate of solid propellants. The quantity ψ was considered constant by previous investigators:

$$\begin{aligned} \psi &= 1 && \text{by Paul et al. (Ref.46);} \\ \psi &= 1/2 && \text{by Parker and Summerfield (Ref.47);} \\ \psi &= 2 && \text{by Von Elbe et al. (Refs. 48-49).} \end{aligned}$$

The above expression and the following equation

$$(2.2) \quad - \left. \frac{dp(t)}{dt} \right|_{cr} = \frac{1}{\psi} \frac{p(t)}{n} \frac{\bar{r}_b^2}{\alpha_c}$$

for critical depressurization rate are still being used (in particular the version with $\psi = 2$), but erroneously, for practical applications. The use of Eq. 2.2 was already proved wrong, on physical grounds, by Merkle et al. Krier analytically showed that ψ depends on the burning surface properties and pressure jump; this function can be computed a priori. Nevertheless, relationships of the type of Eq.2.1 being restricted to small values of dp/dt and small excursions of $r_b(t)$ with respect to \bar{r}_b , are just not applicable to dynamic extinction problems.

A paper by T'ien (Ref.50), in 1974, is the only one

aimed directly at establishing an extinction criterion for fast depressurization. T'ien recognizes the basic difference between static and dynamic burning regimes and argues that heat losses are the mechanism for both static and dynamic extinction of solid propellants; this view is not fully shared in this instance. However, T'ien concludes that for depressurization transients, if the instantaneous burning rate drops below the unstable burning rate solution at the final pressure, extinction will occur. T'ien derives his qualitative criterion from another study (Ref. 51) by him of flammability limits of premixed flames under the influence of environmental disturbances. A somewhat similar result has been found in this investigation, but by a completely different approach.

A subtle error, associated with the appropriate quasi-steady formulations of burning surface boundary condition and gas phase heat feedback, has unfortunately revealed difficult to wipe out from the competent literature (Refs. 52-54). Recent papers (Refs. 55-57) re-introduced basic errors already recognized by Merkle et al. (Ref. 44) in 1969. It should be stated once for all that: (1) quasi-steady gas phase assumption implies a precise mathematical formulation (see pp. 6-7 of Ref. 44a) forbidding different interpretations and (2) linearized flame models cannot be applied to dynamic extinction problems (see p. 42 of Ref. 44a). Incidentally, it should be remarked that some of the criticism expressed in Ref. 44a (pp. 3-13) is in turn not well founded (e.g., the Zeldovich method was misunderstood).

Mongia and Ambs (Ref. 55) assumed a quasi-steady heat feedback with a variable surface heat release; both the mathematical formalization and the physical motivations are questionable. However, Mongia and Ambs rightly recognized the importance of the finite time associated with the condensed phase heat release and its dependence on the instantaneous properties near the burning surface. The importance of condensed phase reactions was first stressed by Marxman and Wooldridge (Refs. 53-54), but their treatment also is suspect. Suhas and Bose (Refs. 56-57) relaxed somewhat the quasi-steady gas phase assumption by taking into account the unsteady gas phase continuity equation in the otherwise standard KTSS linear heat feedback law. The choice of this flame model is surprising, since the linear heat feedback law of KTSS was not intended to be used for extinction transients; in any event, the mathematical approach and the physical motivations are questionable. However, Suhas and Bose recognized the importance of the finite time associated with the gas phase

processes. Likely, the most important area of investigation in solid propellant combustion in the near future will focus on these questions of condensed phase reactions and unsteady gas phase (thick vs thin flames).

The line of research evolved within the framework of the Zeldovich (Refs. 58-59) method is of limited value from the point of view of dynamic extinction. In the original Zeldovich model (constant surface temperature), extinction is assumed to occur when the instantaneous thermal state of the condensed phase (taken as chemically inert) can no longer be matched to the allowed values of surface temperature and thermal gradient at the condensed side of the burning surface. For example, in 1964 Istratov et al. (Ref. 60) used an integral method to determine an approximate solution to the condensed phase energy equation of a propellant burning with a constant surface temperature. Dynamic extinction following instantaneous or exponential pressure decay was taken to occur when the surface thermal gradient on the condensed side exceeds some critical (maximum) value beyond which no solution can be found (this corresponds to a static stability limit). This is not acceptable, since no prediction can be made (without further analysis) about dynamic combustion for burning rates outside the Zeldovich allowed range. Indeed, Marshakov and Leipunskiy (Ref. 61) showed experimentally (by testing a double-base composition) that Zeldovich theory on dynamic extinction has at least three weak points: the initial pressure level (besides the pressure drop and depressurization rate) may be determining, surface temperature is not constant, chemical reactions in the condensed phase are also important. In 1967 Novozhilov (Ref. 62) considered variable surface temperature and recognized that dynamic combustion is permitted also in a range of parameters where statically stable solutions are not found. To explain dynamic extinction the concept was then introduced of limiting points, at constant pressure, corresponding to finite values of burning rates and surface thermal gradients on the condensed side. Combustion, steady or unsteady, is considered impossible beyond these limiting points. The latter should be experimentally established, possibly under nonstationary burning conditions. This "ad hoc" criterion, if feasible, would rely on very delicate experimental results. However, the existence of the limiting points was never proved. Moreover, both models (constant and variable surface temperature) assume a sudden occurrence of extinction: the burning rate immediately prior to extinction is of the order of magnitude of the corresponding steady value. In general, this does not seem plausible from a physical standpoint.

The question of a possible early warning of extinction during a depressurization transient evaluated via the Zeldovich method was examined in a paper by the Princeton group (Ref. 63) in 1971. The possibility was checked that the crossing of the Zeldovich stability boundary is sufficient to subsequently produce dynamic extinction. No clear answer to this question was given. In our opinion the Zeldovich stability boundary has only secondary relevance in a dynamic situation. Indeed, according to the same Princeton reference, "the dynamic conditions of extinguishment tend to shift the stability line" (p. 257 of Ref. 63). Further extensive work in this area (Ref. 64) failed to reach more significant conclusions. Finally Novozhilov (p. 216 of Ref. 4), in 1973, observed that this "question requires certain information about the properties of the system outside the area of smooth burning. Such information cannot be obtained from experiments on steady state combustion. For the calculation of unsteady conditions in the unstable region it is necessary to draw on certain schemes of combustion, which make it possible to predict the properties of propellants beyond the [Zeldovich] stability limit".

Further work by Soviet investigators (Refs. 65-69) offered fresh theoretical considerations, but failed to define a physically sound extinction criterion. In 1972 Frost (Ref. 65) considered the case of the surface temperature depending only on the mass burning rate and reached conclusions similar to those obtained by Zeldovich for constant surface temperature (extinction due to impossibility of matching the temperature distributions in the gas and condensed phases). Frost and Yumashev (Ref. 66) later studied the problem of dynamic extinction by depressurization by numerical integration. They concluded that: 1) introduction of special extinction conditions (limiting points) is not required in order to get extinction; 2) burning rate during extinction changes smoothly; and 3) the passage of the transient burning process outside the Zeldovich limit of stability does not necessarily imply extinction. Frost and Yumashev (Ref. 67) in a successive work in 1976 reviewed the Princeton papers (Refs. 63-64) and formulated criticism similar to that stated above: they emphasized that the Zeldovich stability boundary is valid only for stationary combustion and has no direct bearing on unsteady processes; however, dynamic boundaries were not provided.

2.1.2-Experimental Results on Dynamic Extinction by Fast Depressurization

Experimental results are often ambiguous to interpret due to the interplay and overlapping of several factors. Attention is preferably focused on data collected from laboratory burners (ranging from depressurization strand burners to simulated rocket combustion chambers) rather than actual rocket motors, where fluid dynamic effects may be dominant. However, even results from laboratory burners are not easy to compare due to: (1) implementation of different extinction criteria, diagnostic techniques, and operating conditions; (2) scattering of results; (3) confused theoretical guidelines in data handling.

The pioneering work by Ciepluch (Refs. 41-43) was summarized at the beginning of the preceding subsection. Recall that the critical boundary between (permanent) extinction and continued burning was found with a go/no-go technique to be a straight line in the dp/dt vs p_i (initial pressure) linear plot. Experimental data were provided, among others, by Von Elbe and McHale (Ref. 49) in effort to substantiate Von Elbe's theoretical predictions (Ref. 48). They tested three AP-based composite propellants in a depressurization strand burner (300 cm³ internal volume) furnished with a frangible diaphragm (ruptured by a solenoid-driven plunger) and orifice plate to control the depressurization rate. Flame luminosity in time was monitored with a photodiode simultaneously to pressure decay. Initial pressures of 33 - 5 atm were used. Von Elbe and McHale plotted dp/dt vs p at extinction (as determined by zero luminosity); the critical boundary was found to be straight on a lg/lg plot.

Merkle, Turk, and Summerfield (Ref. 44) produced a rather complete set of data by systematically testing several AP composite and one catalyzed DB propellants. A special laboratory combustor was designed to minimize erosive burning effects and to cause monodimensional "cigarette" burning of the sample. Fast pressure decay was obtained by rupturing a double-diaphragm system. The exhaust gases initially pass through both a primary (large) nozzle and a secondary (small) nozzle; the small nozzle controls the chamber pressure as long as the diaphragms remain in place. When the diaphragms are removed, the small nozzle also becomes ineffective since it is located in the double-diaphragm section. By properly combining nozzles of different diameters, the initial pressure level as well as the depressurization rate could be varied. Pressure and light emission (as seen by a photomul-

tiplier in the visible range) were simultaneously recorded. Extinction was considered to occur when zero light emission from the flame could be observed. Initial pressure in the range of 75 - 14 atm were explored. Venting was always to atmospheric pressure; because of this, reignition was nearly always observed. The following conclusions were reached:

1) The critical boundary between extinction (permanent or temporary) and continued burning was found with a go/no-go technique to be always straight in the dp/dt vs p_i linear plot.

2) Increasing AP loading from 75 to 82.5% makes the propellant harder to extinguish (by a factor of 2) in terms of initial, i.e. maximum, dp/dt .

3) Increasing AP particle size from 45 to 180 μm (unimodal distributions) makes the propellant easier to extinguish (for a fixed loading of 75% AP).

4) Little difference was observed when PBAA, CTPB, and PU binders (for a fixed loading of 80% AP) were tested.

5) Aluminum (16 μm particles) addition up to 15% makes the propellant slightly more difficult to extinguish (for a fixed composition of 77.5% AP/22.5% binder); but the opposite is true for $p_i < 27$ atm.

6) The tested catalyzed DB propellant (N-5 composition) is much easier to extinguish than any of the tested AP composite propellants.

Remark that some of the above conclusions on AP particle size and binder type effects may be in conflict with other experimental studies in which permanent extinction was recorded. Merkle et al. adopted the permanent extinction criterion only for tests using catalyzed DB propellants, since no visible radiation can be detected from DB burning at low pressures.

Experimental works of interest for this investigation include, besides the basic contributions just mentioned, papers reporting data about final pressure as well as propellant composition effects, temperature profiles during depressurization, and attempts to measure unsteady burning rate.

Detailed observations on the flame structure of composite propellants during depressurization were reported by Selzer and Steinz in a series of papers (Refs. 70-72). They showed that, regardless of the depressurization rate, the flame intensity (as seen by spectral emissions from OH, NH, CN, Na lines and carbon continuum) falls to zero soon after the impact of the first rarefaction wave on the burning surface. This event is possibly followed by the reappearance of an incipient flame, after a time span of the

order of the condensed phase thermal wave relaxation time, if the depressurization rate is not too fast. Marked pressure oscillations are observed when this secondary flame develops, the flame decay being otherwise exponential. The authors further claimed that the adiabatic expansion of the flame quenches the active gaseous chemical reactions; this would explain why the first zero intensity of flame radiation is noticed when the instantaneous pressure has dropped only to about 70% of the initial pressure. The average oxygen/fuel (O/F) mixture ratio was observed to be higher during some part of the transient burning than during steady state, due to preferential consumption of AP particles exposed on the propellant surface; the binder surface looked molten and not thicker than a few microns (for depressurization tests at 45 - 1 atm with 76% AP/24% CTPB composition). The implication is that the binder gasification is the first to suffer the effects of a pressure expansion. It was stressed that during depressurizations AP may undergo important postreactions in the condensed phase, which would distort the O/F mixture ratio with respect to steady state and cause 3-D effects. However, it was later concluded that more important steps are the easiness of gas phase reactions and the decomposition mechanism of binder. It was finally confirmed, in agreement with Ciepluch (Ref.41-43) and Merkle (Ref.44), that conditions at the end of the depressurization process (i.e., the final shape of the pressure history and the exhaust pressure) can be determining in extinction.

Baer and Ryan (Refs. 73-74) also furnished detailed information on the flame structure during depressurization from about 7 atm to subatmospheric. AP-based composite propellants were tested in a rarefaction tube. Infrared spectral emissions from H₂O, HCl, CO₂ lines and continuum (presumably from carbon particles) were detected; transient flame temperature was measured by use of an emission-absorption technique at the sodium D-lines (propellants were sodium seeded). Results obtained on the history of the gaseous mixture composition agree with those by Selzer and Steinz mentioned above (Ref. 70). Before the start of the pressure decay, the magnitude of the intensity of the spectral bands fluctuates, apparently as a result of almost periodic combustion irregularities. Intensities decreased rapidly as the pressure dropped and were often observed to increase prior to finally dropping to zero (for extinction transients). Plotting of H₂O/CO₂ intensity ratio, with respect to the corresponding steady-state value, indicated that the O/F ratio increases at the beginning of the depressurization but decreases at the end, in part as a result of faster oxidizer

depletion. The authors suggest that the flame might extinguish for a rich mixture limit effect, since termination of radiation emission (and extinguishment?) occurred as the intensity ratio rose above the steady burning value. The reported flame temperature histories (Ref. 73) are of greatest interest for theoretical modeling. The average steady burning temperature prior to depressurization was in excellent agreement with computed adiabatic flame temperatures. The flame temperature was observed to remain practically constant for a short while immediately after the beginning of pressure decay, then to decrease and possibly feature one or more attempts to recover before extinction. Finally, it was noticed that small pressure drops at low pressures were immediately followed by extinction.

Park, Ryan, and Baer (Ref. 74) presented in 1973 another paper in which static vs dynamic extinction at low pressure (around 1 atm) was experimentally studied. In this pressure range, the two extinction mechanisms tend to overlap each other. Several composite propellants were tested. Propellant strands were burned in a vacuum chamber while supported on a force transducer monitoring their instantaneous weight. Extinction was detected from both the instantaneous burning rate (obtained by differentiating the weight vs time record) and light emission. The following observations are of interest:

(1) Propellants with burning rate catalysts (higher burn rate) require higher depressurization rates than the corresponding uncatalyzed propellants for extinguishment at the same pressure (in the Von Elbe sense).

(2) As depressurization rates are lowered, the extinction pressure approaches a constant minimum value for each propellant (this value is, however, affected by the side burning inhibiting material, ambient gas, and the rate of heat loss).

(3) Extinction pressure (in the Von Elbe sense) is lowered by increasing ambient temperature (or reducing heat losses).

Further data on propellant composition effects were collected by Jensen and Brown (Ref. 75) by testing AP-based composite propellants in two laboratory motors. They confirmed the known effects of exhaust pressure level on extinction and the overlapping effects of motor geometry. Propellants with binders degraded by endothermic thermal decomposition (thermally less stable, e.g. PU and CTPIB) were more easily extinguished than binders degraded by exothermic oxidation (thermally more stable, e.g., CTPB). The addition

of aluminum made both dynamic extinction and reignition easier.

Data on condensed phase thermal profiles during depressurization were published by Zemskikh et al. (Ref. 76). Thin thermocouples (7-10 μm) were used to monitor the temperature history near the burning surface of double-base propellants in a laboratory burner. Fluctuations were observed for both extinction and reignition runs: large temperature drops could be measured following the pressure decay. Further data on double-base propellants tested in a depressurization bomb were offered by Ivashchenko and Komarov (Ref. 77). They claimed the importance of the dispersal of the reacting condensed layer following the expansion of the gas bubbles in response to the rapid pressure fall.

Experimentally, the results reported in Refs. 44 and 49 (go/no-go boundaries), Ref. 70 (flame structure during depressurization), Ref. 73 (flame temperature and emission spectra during depressurization), Ref. 76 (condensed phase temperature during depressurization) are the most interesting. They allow detailed and reliable comparison with analytical and numerical results. Obviously, the most wanted result is the burning rate history during depressurization transients. Unfortunately, no reliable data exist yet in this particularly difficult area of investigation, although a large number of contributions have been offered. For a good summary of the results so far obtained and a critical discussion of the techniques implemented, the reader might consult the excellent review given in Ref. 78 (with the updated comments of Ref. 79). A more recent review (Ref. 80) deals in general with experimental methods capable to measure transient combustion response.

Strand and co-workers have been working for years to set up a microwave technique, with the appropriate time resolution, by monitoring the phase angle difference between the incident and reflected signals. Tests (Ref. 78) on AP-based composite propellants in a laboratory depressurization burner were performed with initial pressures in the range of 22-27 atm, final pressure 1 atm, and maximum (initial) depressurization rates of 1160-6430 atm/s. No correction was made for the compressibility effect on the solid propellant strand, although this may be significant for large pressure variations (Refs. 78-79). The effect of transient flame ionization was later (Ref. 7, pp. 155-172) shown to be not important. In any event, the following results are at least qualitatively correct:

1) Burning rates generally fall below the corresponding steady-state value.

2) Burning rates smoothly go to zero rather than suddenly terminate (for extinction runs).

3) Rather irregular oscillations, roughly below 100 Hz, can be observed; in general, the amplitude and frequency of these oscillations decrease with decreasing depressurization rates.

4) HTPB and CTPB propellants behave similarly; both required a higher (by a factor of two) depressurization rate than PU propellants to extinguish, while the instantaneous burning rate looked more "sluggish" (less oscillatory and slowly recovering when burning continued).

5) Following the pressure decay, burning rate under-shoots down to 5% of the corresponding steady value can be obtained.

The present work on fast depressurization is part of an ample research program about nonlinear stability of solid propellant combustion being carried out at Politecnico di Milano. The specific objective of the report is to check experimentally the analytical predictions on dynamic extinction boundary, obtained by this research group (Refs. 10-13), for heterogeneous thin flames subjected to finite size disturbances. The theory predicts a minimum value of instantaneous burning rate (or surface temperature or flame temperature) under which dynamic extinction necessarily follows for any monotonic decrease of arbitrary forcing functions (pressure, external radiant flux, etc.). This critical burning rate depends on propellant composition and final set of operating conditions. Due to the known difficulties of measuring instantaneous values of burning parameters, the strategy followed in comparing experimental and theoretical results is to resort to a wide range of go/no-go testing. A composite propellant with relatively low oxidizer loading (AP70/PVC30) was already tested (Refs. 8,9,28) by venting a laboratory combustion chamber, furnished of manual and/or solenoid valves, down to 1 atm. In this report a composite propellant with large oxidizer loading (AP83/CTPB16/ Al_2O_3) is tested by venting a laboratory combustion chamber, furnished of a double diaphragm and pressurizable dump tank, down to 1 or 3.25 atm. While the experimental apparatus is described in some detail in Chapter 6, analytical and numerical developments will be illustrated respectively in Chapter 4 and Chapter 5.

2.2 - NONLINEAR DYNAMIC EXTINCTION BY FAST DERADIATION

Studies on dynamic extinction by fast deradiation overlap with those on radiative ignition. Ohlemiller, at Princeton University in 1970, first observed dynamic extinction by fast deradiation while constructing ignition map of noncatalyzed DB (a NC composition) by a CO₂ laser source, providing up to 120 cal/cm²s at the target, in the range 3 to 34 atm of nitrogen. It seems that, independently, the discovery was made in USSR by Mikheev in his Candidate's Dissertation appeared about at the same time (1970), but unavailable to this writer. From successive work published in the open literature, one would guess that Mikheev's data concerned uncatalyzed DB propellants tested in a furnace at low radiant flux (few cal/cm²s) at 1 atm of air or nitrogen. Supporting evidence for the dynamic character of this phenomenon and further experimental data were successively offered mainly at Princeton University (Refs. 12, 38-40) and in USSR (Refs. 81-84 and pp. 173-187 of Ref. 7). The radiative pulse experiment on steadily burning propellants, reported in Ref. 38, was suggested by Yu. A. Gostintsev during a stay at Princeton University.

Theoretical considerations (Refs. 38, 81, 83-84) were offered mainly in the framework of Zeldovich approach. However, just as in the case of dynamic extinction by fast depressurization, the Zeldovich stability boundary is not meant to apply to transient burning stability. The dynamic extinction boundary for fast deradiation was shown to coincide with that for fast depressurization in Ref. 10; details will be given later in Chapter 4. No other attempt to evaluate the dynamic extinction boundary for fast deradiation is known to this author.

All of the successful experimental results collected at Princeton University concern radiation by a 100 W continuous wave, multimode CO₂ laser emitting at 10.6 μm in the far infrared. Cylindrical samples of propellant were tested in a strand burner with two optical windows for high speed cinematography and light emission recording (both visible and infrared photodetectors were available). Two mechanical shutters (of iris leaf type) provided a trapezoidal radiation pulse, the action time of the shutters could be regulated from 1 to 10 ms. Dynamic extinction of steadily burning samples (ignited by hot wire) subjected to laser pulse was observed for two DB uncatalyzed compositions, but it could not be seen for the tested DB catalyzed propellant (Ref. 38). Experiments were made up to 11 atm of nitrogen;

the minimum pulse length required for extinction, determined by a go/no-go technique, was found to increase with pressure but decrease with radiant flux intensity. The radiation cut-off time was 2 ms for all tests; experiments in air were not conducted; composite propellants were not tried.

Ignition tests were performed, in the range 5 to 21 (sometimes up to 34) atm of nitrogen or air, for 12 propellants representative of several classes (uncatalyzed and catalyzed DB, unmetallized and metallized AP composite, HMX composite) both with laser and arc image furnaces. Dynamic extinction associated with ignition was again observed only for several uncatalyzed DB compositions with 0, 0.2 and 1% carbon addition (Refs. 12 and 40). Ignition boundaries, determined by a go/no-go technique, revealed an ignition corridor bounded essentially by two parallel straight lines in the lg radiant heating time vs lg radiant flux intensity plot. The lower boundary defines the minimum exposure time for self-sustained flame propagation; it is not affected by ambient atmosphere (air or nitrogen) and radiation cut-off time. The upper boundary defines the critical (i.e., maximum) exposure time above which a radiation overdriven flame extinguishes when the external radiant beam is removed; this boundary is strongly affected by the ambient atmosphere (extinction occurs in nitrogen but not in air), pressure (increasing pressure widens the ignition corridor), and radiation cut-off time (slow cut-off widens the ignition corridor). For pressures less than 11 atm the ignition corridor was totally wiped out. Dynamic extinction did not occur in air due to the stabilizing effect of a diffusion flame (enveloping the propellant flame) associated with the oxygen contained in the air. All this was confirmed by high-speed movies and photodetectors. However, the same propellants extinguishable at the laser apparatus could not be extinguished when tested, in similar operating conditions, at an arc image apparatus. This used as source a 2.5 kW high-pressure xenon arc lamp with spectral emissions in the visible (similar to sunlight, peak near $0.55 \mu\text{m}$), except for some nonequilibrium high intensity bands in the near infrared. Tests at the arc image apparatus were conducted only for the ignition runs.

The different results obtained with noncatalyzed DB propellants and with the two radiative sources were mainly attributed to different optical properties (volumetric absorption and scattering are strongly wavelength dependent; noncatalyzed DB propellants are much more opaque in the far infrared than in the visible) and larger radiant flux cut-

off time with the arc image apparatus (about twice with respect to the laser apparatus). Other minor differences were also operative: spatial structure of the radiant beams (less sharp with the arc image source), sample positioning (protruding from a metallic holder at the laser apparatus but flush at the arc image; this may cause heat sink effects), different beam geometry (collimated and perpendicular for laser but converging and oblique for the arc image). The different results between noncatalyzed DB vs catalyzed DB and AP composite propellants, observed at both laser and arc image apparatus, were attributed to the different flame structure and different radiation interaction with the combustion products. Indeed, both catalyzed DB and AP composite propellants give a relatively higher ratio of gas phase heat feedback to the burning surface heat release; this is known to be stabilizing. Moreover, radiation is gently terminated and effectively decreased by carbonaceous filaments and particulates generated by the burning samples; this is stabilizing and occurs especially for catalyzed DB propellants. However, it is expected, in principle, that all propellants should manifest dynamic extinction by fast deradiation if tested in the appropriate range of operating conditions.

To the best of the author's knowledge, the only easily available Soviet paper with detailed experimental data on dynamic extinction by fast deradiation is the one by Mikheev and Levashov (Ref.82). Data reported concern a DB composition, without and with carbon addition (1%), at 1 atm of nitrogen, subjected to low (<10 cal/cm²s) radiant flux from an electrically heated incandescent graphite plate. Mechanical shutters, with about 30 ms action time, were used to control the pulse length. Three types of experiments were performed: ignition, radiation pulse of parametrically varied duration on steadily burning samples, radiation pulse of parametrically varied intensity on steadily burning samples. Ignition runs showed the familiar ignition corridor just discussed (cf. Refs. 12 and 40). The second experiment showed a decrease of critical (minimum value leading to extinction) duration of radiant pulse for increasing flux intensity. The third experiment showed critical (minimum value leading to extinction) radiant flux intensity increasing for increasing initial temperature (20°C or 100°C) and for increasing transparency of the sample.

Interesting experimental data on transient burning and surface structure during and after deradiation were provided by Mikheev et al. in a successive paper (pp.173-187 of Ref.7). They used an arc image furnace (the source was a xenon lamp of 10 kW) capable of a radiant flux from 1 to 10 cal/cm²s. Experiments on a DB propellant and pressed nitrocellulose samples, both without and with 1% carbon addition, were carried

out at 1 atm of air or nitrogen. Mechanical shutters with an action time ≤ 2 ms were used to send trapezoidal (square as seen by samples with large thermal and reacting layers relaxation times in the condensed phase) radiation pulses on target. Ignition, fast deradiation, and fast irradiation experiments were performed. A capacitive transducer system was set up to record the instantaneous strand weight and, by inference, the unsteady mass burning rate; the frequency passband of the system was 0-250 Hz.

With the DB + 1% C propellant ($a_\lambda = 100 \text{ cm}^{-1}$) dynamic extinction was observed only for tests in nitrogen; reignition would occur only for tests in air; reignition would not occur for tests in air with samples whose lateral surface was inhibited; self-sustained burning was oscillatory in character (16-20 Hz). For the DB propellant without carbon addition ($a_\lambda = 10 \text{ cm}^{-1}$) dynamic extinction could not be obtained (recall that the maximum radiant flux was $10 \text{ cal/cm}^2\text{s}$); self-sustained burning was again oscillatory (10 Hz). For both propellants, when deradiation occurred, the burning surface was immediately covered with a dense distribution (100% for DB + 1% C and 50% for DB without carbon) of bubbles (0.1 mm diameter). The authors suggested that this may be associated with gas evolution breach, in the subsurface layer, caused by the sharp burning rate decrease. The authors further emphasized the multidimensional nature of phenomena occurring at and near the burning surface; unsteady and nonuniform character of burning surface, on microscale level, even for steady combustion. Low frequency (10-20 Hz) burning was associated with condensed thermal wave relaxation time, while higher frequency (50 to 100 Hz) burning was tentatively associated with local small scales of burning surface.

Further work by the Novosibirsk group in this area was focused on numerical modeling (Refs. 85-86) within the framework of the Zeldovich-Novozhilov approach. The transient burning of DB propellants subjected to sharp radiant flux changes at atmospheric pressure was examined in Ref. 87. Extinction followed by reignition was observed when a noncatalyzed DB (with the addition of 1% carbon black) was subjected to a fast decrease of radiant flux from 10 to $5 \text{ cal/cm}^2\text{s}$. The experimental apparatus from the paper seems to be the one already described by Mikheev et al. (pp. 173-187 of Ref. 7).

At the Politenico di Milano research activities in this field have so far been only theoretical (Refs. 8, 25-27, 33). In particular De Luca (Ref. 10), in 1975, suggested that dynamic extinction occurs in general by removal of a large enough fraction of the condensed phase energy content and

proposed a quantitative criterion for dynamic extinction valid for any monotonic decrease of forcing functions (pressure and/or radiant flux). Extensive check of this theoretical criterion was performed by numerical computations (e.g., see Ref.9). Presently, a laser driven burning apparatus is being set up; it is hoped to collect meaningful experimental results as soon as possible.

2.3 - NONLINEAR OSCILLATORY COMBUSTION

The original work of Huffington (Refs. 88-90) on chuffing and oscillatory burning of cordite goes back to the beginning of the '50. Experimental results and a theoretical interpretation, in terms of condensed phase thermal explosion, were given for both phenomena. The proposed mechanism for oscillatory burning of cordite is the successive explosion, assisted by gas phase heat feedback, of discrete surface layers of decreasing thickness with increasing pressure. The Frank-Kamenetskii thermal explosion theory (Ref. 91) was extended to consider a monodimensional slab of decomposing explosive, enclosed between two parallel walls, with one surface (hot boundary) subjected to a constant rate of heat transfer while the other (cold boundary) is maintained at a constant temperature. For cordite this temperature was taken as the melting temperature (460 K); for other cases it was just the ambient temperature. The solution determines, for a given heat transfer rate to the burning surface, the critical slab thickness and surface temperature above which the volumetric decomposition develops to explosive rates. These critical values were found to depend on the dimensionless parameter $\tilde{E}_C/Q/T_{-\infty}$, being E_C the activation energy of the distributed exothermic reaction (assumed of Arrhenius type) in the condensed phase and $T_{-\infty}$ the cold boundary temperature. The theory was quite successful in predicting, at 20 atm, a thickness of layer burnt off in a single explosion of about 50 μm and a frequency of about 40 Hz. This theoretical approach, remarkable 25 years ago, suffers today the known limitations of the Frank-Kamenetskii type of theory.

Parallel work in the USA was less ready to recognize the real nature of the phenomena, probably because of the confusion generated by the overlapping studies on acoustic instabilities in rocket motors. Huggett (Ref. 92, p.40) attributes the pulsating combustion of chuffing to "the formation of a combustible gas mixture which, when a critical concentration is reached, ignites spontaneously"; but experimental evidence

denies gas phase effects. Inami and Shanfield (Ref. 93) observed the pulsating combustion of AP strands containing aluminum in the pressure range 68-136 atm and found the frequency peak (of the order of several 10 to some 100 Hz) to increase with increasing pressure and aluminum content (15% at most).

Inami and Shanfield (Ref. 93) attributed this nonacoustic instabilities to aggregation of aluminum on the burning surface and its subsequent burning in a single pulse; however, experimental evidence shows that AP-based composite propellants may exhibit oscillatory burning even without aluminum addition.

Eisel et al. (Ref. 94) tested both metallized DB and aluminized AP-based composite propellants in laboratory burners and observed low frequency (below 100 Hz) oscillatory burning for pressures up to 13 atm. The authors recognized that "one or more of the solid phase processes is probably involved" (p.1322 of Ref. 94) in the nonacoustic burning oscillations; quite synthetic, but correct. Angelus and coworkers (Refs. 95-96) went further. They observed that:

- (1) oscillatory frequency increases while oscillatory amplitude decreases when pressure increases;
- (2) oscillatory burning is independent on geometry and other rocket motor parameters;
- (3) the oscillatory frequency is the same in air or nitrogen;
- (4) oscillatory burning occurs for a wide variety of solid propellants;
- (5) frequency and amplitude of the oscillatory burning increase for increasing propellant initial temperature;
- (6) the oscillatory amplitude increases for increasing metal concentration, while the oscillatory frequency is not affected.

Yount and Angelus (Ref. 96, p.1312) conclude: "Chuffing and low frequency instability in composite modified DB solid propellant rocket motors are interpreted to be initiated through a condensed phase thermal explosion mechanism, which is inherent in the propellant combustion process". We fully share these words; however, the proposed theory (in 1964) is a clever but artificial modification of the Frank-Kamenetskii (Ref. 91) or Huffington (Refs. 88-90) theories.

Finally, Price in 1969 reviewed the whole field of solid propellant combustion instability and stated (Ref. 97, p.111): "My personal opinion is that spontaneous oscillations (i.e., independent on environmental oscillations) do not occur with homogenous propellants or with composite propellants of random microstructure, nor do I know of any mechanistic argument that would explain their occurrence. Since this seems to be in contradiction with some experimental result [Ref. 93 and a personal communication by Selzer], this view remains only an

opinion. However, the experimental results may deserve re-examination to verify that no flow oscillations, sample vibrations, or other perturbations occurred during burning to induce combustion oscillations. Likewise, the optical arrangement for photoelectric observations of combustion must be evaluated to assure that the observations do not simply reflect the local transitions from oxidizer to binder as the burning front regresses...".

A relatively large amount of work on oscillatory burning of several reactive materials, including DB and AP-based composite propellant, was performed by Soviet investigators. A good review, mostly focused on the theoretical aspects of this question, is contained in Novozhilov's monograph on solid propellant burning (Ref. 4). In particular, a numerical solution for the unsteady propagation of an exothermic reaction front in a gasless system (condensed phase energy equation coupled with a distributed chemical reaction rate of Arrhenius type) was given in 1971 (Ref. 98). The rather vague mechanism invoked by the authors, to explain the oscillating combustion observed under a wide combination of the relevant parameters, relies on the "excess enthalpy" of the steadily propagating combustion front as compared with the enthalpy of the initial material. Librovich and Makhviladze (Ref. 99) took up this problem in 1974; they simplified the gasless system by considering a collapsed chemical layer separating the initial material from the combustion products. An analytical solution was found via an integral method (Fourier transform) and successfully compared with the previous numerical solution of Ref. 98. In both cases an increase of the activation energy was found to increase the period of the oscillating combustion rate and the amount of movement of the reaction front during one oscillation, but decrease the mean velocity. Frequencies were of the order of several 10 Hz. The oscillating mechanism, according to Librovich and Makhviladze, consists of a succession of fast burn-up of unreacted but heated layers, each requiring a prolonged thermal time lag for the ignition to occur.

Experimental results on self-sustained oscillatory combustion of pure and metallized DB propellants, both in a strand burner and rocket combustion chamber, were published by Svetlichny et al. (Ref. 100) in 1971. In the pressure range 1-140 atm, combustion oscillations (revealed by radiation emission and electrical conductivity of the burning zone) up to several 10 Hz were detected. The authors qualitatively ascribed these oscillations to unstable thermal relaxation of the condensed phase heated layer.

However, according to the same authors (Ref.100), self-sustained oscillatory burning of the same DB propellants at pressure less than 70 atm is due to incomplete combustion. This and other oscillating mechanisms related to burning peculiarities (e.g., incomplete burning invoked in Ref.100 and inhomogeneities of the combustion wave in Refs. 101-102) are out of the scope of this work. Oscillatory burning due to combustion/fluid-dynamics coupling is also out of the scope of this work. In this work self-sustained oscillatory burning of exclusively thermokinetic character is considered for the wide class of heterogeneous combustion systems. It will be shown that this type of oscillatory burning is related to either the presence of exothermic chemical reactions in the condensed phase or too low burning rate. Pressure will be seen to favor stability. The combustion frequency, of the order of few 10-100 Hz, will be found to increase with pressure while the combustion amplitude decreases. The characteristic burning rate spikes associated with these oscillations intuitively confirm the physical mechanism suggested by Librovich and Makhviladze (Ref. 99).

First detailed analytical predictions and numerical results, for a model explicitly considering the heterogeneous burning of a solid propellant (quasi-steady MTS flame), were offered by De Luca (Refs. 11-12) in 1976. Other results and an interpretation in terms of bifurcation diagrams were given by De Luca (Refs. 17-19) later. Kooker and Nelson (Ref.103) numerically confirmed the existence of a self-sustained oscillatory burning regime for solid propellants (the quasi-steady KTSS linearized flame model was adopted), but without making any attempt to predict the existence and the properties of such a special regime. The assumption of quasi-steady gas phase in these developments might be open to criticism, as rightly pointed out by T'ien (Ref. 104). Peters (Ref. 105) numerically observed self-sustained oscillations of hybrid burning of porous spherical particles of combustible material immersed in an infinite stagnant oxidizing atmosphere by solving, via an integral method (polynomial space dependence of the relevant variables), the governing set of 5 ODE's. A rigorous analytical treatment of the oscillating combustion associated with gasless burning of condensed systems discussed in Refs. 93-99 was recently offered by Matkowski and Sivashinski (Ref. 106). They showed that a periodically pulsating solution arises as a Hopf bifurcation from the uniform propagating solution, the bifurcation parameter being the product of a nondimensional activation energy and a factor measuring the difference between nondimensional temperatures of unburned reacting material and the combustion products. The

amplitude, frequency, and velocity of the propagating pulsating front were also computed (within the framework of a nonlinear treatment).

Experimental results collected at Politecnico di Milano are reported in Refs. 32-33; further experimental work is in progress. It will be shown in Chapter 4 (and confirmed numerically in Chapter 5, as well as experimentally in Chapter 6) that oscillatory burning is a general solution of heterogenous thermodiffusive reactive fields and can be found under a variety of situations. For example, we suspect that the oscillatory burning of liquid hydrocarbons recently observed (Ref. 107) is just another manifestation of such a general property of heterogenous reactive media.

2.4 - PRESSURE DEFLAGRATION LIMIT

For a solid rocket propellant the pressure deflagration limit (PDL) is that minimum pressure where a steady combustion regime (either time-independent or steady oscillatory) can still be maintained without adding energy to the system. Besides the scientific importance attached to the understanding of what determines the PDL for a given solid propellant, a very practical reason to investigate the PDL is the possibility of controlling the crucial processes of ignition and extinction. Theoretically, mathematical models and physical explanations of solid propellant PDL have been only partially successful. Experimentally, the determination of PDL has presented specific difficulties because of "reproducibility" problems. Two techniques are generally used to measure solid propellant PDL. In the first, the pressure is fixed and ignition of the propellant sample is attempted in some way. This is essentially a "go/no-go" technique, that has the disadvantage of introducing ignition dynamics into the picture. In the second method, the propellant sample is first ignited at a pressure higher than the presumed PDL and then the pressure is slowly lowered. This also is essentially a "go/no-go" technique, that has the disadvantage of introducing depressurization dynamics into the picture. Although less disturbing than the ignition procedure, this slow depressurization implies different PDL values for different $p(t)$ histories (in particular for different dp/dt); it usually yields PDL values lower than the ignition procedure. Unfortunately, neither experimental procedure is really satisfactory. However, different techniques have rarely been attempted; they will be described in what follows.

2.4.1 - AP monopropellant

A large body of literature deals with pressure deflagration limit (PDL) of pure AP burning as a monopropellant. Friedman et al. (Refs. 108-109) were among the first to observe experimentally that pressed strands of AP cannot deflagrate steadily below some minimum pressure; they assumed that radiative heat losses from the burning surface become more important for decreasing pressure (and overall heat release). Remark that for this minimum pressure Friedman et al. reported first (Ref. 108) a value of 45 atm and later (Ref. 109) 22 atm.; this large difference was attributed to the different efficiency of the ignition procedure implemented to trigger the self-sustained deflagration wave. They also found that PDL is insensitive to the strand size and nature of the inert pressurizing gas, but decreases for increasing particle size or increasing ambient temperature. Almost simultaneously with the conclusion of several years efforts by Friedman et al., Horton and Price (Ref. 110) accidentally discovered that: (1) minimizing radiative heat loss would not affect the PDL (their value of 23 atm is very close to the updated value by Friedman et al. in Ref. 109); (2) the presence of a little amount of fuel at the boundary of a tubular sample of pressed AP would lower the PDL to 3 atm.

Hightower and Price (Ref. 111) tested single crystals of AP by an ignition technique. They found: (1) a PDL of 19 atm (slightly less than the value of 22 atm reported in Ref. 109 for strands of pressed AP); (2) appreciably higher burning rates than the values obtained from strands of pressed AP (but the burning rate limit for "zero particle size" would reasonably agree with the single crystal value); (3) evidence for the existence of a molten layer at the burning surface. Watt and Petersen (Refs. 112-113) tested both pressed pellets and single crystals of AP by an original technique: a linear temperature gradient ($10-20^{\circ}\text{C}/\text{cm}$) along the length of the AP sample is imposed and the deflagration wave, triggered at the warmer end, propagates up to the point where the sample temperature is too low to support steady burning. Since the conductive thermal wave thickness of the samples is much less than the externally imposed thermal gradient, the deflagration wave is essentially steady. The interesting result of a unique curve (for pressed pellets and single crystals of AP) correlating PDL with the sample temperature is obtained: PDL decreases linearly from 26.2 to 15.3 atm when the sample temperature increases from -40°C to $+50^{\circ}\text{C}$ (in particular, the value of 19 atm is recovered at ambient temperature). The results were independent on the nature of the inert pressurizing gas.

Historically, radiative heat losses from the burning surface was the first cause invoked for the existence of a lower limit pressure for self-sustained steady deflagration. Johnson and Nachbar (Ref. 114), in 1962, presented a sound theoretical model of AP steady deflagration with adiabatic gas phase; they could not help concluding that heat losses, in particular of radiative nature from the burning surface, are far too small to explain the experimental values of PDL. In their own words: "The theory can be made to agree with the experimental data for unassisted deflagration of pure AP by a suitable adjustment of the available parameters. This involves, however, the introduction of an energy loss to the system which is not presently accounted for" (p. 687 of Ref. 114).

Attempts to justify the "missing" heat loss contribution (of the order of $5 \text{ cal/cm}^2\text{s}$) by different mechanisms (energy losses from the gas phase and/or convective cooling by the entrained ambient gas) were never put in quantitative terms, probably because rough estimates already indicate that these contributions are far less than required to fit the experimental values of PDL. A totally different approach was taken, in 1971, by Guirao and Williams (Ref. 115) in their model of AP steady deflagration between 20 to 100 atm. They assumed exothermic condensed phase reactions in a liquid layer covering the burning surface, and deflagration completion of the AP unreacted in the liquid phase (about 30%) in the adjacent gas phase. The thickness of the liquid layer was estimated $2 \mu\text{m}$ at most, and decreasing with decreasing pressure. When the surface temperature falls below the AP melting point ($833 \pm 20 \text{ K}$), the model predicts that the condensed phase reaction rates strongly decrease and the liquid layer thickness shrinks to zero. This was thought to cause the lower deflagration limit. Guirao and Williams (Ref. 115) also checked that the addition of heat losses (in the amount of $5 \text{ cal/cm}^2\text{s}$) to their model had no significant effect. This impressive piece of theoretical work overcomes the known (Ref. 114) limitations of the nonadiabaticity assumption for explaining PDL, but rests on the very controversial question of the existence of a molten layer at the burning surface.

A large amount of experimental work was carried out with the intent of clarifying at least the fundamental mechanisms of the intriguing phenomena associated with AP burning. For example, see the papers by Lieberherr (Ref. 116), Casci and De Luca (Ref. 37), Boggs et al. (Ref. 117), Shadman-Yadzi and Petersen (Ref. 118), Cohen Nir (Refs. 119-120). For a matter of space, only the contributions by the

last two authors will be reviewed. Shadman-Yadzi and Petersen (Ref. 118), in 1972, investigated the effects of four catalysts (KMnO_4 , Fe_2O_3 , CuO , copper chromite) on the pressure limits of AP deflagration. Polycrystalline pellets of pure AP were pressed to within 1% of the density of single crystals and tested by an ignition technique. Confirming previous experimental results, by Friedman et al. (Ref. 108) among others, the authors essentially found that all tested catalysts cause an increase of PDL for low concentrations and a decrease of PDL for large concentrations. No explanation is available for this effect; qualitative mechanisms proposed by several investigators are either difficult to support on a quantitative basis or totally speculative. The experimental findings by Shadman-Yadzi and Petersen (Ref. 118) can be summarized as follows:

- 1) the maximum increase of PDL (about 100 atm) corresponds to a concentration of about 0.1% mole of catalyst for all tested catalysts!
- 2) for large concentrations of KMnO_4 (say, above 0.5% mole), AP deflagration features an upper pressure deflagration limit increasing with KMnO_4 concentration (5 atm for 0.5% and above 40 atm for 5%). This may be due to the fact that KMnO_4 decomposes endothermically and quenched burning surfaces were covered with a layer of accumulated catalyst residue in the form of a fused mass" (p. 65 of Ref. 118). The other tested catalysts remained chemically unchanged during combustion.
- 3) PDL of pure AP is independent of the particle size if pellets are "tightly" pressed; the value of 20 atm at 21°C was recovered in agreement with most investigators, in particular Boggs et al. (Ref. 117). However, if the pellets are not packed tightly enough and the size of the void spaces between the particles is comparable to the thickness of the molten layer reported by Boggs et al. (Ref. 117), then PDL is affected by the solid structure.
- 4) catalysts are more effective when their particle sizes decrease.

Of particular interest appear the contributions of Cohen Nir (Ref. 119-120) in 1972 and 1973. He tested a large number of pressed AP pellets by an ignition technique; the following experimental findings were obtained:

- 1) PDL decreases linearly with the strand density: in particular, extrapolation of the results for $\rho_c = 1.95 \text{ g/cm}^3$ (single crystal density) yields $\text{PDL} = 21 \text{ atm}$ at 20°C in agreement with the previous results from Ref. 111 (19 atm), Ref. 116 (21 atm), Ref. 117 (20 atm).
- 2) PDL decreases asymptotically with burning surface area; in particular, a minimum strand size exists below which

no steady deflagration can be found (this critical dimension corresponds to the ratio cross section area/strand perimeter of the order of 0.5 mm).

- 3) PDL decreases less than linearly with the sample temperature.
- 4) PDL is reduced when the strand is pressed for a long time (12 hours); it was obtained a value of about 20 atm very close to that obtained in Ref. 5 by testing a large single crystal.
- 5) PDL decreases when the mean AP particle size increases, as already found in Ref. 108 and elsewhere. Moreover Cohen Nir observes that "the sample temperature positive effect is inversely proportional to the mean size; it follows that PDL tends to be independent on the mean size when testing is performed at large sample temperature.

To interpret his own and other experimental results, Cohen Nir (Ref. 119) heuristically adopted the following theoretical criterion: near PDL, the burning rate is not zero but assumes a constant finite value. The existence of this limiting value might reconcile the theoretical studies by Johnson and Nachbar (Ref. 114), Guirao and Williams (Ref. 115), and Zeldovich (Refs. 5-6). Hightower and Price (Ref. 111) report near PDL a burning rate of about 0.3 cm/s; Watt and Petersen (Refs. 112-113) about 0.2 cm/s (AP single crystals at different sample temperatures). Cohen Nir (Refs. 119-120) found a limiting burning rate of 0.18 cm/s by testing pressed AP strands at different pressures, sample temperatures, and mean particle sizes.

Sohn (Ref. 121), in 1975, revised the whole problem, criticized all previous approaches, and proposed a totally new physical model. This was based on a detailed analysis of the heterogeneous burning surface microstructure and was meant to include within a single framework ignition, burning rate, and PDL of AP. This is the correct viewpoint; the model is developed both for single crystals and high density pellets. Sohn pictures the solid phase covered by a liquid layer through which cylindrical columns of gas flow. He again attributes PDL to heat loss, but through intermediate heat sinks (such as droplets of the liquid layer torn off the surface and/or AP particles escaping the flame zone without burning). When the overall effects are large, the burning sample is microscopically and locally nonadiabatic and extinction follows. "The formulation of the theory involves a critical assumption that the liquid (or other slow burning parts) at the solid surface provides an intermediate heat sink" (p. 151 of Ref. 121); this assumption is speculative. Moreover, several parameters need to be adjusted in order to fully develop

the complex mathematical model. Finally, the overall picture of the complex heterogeneous microstructure of the burning surface may sound artificial. However, Sohn (Ref. 121) offered an interestingly new and unified approach, a full review of the basic literature, and a complex model which may work under the appropriate conditions. Moreover, Sohn found in his theoretical results that a critical burning rate, of the order of 0.20 cm/s, exists over a wide range of PDL and sample temperature.

Godon (Ref. 122), in 1982, proposed a model for AP steady burning based on a flat premixed flame at some distance (to be defined) from the burning surface. Godon accepts the view previously proposed that PDL arises when the surface temperature falls below the AP melting temperature (taken as 830 K), which implies also a limiting burning rate of about 0.27 cm/s. Godon (Ref. 122) found an excellent agreement between his calculation and the experimental results (of PDL vs sample temperature) obtained by Cohen Nir (Refs. 119-120). The proposed physical mechanism rests on the increasing of the premixed flame height for decreasing pressure and subsequent surface temperature decrease.

2.4.2 - AP Composite Propellants

Only few papers deal with the PDL of AP-based composite solid propellants. A careful review of the previous work was presented in 1969 by Steinz and Summerfield (Ref. 123). Theoretically, a "distended" version of the GDF model for steady burning of composite propellants was offered; experimentally, a large number of propellant formulations was tested by a depressurization technique. First, ignition was performed in nitrogen above 0.3 atm, and then pressure was reduced "as slowly as possible". PDL "was taken as the lowest value (out of a number of tests) at which the propellant could be made to burn" (p. 283 of Ref. 123). Reproducibility was estimated within 10%, but the possible presence of side burning inhibitors caused the PDL to increase (e.g., from 0.045 to 0.060 atm). These carefully performed experiments confirmed the results already known from the literature and, in addition, allowed to observe burning at lower pressures. The results obtained by Steinz and Summerfield (Ref. 123) can be summarized as follows:

- 1) In the subatmospheric pressure range, burning rates on a $\ln(r_b)$ vs $\ln(p)$ plot follow a straight line of 0.7 slope. But exceptions exist: e.g., AP/PIB features a slope close to 1.
- 2) PDL is not less than 0.05 atm for most tested propellants. Notable exception: a propellant with 35% PS (denoted as LP3) binding unimodal 5 μ m AP, for which PDL falls down

- to 0.005 atm thanks to a protective ash layer retaining heat near the burning surface.
- 3) For the propellant 65% AP/35% PS, increasing the AP particle size makes combustion more difficult (burning rate decreased, especially near PDL, and PDL increased).
 - 4) Propellant containing PBAA and CTPB as binders burn with a dry surface. Propellants with HTPB cured with TDI (known to be a polyurethane type of binder) feature a layer of molten fuel encasing AP particles; periodical eruptions of this mixture from the burning surface yield burning inefficiency. PDL was about 0.05 atm for AP/PBAA and AP/CTPB, against 0.18 atm for AP/HTPB (cured with TDI). Notice that AP/HTPB (cured with TDI) with the addition of 0.75% copper chromite behaved like AP/PBAA and AP/CTPB. All comparisons made with unimodal 5 μ m AP.
 - 5) PDL depends on the strand size: it decreased by a factor of 2 when the strand size increased from 6.35x6.35 mm to 15.24 x 15.24 mm.
 - 6) Low pressure burning is inefficient due to: unreacted AP particles ejection from the burning surface; ash formation (containing 60% unreacted AP); smoke (containing 25% unreacted AP), white and dense, emitted from the flame edges, especially below 0.05 atm.
 - 7) "The dominant cause of low pressure extinction (at about 0.05 atm) in normal burning propellants in strand form appears to be convective cooling by the entrained ambient gases in the combustion chamber together with lost of available heat owing to escape of unreacted AP from the edges of the $\text{NH}_3/\text{HClO}_4$ flame zone. In motors under more nearly adiabatic conditions, these losses might be avoidable and still lower pressures might be attainable" (p. 290 of Ref. 123).

Cookson and Fenn (Ref. 124), in 1968, tested AP-based composite propellants (with a polyester type of binder) by a depressurization technique. By properly recasting their own data and those obtained with similar propellants by Sil-la (Ref. 125), they concluded that some finite value of pressure might exist at which burning rates vanish even under adiabatic combustion conditions. The results by Steinz and Summerfield (Ref. 123) were already known to Cookson and Fenn. Therefore, they could point out the following contradictory conclusions reached by the previous investigators:

- 1) Levy and Friedman (Ref. 108) claim that PDL is strand size independent from experiments with pure AP (by an ignition technique); Steinz and Summerfield (Ref. 123)

claim that PDL is sensibly dependent on the strand size from experiments with AP-based composite propellants (by a depressurization technique).

- 2) Johnson and Nachbar (Ref. 114), ascribed PDL to radiative heat loss (but without justification according to their own words) in their theoretical treatment of pure AP deflagration; Steinz and Summerfield (Ref. 123) ascribed PDL of AP-based composite propellants to convective heat loss and combustion inefficiency (but without ascribing quantitative criteria).

Their experimental results (Ref. 124) can be summarized as follows. Rectangular cross section strands with no inhibitor were used; the long dimension was always 25.4 mm, the short dimension ranged from 1.59 mm to 2.54 mm. It was found that:

- 1) PDL is sensibly dependent on the strand size. In particular: there is a minimum strand size below which steady combustion is not allowed no matter what the pressure is; viceversa there is a minimum pressure below which steady combustion is not allowed no matter what the strand size is.
- 2) The hotter propellant tested (80% AP) burns to a lower pressure than a cool propellant (78% AP) for a given strand size. For a short side of the rectangular strand above 15 mm, PDL is independent on the geometry and is about 0.05 atm for 80% AP against 0.07 atm for 78% AP.

At least for homogeneous solid propellants, Williams et al. (p. 372 of Ref. 2) concede that mechanisms other than heat loss might as well be responsible for PDL. In their own words: "... the magnitude of the heat loss q_c (that occurs in addition to the radiant heat loss from the surface) can be estimated from the known environmental conditions. Estimates of all possible heat loss mechanisms, e.g., gas-phase radiation, convective losses from the solid, etc., yield a much smaller total heat loss than the value of q_c , needed to fit the observed deflagration limit. Hence, the correlation of the deflagration limit is unsatisfactory.

Although it is, of course, conceivable that chemical effects could be responsible for the observed deflagration limit or that a dynamically unstable steady-state solution is encountered on the upper branch of the $m(p)$ curve at pressures well above the critical limiting value, nevertheless a suitable modification of the surface boundary condition within the present theory, may conceivably produce satisfactory agreement. There is some question concerning the validity of the published pyrolysis results for B_s and \tilde{E}_s [the dimensional pre-exponential factor and activation energy of the surface pyrolysis law] and of the hypothesis of an unopposed surface rate process for NH_4ClO_4 . It would therefore be of interest to employ in the John-Nachbar theory a more general surface boundary condition, ..., in order to see whether the observed deflagration limit can then be correlated by choosing a more reasonable value for the heat loss term q_c ".

Northam et al. (Ref. 126), in 1972, tested an AP/CTPB composite propellant by a depressurization technique. AP was chemically altered in order to obtain wide changes, within one order of magnitude, of low temperature (100-300°C) AP decomposition. PDL showed no change. Noticed that the implemented depressurization rate of 2 psi/s was probably too fast to neglect dynamic effects; however, this seems irrelevant since other tests, including extinction by fast depressurization, did not reveal any significant effect.

Park, Ryan, and Baer (Ref. 74) presented in 1973 a paper in which static vs dynamic extinctions at low pressure (below 1 atm) were experimentally studied. In this pressure range, the two extinction mechanisms overlap. Side-inhibited strands of several AP-based composite propellants were tested in nitrogen. Two different experimental techniques were implemented. In the first, propellant samples were subjected to "slow" (see below) and fast depressurization. It was found that slow depressurization rates ($d \ln(p)/dt$ of the order of 5 to 0.005 s^{-1}) did not usually influence the extinction pressure (PDL?), if the initial pressure was at least twice the extinction pressure itself. This first experimental procedure allowed to measure the instantaneous burning rate during slow depressurization. The transient burning rate was found to follow the steady dependence on pressure: in some cases all the way down to extinction (AP/PU propellants), and in other cases only partially (down to 0.01 atm for AP/PBAA propellants with $PDL \approx 0.05 \text{ atm}$). Lack of reproducibility and residual dependence on the depressurization rate moved the authors to device a specific go/no-go ignition technique in order to evaluate PDL. In this second experimental procedure, propellant samples were ignited under carefully controlled (Ref. 74) conditions: the pressure was considered below the deflagration limit if extinction occurred before the burning surface had regressed 12 mm from the initial position. The results obtained by the authors can be summarized as follows:

- 1) PDL reveals no effect of AP particle size for hard-to-melt binders (e.g., PBAA), while decreases sharply as particle size increases for easy-to-melt binders (e.g., PU). This confirms a previous suggestion by Steinz and Summerfield (Ref. 123) to the effect that AP crystals coated by molten polymer cannot participate to surface reactions, except those large crystals ($> 400 \mu\text{m}$) which project beyond the molten layer. The effect of binder melting disappears for large AP loading ($> 80\%$), presumably because not enough melt is available.

- 2) Confirming a previous remark by Steinz and Summerfield (Ref. 123), a significant amount of unreacted AP was observed to be ejected from the regressing surfaces of AP/PBAA and AP/HTPB burning at low pressures. The phenomenon was noticeably more evident at higher AP loadings. This would in fact make the AP/binder ratio for the nominal 75% AP propellant larger than for the nominal 85% AP. Supporting evidence for this surprising conclusion is that, near the deflagration limit, burning rate for the nominal 75% AP propellant is larger than for the nominal 85% AP (at the same operating pressure).
- 3) PDL was expected to be lower with the hottest compositions (e.g., for larger AP loading). In fact, PDL was found to decrease with AP loading when PBAA and HTPB binders were used. The authors ascribed this effect to burning inefficiencies (see the previous point).
- 4) PDL decreased from few atm down to less than 0.002 atm (the minimum attainable pressure of the apparatus) by: increasing AP particle size (for easy-to-melt binders); decreasing AP loading for PBAA or HTPB binders but increasing AP loading for PU binder; heating the surroundings after sample ignition.

An important application of PDL studies is the safety of solid propellant handling and of rocket motor operation: PDL larger than 1 atm avoids accidental deflagrations and ensures permanent extinction of controllable rocket motor as well as precise termination of multistage rocket motors. An example of these applications is in a paper by Petersen et al. (Ref. 127) published in 1967. By properly combining several chemical and physical factors, the authors were able to raise PDL to above 3 atm for the current AP-based composite propellants with only a slight loss in performances. Of interest for this review is that PDL could be increased in particular by: replacing hydrocarbon binders (PBAA) with oxygenated binder (PU or polyesters); increasing binders content (results given for PU binder only); and using small AP particles. Remark that the effects due to PU binders were later explained in physical terms (molten layer) in Ref. 123 and Ref. 74, while in Ref. 127 thermochemical effects were invoked.

Baliga and T'ien published in 1975 an excellent paper (Ref. 128), in which for the first time PDL was explicitly associated with combined unsteady effects and heat loss mechanisms (only radiation from the burning surface). "The unsteady effects include dynamic extinctions induced both by natural flame oscillation and by forced flame vibration in response to external pressure disturbances. The present analysis shows that part of the steady state solution at

low pressure is linearly unstable, so it cannot be physically observed. The existence of this branch of unstable solution is the consequence of heat loss from the flame. The heat loss also provides a mechanism to interpret the final outcome of the growing oscillatory unstable flame, i.e. dynamic extinction" (p. 1653 of Ref. 128). We could fully share these illuminating words, except that the burning stability analysis conducted under nonlinear conditions would reveal that an heterogeneous flame becomes unstable, for decreasing pressure, even if adiabatic.

Experimentally, oscillatory thermal profiles in the gas phase for low burning rates are reported for both double-base and AP-based composite propellants by Zenin (Ref.129). Likewise, an oscillatory thermal profile in the gas phase can be observed in Fig. 1 of Ref. 130, where again Zenin reports results obtained by a microthermocouple testing N-powder (a Russian double-base) burning at pressure less than 0.5 mm Hg. This experimental evidence is of interest because the nonlinear stability theory developed by the Milano group (Refs. 17,25-27) predicts, near PDL, self-sustained oscillatory burning of decreasing frequency with decreasing pressure. This fact should also be related to the lack of reproducibility and fluctuating signals often reported by the experimentalists in the marginal burning domain associated with PDL. The cigarette burning, tacitly assumed by the experimentalist, is often of oscillatory character.

In general, oscillations in solid propellant combustion and their relationships with low pressure extinction have been the object of numerous investigations; for a critical review of this area see the previous sec. 2.3. Evidence on an oscillatory regime preceding extinction in a premixed flame (porous burner) goes back to Kydd and Foss (Ref. 131). More recent experimental results were obtained by Chan and T'ien (Ref. 132). This area can be seen as a subdomain of the vaster field of stability in chemically reacting systems. De Luca (Ref. 17), in 1979, analytically predicted that burning regime of AP-based composite propellants goes from time-independent steady state through self-sustained oscillatory to extinction when going from (constant) high to (constant) low pressure. This result raised interesting questions about the nature of the PDL. Detailed analytical predictions and numerical verifications were offered in Ref.9. Extension to temperature-dependent condensed phase thermal properties was performed in Ref. 25. Theoretical and experimental work (Ref. 32) was simultaneously effected on the often overlapping phenomenon of extinction by fast depres-

surization. It was predicted theoretically and verified experimentally that fast depressurization extinction is a dynamic burning stability problem, whereas low pressure extinction is a static burning stability problem.

The purpose of this contribution is to show how the nonlinear deflagration developed by this research group (Refs. 21-27) predicts different stability regions corresponding to different solid propellant burning regimes, predicts a nonzero minimum combustion pressure (i.e., a PDL) for a given propellant formulation, predicts that near PDL fast depressurization extinction and low pressure extinction merge, can evaluate the amplitude and frequency of the self-sustained oscillations associated with the PDL. Chapter 6 will show that these predictions are in reasonable agreement with the experimentally observed behavior of composite propellants near PDL.

2.5 - VARIABLE THERMAL PROPERTIES

Variable thermal properties in the condensed phase are seldom taken into account, although it is well known that thermal conductivity and (especially) specific heat are sensibly temperature dependent. Imber (Ref. 133), in 1966, first considered the effect of thermal conductivity, linearly dependent on temperature,, on small perturbations stability of burning solid propellants. Experimental data were reported for two DB compositions, whose thermal conductivity was linearly increasing with temperature over the range from -10 to +110 °F. The author found the stability modes affected by variable thermal conductivity, especially at low instability frequency. Moreover, Imber analytically determined the steady temperature distribution in the condensed phase and suggested a convenient way to transform the exact implicit solution into an approximate explicit expression. His suggestion has been used in this investigation also; for details, see Sec. 3.2.

Williams and Lengellé (Ref. 134), in 1964, published a substantial piece of work intended to explain nonacoustic or intrinsic burning oscillations of unmetallized composite propellants. The assumption was made that the condensed phase heterogeneity could be visualized as a locally layered propellant (with layers of different properties parallel to the burning surface); the properties would vary continuously and sinusoidally in the normal direction, with amplitudes of variation small compared with their mean values. The authors show that thermal conductivity heterogeneity (in the sense just mentioned) yields to first order mass burning rate

oscillating in time about the mean value; the same result applies for specific heat heterogeneity (for details see p. 102 of Ref. 134). The authors further show how phase synchronization of otherwise randomly distributed oscillations over the burning surface occurs through second order terms; but this is out of the scope of this section.

Nelson (Ref. 135), in 1979, is the only known author to consider variable thermal conductivity and specific heat in numerical simulations of transient propellant burning by both flame models and Zeldovich approach. Nelson reports the following experimentally measured (by other authors) linear dependencies on temperature: specific heat, for a propellant denoted X14, gives over the temperature range 283-343 K

$$c_c(T) = 0.118 + 0.66 \cdot 10^{-5} T \text{ cal/gK;}$$

while thermal conductivity, for a DB composition, gives over the temperature range 267-317 K

$$k_c(T) = 1.90 \cdot 10^{-5} + 2.46 \cdot 10^{-6} T \text{ cal/cm s K.}$$

The two laws were extrapolated to temperature however high in the condensed phase. Nelson found that computer simulated pressurization tests feature less pronounced transient burning effects, if variable thermal properties are enforced. The same conclusion will be reached in this report, together with many other findings. No analytical work was offered by Nelson in Ref. 135.

Price, Boggs, and Derr at NWC accounted for variable thermal conductivity and specific heat in their numerical modeling of AP monopropellant (Ref. 169, 1978) and HMX monopropellant (Ref. 170, 1979). Thermal conductivity of AP was computed from the experimental values of thermal diffusivity

$$\alpha_c(T-273) = 2.50 \cdot 10^{-3} - 4.55 \cdot 10^{-6} (T-273) \text{ cm}^2/\text{s}$$

measured by Rosser, Inami, and Wise in Ref. 171. Specific heats of AP were those reported by the JANNAF tables:

orthorombic	$c_c(T) = 0.13626 + 0.000415 T$	cal/g K
cubic	$c_c(T) = 0.15309 + 0.000414 T$	cal/g K.

These values were obtained by experimental measurements in the range from 5 to 350 K and by extrapolation above 350 K. The transition temperature from orthorombic to cubic phase is 240 °C, i.e. 513 K. No specific assessment on the effects of these variable properties was offered in Refs. 169-170.

CHAPTER 3 - NONLINEAR UNSTEADY BURNING OF SOLID PROPELLANTS

In this chapter an overview of the analytical developments concerning nonlinear unsteady burning of solid propellants is offered. First, the basic assumptions and equations are illustrated; then, some steady state solutions of the temperature profile in the condensed phase are reported; finally, a range of thermal flame models properly modified to include the effects of variable thermal properties and chemical reactions in the condensed phase is revised.

For the first time with respect to previous Progress Reports (e.g., Ref. 9) by this research group:

- (a) temperature dependent thermal conductivity and specific heat in the condensed phase are taken into account.
- (b) chemical reactions volumetrically distributed in the condensed phase are included.
- (c) polychromatic, rather than necessarily monochromatic, radiation impinging from an external, continuous wave source is allowed.
- (d) some particular solutions of the steady state temperature profile in the condensed phase, usually not available in literature, are reported.

The nonlinear stability burning based on the present model of solid propellant unsteady burning will be developed in Chapter 4. Computer simulated tests assessing the validity of the analytical work will be described in Chapter 5. Experimental results (from a depressurization strand burner, piston tube, subatmospheric strand burner, etc.) collected with the intent of checking the whole theoretical approach will be discussed in Chapter 6.

3.1- FORMULATION OF THE GENERAL HETEROGENEOUS THIN FLAME PROBLEM

The following set of assumptions is valid throughout this work. With reference to Fig. 1:

- a) Entire Strand.
 1. Monodimensional.
 2. At cold boundary, in thermal equilibrium with ambient.
 3. Subjected to no external forces (acceleration, gravity, electromagnetism).

4. No emission of radiation (only external radiation sources).
- b) Condensed Phase.
1. Semi-infinite slab.
 2. Uniform and isotropic composition.
 3. Adiabatic, except at the burning surface.
 4. No radiation scattering.
 5. No photochemical effects.
- c) Interface.
1. Infinitesimally thin and planar surface layer (collapsed burning surface reacting layer).
 2. One-step, irreversible gasification processes (pyrolysis).
- d) Gas Phase.
1. Semi-infinite column of gas.
 2. Mixture of thermally perfect gases of average molecular weight \bar{W} .
 3. One-phase, laminar, nonviscous, low subsonic flow.
 4. Adiabatic, except at the burning surface.
 5. No interaction with (external) radiation.
 6. Lewis number = 1, each chemical species has the same specific heat c_g , mass diffusion is expressed by Fick's law. Therefore, the gas phase can be described by a simple thermal model.
 7. Quasi-steady behavior, with finite reactive layer thickness.

The following set of reference parameters is used for non-dimensionalizing (with specific reference to the propellant AP/PBAA No. 941 taken as datum case; see also Tab. 1):

P_{ref}	$\equiv 68$	atm
T_{ref}	$\equiv 300$	K
$r_{b,ref}$	$\equiv r_b(p_{ref}) = 0.837$	cm/s
$T_{s,ref}$	$\equiv T_s(p_{ref}) = 1.000 \times 10^{+3}$	K
$T_{f,ref}$	$\equiv T_f(p_{ref}) = 2.430 \times 10^{+3}$	K
d_{ref}	$\equiv \alpha_{ref}/r_{b,ref} = 1.673 \times 10^{-3}$	cm
t_{ref}	$\equiv \alpha_{ref}/r_{b,ref}^2 = 1.998 \times 10^{-3}$	s
Q_{ref}	$\equiv c_{ref}(T_{s,ref} - T_{ref}) = 231$	cal/g
ψ_{ref}	$\equiv \rho c_{ref} r_{b,ref} (T_{s,ref} - T_{ref}) = 297.8$	cal/cm ² s

from which one gets the following nondimensional variables:

P	= p/p_{ref}	nondim. pressure
R	= $r_b/r_{b,ref}$	nondim. burning rate
X	= x/d_{ref}	nondim. distance
δ_a	= $(1/a_\lambda)/d_{ref}$	nondim. optical absorption layer thickness
τ	= t/t_{ref}	nondim. time
H	= Q/Q_{ref}	nondim. heat release
F_o	= I_o/ϕ_{ref}	nondim. radiant flux intensity
q	= ϕ/ϕ_{ref}	nondim. conductive heat flux.

Notice that, both of the following definitions are used, according to need, for the temperature:

$$(3.1.1a) \quad \theta () \equiv \frac{T () - T_{ref}}{T_{s,ref} - T_{ref}}, \text{ e.g. } \theta_f = \frac{T_f - T_{ref}}{T_{s,ref} - T_{ref}}$$

$$(3.1.1b) \quad T () \equiv \frac{T ()}{T (),ref}, \text{ e.g. } T_f = \frac{T_f}{T_{f,ref}}$$

where the choice of the particular definition depends on the specific physical phenomenon being considered.

The general nondimensional quasi-steady gas phase transient formulation includes the unsteady condensed phase problem, relationships accounting for the surface mass production, the quasi-steady gas phase problem, some auxiliary relationships assigning the gas phase and burning surface heat releases and the time history of the controlling parameters. Obviously, the gas phase treatment is not complete without the energy equation whose first integral gives the heat feedback law; this is discussed in Sec. 3.3. For details about the writing of the equations, the reader is referred to Ref. 14. The energy balance in the condensed phase gives:

$$(3.1.2) \left\{ \begin{array}{l} c_c(\theta) \left(\frac{\partial \theta}{\partial \tau} + R \frac{\partial \theta}{\partial X} \right) = \frac{\partial}{\partial X} \left[K_c(\theta) \frac{\partial \theta}{\partial X} \right] + F_0 \int_{\lambda_1}^{\lambda_2} f_1(X, \lambda) d\lambda + H_c \epsilon_c \\ \theta(X, \tau=0) = \text{assigned function} \\ \theta(X \rightarrow -\infty, \tau) = \theta_{-\infty} \\ \left(K_c \frac{\partial \theta}{\partial X} \right)_{c,s} = \left(K_g \frac{\partial \theta}{\partial X} \right)_{g,s} + H_s R - q_{out}(\theta_s) \end{array} \right.$$

being

$$(3.1.3) \quad f_1(X, \lambda) \equiv \frac{1 - \bar{\tau}_\lambda}{\epsilon_a} \left(\frac{F_\lambda}{F} \right)_0 \exp(X/\delta_a);$$

$$(3.1.4) \quad q_{out} = \bar{\epsilon}_\lambda \sigma \frac{T^4 - T_{-\infty}^4}{\varphi_{ref}};$$

$$(3.1.5) \quad H_s = \frac{Q_{s,ref} + T_{s,ref} [c_g(T_{s,ref}) - c_c(T_{s,ref})]}{Q_{ref}} - \frac{T_s [c_g(T_s) - c_c(T_s)]}{Q_{ref}}.$$

The function

$$q_{g,s}(P, R) \equiv \left(K_g \frac{\partial \theta}{\partial X} \right)_{g,s}$$

requires a flame model to be evaluated (see appropriate section). The following combined pyrolysis law is implemented both for steady and unsteady states:

$$(3.1.6a) \quad R = P^n \exp \left[-E_s \left(\frac{1}{T_s} - 1 \right) \right] \quad T_s \geq T_k \quad \text{Arrhenius pyrolysis}$$

$$(3.1.6b) \quad R = P^n \left(\frac{T_s - T_m}{1 - T_m} \right)^w \quad T_k \geq T_s \geq T_m \quad \text{KTSS pyrolysis}$$

$$(3.1.6c) \quad R = 0 \quad T_m \geq T_s \geq 0$$

where $T_m \equiv T_m / T_{s,ref}$ is some empirically defined minimum temperature under which the solid propellant undergoes no chemical activity and w is determined by matching the two pyrolysis laws at some given $T_k \equiv T_k / T_{s,ref}$ near the ambient temperature.

A standard Arrhenius form is assumed for the reaction rate ϵ_c of zero-th order

$$(3.1.7) \quad \epsilon_c(P,T) = A_c(P) \exp(-E_c/T),$$

while no assumption whatsoever is made for the temperature dependence of thermal conductivity and specific heat in the condensed phase:

$$K(\Theta) \equiv k_c(T)/k_{ref} = \text{arbitrary}, \text{ being } k_{ref} \equiv k_c(T_{ref})$$

$$C(\Theta) \equiv c_c(T)/c_{ref} = \text{arbitrary}, \text{ being } c_{ref} \equiv c_c(T_{ref}).$$

$$\text{Therefore: } \alpha_{ref} \equiv \alpha_c(T_{ref}) = \frac{k_c(T_{ref})}{\rho_c c_c(T_{ref})}.$$

The quasi-steady gas phase assumption implies the following conservative equations:

$$(3.1.8) \quad U(X,\tau) = \frac{\rho_c}{\rho_g(X,\tau)} R(\tau) \rightarrow m = \rho_c r_b = \text{const} \quad \text{continuity}$$

$$(3.1.9) \quad P = P(\tau) \quad \text{momentum}$$

$$(3.1.10) \quad \frac{\partial^2 \Theta}{\partial X^2} - R \frac{C_g}{K_g} \frac{\partial \Theta}{\partial X} + \frac{\rho_g}{\rho_c} \frac{H_f}{K_g} \epsilon_g(X) = 0 \quad \text{energy}$$

$$\text{being } \epsilon_g(X) \equiv \frac{\tilde{\epsilon}_g(X)}{(\alpha_{ref}/r_{b,ref}^2)}$$

where $\tilde{\epsilon}_g$ is the dimensional reaction rate measured in 1/s while $\epsilon_g \rho_g / \rho_c$ is the nondimensional mass reaction rate per unit volume. Further relationships, required to complete the set of gas phase equations, are:

the state equation (in dimensional terms)

$$(3.1.11) \quad p = \rho_g \frac{R}{\bar{W}} T;$$

the quasi-steady flame temperature

$$(3.1.12) \quad \theta_f(\tau) = \theta_s(\tau) + (H_f - \frac{q_{g,s}}{R}) / C_g;$$

the heat release in the gas phase depending only on pressure and ambient temperature

$$(3.1.13) \quad \bar{H}_f(P, \theta_{-\infty}) = \int_{\theta_{-\infty}}^{\bar{\theta}_s} C_c(\theta) d\theta + C_g(\bar{\theta}_f - \bar{\theta}_s) - \bar{H}_s - H_c;$$

the steady flame temperature in the presence of an external radiant flux

$$(3.1.14) \quad \bar{\theta}_f(P, F_o, \theta_{-\infty}) = \bar{\theta}_s(P, F_o, \theta_{-\infty}) + H_c + \bar{H}_s + \bar{H}_f - \int_{\theta_{-\infty}}^{\bar{\theta}_s(P, F_o, \theta_{-\infty})} C_c(\theta) d\theta + \left. \frac{(1 - \bar{r}_\lambda) F_o - q_{out}(\bar{\theta}_s)}{\bar{R}(P, F_o)} \right] / C_g.$$

The following external functions and parameters are assumed known:

$$P(\tau) = \text{assigned}$$

$$(3.1.15) \quad F_o(\tau) = \text{assigned}$$

$$T_{-\infty} = \text{assigned}$$

The nature of the solid propellant is "identified" by two pieces of information concerning adiabatic burning rate and adiabatic flame temperature:

$$(3.1.16) \quad \begin{aligned} \bar{R}(P) &= \text{known from experiments (at a given ambient temperature);} \\ \bar{\theta}_f(P, \theta_{-\infty}) &= \text{known from experiments or thermochemistry.} \end{aligned}$$

The quantity $Q_{s,ref}$ (used in Eq.3.1.5) depends on the original condensed phase composition only. For example, for non-metallized AP composite propellants:

$$(3.1.17) \quad Q_{s,ref} = \psi(Q_{NH_3/HClO_4} + Q_{cr,AP} + Q_{v,AP}) + (1-\psi)Q_{v,binder}$$

being:

$Q_{NH_3/HClO_4}$ the heat released by the premixed $NH_3/HClO_4$ flame due to AP decomposition;

$Q_{cr,AP}$ the energy associated to the endothermic processes of AP crystalline transition from orthorombic to cubic at $240^\circ C$;

$Q_{v,AP}$ the energy associated to the endothermic AP dissociative sublimation of zero-th order with respect to the pressure;

$Q_{v,binder}$ the energy associated to the endothermic binder gasification.

The pre-exponential factor $A_c(P)$ (see Eq. 3.1.7) is evaluated by imposing that the proper amount of energy is released in the solid phase under steady adiabatic conditions. Indeed an overall energy balance through the combustion wave gives

$$(3.1.18) \quad \int_{\theta_{-\infty}}^{\bar{\theta}_s} C_c(\theta) d\theta + C_g(\bar{\theta}_f - \bar{\theta}_s) = \bar{H}_s + \bar{H}_f + H_c \cdot$$

The following compatibility relationship has to be respected:

$$(3.1.19) \quad R = \int_{-\infty}^0 \bar{\epsilon}_c(P, T) dX \cdot$$

If one assumes the Arrhenius form of Eq. 3.1.7 for the reaction rate $\bar{\epsilon}_c$, the pre-exponential factor can be evaluated as

$$(3.1.20) \quad A_c(P) = \frac{\bar{R}(P)}{\int_{-\infty}^0 \exp\left(-\frac{E_c}{\bar{T}(X)}\right) dX} \cdot$$

where $\bar{T}(X) \equiv \bar{T}(X)/T_{s,ref}$ is the steady temperature profile prevailing under a given set of operating conditions.

Any flame model (see Sec.3.3), defining the reaction rate $\epsilon_g(X)$, allows to obtain the conductive heat feedback from the gas phase to the burning surface through the first integral of the gas phase energy equation:

$$(3.1.21) \quad \left(\frac{\partial \theta}{\partial X}\right)_{g,s} = \int_{0^+}^{X_f} \frac{\rho_g}{\rho_c} \frac{H_f}{K_g} \epsilon_g(X) \exp\left(-\frac{C_g}{K_g} RX\right) dX ,$$

where the usual assumption $(\partial \theta / \partial X)_f \exp(-R^2 \bar{\tau}'_{re}) \ll (\partial \theta / \partial X)_{g,s}$ was made. The average characteristic flame thickness \bar{X}_f is given by

$$(3.1.22) \quad \bar{X}_f = R \bar{\tau}'_{re} \rho_c / \bar{\rho}_g = \frac{K_g}{C_g} R \bar{\tau}'_{re} .$$

The characteristic gas phase reaction time $\bar{\tau}'_{re}$ has to be defined by a flame model.

3.2- STEADY THERMAL PROFILES IN THE NONREACTIVE CONDENSED PHASE

Analytical expressions of the steady state thermal profiles in the condensed phase, for given values of the surface temperature θ_s and the cold boundary temperature $\theta_{-\infty}$, are extremely useful for the numerical integration of the governing set of equations (in that, they provide the initial condition of Eq. 3.1.2) as well as for the burning stability analysis (in that, they provide the reference condition with respect to which finite size disturbances are evaluated). Moreover, steady solutions of the condensed thermal profile with temperature dependent thermal properties are not usually available in the literature, although their obvious importance "per se".

Unfortunately, the presence of distributed chemical reactions is too difficult to be accounted for; therefore, the results of this section are restricted to chemically inert condensed phase. Mathematically, the problem is stated as follows:

$$(3.2.1) \quad \begin{cases} c_c(\theta) \bar{R} \frac{d\bar{\theta}}{dX} = \frac{d}{dX} \left[(K_c(\theta) \frac{d\bar{\theta}}{dX}) \right] + \bar{F}_o \int_{\lambda_2}^{\lambda_1} f_1(X, \lambda) d\lambda \\ \bar{\theta}(X=0) = \bar{\theta}_s \\ \bar{\theta}(X \rightarrow -\infty) = \theta_{-\infty} \end{cases}$$

In the simple case of no temperature dependence of the thermal properties and no impinging external radiation, one obtains the familiar temperature distribution (called Michelson profile in the Soviet literature):

$$(3.2.2) \quad \bar{\theta}(X) = \theta_{-\infty} + (\bar{\theta}_s - \theta_{-\infty}) \exp(X\bar{R}).$$

For no temperature dependence of the thermal properties but with impinging external radiation of monochromatic nature, one obtains:

$$(3.2.3) \quad \bar{\theta}(X) = \theta_{-\infty} + (\bar{\theta}_s - \theta_{-\infty}) \exp(X\bar{R}) + \bar{F}_o \frac{1 - \bar{r}}{\bar{R} - 1/\delta_a} \left[\exp(X/\delta_a) - \exp(X\bar{R}) \right].$$

For no impinging external radiation, constant value of the specific heat, but temperature dependent thermal conductivity according to a linear law $K_c(\theta) = 1 + b\theta$, the following implicit form solution can be easily found:

$$(3.2.4) \quad \frac{\bar{\theta}(X) - \theta_{-\infty}}{\bar{\theta}_s - \theta_{-\infty}} \exp \left[\left(\frac{\bar{\theta}(X) - \theta_{-\infty}}{\bar{\theta}_s - \theta_{-\infty}} - 1 \right) \left(\frac{K_c(\bar{\theta}_s)}{K_c(\theta_{-\infty})} - 1 \right) \right] = \exp \left(\frac{X\bar{R}}{K_c(\theta_{-\infty})} \right).$$

Imber (Ref.133), who first derived the above expression during a study of burning stability of solid propellants, proposed to use the following approximate but explicit expression:

$$(3.2.5) \quad \bar{\theta}(X) \cong \theta_{-\infty} + (\bar{\theta}_s - \theta_{-\infty}) \exp \left[\frac{X\bar{R} f(K_c)}{K_c(\theta_{-\infty})} \right],$$

where $f(K_c) = \frac{1}{1 + 0.75 \left(\frac{K_c(\bar{\theta}_s)}{K_c(\theta_{-\infty})} - 1 \right)}$.

For no impinging external radiation, constant value of the thermal conductivity, but temperature dependent specific heat according to a linear law $C_c(\theta) \equiv c_c(T)/c_{ref} = 1+a\theta$, the following explicit solution can be easily derived:

$$(3.2.6) \quad \bar{\theta}(X) = \bar{\theta}_{-\infty} + \frac{(\bar{\theta}_s - \bar{\theta}_{-\infty}) C_c(\bar{\theta}_{-\infty}) \exp [C_c(\bar{\theta}_{-\infty}) \bar{R} X]}{C_c(\bar{\theta}_{-\infty}) + \frac{a}{2} (\bar{\theta}_s - \bar{\theta}_{-\infty}) \left\{ 1 - \exp [C_c(\bar{\theta}_{-\infty}) \bar{R} X] \right\}}$$

For no impinging external radiation, but both thermal properties temperature dependent according respectively to the linear laws $K_c(\theta) \equiv k_c(T)/k_{ref} = 1+b\theta$ and $C_c(\theta) \equiv c_c(T)/c_{ref} = 1+a\theta$, the following implicit solution can be easily derived:

$$(3.2.7) \quad \bar{\theta} \left(1 + \frac{a}{2} \bar{\theta}\right)^{(2b/a-1)} = \bar{\theta}_s \left(1 + \frac{a}{2} \bar{\theta}_s\right)^{(2b/a-1)} \exp(X\bar{R}),$$

which however requires $\bar{\theta}_{-\infty} = 0$, as usually but not necessarily true. Remark that for $b=a/2$ a particularly simple explicit solution is obtained:

$$(3.2.8) \quad \bar{\theta}(X) = \bar{\theta}_s \exp(X\bar{R}),$$

while for $b=a$ the following solution is found

$$(3.2.9) \quad \bar{\theta} \left(1 + \frac{a}{2} \bar{\theta}\right) = \bar{\theta}_s \left(1 + \frac{a}{2} \bar{\theta}_s\right) \exp(X\bar{R}).$$

Remark that whenever the thermal properties depend on temperature with the same nondimensional law (whichever it is)

$$(3.2.10) \quad k_c(T)/k_{ref} = c_c(T)/c_{ref} = f(\theta),$$

it is convenient to resort to the following Kirchoff's transformation:

$$(3.2.11) \quad \theta \equiv \int_0^\theta f(\theta) d\theta.$$

From this position one immediately obtains that

$$\frac{d\vartheta}{dX} = \frac{d\vartheta}{d\theta} \frac{d\theta}{dX} = f(\theta) \frac{d\theta}{dX},$$

$$\frac{d^2\vartheta}{dX^2} = \frac{d}{dX} \frac{d\vartheta}{dX} = f(\theta) \frac{d^2\theta}{dX^2}$$

Therefore, the steady thermal profile for the same nondimensional temperature dependence of the thermal properties and no impinging external radiation is

$$(3.2.12) \quad \bar{\vartheta}(X) = \vartheta_{-\infty} + (\bar{\vartheta}_s - \vartheta_{-\infty}) \exp(X\bar{R}),$$

where
$$\bar{\vartheta}_s = \int_0^{\bar{\theta}_s} f(\theta) d\theta$$

and
$$\bar{\vartheta}_{-\infty} = \int_0^{\theta_{-\infty}} f(\theta) d\theta.$$

For example, if $k_c(T)/k_{ref} = c_c(T)/c_{ref} = 1+a\theta$,

then: $f(\theta) \equiv 1+a\theta$,

$$\bar{\vartheta} = \int_0^{\bar{\theta}} (1+a\theta) d\theta = \bar{\theta} \left(1 + \frac{a}{2} \bar{\theta}\right),$$

$$(3.2.13) \quad \bar{\theta}(X) \left[1 + \frac{a}{2} \bar{\theta}(X)\right] = \theta_{-\infty} \left(1 + \frac{a}{2} \theta_{-\infty}\right) + \left[\bar{\theta}_s \left(1 + \frac{a}{2} \bar{\theta}_s\right) - \theta_{-\infty} \left(1 + \frac{a}{2} \theta_{-\infty}\right)\right] \exp(X\bar{R}),$$

showing that the quantity $\bar{\theta} \left(1 + \frac{a}{2} \bar{\theta}\right)$ decays over the space X for $f(\theta) = 1+a\theta$ just as $\bar{\theta}(X)$ for $f(\theta) = 1$. Remark moreover that the solution coincides with the Eq. 3.2.9 for $\theta_{-\infty} = 0$.

Another common case is $k_c(T)/k_{ref} = c_c(T)/c_{ref} = \exp(a\theta)$, for

which one obtains

$$f(\theta) \equiv \exp(a\theta) \quad ; \quad \bar{\theta} = \int_0^{\bar{\theta}} \exp(a\theta) d\theta = \frac{\exp(a\bar{\theta}) - 1}{a} \quad ;$$

$$\frac{\exp[a\bar{\theta}(X)] - \exp(a\theta_{-\infty})}{\exp(a\bar{\theta}_s) - \exp(a\theta_{-\infty})} = \exp(X\bar{R}) \quad ,$$

showing that the quantity $\exp[a\theta(X)]$ decays over the space X for $f(\theta) = \exp(a\theta)$ just as the quantity $\bar{\theta}(X)$ for $f(\theta) = 1$. The previous expression can be written explicitly as

$$(3.2.14) \quad \bar{\theta}(X) = \frac{1}{a} \lg \left\{ \exp(a\theta_{-\infty}) + \left[\exp(a\bar{\theta}_s) - \exp(a\theta_{-\infty}) \right] \exp(X\bar{R}) \right\} .$$

3.3- QUASI-STEADY FLAME MODELS

In order to assign the function $q_{g,s}(P,R)$ required at the boundary condition of the PDE describing the transient thermal profile in the condensed phase (Eq. 3.1.2), a flame model has to be chosen. Several quasi-steady flame models were already reviewed in a previous Final Technical Report (Ref. 9). In this section, the formulation of the flame models will be extended to include variable thermal properties and distributed chemical reactions in the condensed phase. To make the exposition concise, only the variations with respect to the original models will be emphasized.

3.3.1- MTS flame

The relationship giving the heat feedback according to the MTS flame model is not directly affected by the variability of the thermal properties and the presence of chemical reactions in solid phase. In fact, such effects influence only the kinetic (A_m) and diffusive (B_m) characteristic time parameters, whose computation is based on the optimization of the heat feedback expression with respect to the experimental burning rate data obtained under steady and adiabatic conditions (Ref. 44 a , pp.37-38).

The first integral of the steady and adiabatic energy equation in the condensed phase gives:

$$(3.3.1) \quad (K_c \bar{\theta}) \frac{d\bar{\theta}}{dX} \Big|_{c,s} = \bar{R} \int_{\theta_{-\infty}}^{\bar{\theta}_s} C_c(\theta) d\theta - \int_{-\infty}^0 H_c \bar{\epsilon}_c dX .$$

By combining the energy conservation at the interface with the previous expression, one obtains

$$(3.3.2) \quad (K_g \frac{d\bar{\theta}}{dX}) \Big|_{g,s} = \bar{R} \left[\int_{\theta_{-\infty}}^{\bar{\theta}_s} C_c(\theta) d\theta - \bar{H}_s \right] - \int_{-\infty}^0 H_c \bar{\epsilon}_c dX .$$

The function required to determine the kinetic and diffusive time parameters, once Eq. 3.1.19 is taken into account, is:

$$(3.3.3) \quad \int_{\theta_{-\infty}}^{\bar{\theta}_s} C_c(\theta) d\theta - H_c \bar{H}_s = \frac{H_f}{\sqrt{\tau'_{re}}} \left[\sqrt{\tau'_{ki}} \exp(-R^2 \tau'_{re}) + \sqrt{\tau'_{di}} \frac{1 - \exp(-R^2 \tau'_{re})}{R^2 \tau'_{re}} \right] .$$

Some values of the parameters A_m and B_m , obtained allowing variable specific heat in the condensed phase $C_c(\theta) = c_c(T)/c_{ref} = 1 + a\theta$, are reported in Tab. 3 for two different pressure ranges. Once the gas phase characteristic times have been properly computed, one can obtain the heat feedback law:

$$(3.3.4) \quad (K_g \frac{d\theta}{dX}) \Big|_{g,s} \equiv q_{g,s} = \frac{H_f}{\sqrt{\tau'_{re}}} \left[\sqrt{\tau'_{ki}} \exp(-R^2 \tau'_{re}) + \sqrt{\tau'_{di}} \frac{1 - \exp(-R^2 \tau'_{re})}{R^2 \tau'_{re}} \right] .$$

where:

$$\sqrt{\bar{\tau}'_{ki}} = A_m \frac{T_f}{P} \exp \left[\frac{E_f}{2} \left(\frac{1}{T_f} - 1 \right) \right]$$

is a nondimensional kinetic time parameter associated with a second order gas phase reaction assumed to occur wholly at the highest temperature T_f ;

$$\sqrt{\bar{\tau}'_{di}} = B_m \frac{(T_f)^{5/6}}{(P)^{1/3} (T_s)^{7/8}}$$

is a nondimensional diffusion time parameter obtained by assuming that the diffusional mixing rate of fuel pockets with the surrounding atmosphere of oxygen rich gases depends on the surface temperature T_s ;

$$\sqrt{\bar{\tau}'_{re}} = \sqrt{\bar{\tau}'_{di}} + \sqrt{\bar{\tau}'_{ki}}$$

is a nondimensional reaction time parameter obtained as a simple combination of the two above limiting cases. This last relationship was shown in Ref. 123a to represent the pressure dependence of the burning rate quite accurately for a wide range of composite propellants and also to describe the depressurization extinction correctly for composite and, to some extent, double base propellants (Ref. 44). Several plots of heat feedback vs burning rate are reported in Ref. 9 ($C_g = 1$ or $\neq 1$ and $C_c(\theta) = 1$) and Ref. 36 ($C_g \neq 1$ and $C_c(\theta) \neq 1$).

By further space integration of the

gas phase energy equation over the interval from $X=0$ to X_f , the overall quasi-steady gas phase thermal profile can be obtained:

$$(3.3.5) \quad \Theta(X, \tau) = \Theta_s(\tau) + \frac{X}{K_g} \sqrt{\frac{\bar{\tau}'_{di}}{\bar{\tau}'_{re}}} \frac{H_f}{R\bar{\tau}'_{re}} +$$

$$+ \left[\exp\left(R^2 \bar{\tau}'_{re} \frac{X}{X_f} \right) - 1 \right] \left[\frac{X_f}{K_g} \frac{H_f}{R\bar{\tau}'_{re}} \exp\left(-R^2 \bar{\tau}'_{re} \right) \right.$$

$$\left. \left(\sqrt{\frac{\bar{\tau}'_{ki}}{\bar{\tau}'_{re}}} - \frac{1}{R^2 \bar{\tau}'_{re}} \sqrt{\frac{\bar{\tau}'_{di}}{\bar{\tau}'_{re}}} \right) \right] \quad 0 \leq X \leq X_f$$

and $\Theta(X, \tau) = \Theta_f(\tau) \quad X > X_f.$

Plottings of quasi-steady gas phase thermal profiles according to MTS flame model are reported in Ref. 36 for variable specific heat (linear temperature dependence) at $p=10$ and 50 atm.

3.3.2-KTSS flame

As in the case of MTS flame, the characteristic diffusive time (the only considered in this model) is the parameter through which the condensed phase properties affect the gas phase behavior. This is not surprising because KTSS flame (Ref.136) can be considered as a particular case of MTS model, when chemical kinetics is not important. The diffusive characteristic time, according to KTSS flame model, can be obtained in a very simple manner. The "linearized" expression of the KTSS heat feedback can be written in a compact form as

$$(3.3.6) \quad q_{g,s}(P, R) = \frac{H_f}{R \bar{\tau}'_{di}} = \frac{\Phi(P, \epsilon_{-s})}{R}$$

The energy balance at the solid-gas interface under steady conditions, allows to reformulate the previous expression as follows:

$$(3.3.7) \quad \Phi \equiv \bar{q}_{g,s} \bar{R} = (\bar{q}_{c,s} - \bar{q}_s) \bar{R},$$

being

$$(3.3.8) \quad \bar{q}_{c,s} \equiv (K_c(\bar{\theta}) \frac{d\bar{\theta}}{dX})_{c,s} = \bar{R} \int_{\bar{\theta}_{-\infty}}^{\bar{\theta}_s} C_c(\theta) d\theta - \int_{-\infty}^0 H_c \bar{\epsilon}_c dx$$

and

$$(3.3.9) \quad \bar{q}_s = \bar{R} \bar{H}_s.$$

Once the steady burning rate is expressed as $\bar{R}=P^n$ and upon substitution in Eq. 3.3.7, one obtains:

$$(3.3.10) \quad q_{g,s} = \frac{\bar{R}^2}{R} \left(\int_{\bar{\theta}_{-\infty}}^{\bar{\theta}_s} C_c(\theta) d\theta - \bar{H}_s - H_c \right).$$

A comparison between Eq. 3.3.10 and Eq. 3.3.6 gives immediately the required characteristic time:

$$(3.3.11) \quad \bar{\tau}'_{di}(P) = \frac{H_f}{\bar{R}^2 \left(\int_{\bar{\theta}_{-\infty}}^{\bar{\theta}_s} C_c(\theta) d\theta - \bar{H}_s - H_c \right)}.$$

The heat feedback law in its nonlinear version becomes

$$(3.3.12) \quad \left(K_g \frac{d\theta}{dX} \right)_{g,s} \equiv q_{g,s}(P,R) = \frac{H_f}{R \bar{\tau}'_{di}} \left[1 - \exp(-R^2 \bar{\tau}'_{di}) \right].$$

A plot of $q_{g,s}$ vs R according to KTSS flame model is shown in Fig. 3, where the effect of variable specific heat and ambient pressure is put in evidence.

The gas phase thermal profile is

$$(3.3.13) \quad \theta(X,\tau) = \theta_s(\tau) + \frac{H_f}{C_g} \left[\frac{X}{X_f} + \frac{1 - \exp\left(\frac{C_g}{K_g} R X\right)}{R^2 \bar{\tau}'_{di} \exp\left(R^2 \bar{\tau}'_{di}\right)} \right] \quad 0 \leq X \leq X_f$$

$$\theta(X,\tau) = \theta_f(\tau)$$

$$X > X_f.$$

Plottings of the thermal profiles referring to the previous expression and including the effects of the most influent parameters are reported in Fig. 4.

3.3.3- KZ flame

The Kooker-Zinn flame model, in its original version, does not differ significantly from the KTSS model, despite the different physical justification of the heat release in the gas phase (Ref.137). The "nonlinearized" expression of the heat feedback assumes the following form:

$$(3.3.14) \quad q_{g,s} = \frac{Z}{R} P^\beta \left[1 - \exp(-R \frac{Z}{R} \tau_{ki}) \right].$$

In order to make the model able to reproduce correctly the steady burning rates corresponding to different values of the pressure, the parameter Z cannot be kept constant. If the condensed phase properties are taken into account, one finds

$$(3.3.15) \quad Z(P) = \frac{\bar{R} \left[\int_{-\infty}^{\bar{\theta}_s} C_c(\theta) d\theta - H_c - \bar{H}_s \right]}{P^\beta}.$$

The Eq. 3.3.15 is obtained again combining the energy balance of the interface with the first integral of the solid phase energy equation. It is immediate to remark that no difference exists between KTSS and KZ models, once the latter is extended to reproduce the steady state for different sets of operating conditions. In the linearized version, KZ heat feedback law is

$$q_{g,s}(P, R) \approx Z \frac{P^\beta}{R}.$$

3.3.4 - LC flame

This model does not invoke a particular mechanism (kinetic or diffusion) to justify the heat release in gas phase (Ref.138) but assumes that the pressure dependence of the reaction rate $w = \rho_g \tilde{\epsilon}$ holds both in steady and unsteady conditions. The first

integral of the gas phase energy equation (Eq. 3.1.21), once the term $w = \rho_g \tilde{\epsilon}$ is kept constant, leads to the following relationship:

$$(3.3.16) \quad (K_g \frac{d\theta}{dX})_{g,s} \equiv q_{g,s}(P,R) = \frac{H_f k_g w}{R c_{g,ref}^2} \left[1 - \exp\left(-\frac{C}{K_g} R X_f\right) \right],$$

where the term w has to be defined. The pyrolysis law used by LC is a generalized version of the Arrhenius expression including a pressure dependence through the power n_s . In terms of our nondimensional variables, the burning rate is given by

$$(3.3.17) \quad \bar{R} = P^{n_s} \exp\left\{-\frac{\tilde{E}_s}{Q} \left[\frac{1}{\theta_s (T_{s,ref} - T_{ref}) + T_{ref}} - \frac{1}{T_{s,ref}} \right]\right\}.$$

The usual procedure, requiring the first integral of the solid phase energy equation (under steady and adiabatic conditions) and the energy balance at the interface, leads to define the wanted parameter:

$$(3.3.18) \quad w = \frac{-2}{H_f k_g} \frac{c_g}{m} \int_{\theta_{-\infty}}^{\theta_s} C_c(\theta) d\theta - H_c - \bar{H}_s,$$

where the surface temperature is obtained from Eq. 3.3.17 by considering the experimental relationship $\bar{R} = P^n$:

$$(3.3.19) \quad \bar{\theta}_s = \frac{1}{1 - \frac{T_{ref}}{T_{s,ref}} + \frac{Q}{\tilde{E}_s} (T_{s,ref} - T_{ref}) \lg P^{(n_s - n)} T_{s,ref} - T_{ref}} \frac{T_{ref}}{T_{s,ref}}$$

The Eq. 3.3.18 holds also under quasi-steady conditions once the steady values of surface temperature, pressure, and energy releases have been replaced by the corresponding quasi-steady values :

$$(3.3.20) \quad w = \frac{m^2(t) c_g}{H_f k_g} \int_{-\infty}^{\theta_s} C_c(\theta) d\theta - H_c - H_s \quad .$$

The previous expression permits to evaluate the heat feedback according to Eq. 3.3.16 or, when allowed, to its "linearized" version :

$$q_{g,s}(P,R) \approx \frac{H_f k_g w}{R c_g m_{ref}^2} \quad .$$

3.4 - A WORKING MAP

It is instructive to consider the working map in the form of Fig. 5. This is a R vs $q_{g,s}(P,R)$ plot applicable to any quasi-steady flame model. In Fig. 5 KTSSN flame was implemented under the indicated set of operating conditions. Isobaric curves describe the available heat feedback at the corresponding pressure; note that $q_{g,s}(P,R=0)=0$. Lines at constant ambient temperature (for adiabatic burning) or at constant radiant flux (for $\theta_{-\infty}=0$) describe the heat feedback required by the condensed phase for steady burning

$$q_{g,s}(P, F_o, \theta_{-\infty}) = \bar{R} \int_{\theta_{-\infty}}^{\bar{\theta}_s} C_c(\theta) d\theta - \bar{H}_s - (1 - \bar{r}_\lambda) \bar{F}_o + q_{out}(\theta_s)$$

At the crossing of $q_{g,s}(P,R)$ with $\bar{q}_{g,s}(P, F_o, \theta_{-\infty})$, steady solutions $\bar{R}(P, F_o, \theta_{-\infty})$ vs $q_{g,s}$ are singled out. Curves $q_{g,s}(P,R)$ depend on flame modeling, curves $\bar{q}_{g,s}(P, F_o, \theta_{-\infty})$ depend on external parameters only. It is seen immediately that two steady solutions are found for each set of external parameters: the trivial $\bar{R} = 0$ (unreacting state and some $\bar{R} \neq 0$ (reacting state). For quasi-steady gas phase transients driven by deradiation, for example, the instantaneous solution in time runs on the isobaric curve of interest; only when a steady burning configuration is reached, will the solution stop at the crossing with the relevant $q_{g,s}$ curve. Similar remarks hold true for any flame model, except that the unreacting or extinguished state $\bar{R} = 0$ is not allowed for linearized models.

By decreasing ambient temperature and/or radiant flux (negative values of F_0 imply heat loss from burning surface), the corresponding $\bar{R}(P, F_0, \theta_\infty)$ are seen in Fig. 5 to become lower and lower at any pressure. The question arises: are there minimum values of P, F_0 , and θ_∞ below which $\bar{R} \neq 0$ is not allowed or, if allowed, is unstable? This would assign static limits to burning domain of the flame model under consideration. The answer for decreasing heat loss will be shown in Fig. 12: the point of maximum heat feedback roughly corresponds to the minimum allowed steady burning rate at any given pressure. For $\theta_\infty \rightarrow -0.429$ it is found (not shown in the figure) that the steady solution does not reach this minimum steady burning rate; but obviously other effects would come into play at such low ambient temperatures. For decreasing pressure (with adiabatic burning at $\theta_\infty = 0$, i.e. $T_\infty = 300$ K), a steady solution is always found. However, it will be seen in Sec. 4.6, that burning instability develops, defining a pressure deflagration limit PDL; this will require further analysis. Note that so far no constraint whatsoever has been placed on unsteady burning.

3.5 - CONCLUDING REMARKS

The modeling approach discussed in this chapter, being of rather general formulation, can be specialized to any transient burning problem within the basic limitation of monodimensional thin flames of thermal character. In particular, dynamic burning associated with fast depressurization and/or deradiation can be studied. The range of validity is essentially established by that of the flame model. Among the flame models reported in this chapter, the most general is MTS whose range of validity, with the formulation given in Eq. 3.3.4, covers 1-100 atm (Ref. 44a, p.27). For pressures above 100 atm, the assumptions of monodimensionality (condensed and gaseous thermal waves much larger than burning surface roughness) and condensed phase homogeneity (condensed phase thermal wave much larger than mean particle size) fail for MTS as well as all other flame models considered in this chapter. For pressures less than 1 atm, a distended $\text{NH}_3/\text{HClO}_4$ premixed flame should be considered in MTS flame; this was done by Merkle (Ref. 44a, pp. 49-43), but is not reported here.

In its linearized version, (Eq. 3.3.6) the non-dimensional KTSS heat feedback law is a particular case of the full expression (Eq. 3.3.12), when the further assumption is made that

$$(3.5.1) \quad \exp(-R^2 \frac{=}{\tau_{di}}) \ll 1$$

corresponding to $\bar{\tau}'_{di}$ very large but finite burning rate. This constraint is usually valid for steady burning, but is not acceptable in extinction transients, since under this circumstance $R \rightarrow 0$ while $\bar{\tau}'_{di}$ remains finite and, therefore,

$$\exp(-R^2 \bar{\tau}'_{di}) \rightarrow 1.0$$

An essential ingredient for all flame models is the experimental stationary $\bar{R}(P)$ curve. This steady state structure is embodied by MTS, KTSS and LC models. It is worthwhile to remark that even the linearized version of the KTSS model can accurately reproduce the experimental stationary $\bar{R}(P)$.

The pressure dependent portion of the heat feedback law, assumed the same as in the steady state, is embodied in LC flame without ever specifying what the dependency is. KTSS and KZ also assumed the pressure dependent portion of the heat feedback law to be the same as in the steady state, but enforced respectively a diffusion and a kinetics controlled burning mechanism.

Both KZ and LC flame models were derived under the same constraint (large characteristic times) as the linearized KTSS; they are subjected to the same limitations of applicability as well. While KTSS and LC recover the steady state burning rate dependence on pressure when transient effects vanish, KZ does not. Although differences at steady state can be small if an appropriate choice of β is made, this is a weakness of KZ flame.

From a rigorous point of view, even within these validity limits, extinction (and ignition) transients cannot be described by quasi-steady gas phase models. Indeed, these phenomena are intrinsically unsteady. However, error due to applying the quasi-steady gas phase assumption is estimated negligible to the extent in which the gas phase characteristic times are small with respect to the condensed phase thermal wave characteristic time.

With these restrictions in mind, one can pick up a favorite pyrolysis law and flame model, assign the wanted external laws $P(\tau)$ and $F_o(\tau)$, select the appropriate optical model and thermal properties for the condensed phase, enforce the correct initial condition, and finally numerically integrate the PDE of Eq.3.1.2. What do we get? Trends and bounds, but no predictions. For static as well as dynamic burning, more sophisticated analyses are required. This is discussed in next section. Nevertheless, the importance of a numerical approach cannot be overlooked; complete burning transients cannot be evaluated otherwise.

CHAPTER 4 - NONLINEAR BURNING STABILITY OF SOLID PROPELLANTS

In this chapter an overview of the analytical developments concerning nonlinear burning stability of solid propellants is offered. First, some introductory concepts and nomenclature are recalled; then, the theory is formally developed for heterogeneous thin flames; finally, specific effects of particular parameters are illustrated in detail.

For the first time with respect to previous Progress Reports by this research group:

1. Temperature dependent thermal conductivity and specific heat in the condensed phase are taken into account.
2. Chemical reactions volumetrically distributed in the condensed phase are included.
3. Polychromatic, rather than necessarily monochromatic, radiation impinging from an external, continuous wave source is allowed.
4. Exponential or polynomial temperature disturbance profiles in space are considered.

This nonlinear burning stability theory of solid propellants is based on the unsteady burning models previously presented in Chapter 3. Computer simulated tests assessing the validity of the analytical work, developed in the Chapters 3 and 4, will be described in Chapter 5. Experimental results (from a depressurization strand burner, piston tube, sub-atmospheric strand burner, etc.), collected with the intent of checking the whole theoretical approach, will be discussed in Chapter 6.

4.1 - BACKGROUND AND NOMENCLATURE

The physical system dealt with is presented in its most general form in the schematic of Fig. 1a. The pressure of the vessel, the radiant flux impinging on the surface of the strand (originating exclusively from some external energy source), the ambient temperature measured at the cold boundary of the propellant sample (supposed to be infinitely long), and any other parameter which can be controlled in a known way from the outside of the vessel are designated as controlling parameters. A change of one or more of these controlling parameters will affect, in some way, the state of the burning propellant; consequently, they are also called external perturbations.

On the other side, we designate as intrinsic perturbations sources all those "small" (in a sense to be specified)

irregularities and imperfections always present in the real world but which are nevertheless neglected in the idealized picture of Fig. 1a. For example, nonuniform composition of the strand, impurities variously scattered in the condensed phase, complicated geometry of the burning surface, etc., all contribute to hopefully small but persistent differences of the actual phenomena from those described by mathematical models.

Whether the perturbation sources are external or intrinsic, the prior, supposedly unperturbed steady state profile of temperature in the combustion wave will be modified to some new perturbed unsteady profile. Let us define the disturbance temperature profile as the profile of the point-by-point difference between the perturbed profile and the original, unperturbed profile. The general problem of static stability may be stated as follows: given a stationary combustion state, the propellant is forced to a close but nonstationary combustion state and it is asked whether the propellant, after a long enough period of time, will go back to its initial state or will move away from it. In the specific physical configuration considered in this study, it is asked whether the disturbance temperature profile will die out in time or not. Mathematically, the problem is an initial value problem and is usually described by a parabolic type of partial differential equation.

It is of concern to distinguish between static and dynamic stability. The general problem of dynamic stability may be stated as follows: given an initial stationary combustion state, the propellant is forced to a different (final) stationary state by means of appropriate changes in time of pressure and/or radiant flux and it is asked whether the propellant, after a long enough period of time, will reach the wanted final state or another (unwanted) final state. In other words, the combustion stability of a propellant where intrinsic perturbation sources exclusively are considered to be acting (stability of an equilibrium state) is called static. Conversely, the combustion stability of a propellant for which the external controlling parameters are changing in time and multiple final steady state exist (stability of a burning transition) is called dynamic (or, better, transitional). It is well known that in the latter case the rate of change in time of the external controlling parameters (typically, pressure and/or external radiant flux) is of fundamental importance and this explains the expression "dynamic stability" (which may however be confusing in other fields of applied sciences).

The ultimate objective of this research program is to establish boundaries separating regions of static and/or dynamic burning stability from region of static and/or dynamic burning instability on some convenient graphical plot. While at the beginning of this research the preferred plot was that of nonlinear static function vs surface temperature, later on plotting of the bifurcation diagrams vs the relevant parameters revealed much more powerful (see below).

Since the mathematical problem is formidable, no general method has been set up so far for solving the stability problem in all of its intriguing aspects. In this study, the approximate approach proposed by the senior author in 1975 (Ref. 10) and implemented since then with continuous improvements is resorted to. This consists of transforming the governing PDE-based set of equation into an ODE-based set of equation via an integral method. A nonlinear algebraic function, called static restoring function, is then determined which contains all basic properties of equilibrium and stability of burning solid propellants. Plotting the zeroes of this algebraic function vs any relevant parameter generates the above mentioned bifurcation diagrams.

Notice that this approach requires the implementation of a flame model, since the Zeldovich method is of no help (see Sec. 2.1.1). The choice of the flame model is at the option of the investigator. But it should be extremely clear that any stability theory can only extract the stability properties (static as well as dynamic) implicitly buried in the flame model. A flame model of limited validity will yield stability predictions of limited validity.

4.2 - THE NONLINEAR BURNING STABILITY EQUATION

Basically, the mathematical method implemented to reduce a PDE into an ODE is the one set up by Von Karman and Polhausen in the study of boundary layers and later generalized by Goodman to thermal problems. The method can be extended to any other problem described by nonlinear PDE of parabolic type. In our case, the approach consists in defining a parameter $\xi(\tau)$, called the penetration distance of the thermal wave in the condensed phase, "such that for $X \geq \xi(\tau)$ the propellant slab, for all practical purposes, is at an equilibrium temperature and there is no heat transferred beyond this point" (p. 53 of Ref. 139). The evolution in time of the thermal profile in the condensed phase is obtained by following the time history of

the penetration distance propagating into an initially uniform temperature field. Within this penetration layer, progressing in time, the qualitative space distribution of temperature is assumed known a priori; but we make sure that, in so doing, the integral balance of thermal energy in the condensed phase is preserved. In other works, the price to be paid for making the transformation from PDE to ODE formulation is an approximate solution of the local space distribution of temperature. This is not such a serious drawback because the interest is in the time evolution of the surface temperature. In any event, several investigations found an error of only some percents for various cases in which both the exact and the integral solutions were evaluated. For example, see Fig. 5 on p.89 of Ref. 139 showing the temperature time history at the surface of a semi-infinite slab with triangular surface heat flux.

In order to get a deeper understanding of questions related to the integral method as applied to thermal problems, the interested reader might wish to consult the excellent review by Goodman (Ref. 139) and the references given there. Before getting involved in mathematical details, the reader should be warned about the limits of the integral method. Any solution obtained by the integral method contains hopefully small but irrevocable errors in the final numerical results. The question of how to improve the accuracy then arises. It has been argued that "there is no a priori guarantee that increasing the order of the polynomial (used to represent the space distribution of the unsteady temperature profile) will improve the accuracy. Although the accuracy is frequently improved with this technique, it can be demonstrated, nonetheless, that there are cases for which it actually worsens" (p. 96 of Ref. 139). In this same reference it is suggested that the method of weighted residuals provides a very efficient method for improving the accuracy of the results obtained by using the integral method. The simple integral method implemented in this work can be considered a special case of the method of weighted residuals when just one parameter (the penetration distance ξ) and one weighting function are considered. Under these circumstances, the only equation to be considered is the heat balance integral (see below).

Let us define the finite size thermal disturbance profile as:

$$(4.2.1) \quad u(X, \tau) \equiv \theta(X, \tau) - \bar{\theta}(X) \quad X \leq 0$$

where $\bar{\theta}(X)$ is the initial steady state distribution of temperature and $\theta(X, \tau)$ is the temperature distribution following some perturbation. The new variable $u(X, \tau)$ may therefore be conveniently interpreted as the finite temperature disturbance propagating inside the condensed phase and superimposed on the initial temperature distribution after the action of perturbation. At the initial instant $\tau=0$, by definition $\theta(X, \tau) = \bar{\theta}(X)$ and $u(X, \tau) = 0$. Suppose now that, in the following instant, a perturbation starts acting on the system and makes $u(X, \tau) \neq 0$: the goal of the analysis is to determine the ultimate effect of such a temperature disturbance after waiting a period of time sufficiently long for the perturbation to disappear. No assumption whatsoever is made as to the size of the temperature disturbance. The analysis will be restricted to the case of constant (not necessarily reference) ambient temperature $\theta_{-\infty}$.

Let us assume that the disturbance thermal profile, in general depending on time and space, can be written in a "separate" form of the type

$$(4.2.2) \quad u(X, \tau) = u_s(\tau) u_c(X, \tau)$$

where $u_s(\tau)$ is the unknown temperature disturbance at the surface s and $u_c(X, \tau)$ is the unknown temperature disturbance profile in the condensed phase. Based on the physical nature of the problem, let us restrict our attention to perturbations monotonically decaying in space: typically, of polynomial

$$(4.2.3) \quad u(X, \tau) = u_s (1+X/\xi)^n$$

or exponential nature

$$(4.2.4) \quad u(X, \tau) = u_s \exp(nX/\xi)^n.$$

In both cases, the penetration thickness $\xi(\tau)$ of the disturbance thermal boundary layer is given (see Ref. 25) by

$$(4.2.5) \quad \xi(\tau) = n \frac{u_s}{(u_X)_{c,s}}.$$

The thermal gradient at the solid side of the burning surface, $(u_X)_{c,s}$, is evaluated through the energy balance at the solid-gas interface in perturbed conditions:

$$(4.2.6) \quad (u_X)_{c,s} = \frac{1}{K_c(\theta_s)} \left[(K_g \frac{\partial \theta}{\partial X})_{g,s} + RH_s - q_{out}(\theta_s) \right] - (\bar{\theta}_X)_{c,s}$$

The integral method, when applied to the energy equation in the condensed phase (Eq. 3.1.2), leads to a reformulation of the problem in terms of an ordinary differential equation. The analytical procedure requires to consider the unsteady thermal profile as the sum of the steady temperature distribution and the disturbance thermal profile (Eq. 4.2.1). A space integration from 0 to $-\xi(\tau)$ is then performed:

$$\int_{-\xi}^0 C_c(\theta) \frac{\partial u}{\partial \tau} dX = \int_{-\xi}^0 \left\{ -C_c(\theta) R \frac{\partial \theta}{\partial X} + \frac{\partial}{\partial X} \left[K_c(\theta) \frac{\partial \theta}{\partial X} \right] + F_o \int_{\lambda_1}^{\lambda_2} f_1(X, \lambda) d\lambda + H_c \epsilon_c \right\} dX$$

The analytical treatment of the right-hand side of the previous expression is straightforward; only details about the left-hand side term will be offered. From the assumption of Eq. 4.2.2 the following development follows:

$$\int_{-\xi}^0 C_c(\theta) \frac{\partial u}{\partial \tau} dX = \int_{-\xi}^0 C_c(\theta) \left(u_c \frac{du_s}{d\tau} + u_s \frac{du_c}{d\tau} \right) dX$$

By expressing the time derivative of the space and time dependent portion of the temperature disturbance as

$$\frac{du_c}{d\tau} = \frac{\partial u_c}{\partial \xi} \frac{d\xi}{d\tau}, \text{ one obtains:}$$

$$\int_{-\xi}^0 C_c(\theta) \frac{\partial u}{\partial \tau} dX = \int_{-\xi}^0 C_c(\theta) u_c \left\{ \frac{du_s}{d\tau} + \frac{X}{G(X)} \left[\frac{(u_X)_{c,s}}{u_s} \frac{du_s}{d\tau} - \frac{d(u_X)_{c,s}}{d\tau} \right] \right\} dX$$

where $G(X)=1+X/\xi$ for polynomial disturbance (Eq.4.2.3) or $G(X) = 1$ for exponential disturbance (Eq. 4.2.4). Since the disturbance gradient at the burning surface depends on time through $u_s(\tau)$ and $P(\tau)$, one can write:

$$\frac{d(u_X)_{c,s}}{d\tau} = \left(\frac{\partial(u_X)_{c,s}}{\partial u_s} \right)_P \frac{du_s}{d\tau} + \left(\frac{\partial(u_X)_{c,s}}{\partial P} \right)_{u_s} \frac{dP}{d\tau}.$$

After substitution and algebraic manipulations, the following ODE is obtained:

$$(4.2.7) \quad \frac{du_s}{d\tau} =$$

$$\frac{-R \int_{-\xi}^0 C_c(\theta) d\theta + \left[K_c(\theta) \frac{\partial \theta}{\partial X} \right]_{c,s} - \left[K_c(\theta) \frac{\partial \theta}{\partial X} \right]_{-\xi} + F_0 \int_{-\xi}^0 \int_{\lambda_1}^{\lambda_2} f_1(X, \lambda) d\lambda dx + H_c \int_{-\xi}^0 \epsilon_c(\xi) dx}{\int_{-\xi}^0 C_c(\theta) u_c \left\{ 1 - \frac{X}{G(X)} \left[\frac{(u_X)_{c,s}}{u_s} - \left(\frac{\partial(u_X)_{c,s}}{\partial u_s} \right)_P \right] \right\} dx}$$

$$- \frac{\int_{-\xi}^0 C_c(\theta) u_c \frac{X}{G(X)} \left[\left(\frac{\partial(u_X)_{c,s}}{\partial P} \right)_{u_s} \frac{dP}{d\tau} \right] dx}{\int_{-\xi}^0 C_c(\theta) u_c \left\{ 1 - \frac{X}{G(X)} \left[\frac{(u_X)_{c,s}}{u_s} - \left(\frac{\partial(u_X)_{c,s}}{\partial u_s} \right)_P \right] \right\} dx}$$

being $u_s(\tau=0) = 0$. This is approximately equivalent to the initial PDE+boundary conditions formulation. Notice that in the above equation $\theta(X)$ is known and only the surface temperature appears.

The above nonlinear ODE in the unknown $u_s(\tau)$ describes the response of the system to a finite size departure of the surface temperature from the stationary value due not only to intrinsic perturbation sources acting on the system (static stability), but also to arbitrary but assigned mono-

tonical changes in time of pressure and radiant flux (dynamic stability).

Considerations of a general character on the static stability of the system described by Eq. 4.2.7 can be made. A given equilibrium configuration of the burning propellant is asymptotically stable if

$$\text{or } \left. \begin{array}{l} u_s(\tau) \rightarrow 0 \\ \theta(X, \tau) \rightarrow \bar{\theta}(X) \end{array} \right\} \text{ for } \tau \rightarrow \infty .$$

In other words, the equilibrium configuration is (asymptotically) stable if the disturbance disappears at large time and the propellant returns to its initial steady configuration. Following Lyapunov (p. 216 of Ref. 140), Eq. 4.2.7 can be written more concisely as

$$(4.2.8) \quad \left\{ \begin{array}{l} \frac{du_s}{d\tau} = f(u_s) - g(\tau, u_s) \\ u_s(\tau=0) = 0 \end{array} \right.$$

where

$$(4.2.9) \quad f(u_s) \equiv$$

$$-R \int_{-\xi}^0 C_c(\theta) d\theta + \left[K_c(\theta) \frac{\partial \theta}{\partial X} \right]_{c,s} - \left[K_c(\bar{\theta}) \frac{\partial \bar{\theta}}{\partial X} \right]_{-\xi} + F \int_0^{\lambda_2} \int_{-\xi}^{\lambda_1} f_1(X, \lambda) d\lambda dX + H_c \int_{-\xi}^0 \epsilon_c(\epsilon) dX$$

$$\int_{-\xi}^0 C_c(\theta) u_c \left\{ 1 - \frac{X}{G(X)} \left[\frac{(u_x)_{c,s}}{u_s} - \left(\frac{\partial (u_x)_{c,s}}{\partial u_s} \right)_P \right] \right\} dX$$

is the autonomous (i.e., time independent) contribution, and

(4.2.10) $g(\tau, u_s) \equiv$

$$\frac{\int_{-\xi}^0 c_c(\theta) u_c \frac{X}{G(X)} \left[\left(\frac{\partial (u_X)_{c,s}}{\partial P} \right)_{u_s} \frac{dP}{d\tau} \right] dx}{\int_{-\xi}^0 c_c(\theta) u_c \left\{ 1 - \frac{X}{G(X)} \left[\frac{(u_X)_{c,s}}{u_s} - \left(\frac{\partial (u_X)_{c,s}}{\partial u_s} \right)_P \right] \right\} dx}$$

is the nonautonomous (i.e. time dependent) contribution. Remark that, for optically opaque condensed phase, the term

$$\int_{-\xi}^0 c_c(\theta) u_c \frac{X}{G(X)} \left(\frac{\partial (u_X)_{c,s}}{\partial F_o} \right)_{u_s, P} \frac{dF_o}{d\tau} dx$$

should be added to the numerator of Eq. 4.2.10. If no forcing function is acting, i.e. $P = \text{const}$ and $F = \text{const}$ (for optically opaque propellants), Eq. 4.2.8 reduces to:

(4.2.11) $\frac{du_s}{d\tau} = f(u_s)$

by which the autonomous contribution assumes the meaning of a static restoring function. Indeed, under these circumstances, one can think of the chemically reacting system comprised of the deflagrating condensed material as analogous to a mass-spring type of mechanical system which the nonlinear characteristic $f(u_s)$. Considering the $u_s(\tau)$ definition of Eq. 4.2.1, Eq. 4.2.8 can also be written as

4.2.12
$$\left\{ \begin{array}{l} \frac{d\theta_s}{d\tau} = f(\theta_s - \bar{\theta}_s) - g(\tau, \theta_s - \bar{\theta}_s) \quad 0 \leq |X| \leq \xi(\tau) \\ \theta_s(\tau=0) = \bar{\theta}_s \end{array} \right.$$

The static restoring function $f(\theta_s - \bar{\theta}_s)$ depends on the

nature of the deflagrating substance but not on its burning history; however it is affected by the operating conditions (pressure, ambient temperature, and heat exchange with environment), flame model, and approximating profile order. The nonautonomous term $g(\tau, \theta_s - \theta_s)$ changes in time according to the first derivatives of the external controlling parameter (see Eq. 4.2.10). The static restoring function, being a property of the deflagrating substance, can be examined a priori (see next section) independently on any specific burning process. On the contrary, nothing can be said a priori for the nonautonomous term. Nevertheless, the following important remark can be made immediately. The final outcome of a burning process is controlled only by the static restoring function when:

- (1) no forcing function is acting (static stability); see Sec. 4.4.
- (2) forcing functions monotonically change in time from some initial to some final value (dynamic stability); e.g., depressurization or deradiation; see Sec. 4.5.
- (3) forcing functions are of arbitrary shape but level off in time (dynamic stability); e.g., pressure or radiation pulses ; see Sec. 4.5.

4.3 - THE STATIC RESTORING FUNCTION

The static restoring function is an algebraic nonlinear function strictly dependent on the nature of the burning propellant (including the specific way its flame is described, i.e. the flame model implemented and the order of the approximating profile used in Sec. 4.2) and the operating conditions. Before examining quantitative plots, consider the qualitative plots of Fig. 6. This allows to extract the basic properties of the static restoring function independently of the flame description.

4.3.1 - Meaning of the Algebraic Roots

Consider the qualitative plot of Fig. 6. According to Eq. 4.2.12, when no forcing function is acting on the system, the points (algebraic roots) for which $f(\theta_s - \theta_s) = 0$ define potential equilibrium configurations for the burning propellant, since they correspond to $d\theta_s/d\tau = 0$. It will be shown below that this is a necessary but not sufficient condition for a root of the static restoring function to represent a burning equilibrium state.

It is seen in Fig. 6 that, in addition to the trivial $\theta_s = 0$ (unburning propellant, root C), two more possible equilibrium solutions (roots A and B) are allowed, in general, for a given set of parameters. Let us consider the equilibrium configuration corresponding to root A. Suppose that, for some unspecified reason, the burning rate or the surface temperature increases a finite amount; then the burning propellant is no longer in a stationary configuration, $d\theta_s/d\tau = f(\theta_s - \bar{\theta}_s)$ is negative, and the system reacts by decreasing its surface temperature. Conversely, if for a unspecified reason, the surface temperature of a propellant burning according to the configuration of root A decreases, the propellant reacts by increasing its surface temperature. These movements, around point A, are indicated by arrows in Fig. 6. It is concluded that the equilibrium configuration corresponding to root A is stable because, when disturbed, the propellant always moves back toward A. In mathematical terms, this physical mechanism finds an elegant interpretation due to Lyapunov (see Sec. 4.4.3). By the same arguments, it is concluded that the potential equilibrium configuration corresponding to root B is unstable; any disturbance yields movement away from the point. In steady state experiments only solution A is observed. In any event, the exact nature of root B will be classified in what follows.

If the set of parameters is changed, for example the pressure is decreased from P to P_1 , the initial condition of the ODE (see Eq. 4.2.12) is changed so that a new pair of roots, A_1 and B_1 , is found in addition to the trivial $\theta_s = 0$ of root C. Again, root A_1 defines a stable equilibrium configuration, while root B_1 defines an unstable configuration corresponding to the new set of parameters. Likewise, a new pair of roots, in addition to the trivial $\theta_s = 0$ of root C, is found if the pressure is increased. It follows that the θ_s axis in Fig. 6 includes, in addition to the trivial solution of nonburning propellant at the root C, a segment of stable solution A_1 and a segment of associated unstable configurations B_1 (each pair of roots corresponds to a given set of parameters).

It should be explicitly observed that the trivial $\theta_s = 0$ solution may be obtained only if the exponential Arrhenius-type pyrolysis law for mass production at the surface is dropped. Moreover, the trivial $\theta_s = 0$ solution implies that no external energy source (e.g., radiation) is acting on the solid propellant.

The qualitative picture of Fig. 6 illustrates the general behavior of the static restoring function when the

pressure varies within "regular" bounds. When the pressure becomes too low (in a sense which will be better understood below), the static restoring function features a new couple of roots D and E. At first, this is rather surprising: in principle there are now five potential equilibrium configurations of the combustion wave!

Let us examine the meaning of these roots. The total number of roots is in general odd, being the sum of couple of reacting roots (A and B, D and E, ecc.) with one trivial unreacting root ($R=0$). The trivial root, corresponding to the equilibrium configuration of the unreacting state, shall be called C. For adiabatic propellants, root C always exists and is stable in the Lyapunov sense previously mentioned. On the other hand, all reacting roots are potentially reacting equilibrium configurations, since by definition $d\theta_s/d\tau = f(\theta_s - \bar{\theta}_s) = 0$. However, this condition includes configurations of maximum or minimum acceleration as well: only those roots for which simultaneously $\theta_s(\tau) = \bar{\theta}_s$ are reacting equilibrium configurations. In practical terms, the reacting equilibrium configuration corresponds to that special root which is solution simultaneously of the steady state energy equation (Eq. 3.2.1) and the disturbance energy equation (Eq. 4.2.7). This special root shall be called A. The working map plotted in Fig. 5 shows that there is in general one root C and one root A, whose physical meaning is well illustrated graphically in the same Fig. 5.

All other roots (B, D, and E) correspond to configurations of maximum or minimum acceleration, but they are not solutions of the steady state energy equation. In different words roots B, D, and E are in general solutions only of the disturbance energy equation. Exceptional cases will be discussed later, when introducing burning stability boundaries.

For further decreases of pressure, it is observed that A- and D-type roots respectively increase (moving to right) and decrease (moving to left) in the plot of Fig. 6, until coalescence and then crossing over occur with exchange of stability character. This important point will be discussed in detail later (see Sec. 4.6). For further decreasing of pressure, B- and D-type roots disappear after coalescence, while both A_2 and E_2 roots, for different reasons, are eliminated as being stable reacting solutions (curve CA_2E_2 in Fig. 6). Under these circumstances, it follows that the only allowed solution is the trivial unreacting configuration represented by root C. Any attempt to produce a

stationary combustion wave with a static restoring function of type CA_2E_2 will inevitably result in extinction. This type of extinction, however, cannot be qualified as "dynamic".

It will be shown in Sec. 4.6 that this pattern of evolution of the static restoring function from CBA to CBADE to CBDAE to CAE is generally observed for most parameters (operating conditions and/or physical properties) of the combustion wave.

Quantitative plots of the static restoring function $f(\theta_s - \bar{\theta}_s)$ vs the nondimensional surface temperature θ_s are given for the propellant AP/PBAA No. 941. A quantitative plot requires the choice of a specific flame model and a specific order of the approximating profile (see Sec. 4.2). By applying different flame models to the same propellant, different stability properties are predicted: this offers a criterium for discriminating potentially good from bad flame models. In this work MTS, KTSS (both linear and nonlinear), KZ, and LC flame models are implemented. As to the order of the approximating profile, a cubic polynomial law was often chosen to represent the space distribution of the disturbance thermal profile. This choice was suggested by a large body of literature on heat transfer problems (e.g. Ref. 139) and by similar solid propellant rocket problems (Refs. 141-142). However, there is no a priori guarantee that is the best choice. The choice has to be verified, somehow. This is discussed in Sec. 4.3.4.

4.3.2 - Effect of Operating Conditions (Pressure and Diabaticity)

Plots obtained implementing MTS, KTSS nonlinear, and KTSS linear (or, equivalently, LC or KZ) flame models, with a cubic polynomial profile, are respectively shown in Figs. 7-8, Fig. 9 and Fig. 10. MTS flame was applied by assuming a combined exponential-power pyrolysis law at the burning surface (see Eqs. 3.1.6 with: $\theta_k = 0.15$, $\theta_m = 0$ and $n_s = 0$). KTSS flame was applied by assuming a power pyrolysis law (see Eq. 3.1.6b with: $w=6$, $\theta_m = 0$ and $n_s = 0$) over the whole range of surface temperature of interest. Comparative results are shown in Fig. 10, for some standard operating conditions, leading to the conclusion that MTS is perhaps the best flame model but KTSS nonlinear is strongly competitive; KTSS linear (or LC or KZ in the appropriate form) yield identical results.

The effect of ambient pressure on the static restoring function vs the nondimensional surface temperature is illustrated in Fig. 7 for the indicated set of parameters (MTS flame and $n=3$ polynomial); further effects due to the combined action of pressure and other parameters will be discussed successively. An increase of pressure implies an increase of the stable equilibrium surface temperature, but a less pronounced increase of the unstable equilibrium surface temperature. The strength of the stability (see Sec. 4.4.3) is enhanced by an increase of pressure. Similar comments hold true as to the effect of external radiant flux on the restoring function (Fig. 8). It is important, however, to note that an increase of external radiant flux decreases the unstable equilibrium surface temperature and above a certain value of radiant flux intensity (e.g., $40 \text{ cal/cm}^2\text{-s}$ for the set of parameters in Fig. 8) unstable solutions are no more found. This implies that, in principle (see Sec. 4.5), at each pressure a minimum value of external radiant flux intensity exists above which the dynamic boundary can no longer be defined.

The effects of physical properties and their interactions with the operating conditions will be examined in Sec. 4.6.

4.3.3 - Effect of Flame Models

Similar trends are observed for the nonlinear KTSS flame model, again with $n=3$ polynomial. The effect of ambient pressure in Fig. 9 is very close to that found with MTS (cf. Fig. 7); minor differences are found in the region near the statically unstable root.

Drastically different results are observed for the linear KTSS (or KZ or LC) flame model, always with $n=3$ polynomial. The effect of ambient pressure is virtually the same (as compared both to MTS and KTSS nonlinear) for surface temperature about or larger than the steady state value, but is physically meaningless for surface temperature less than about 90% of the steady state value (no zero solution and no unstable root; See Fig. 21 of Ref. 9).

The static restoring functions for the three flames are plotted simultaneously in Fig. 10, always with $n=3$ polynomial, for the standard conditions specified in the figure ($p=30 \text{ atm}$, $T_{-\infty}=300 \text{ K}$, $Q_{s,ref}=+158.2 \text{ cal/g, adiabatic}$). The comparison graphically emphasizes the differences just mentioned. The linear KTSS (or LC or KZ) are discarded from being in principle acceptable flame models, the nonlinear KTSS is acceptable for most of the surface temperature range of values (except near extinction, since chemical kinetics is not considered), MTS flame is in

principle acceptable over the whole range of surface temperature of interest.

4.3.4 - Effect of Approximating Polynomial Order

The effect of the order of the polynomial approximating disturbance thermal profile on the static restoring function is illustrated in Fig. 11 ($p=20$ atm) for the MTS flame. The shape of the static restoring function is kept for n varying from 2 to 4; the steady state (or stable reacting) solution is always recovered (by construction); the trivial zero solution is also always recovered; the surface temperature associated with the unstable reacting configuration slightly increases for n decreasing. Numerical values can be better appreciated in Tab. 3 of Ref. 9; typically, the surface temperature associated with the B root increases of less than 10% when n decreases from 3 to 2. However, upper dynamic stability is sensibly favored by n decreasing. Detailed investigations indicate that the best results are found for n ranging from 2.5 to 3.

4.3.5 - Effect of Approximating Profile Type

In order to assign the spatial temperature distribution under perturbed conditions inside the solid phase, two different types of disturbance profiles are used: polynomial or exponential (see Sec. 4.2). Both expressions represent functions monotonically decaying in space, starting from the burning surface. The parameter n was kept constant. The results concerning the tested disturbance profiles evidence the following facts:

- For inert solid phase: the roots of the static restoring function are not affected by the type of the thermal disturbance.
- For exothermic reactions in solid phase: negligible differences are observed for the B root, while the exponential form induces a decrease of the D root and an increase of the E root.
- The static stability strength of two different combustion configurations can be compared only if evaluated by the same type of approximating profile.

4.3.6 - Concluding remarks

The static restoring function $f(\theta_s - \bar{\theta}_s)$ assumes a considerable importance in the static and dynamic combustion stability analysis, allowing to define both the strength of the steady burning configuration and the limits beyond which the externally induced dynamic burning leads to the extinction of the combustion processes. These points are respectively discussed in Sec. 4.4 and 4.5.

A more complete set of information related to the dynamic stability can be obtained through the bifurcation diagrams, where the zeros of several static restoring functions are plotted vs a "bifurcation parameter". By this approach, several and apparently uncorrelated combustion phenomena (such as PDL, self-sustained oscillatory combustion, and dynamic extinction) are explained from a single point of view. This is discussed in Sec. 4.6.

4.4 - NONLINEAR STATIC BURNING STABILITY

Static stability analysis of a burning propellant relates to the capability of the propellant to keep its burning equilibrium configuration in time. It was shown in Sec. 4.2 that this implies to study the properties of nonlinear ODE

$$(4.4.1) \quad \frac{d\theta_s}{dt} = + f(\theta_s - \bar{\theta}_s)$$

which in turn depends on the shape of the algebraic nonlinear static restoring function $f(\theta_s - \bar{\theta}_s)$ examined in Sec. 4.3. The following problems are of relevance in the area of static stability:

1. prediction of number and nature of the allowed static solutions (see Sec. 4.4.1).
2. prediction of static burning boundary (see Sec. 4.4.2).
3. measurement of static stability strength (see Sec. 4.4.3).

4.4.1 - Number and Nature of the Allowed Static Solutions

It will be shown in Sec. 4.6 that three regions of interest can be distinguished:

1. before A-D roots coalescence (static restoring function of the type CBADE), the static reacting solution is the usual time-independent combustion wave strictly defined by root A.
2. after A-D roots coalescence but before B-D roots coalescence (static restoring function of the type CBDAE), the static reacting solution is a self-sustained oscillating combustion wave around root A.
3. after B-D roots coalescence (static restoring function of the type CAE), no static reacting solutions whatsoever is allowed.

Obviously, the trivial unreacting solution $\bar{\theta}_s = \bar{R} = 0$ (when allowed) is always statically stable. All of the above predictions were verified by numerical integration of the governing PDE. Results concerning self-sustained oscillatory burning are discussed in detail in Sec. 4.6.

4.4.2 - Static Burning Boundary

An important preliminary information in the static stability analysis of a burning propellant is the minimum value of surface temperature (or burning rate) above which steady burning exists. In order to evaluate this value, a common feature of all static restoring functions is emphasized. The specific surface temperature value, θ_s^{ST} , at which the pair of solution A_i^{ST} stable and B_i^{ST} unstable coalesces, at a given pressure (Fig. 6) and for a given set of parameters,

$$A_i^{ST} = B_i^{ST} = \theta_s^{ST}$$

defines the branching or metastable point at that pressure (and for that set of parameters). Corresponding to this special value of the surface temperature, a change of the character of stability occurs at a given pressure: for $\theta_s < \theta_s^{ST}$ all the potential equilibrium solutions at that pressure (corresponding to different ambient temperature and/or heat loss from the burning propellant) are statically unstable (roots B_i), while for $\theta_s > \theta_s^{ST}$ all the equilibrium solutions at that pressure are statically stable (roots A_i).

Therefore, the branching point at a given pressure isolates the critical static stability value, θ_s^{ST} , of the surface temperature at that pressure under which no steady reacting solution is allowed. Construction of the static burning boundary on the R vs $q_{g,s}$ plane, in a range of pressure, consists of connecting the critical static burning points defined for each pressure of interest in the wanted range (and for a given set of parameters). This implies the search of the branching point at any fixed pressure.

A general method (based on nonadiabaticity of the propellant) for solving this problem consists in assigning a larger and larger heat loss to the burning propellant until just one solution is found (coalescing from the statically stable and unstable roots). Obviously, this search can be made directly for any flame model, without knowledge of the static restoring function (see Fig.12). However, the same results should be obtained by searching the coalescence of the corresponding A and B roots of the static restoring function. This is illustrated in Fig. 13 ($p=20$ atm) for the MTS flame with $n=3$ polynomial. The closeness of the two sets of results confirms the validity of the ODE formulation of the problem. Obviously, this second approach is affected by the choice of the approximating profile. The quantitative differences between the two sets of results may be appreciated by comparing Tab. 6 (based on heat feedback) with Tab. 7 (based on static restoring function with $n=3$) of Ref. 9. Other burning limits, such as the pressure deflagration, will be more profitably discussed in Sec. 4.6.

4.4.3 - Measurement of Static Stability Strength

The static stability analysis can be put on a quantitative basis by means of the "first" Lyapunov criterion (Ref. 140). According to this, the solution of the nonlinear autonomous ODE of Eq. 4.4.1 is stable in the neighborhood of a point θ_s^* if

$$\left[\frac{df(\theta_s - \bar{\theta}_s)}{d\theta_s} \right]_{\bar{\theta}_s = \theta_s^*} < 0$$

at the point of interest θ_s^* . The physical meaning of this criterion was explained in Sec. 4.3.1. In keeping with the spirit of this physical interpretation, the strength of the stability of the solution at a point θ_s^* may be measured by the magnitude of the derivative $df/d\theta_s$ evaluated at $\bar{\theta}_s = \theta_s^*$. How this value is affected by typical parameters s is shown in Tab. 3. In the exceptional case of a branching, or metastable, point in which the unstable and the stable solutions coalesce, the above first criterion is not valid. In the present situation, however, it is enough to say that the point θ_s^{ST} is stable from one side ($\theta_s > \theta_s^{ST} + \epsilon$) while it is unstable on the other side ($\theta_s < \theta_s^{ST} - \epsilon$), so that, overall, the point θ_s^{ST} is said to be unstable. It should be clear that the first Lyapunov criterion (used for measuring the strength of the stability) is essentially a linearization criterion of the originally nonlinear ODE. However, it is plausible that both roots C and A are stable to finite disturbances of an unknown size, also. The extent of the stability region around the stable roots could be estimated by the Lyapunov "direct" method; but this is not a purpose of this analysis. Physically, it is expected that the range of stability of C root (always stable) is limited upward by B, while the range of stability of A root (if stable) is limited downward by B. But dynamic effects may increase the range of stability of C root against the range of stability of A root.

4.5 - NONLINEAR DYNAMIC BURNING STABILITY

It is wished to predict, under an appropriate set of assumptions, the behavior of a combustion wave initially propagating steadily under a given set of operating conditions and then subjected to arbitrary but known changes in time of pressure and/or radiant flux. This is easily done if an ODE formulation of the problem is available.

Dynamic stability of a burning propellant relates to transition of the propellant, from a given initial, to some final set of operating conditions for which multiple equilibrium configurations (statically stable) are allowed. A burning propellant is dynamically stable if the wanted transition is successful; if the transition leads to a final configuration different from the wanted one, the burning propellant is dynamically unstable.

The nonlinear ODE of Eq. 4.2.12 describes the instantaneous response of the system to a finite size departure

of the surface temperature from the stationary value due not only to intrinsic perturbation sources (static stability), but also to any arbitrary but externally assigned monotonical change in time of pressure and/or radiant flux (dynamic stability). This can be of great advantage for describing time histories of ignition and/or extinction transients. However, a more important and fruitful point of view can be taken. Indeed, it was already emphasized in Sec. 4.2 that the surface temperature time derivative is governed by the static restoring $f(\theta_s - \bar{\theta}_s)$, even for finite size disturbances, both for static and dynamic burning stability. It was shown that this holds true after the disturbance for forcing functions levelling off in time and instantaneously for forcing functions monotonically decreasing in time (Ref. 22). Studying the nature of the algebraic static restoring function leads to a very general burning stability analysis without ever solving the nonlinear ODE of Eq. 4.2.12 or PDE of Eq. 3.1.2.

4.5.1 - Dynamic Extinction of Solid Propellants

In this subsection inquiry is made about the possibility of dynamic extinction of the solid propellant even though it may be capable of statically stable burning for the given final set of operating conditions. It is expected that this will be a function of the rate of decrease of the operating conditions from the initial set of values. Specific reference to this question will be made, but the overall line of attack is of a general nature.

The objective is to predict when an allowed static transition (realized through a succession of exclusively steady state configurations) becomes forbidden if one attempts to realize it in a transient (quasi-steady gas phase) fashion.

Dynamic stability analysis requires consideration of the nonlinear ODE of Eq. 4.2.12. The basic difference from the static stability analysis is that the rate of return of the surface temperature toward the equilibrium value now depends explicitly on time, so that no a priori analysis is possible. However, Eq. 4.2.12 shows that the rate of the response of the system can be separated in two terms: of these, $f(\theta_s - \bar{\theta}_s)$ is the autonomous contribution previously discussed while $g(\tau, \theta_s - \bar{\theta}_s)$ is the nonautonomous contribution due to the finite disturbance subsequent to the given timewise change of forcing functions.

The main interest is the asymptotic behavior of the system for $\tau \rightarrow \infty$: to predict whether the final stable equilibrium point A_f or the trivial solution $\theta_s = 0$ will be reached (Fig. 14). For the wide range of controlling parameters varying in time according to monotonically decreasing functions, it follows from Eq. 4.2.10 that before and after the externally controlled transition, the rate of return of surface temperature toward the equilibrium value is governed by the autonomous term $f(\theta_s - \bar{\theta}_s)$, whose properties have been already illustrated.

A qualitative picture of the behavior of the burning propellant, for a given set of initial conditions, can be portrayed in the plane $d\theta_s/d\tau$ vs θ_s (Fig. 14). Points A_i and A_f are respectively the statically stable initial and final equilibrium configurations. All trajectories (representing the history of the system) in Fig. 14 start from the point A_i and terminate either at the point A_f or at the origin of the axes (root C, dynamic extinction). In the qualitative portrait of Fig. 14 the nonlinear characteristics $f(\theta_s - \bar{\theta}_{i,s})$ at $\tau=0$ and $f(\theta_s - \bar{\theta}_{f,s})$ at $\tau \rightarrow \infty$ have been represented. On the horizontal axis, the surface temperature corresponding to the branching point θ_s^{ST} at the operating pressure has been marked. This value (statically critical point) separates the statically stable points (A_i, A_f) from the statically unstable points (B_i, B_f). For a quasi-steady transition, the trajectory starting from point A_i progresses into the negative half-plane $d\theta_s/d\tau < 0$, since the term $g(\tau, \theta_s - \bar{\theta}_{i,s})$ initially dominates the term $f(\theta_s - \bar{\theta}_{i,s})$ in the ODE of Eq. 4.2.12. But $g(\tau, \theta_s - \bar{\theta}_{i,s})$ decreases monotonically toward zero. When $g(\tau, \theta_s - \bar{\theta}_{i,s})$ becomes negligible compared to $f(\theta_s - \bar{\theta}_{i,s})$, the latter term might drive the trajectory toward the final root A_f .

The rate of return of the surface temperature toward equilibrium for $\tau \rightarrow \infty$ (in the sense $\tau > \tau_{ext}$) is controlled only by the autonomous term. This means that, in the disturbance history, it is the intrinsic stability of the final state that tends to govern the behavior of the system. At a given value of pressure, the critical "no-return" point is defined by the statically unstable root B_f associated with the final statically stable root A_f through the function $f(\theta_s - \bar{\theta}_s)$. The whole segment between θ_s^{ST} and B_f is statically unstable but allows a dynamic burning regime. The statically unstable root B_f in Fig. 14 represents a limiting condition which is a unique property of the system at the operating (final) pressure. This analysis can be repeated for different values of pressure, so that a dynamic

stability boundary may be constructed. The dynamic stability boundary just determined will be called, for the remainder of this work, lower dynamic stability boundary (cf. Sec. 4.4.2)

The statically unstable root B_f in Fig. 14 represents a limiting condition which is a unique property of the propellant at the operating pressure (for a given set of parameters, it depends only on the properties of the intended final state). The line connecting all the points B_f is the lower dynamic stability boundary for any combination of forcing functions monotonically decaying. No problem arises if one wishes to consider the effect of other parameters (for example the ambient temperature) on the lower dynamic stability boundary: it is enough to determine the statically unstable root for each set of parameters of interest. An example is given in Fig. 15.

The existence of a lower dynamic stability boundary different from the static burning boundary (see Sec.4.4.2) and the static burning stability boundary (see Sec.4.6) has been shown. Crossing of this boundary is enough to assure dynamic extinction. At least two large classes of situations can be envisaged. For the wide range of controlling parameters varying in time according to monotonically decreasing functions (e.g.: linear, parabolic, exponential, etc.), the lower dynamic stability boundary holds true instantaneously, in that crossing of the boundary at any instant, even during the action of the external disturbance, is sufficient to yield dynamic extinction. Indeed, for monotonically decreasing functions the effect of $g(\tau, \theta_s - \bar{\theta}_s)$ is to favor extinction independently of $f(\theta_s - \bar{\theta}_s)$. For the wide range of controlling parameters varying in time according to levelling off (i.e., with zero final derivative in time) functions not necessarily monotonic (e.g., pulses of arbitrary shape), the lower dynamic boundary holds true "asymptotically", in that crossing of the boundary assures dynamic extinction only after the action of the external disturbance. Indeed, for levelling off functions the effect of $g(\tau, \theta_s - \bar{\theta}_s)$ depends on the details of the specific function g being used. A priori it can only be said that, following the action of the external disturbance (i.e., for $\tau > \tau_{ext}$), the term $g(\tau, \theta_s - \bar{\theta}_s) \rightarrow 0$ and dynamic extinction is exclusively controlled by $f(\theta_s - \bar{\theta}_s)$.

In the general ODE formulation of Eq. 4.2.12, the influence of time varying external parameters is felt only

through time derivatives. This implies that, if no change of forcing functions occurs, the burning propellant is only subjected to random intrinsic fluctuations and the results from the static stability analysis apply. It is also implied that, in the case that $g(\tau, \theta_s - \bar{\theta}_s) \ll f(\theta_s - \bar{\theta}_s)$, the dynamic stability boundary is a no-return boundary for any τ and for any external law. Under these circumstances, the dynamic stability range coincides with the range of influence of the statically stable configuration $\bar{\theta}_s$.

4.5.2 - Lower and Upper Dynamic Combustion Stability

So far, only dynamic effects associated with a B-type root (see Fig. 6) have been discussed. In fact, similar dynamic effects are also associated with a D-type root (see Fig. 6). The former is called lower dynamic stability and the latter is called upper dynamic stability. Although the last has been essentially neglected in the literature, both types of instabilities are very important in practice. Lower dynamic stability relates to extinction. Upper dynamic stability relates to vigorous accelerations of the combustion wave and pressure build-up due to large mass production; eventually mechanical failure of the enclosing vessel or dynamic extinction might follow. Upper instability is treated in detail in Sec. 4.6.

4.6-BIFURCATION PHENOMENA

Plotting of the static restoring function is useful for discriminating between (statically) stable and unstable roots. The stability character of any root changes with the operating conditions (including values of the external controlling parameters and thermokinetic properties of the propellants). Static restoring function plots, under a wide variety of operating conditions, are reported in Ref. 9.

A more significant representation is obtained by plotting the nondimensional surface temperature vs a given parameter of interest. This plot shall be called bifurcation diagram. Plotting of bifurcation diagrams is useful for discriminating between different static domains of burning. The following sections are dedicated to self-sustained oscillatory burning, seen as a bifurcated solution from the common time-independent steady burning.

4.6.1 - Morphology of the Static Restoring Function

By proper variations of the operating conditions, the static restoring function typically evolves from the "regular" CBA-type to CBADE, then to CBDAE after A-D roots coalescence, and finally to CAE after B-D roots coalescence. The only known alternative behavior to this general pattern is the "regular" CBA-type of restoring function reducing to C only (after B-A roots coalescence); this is associated with large enough increases of heat loss rate from the burning propellant and originates the static burning boundary discussed in Sec. 4.5.2.

When the static restoring function is of the type CBA, the only dynamic effects permissible are those associated with B-root. This implies the possible occurrence of dynamic extinction.

When the static restoring function is of the type CBADE, two unstable roots (B and D) of the perturbed energy equation sit at the sides of the stable steady state configuration of A-root. Under these circumstances, if the surface temperature during a transient goes past B or D, the combustion wave will accelerate respectively toward C ($R=0$; lower dynamic instability) or E ($R\neq 0$; upper dynamic instability). In the case of lower dynamic instability, the fate of the combustion wave is dynamic extinction. In the case of upper dynamic instability, the fate of the combustion wave is more involved. As soon as root D is passed, a vigorous acceleration occurs. The increase of burning rate may be of

orders of magnitude. Root E, strongly stable, violently pulls back the combustion wave toward a stable steady state configuration. Depending on the dynamics of the whole process, this can be either the reacting mode A or the unreacting mode C (dynamic extinction due to overstability). Dynamic extinction may be the unexpected result of a too fast pressurization (for example) transient; but this holds true only for quasi-steady gas phase!

When the static restoring function is of the type CBDAE, two stable roots (D and E) of the perturbed energy equation sit at the sides of the unstable steady state A-root. Under these circumstances, even in a static environment, the burning propellant is not capable of finding an equilibrium reacting configuration and bounces back and forth around A under the competing influences of D and E. It is confirmed by numerical integration that, after a transient, the combustion wave undergoes sharp self-sustained oscillations around A with peaks near D and E. This suggests the existence of a limit cycle. Being a limit cycle an overall property of the governing differential equation, once triggered this oscillatory behavior would not depend on the initial conditions of the system (see sec. 4.6.2). With this notable difference, i.e. self-sustained oscillations substituting for the time-independent solution as the stationary reacting state, all previous considerations on transients are valid. If the surface temperature momentarily goes past B, the combustion wave will irresistibly accelerate toward C (dynamic extinction). This may happen if the combustion wave is slowed down (e.g. by depressurization) and also if, in trying to accelerate the combustion wave (e.g., by pressurization), the system goes too much past E during the initial transient. Depending on the dynamics of the whole process, the final result of a transient toward a state controlled by a static restoring function of the type CBDAE is either a self-sustained oscillating combustion wave or dynamic extinction.

When the static restoring function is of the type CAE, two stable roots (C and E) respectively of the steady state energy equation and its perturbed form sit at the sides of the unstable steady state A-root. Under these circumstances, even in a static environment, the only possible steady solution is the trivial unreacting state corresponding to C-root. Since there is no alternative solution, this should be considered a static type of extinction. Notice, however, that the reason of this is lack of stability rather than lack of steady solution (cf. Sec. 4.4.2).

4.6.2 - Bifurcation Diagrams

Self-sustained oscillatory propagation of the combustion wave is strictly associated with static restoring function of the type CBDAE, that is between A-D roots coalescence and B-D roots coalescence. To detect this special configuration of the static restoring function, it is convenient to plot the values of its roots vs the parameter of interest (an external controlling parameter or a physical property) for the relevant set of operating conditions. These plottings shall be called bifurcation diagrams, because they show when the steady solution bifurcates from the time-independent A-root configuration to self-sustained oscillations between D and E roots. If such a bifurcation occurs, the independent variable takes the nature of a "bifurcation parameter".

Results found in the range 10 - 60 atm are graphically illustrated in the bifurcation diagrams of Fig. 16 (10 atm), Fig. 17 (20 atm), Fig. 18 (30 atm), Fig. 19 (40 atm), Fig. 20 (50 atm), and Fig. 21 (60 atm) for an hypothetical family of solid propellant formulations. In these bifurcation diagrams the values of the non-trivial roots A,B,D,E vs surface heat release (bifurcation parameter) are plotted for a given set of operating conditions. The plots of Figs. 16-21 were obtained implementing the MTS flame model with $n=3$ polynomial. It can be seen that:

- (1) the fundamental A-root monotonically increases with $Q_{s,ref}$;
- (2) B,D and E roots all lie on the same curve;
- (3) this S-shaped curve crosses the A-curve (bifurcation point).

For $Q_{s,ref}$ low enough, A and B are the only reacting roots; A defines the steady time-independent solution, while B defines the lower dynamic stability point. For increasing $Q_{s,ref}$, D and E roots branch off; A still is the steady solution, while B and D respectively define the lower and upper dynamic stability points. For further increases of $Q_{s,ref}$, A and D roots cross over and exchange their stability character; the steady solution, even in a static environment, is now self-sustained oscillatory burning, between D and E, around A. For $Q_{s,ref}$ even larger, B-D roots coalesce; under these circumstances there is no steady reacting solution.

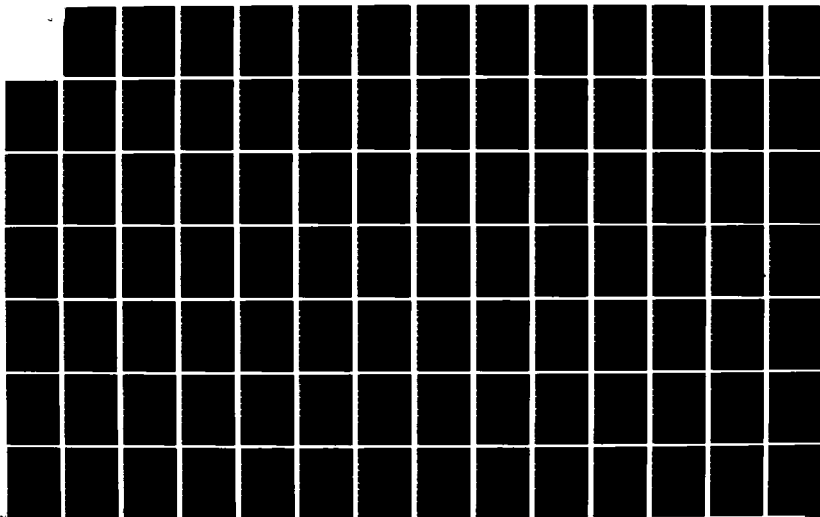
AD-A143 573

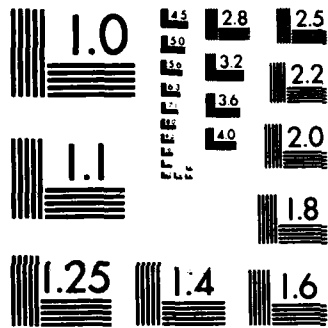
NONLINEAR BURNING STABILITY OF SOLID PROPELLANTS(U)
POLITECNICO DI MILANO (ITALY) IST DI MACCHINE
L DE LUCA ET AL. 31 DEC 83 DAJ37-81-C-0215

2/4

UNCLASSIFIED

F/G 21/9. 2 NL





MICROCOPY RESOLUTION TEST CHART
NATIONAL BUREAU OF STANDARDS-1963-A

4.6.3 - Self-Sustained Oscillatory Burning

Self-sustained oscillatory burning may only be found, at a given pressure, for $Q_{s,ref}$ values ranging between A-D roots coalescence and B-D roots coalescence. Both A-B roots and B-D roots coalescence occur for increasing $Q_{s,ref}$ with increasing pressure. However, the extent of this critical $Q_{s,ref}$ interval shows only minor increases with increasing pressure. A maximum amount of surface heat release is allowed by KTSSN flame according to Eq. 3.3.11. No such a limitation exists for MTS flame.

Remark that $Q_{s,ref}$ ranging within the proper values (restoring function of the type CBDAE) is a necessary, but not sufficient condition for the occurrence of self-sustained oscillatory burning. Dynamic extinction, due to decelerating deflagration waves or overstability, is always an alternative to the self-sustained oscillatory burning. Even without external disturbance, the actual range of $Q_{s,ref}$ values for which self-sustained oscillatory burning may occur is narrower than the nominal range obtained from the corresponding bifurcation diagrams. Indeed, in this oscillatory regime, the burning propellant bounces back and forth under the competing influence of D and E roots. For dynamic reasons, the amplitude of the surface temperature oscillations has to be somewhat larger than $\theta_s(E) - \theta_s(D)$. This implies that, especially near B-D roots coalescence, extinction will somewhat shrink the $Q_{s,ref}$ range of self-sustained oscillatory burning.

It will be seen in next section that $Q_{s,ref}$ is not the only parameter capable to generate self-sustained oscillatory burning. Therefore, the comments offered in this section have a general validity and are not at all restricted to the influence of $Q_{s,ref}$ only.

The frequency of the self-sustained burning oscillations is expected to be somewhat related to the condensed phase thermal wave relaxation time (at the final operating conditions of a burning transient):

$$(4.6.1) \quad \Omega \cong 1/\tau_{th,c} = \bar{R}^2(P, F_o, \theta_{-\infty}) = \bar{P}^{2n}$$

However, the exact meaning of this parameter is open to questions, in the present context. This point will be dealt with further.

A physical interpretation of the mechanism driving the self-sustained burning oscillations is offered in Sec.4.6.5. In the meanwhile, observe that the transition from the time-independent steady solution to the self-sustained oscil-

4.6.2 - Bifurcation Diagrams

Self-sustained oscillatory propagation of the combustion wave is strictly associated with static restoring function of the type CBDAE, that is between A-D roots coalescence and B-D roots coalescence. To detect this special configuration of the static restoring function, it is convenient to plot the values of its roots vs the parameter of interest (an external controlling parameter or a physical property) for the relevant set of operating conditions. These plottings shall be called bifurcation diagrams, because they show when the steady solution bifurcates from the time-independent A-root configuration to self-sustained oscillations between D and E roots. If such a bifurcation occurs, the independent variable takes the nature of a "bifurcation parameter".

Results found in the range 10 - 60 atm are graphically illustrated in the bifurcation diagrams of Fig. 16 (10 atm), Fig. 17 (20 atm), Fig. 18 (30 atm), Fig. 19 (40 atm), Fig. 20 (50 atm), and Fig. 21 (60 atm) for an hypothetical family of solid propellant formulations. In these bifurcation diagrams the values of the non-trivial roots A,B,D,E vs surface heat release (bifurcation parameter) are plotted for a given set of operating conditions. The plots of Figs. 16-21 were obtained implementing the MTS flame model with $n=3$ polynomial. It can be seen that:

- (1) the fundamental A-root monotonically increases with $Q_{s,ref}$;
- (2) B,D and E roots all lie on the same curve;
- (3) this S-shaped curve crosses the A-curve (bifurcation point).

For $Q_{s,ref}$ low enough, A and B are the only reacting roots; A defines the steady time-independent solution, while B defines the lower dynamic stability point. For increasing $Q_{s,ref}$, D and E roots branch off; A still is the steady solution, while B and D respectively define the lower and upper dynamic stability points. For further increases of $Q_{s,ref}$, A and D roots cross over and exchange their stability character; the steady solution, even in a static environment, is now self-sustained oscillatory burning, between D and E, around A. For $Q_{s,ref}$ even larger, B-D roots coalesce; under these circumstances there is no steady reacting solution.

latory steady solution is "abrupt"; indeed immediately after the bifurcation, oscillating combustion of finite amplitude and frequency is expected. This can be viewed as "hard excitation".

4.6.4 - Bifurcation parameters

The quantity $Q_{s,ref}$ (net heat release at the burning surface under reference conditions) was the first to be recognized as a bifurcation parameter in 1976 (Ref. 11). The peculiar effects of $Q_{s,ref}$ were observed in a previous paper (Ref. 136a, p. 284), but were not thoroughly investigated (perhaps because suspected to be a numerical failure). Kooker and Nelson, in 1979, confirmed the bifurcating property of $Q_{s,ref}$ thanks to a careful numerical work (Ref. 103).

This research group dedicated much attention to bifurcation phenomena. By systematic plotting of bifurcation diagrams, it was inquired whether other quantities would exhibit the same bifurcation character illustrated in the previous section for $Q_{s,ref}$. The surprising answer is that the peculiar effects initially attributed only to $Q_{s,ref}$ seem to be a general property of the combustion parameters! It was found that Q_c , heat release of the condensed phase distributed reactions (if any), behaves just like $Q_{s,ref}$: see Fig. 22 ($p=50$ atm, $Q_{s,ref}=125$ cal/g, $\tilde{E}_c=30$ kcal/mole), Fig. 23 ($p=20$ atm, $Q_{s,ref}=125$ cal/g, $\tilde{E}_c=30$ kcal/mole), Fig. 24 ($p=50$ atm, $Q_{s,ref}=125$ cal/g, $\tilde{E}_c=15$ kcal/mole), and Fig. 25 ($p=50$ atm, $Q_{s,ref}=145$ cal/g, $\tilde{E}_c=15$ kcal/mole). All of these plots were obtained by implementing the KTSSN flame model with $n=3$ polynomial. The general features remarked in the previous section hold true, except that now the fundamental A-root remains constant with Q_c due to the different flame model implemented. By comparing Figs. 22-25, it is predicted that bifurcation occurs for increasing Q_c (larger range of static stability) when: pressure increases, $Q_{s,ref}$ decreases, \tilde{E}_c decreases.

The quantity E_c , activation energy of the condensed phase distributed reactions (if any), is also a bifurcation parameter: see Fig. 26 ($Q_{s,ref}=125+Q_c=100$ cal/g), Fig. 27 ($Q_{s,ref}=125+Q_c=50$ cal/g), and Fig. 28 ($Q_{s,ref}=100+Q_c=25$ cal/g). These plots were again obtained by implementing the KTSSN flame model with $n=3$ polynomial. By comparing Figs. 22-25 with Figs. 26-28 it is predicted that bifurcation occurs for increasing E_c (larger range of static stability) when: pressure increases, $Q_{s,ref}$ decreases, Q_c decreases.

Another important bifurcation parameter, the operating pressure p , is discussed in next section.

The quantity \tilde{E}_s , activation energy of the Arrhenius type of pyrolysis law, and the corresponding quantity w , power of the KTSS type of pyrolysis law, are the only parameters so far tested not yielding marked bifurcation: see respectively Fig. 29 (\tilde{E}_s) and Fig. 30 (w). Several plots performed for a wide range of operating conditions confirmed such a particular behavior of the roots A-D. This implies that the steady solution is usually given by the time-independent equilibrium configuration defined by root A; however oscillations can be found in the regions where the root D approaches the root A.

4.6.5 - Pressure Deflagration Limit

The most important bifurcation parameter investigated during this research program is the pressure. Bifurcation plottings reveal that decreasing values of pressure yield first self-sustained oscillations and then instability of the steady state solution. For example, see Fig. 31 ($Q_{s,ref} = 125 + Q_c = 50$ cal/g) and Fig. 32 ($Q_{s,ref} = 125$ cal/g) for the propellant AP/PBAA No. 941; Figs. 33-37 ($Q_{s,ref} = 125$ cal/g and optimum values of \tilde{E}_s and n_s) for the propellant AP84/CTPB 16. All of these plots were obtained by implementing the KTSSN flame model with $n=3$ polynomial. By comparing these and other plots not reported, it is predicted that bifurcation occurs for decreasing pressure (larger range of static stability) when $Q_{s,ref}$ decreases, Q_c decreases, \tilde{E}_c decreases, \tilde{E}_s or w decrease, C_c decreases, K_c increases.

Notice that the bifurcation plottings of Fig. 31-37 naturally yield a PDL prediction, when the pressure is such that B-D roots coalesce. Indeed, for $p < p(B=D)$ no self-sustained steady combustion regime can exist. Notice also that for $p(B=D) < p < p(A=D)$ self-sustained oscillations are expected; this allows an easy experimental verification of the theory and moreover points to the burning stability character of the PDL. To this respect, remark that radiative heat loss from the burning surface with $\bar{\epsilon}_\lambda = 0.75$ was found to be too small to be of any consequence. Finally, notice that for $p = p(B=D) = PDL$ is no longer possible to distinguish fast depressurization extinction (surface temperature dropping below B-root) from low pressure extinction (steady state solution impossible because A-root is unstable and D-root disappears).

A physical interpretation of these results can be summed up saying that for heterogeneous thin flames two

main propagating regimes are possible: in the first (time-independent steady state), typical of higher pressures, the coupling between gas and solid phases is very tight, so that at each instant only one distribution of temperature is allowed. This can be also expressed by saying that, in a broad sense, the energy transfer between the two phases is matched. In the second regime, typical of lower pressures, the burning mode is steady oscillatory, i.e. periodic in time, with constant amplitude and frequency. This implies a looser coupling between solid and gas. For instance, following a burning rate spike, the condensed phase temperature will drop and reach values lower than the ones corresponding to steady state burning. At that point the heat feedback from the gas will be much larger, and drive slowly (the characteristic conductive condensed phase time is long at low pressure) the surface temperature high again. Being the warming time long, a thick heated layer is generated at relatively low surface temperature. When the surface temperature reaches the proper value, a burning spike again occurs in the form of volumetric thermal explosion, closing the cycle that can continue indefinitely ("onion peeling" mechanism). At lower and lower pressure the oscillations have larger and larger amplitudes; during a cycle the surface temperature moves closer and closer to values below which the increase in heat flux from the gas to the solid is not enough to compensate the decrease of heat release at the burning surface and support in a stable way the thickening of the thermal conductive layer in the condensate phase. When that happens, "recovery" after a temperature fall is not possible. The corresponding pressure is the pressure deflagration limit.

4.6.6 - A Physical Interpretation of the Bifurcation Diagram

For sake of clarity reference is made to Fig. 38, but the discussion is valid for bifurcation diagrams in general. The symbol (-) denotes regions where heat conducted away in the condensed phase is dominant; in these regions the instantaneous burning rate tends to decrease. The symbol (+) denotes regions where energy releases (in the gas phase or at the burning surface or in the condensed phase) are dominant; in these regions the instantaneous burning rate tends to increase. It follows that root C (not shown) when allowed is always stable, while root A loses its stability after crossing the D-root branch. The transition from root A stable (time-independent steady state solution) to self-sustained D-E oscillations occurs for: decreasing p , increasing $Q_{s,ref}$, increasing Q_C , increasing \bar{E}_C .

If the burning propellant suffers heat losses, root A decreases and root B increases (as shown by the arrows in Fig. 38). For a critical maximum value of heat loss rate, root A and root B merge: this is the static burning boundary for the given set of operating conditions.

4.7 - EFFECTS OF THERMAL PROPERTIES

To observe the influence of the ratio $C_g = c_g/c_{ref}$, the bifurcation diagram of Fig. 18 (MTS flame and $C_g=1$) was re-plotted in Fig. 38 with $C_g = 1.12$. By comparing the two figures, it is predicted that increasing values of C_g moves the bifurcation point (A=D coalescence) toward larger $Q_{s,ref}$ and reduces the amplitude of self-sustained oscillations. In a broad sense, $C_g \neq 1$ favors the static burning stability.

Thermal conductivity of condensed substances is usually temperature dependent; both increasing and decreasing functions are common. In this research program the mathematical model can accommodate any law. To fix the ideas, let us consider the common case

$$(4.7.1) \quad K_c(\theta) \equiv k_c(T)/k_{ref} = 1+b\theta$$

where b is an arbitrary constant of positive or negative sign. A bifurcation diagram vs $Q_{s,ref}$ is plotted in Fig. 39 with $b=0$ or $b=1$ and $C_g = 1.12$ or 1.24 . By comparing the curves, it is predicted that thermal conductivity increasing with temperature moves the bifurcation point (A=D coalescence) toward larger $Q_{s,ref}$ and reduces the amplitude of self-sustained oscillations. In a broad sense, $K_c(\theta)$ increasing with temperature favors the static burning stability. It was also found that changing the constant b from negative to positive values makes dynamic extinction more and more difficult (lower B-root). A similar effect can be observed in Fig. 36 for increasing C_g .

Specific heat of condensed substances is usually temperature dependent; typically, increasing functions are found. In this research program the mathematical model can accommodate any law. To fix the ideas, let us consider the common case

$$(4.7.2) \quad C_c(\theta) = c_c(T)/c_{ref} = 1+a\theta$$

where a is an arbitrary constant of positive or negative sign. Obviously, the value of $C_c(\theta)$ has to be properly

matched with C_g at the burning surface. Static stability burning, in a broad sense, is favored by large values of C_g and/or small positive values of a . Likewise dynamic extinction is made more difficult, i.e. B-root decreases, by large values of C_g and/or small positive values of a . In general terms, realistic physical results are obtained with large values of c_g (say, 0.5 cal/gK) and small values of a (say, 0.1-0.2), being $c_{ref} \approx 0.3$ cal/gK typically.

4.8 - EFFECTS OF CONDENSED PHASE DISTRIBUTED REACTIONS

For sake of simplicity only one-step, zero order reactions have been considered so far. By recalling the constraint of Eq. 3.1.20, the characteristic thickness of the condensed phase chemical layer is found to be

$$(4.8.1) \quad \delta_{ki,c}(P) \equiv \bar{R} \tau_{ki,c} = \frac{\int_{-\infty}^0 \exp(-\bar{E}_c/\bar{T}) dX}{\exp(-\bar{E}_c/\bar{T}_s)}$$

The characteristic thickness of the condensed phase conductive thermal layer, for inert solid and constant thermal properties, is usually defined as

$$\delta_{th,c}(P) \equiv 1/\bar{R},$$

implying that $\bar{\theta}(X=3\delta_{th,c})=0.05 \bar{\theta}_s$. For consistency, the above definition was generalized to reacting solids as follows

$$(4.8.2) \quad \delta_{th,c}(P) = X(\bar{\theta}/\bar{\theta}_s = 0.05) / 3.$$

Plottings of $\delta_{th,c}$ and $\delta_{ki,c}$ vs pressure are reported in Fig. 40 for several values of Q_c and \bar{E}_c . The thermal properties were kept constant, except few cases where variable thermal conductivity was considered. Both thicknesses decrease with pressure; in particular, the chemical layer thickness decreases also with decreasing Q_c and increasing \bar{E}_c . However, for the tested range of the parameters, the thermal layer thickness is not significantly affected by the presence of chemical reactions. Despite this fact the effects on the combustion stability of distributed chemical reactions is perceivable. The results obtained show that

both static and dynamic stability are depressed by large values of \bar{E}_c , while large values of Q_c depress static stability but favor dynamic stability (lower values of B-root).

4.9 - THE BURNING RATE VS PRESSURE PLOT REVISITED

The practical meaning of the nonlinear combustion stability analysis developed in this chapter is perhaps better appreciated in the plot shown in Fig. 41. This is a standard burning rate (nondimensional) vs pressure diagram plotted on logarithmic scales for graphical convenience. The $\bar{R}(p)$ curve is obtained experimentally and corresponds to A-root. MTS flame reproduces the experimental $\bar{R}(p)$ curve with some tolerance due to the fitting procedures required to evaluate the proper gas phase parameters; however, this tolerance can be made negligible. All other flame models reproduce $\bar{R}(p)$ perfectly, except KZ which needs to be properly modified. The combustion stability properties shown in Fig. 41 were obtained implementing KTSSN flame with $n=3$ polynomial. The nonlinear combustion stability analysis predicts for large pressures the usual time-independent steady burning rate; for decreasing pressure, the steady burning rate is self-sustained oscillatory; for further decreasing pressure, the only stable steady solution left is the unreacting state $\bar{R}=0$. The minimum pressure permitting self-sustained steady burning is the pressure deflagration limit PDL. It is emphasized that PDL is associated with loss of static burning stability rather than lack of steady burning rate solution. The fact that, for decreasing pressure, the burning wave "jumps" abruptly from the usually time-independent steady configuration to a large amplitude self-sustained oscillatory configuration before getting fully extinguished was predicted in Ref. 98 from a totally different standpoint. The nonlinear combustion stability analysis furthermore predicts in Fig. 41 the dynamic extinction boundary and the static burning boundary. The region of dynamic stability is bounded also upward by an upper dynamic stability boundary (drawn only partly for graphical reasons), which lies somewhat above the $\bar{R}(p)$ curve from $p > p(A=D)$ up to some maximum pressure; in this pressure range damped oscillatory burning may occur.

For a given propellant composition, pressure is seen in general to favor combustion stability; however, remark that the plot of Fig.41 was obtained for adiabatic burning at reference ambient temperature. A possible physical explanation of the stabilizing effect of pressure is the following. Any self-sustained reactive system is capable of exothermic

reactions. These generally occur in the gas phase (H_f), at the burning surface (H_s), and in the condensed phase (H_c). The total energy release $H_f(P) + H_s(\theta_s) + H_c(\theta < \theta_s)$ is determined by the energy balance on the overall steadily burning propellant for the given set of operating conditions. For a fixed set of operating conditions, q_s increases while $q_{g,s}$ decreases for increasing burning rate. For low values of H_s , an increase of burning rate and thereby of $q_s \equiv R H_s$ is counterbalanced through a simultaneous decrease of $q_{g,s} \sim 1/R$ and increase of the heat flux $q_{c,s} \sim R\theta_s$ absorbed into the condensed phase. However, for large values of H_s , an increase of burning rate might be destabilizing if q_s increases more than $(q_{c,s} - q_{g,s})$. This implies an acceleration of the combustion wave, that is the appearance of a D-type root in the nonlinear static restoring function. On the other hand, for the same set of operating conditions, a large increase of burning rate (up to orders of magnitude) is strongly stabilizing. Indeed, under these circumstances, the increase of $q_{c,s}$ is much larger than the increase of $(q_s + q_{g,s})$ due to the Arrhenius-type dependence of the surface temperature on the burning rate. This corresponds to the appearance of an E-root in the nonlinear static restoring function. Therefore, at each pressure a critical (A-D roots coalescence) value of surface heat release exists above which the energy coupling between condensed and gas phases becomes locally unstable, i.e. a burning rate disturbance due to the change of heat flux absorbed into the condensed phase is counterbalanced only "in the large" (through a limit cycle process) by an appropriate change of heat feedback from the flame and the surface reacting layer. At each pressure a second larger critical (B-D roots coalescence) value of surface heat release exists above which the energy coupling between condensed and gas phases becomes totally unstable (except at the trivial root C), due to the excessively large thermal gradients occurring in the condensed phase near the burning surface.

As to the pressure effect, increasing pressure implies increasing H_f and shrinking the flame thickness (see Eq. 3.1.22). Both effects imply increasing $q_{g,s}$, which subsequently require a larger value of $H_s + H_c$ for destabilizing the combustion wave. Larger pressure requires larger value of $H_s + H_c$ for triggering both upper instability and the self-sustained oscillation mechanism.

4.10 - CONCLUDING REMARKS ON COMBUSTION STABILITY

All stability features discussed in this chapter were determined within the framework of a thermal model of thin (quasi-steady) heterogeneous flames. Both static and dynamic combustion properties, including self-sustained oscillatory burning, are related to the thermokinetics of the deflagrating surface. Diffusive effects and wave propagation in the gas phase were neglected.

The general behavior of thin heterogeneous flames, for decreasing pressure, in the standard burning rate vs pressure plot (Fig. 41) includes stationary burning, damped oscillatory burning, self-sustained oscillatory burning, and no self-sustained reacting solution. The critical value of pressure under which self-sustained reacting solutions are no longer allowed is the pressure deflagration limit. The available quasi-steady flame models are questionable in this marginal burning domain; however, this new concept of pressure deflagration limit associated with heterogeneous (thermokinetic) burning instability rather than non adiabaticity of the combustion waves makes sense. Nonadiabaticity increases the value of pressure deflagration limit; other stability boundaries are affected as well.

The overall picture of thin heterogeneous flames seems fully understood. Remark that the transient behavior of such flames is predicted for both pressure and radiation driven combustion waves. Thin heterogeneous flames are (Fig. 41): statically impossible and dynamically unstable below the dynamic stability limit, statically and dynamically stable above the static burning limit, statically impossible but dynamically stable in the region between the two limits, statically and dynamically unstable for pressures below PDL. Recall that the dynamic limit is valid instantaneously for forcing functions monotonically decreasing in time, asymptotically ($\tau \gg \tau_{ext}$) for forcing functions of arbitrary shape but levelling off in time (in particular, pressure or radiation pulses).

A review of the results presented throughout this chapter shows that in general physical properties increasing the static stability strength (according to Lyapunov) of a given steady state configuration will also increase the B-root value, which implies easier dynamic extinction. This means that a burning propellant with a large enough reservoir allows larger instantaneous surface temperature drops without suffering dynamic extinction, but also finds more difficult to dissipate energy excess near the steady state configuration.

CHAPTER 5 - NUMERICAL APPROACH

The numerical solution of the governing equations (see Chapter 3), together with the experimental approach, is required in order to check the validity of the analytical predictions (see Chapter 4) about the stability characteristics of heterogeneous deflagration waves. In this chapter, details of the numerical approach and typical results will be discussed.

5.1 - THE MATHEMATICAL PROBLEM

The mathematical model, whose numerical solution will be treated in this chapter, was introduced in Chapter 3. Equation 3.1.2 is a parabolic, strongly nonlinear partial differential equation in the unknown $\Theta(x, \tau)$, with the appropriate initial and boundary conditions. Other relationships required for the complete definition of the problem are reported in the same Chapter (Eqs. 3.1.3-3.1.22). The gas phase, exerting his influence through the energy balance at the burning surface, is treated by one of the thermal flame models previously discussed. In summary, we are dealing with a heat transfer problem inside a homogeneous solid material with variable thermal properties, assigned optical properties, and distributed chemical reactions according to the model described in Chapter 3. The burning surface regresses with rate $R(\tau)$, that is one of the unknowns of the problem. The forcing functions may be any assigned combination of pressure $P(\tau)$ and radiant flux intensity $F_0(\tau)$ coming from an external source. A further term taken into account is the radiant energy lost through the burning surface, while the convective phenomenon is neglected. The lateral surface of the sample is considered adiabatic.

Several interesting works (Refs. 144-146) about heat transfer problems were recently published. However, the numerical solution of the energy equation in a solid material, at least in the simple formulation including only unsteady and diffusive terms, has extensively been treated in the specialized literature. All the numerical schemes and the solution procedures implemented in this work were taken from standard textbooks (Refs. 147-148) and extended to include the further terms considered in this investigation.

5.2 - FORMULATION OF THE FINITE DIFFERENCE PROBLEM

This section, based on Ref. 24, extends the validity of the solution to include chemically reacting condensed phase. The mathematical formulation of the simple thermal diffusion problem in a solid strand leads to the following expression:

$$(5.2.1) \quad \frac{\partial \theta}{\partial \tau} = \sigma \frac{\partial^2 \theta}{\partial X^2} \quad \tau \geq 0 \text{ and } X \leq 0,$$

where σ is a positive constant. The discretization of Eq. 5.2.1 is widely discussed in Refs. 147-148. Two schemes taken from Ref. 147, pp. 189-191, will now be presented. The former (No. 13, p. 191, Ref. 147), synthetically shown in Fig. 42a, approximates the time derivative by the following weighted average in the neighborhood of the point we are solving for θ_j^{n+1} :

$$(5.2.2) \quad \frac{\partial \theta}{\partial \tau} \approx \frac{1}{12} \frac{3/2 \theta_{j+1}^{n+1} - 2 \theta_{j+1}^n + 1/2 \theta_{j+1}^{n-1}}{\Delta \tau} + \\ + \frac{5}{6} \frac{3/2 \theta_j^{n+1} - 2 \theta_j^n + 1/2 \theta_j^{n-1}}{\Delta \tau} + \frac{1}{12} \frac{3/2 \theta_{j-1}^{n+1} - 2 \theta_{j-1}^n + 1/2 \theta_{j-1}^{n-1}}{\Delta \tau}.$$

The second space derivative is numerically approximated by a standard central difference:

$$(5.2.3) \quad \frac{\partial^2 \theta}{\partial X^2} \approx \frac{\theta_{j+1}^{n+1} - 2 \theta_j^{n+1} + \theta_{j-1}^{n+1}}{(\Delta X)^2}.$$

From the point of view of the truncation errors (order of $(\Delta X)^4$), this scheme is one of the most advantageous. However, its utilization may give some problems in terms of computer core required for the simultaneous treatment of three thermal profiles: one "present" and two referring to the previous time steps. Due to this notable "memory of the past", this scheme is suitable for treatment of rapidly varying phenomena.

An alternative numerical method (No. 2, p. 189, Ref. 147), reported in Fig. 42b, resorts to the Crank-Nicholson scheme, where the time derivative is given by:

$$(5.2.4) \quad \frac{\partial \theta}{\partial \tau} \approx \frac{\theta_j^{n+1} - \theta_j^n}{\Delta \tau},$$

while the second space derivative is approximated by the following average

$$(5.2.5) \quad \frac{\partial^2 \theta}{\partial X^2} \approx \frac{(\theta_{j+1} - 2\theta_j + \theta_{j-1})^{n+1} + (\theta_{j+1} - 2\theta_j + \theta_{j-1})^n}{2(\Delta X)^2}.$$

This method, obviously simpler and less expensive in terms of computer core, presents the disadvantage of larger truncation errors (order of $(\Delta X)^2$).

Both the numerical schemes previously described are implicit and unconditionally stable when applied to the problem of Eq. 5.2.1. In Ref. 147, p. 195, it is also shown that the stability of both the methods is not affected by the presence of lower order terms weighted by constant coefficients. Unfortunately, in the problem we need to solve, the convective term (the first space derivative) contains a coefficient strongly nonlinear in the temperature. This fact not only affects the choice of the time step size, but also might influence the stability of the overall approach. The presence of further terms depending on temperature, both in the equation and in the boundary condition at the burning surface, makes any prediction about the stability characteristics of the approach even more questionable.

Independently on the numerical scheme used, the first space derivative is approximated by the "forward" difference (remark that the integration proceeds from $X \rightarrow \infty$ to $X=0$):

$$(5.2.6) \quad \frac{\partial \theta}{\partial X} \approx \frac{\theta_{j-1}^{n+1} - \theta_j^{n+1}}{\Delta X},$$

having verified that the backward scheme induces numerical instability.

The solution procedure is based on the following canonical form of the finite difference equation:

$$(5.2.7) \quad -A_j \theta_{j+1}^{n+1} + B_j \theta_j^{n+1} - C_j \theta_{j-1}^{n+1} = D_j \quad j=2, \dots, JF-1.$$

If the numerical scheme of Eqns. 5.2.2-5.2.3 is used, the coefficients are given by:

$$A_j = -\frac{1}{8} + \frac{\Delta\tau}{(\Delta X)^2} K_c(\theta_j^{n+1}) / C_c(\theta_j^{n+1})$$

$$B_j = \frac{5}{4} - R \frac{\Delta\tau}{\Delta X} + 2 \frac{\Delta\tau}{(\Delta X)^2} K_c(\theta_j^{n+1}) / C_c(\theta_j^{n+1}) + \frac{\Delta\tau}{(\Delta X)^2} [K_c(\theta_{j-1}^{n+1}) - K_c(\theta_j^{n+1})] / C_c(\theta_j^{n+1})$$

$$C_j = \frac{1}{8} - R \frac{\Delta\tau}{\Delta X} + \frac{\Delta\tau}{(\Delta X)^2} K_c(\theta_j^{n+1}) / C_c(\theta_j^{n+1}) + \frac{\Delta\tau}{(\Delta X)^2} [K_c(\theta_{j-1}^{n+1}) - K_c(\theta_j^{n+1})] / C_c(\theta_j^{n+1})$$

$$D_j = \left(\frac{1}{6} \theta_{j+1} + \frac{5}{3} \theta_j + \frac{1}{6} \theta_{j-1}\right)^n - \left(\frac{1}{24} \theta_{j+1} + \frac{5}{12} \theta_j + \frac{1}{24} \theta_{j-1}\right)^{n-1} +$$

$$+ \Delta\tau F_o^{n+1} \frac{1-\bar{\Gamma}}{\delta_a} \exp \left[\Delta X(j-1) / \delta_a \right] / C_c(\theta_j^{n+1})$$

$$- \bar{E}_c / R$$

$$+ \Delta\tau H_c A_c^{n+1} \exp \left[\frac{-\bar{E}_c / R}{\frac{1}{2}(\theta_j^{n+1} + \theta_{j-1}^{n+1}) (T_{s,ref}^{-T_{ref}})^{T_{ref}}} \right] / C_c(\theta_j^{n+1}) .$$

If the numerical scheme of Eqns. 5.2.4-5.2.5 is used, the coefficients are:

$$A_j = \frac{1}{2} - \frac{\Delta\tau}{(\Delta X)^2} K_c(\theta_j^{n+1}) / C_c(\theta_j^{n+1})$$

$$B_j = 1 - R \frac{\Delta\tau}{\Delta X} + \frac{\Delta\tau}{(\Delta X)^2} K_c(\theta_j^{n+1}) / C_c(\theta_j^{n+1}) + \frac{\Delta\tau}{(\Delta X)^2} [K_c(\theta_{j-1}^{n+1}) - K_c(\theta_j^{n+1})] / C_c(\theta_j^{n+1})$$

$$C_j = -R \frac{\Delta\tau}{\Delta X} + \frac{1}{2} - \frac{\Delta\tau}{(\Delta X)^2} K_c(\theta_j^{n+1}) / C_c(\theta_j^{n+1}) + \frac{\Delta\tau}{(\Delta X)^2} [K_c(\theta_{j-1}^{n+1}) - K_c(\theta_j^{n+1})] / C_c(\theta_j^{n+1})$$

$$\begin{aligned}
 D_j = & \theta_j^n \left[1 - \frac{\Delta\tau}{(\Delta X)^2} K_c (\theta_j^n) / C_c (\theta_j^n) \right] + (\theta_{j+1}^n + \theta_{j-1}^n) \frac{1}{2} \frac{\Delta\tau}{(\Delta X)^2} K_c (\theta_j^n) / C_c (\theta_j^n) + \\
 & + \Delta\tau F_o^{n+1} \frac{1 - \bar{r}_\lambda}{\delta_a} \exp \left[\Delta X (j-1) / \delta_a \right] / C_c (\theta_j^{n+1}) \\
 & + \Delta\tau H_c A_c^{n+1} \exp \left[\frac{-\bar{E}_c / R}{\frac{1}{2} (\theta_j^{n+1} + \theta_{j-1}^{n+1}) (T_{s,ref} - T_{ref}) + T_{ref}} \right] / C_c (\theta_j^{n+1}) .
 \end{aligned}$$

For $j=1$ or $j=JF$, Eq.5.2.7 accomodates the appropriate boundary conditions. The algebraic system derived from the above discretization of the PDE is then cast in a tridiagonal matrix. An efficient method of solution suitable for automatic computation is suggested, for example, in Ref. 147 (p. 199).

5.3 - STABILITY AND CONVERGENCE OF THE NUMERICAL SOLUTION

The strongly nonlinear nature of the problem imposes the assumption of small values of both time and space steps. Moreover, in order to accelerate the convergence of the solution during fast changes of the controlling parameters, the time evolution of the thermal profile is "guessed" at each time step by parabolic extrapolation, allowing to evaluate the temperature dependent coefficients in more realistic terms. A comparison between extrapolated and computed solutions is then performed and, if they differ of more than a prefixed tolerance, the procedure is repeated with a reduced time step size. On the contrary, when the agreement between predicted and computed solutions is very good, the time step size is automatically increased. In all cases, the time step will assume values within a prefixed range depending on the characteristic diffusive time in condensed phase ($\tau_{th,c} \times 10^{-6} \leq \Delta\tau \leq \tau_{th,c} \times 10^{-1}$). The practical consequence of this procedure is to keep strongly bounded the time gradient of the surface temperature (that is of the burning rate). The space step size is also subjected to several constraints: in particular the choice of ΔX is affected by the characteristic thicknesses of thermal, chemical, and radiant phenomena inside

the condensed phase besides the stability requirements of the numerical method. Large values of the extinction coefficient in the Beer's law and/or large activation energies of chemical reactions in the solid phase impose the choice of a small space step. Typical values are $\Delta X=0.01-0.05$ (remember that $\delta_{th,c}=1$ for adiabatic systems at $p=68$ atm) depending on the operating conditions.

Several checks were made in order to make sure that the overall numerical approach was performing as intended. The difficulties inherent in the numerical solutions deserve a full study by themselves; therefore, only semi-empirical tests were performed. For example, an obvious check is to compare the steady state solutions found numerically with the corresponding analytical solutions (when available). The appropriate choice of the time and space step sizes was verified by varying them in a programmed manner, while keeping the input data fixed, and making sure that no appreciable difference in the results could be detected by halving or doubling the mesh size. The stability of the overall numerical approach was checked by letting the computer run free on hypothetical transients with no change in time of the controlling parameters. In such operating conditions the two schemes show a slightly different behavior, specially when temperature dependent coefficients are considered: the scheme working on two time levels (Fig. 42b) presents oscillations of small (but sometimes not negligible) amplitude around the correct solution, while for the scheme working on three time levels (Fig. 42a) such oscillations are of amplitude absolutely negligible in all the tested cases. However, these are not conclusive tests and are, in principle, restricted to those specific situations in which they were performed. It was felt convenient to have some form of internal checks in the program itself, so that each run could at least be considered selfconsistent. Therefore, at each integration step, not only the cold boundary temperature and the BC1 error below mentioned, but also the integral balances of energy in the solid phase and across the whole deflagration wave are monitored. These must be viewed only as effective warning signal at any stage of the computation.

5.4 - SOME PROBLEMS RELATED TO THE BOUNDARY CONDITIONS

The boundary conditions of Eq. 3.1.2 are the energy balance at the burning surface and the thermal equilibrium with the surroundings at the cold end. The former should be applied to a thickness as small as possible, the latter refers to a part of the system as far as possible from the burning surface. To realize both these opposite requirements

two parameters are available: the number of nodes in the space net JF and the space step size ΔX . The values of such parameters are subjected to limitations of practical character. Several constraints on the space step size were already discussed in Sec. 3. Errors are introduced whenever the temperature gradient at the surface is evaluated using a too large space step. Physically, this is due to the fact that volumetric terms (radiation penetration, chemical reactions, convective and unsteady effects) become important compared to surface terms (collapsed reacting layer, condensed and gas phase side thermal gradients) and cannot be neglected in the energy balance across the finite thickness ΔX required by the numerical approach. The space mesh size ΔX is then chosen by requiring that across the first ΔX

$$\text{BC1 error} \equiv \frac{\Delta\theta \text{ due to volumetric terms}}{\Delta\theta \text{ due to surface terms}} \ll 1.$$

The above check is made at each time integration step. Computer runs, performed for different sets of input data and operating conditions, indicate that a BC1 error up to a few percent has no appreciable influence on the overall numerical solution.

The number of nodes in the space net, JF , is also the number of algebraic equations to be solved at each time step. Moreover, the parabolic extrapolation and the solution procedures require the simultaneous treatment of six vectors containing JF elements. Both these facts evidence the strong influence of the parameter JF on the computer core and time required for the numerical treatment of the problem.

The previous considerations, together with several numerical checks, define a range of variation for the parameters of interest. Typical values are $800 \leq JF \leq 3000$ and $0.01 < \Delta X < 0.05$. Remark that the selected ΔX is kept constant during the run. The operating conditions allowing large space steps are: low pressure, no chemical activity in solid phase or low activation energies, no external radiation or large transparency coefficient of the solid. These conditions have, however, the effect to increase the thickness of the thermal profile.

The temperature at the cold boundary is considered to be approximately zero when it is several orders of magnitude less than the surface temperature. Computer runs, performed for different sets of input data and operating conditions, indicate that a cold boundary temperature $\theta(X \rightarrow \infty, \tau) = 0(10^{-6})$ or less have no appreciable influence on the structure of the thermal profile near the solid-gas interface. At each

time step, the total number JF of space steps is then chosen, by requiring that the cold end temperature is conveniently small, but not too small (in such a case JF is decreased). The allowed range is 10^{-9} - 10^{-6} ; remark that $\theta_s = O(1)$

In normal operating conditions ($1 < p < 70$ atm, $0 < I_0 < 100$ cal/cm²s, $d_a < 0.005$ cm, $Q_c \leq 0.1 Q_{tot}$, $15 \leq \bar{E}_c \leq 45$ kcal/mole), an appropriate choice of ΔX , according to the previously defined range, leads to a selection of the parameter JF of the order 1000-2000.

5.5 - THE INITIAL CONDITION

The numerical solution of the unsteady problem (Eq.3.1.2) requires the knowledge of the initial thermal profile. In the simple cases where such profile can be obtained analytically, no problem exists. However, in the case of arbitrary temperature dependence of thermal properties and/or chemical activity in condensed phase, the initial condition must be obtained numerically. In particular, the presence of the chemical term implies the evaluation of the parameter $A_c(P)$ (see Eq. 3.1.20), whose dependence on the steady thermal profile makes necessary an iterative procedure.

Once the integration procedure of the unsteady problem is available, the most immediate solution for obtaining the initial condition is to use the same algorithm for integration of PDE at fixed (initial) ambient conditions. The initial condition required for starting this preliminary computation may be any assigned thermal profile (for example, the solution of the simpler case at constant coefficients). The surface temperature, known from the energy balance at the burning surface under steady conditions, is kept constant ($\theta(X=0, \tau) = \theta_s$), while at the cold boundary the usual thermal equilibrium $\theta(X \rightarrow -\infty, \tau) = \theta_{-\infty}$ is imposed. At each integration step, a new value of $A_c(P)$ is evaluated in the appropriate coefficient D_j of the finite difference equation. The iterative procedure terminates when the change in time of the temperature profile is less than a prefixed tolerance.

It is important to remark that the procedure previously described leads to numerical solutions also for combination of parameters and ambient conditions known to originate physically unstable situations (for instance: very low pressure, large values of heat release in solid phase or at the burning surface, etc.). This is very useful when the computation of the steady thermal profile is a preliminary step for the non-linear stability analysis discussed in Chapter 4. In fact,

such analysis is based on the knowledge of the steady thermal profile, and could not be extended to physically unstable configurations (for instance self-sustained oscillatory combustion) if the steady solution were not available.

5.6 - THE NUMERICAL CODE

The numerical schemes discussed in the previous sections constitute the nucleus of a computer code, UNCAP, which simulates the unsteady combustion of composite solid propellants. The code has been written in FORTRAN IV language and has been run mainly on UNIVAC 1100/80; however, successful tests were also performed on IBM, Honeywell, Gould, Digital and Perkin-Elmer computers. Several subroutines are also available in BASIC and implemented on Hewlett-Packard HP-85 personal computer.

The execution time strongly depends on the kind of transient under simulation. It ranges, on UNIVAC 1100/80, from about one minute for "easy" transients to about 10 minutes for self-sustained oscillatory combustion with sharp spikes of burning rate. A typical double precision run takes about 50,000 words of computer core.

Combustion transients driven by any combination of pressure and radiant flux changes can be simulated, namely:

- transients driven by pressure changes only;
- transients driven by changes of radiant flux intensity only (including ignition);
- transients driven by simultaneous changes of pressure and radiant flux intensity;
- transients driven by consecutive changes of pressure and radiant flux intensity;
- relaxations to (or direct evaluation of) steady states.

The computation of the static restoring function (Eq.4.2.9) is a further possibility of the code.

The structure of the numerical code (see flow chart in Fig. 43) is based on a main routine (UNCAP) and eight subroutines (SSTATE, FLAME, MESSNU, PYROL, RTMI, VELGAS, DELAW, PPSTPL). The input data set is divided in several blocks:

- physical properties of the propellant;
- reference quantities;
- ambient conditions and forcing law parameters;
- working quantities and coefficients;
- numerical parameters
- options and integer quantities.

All the above mentioned data, together with the immediately computable quantities (reference heat flux, characteristic thicknesses and times, etc.) are printed at the beginning of each run.

The effective computation procedure starts in all cases with the evaluation of the steady surface temperature referring to the initial conditions. This first step implies the solution of the energy balance at the burning surface, mathematically described by a nonlinear algebraic equation in θ_s . Five subroutines are involved in this procedure: MESSNU' (giving the algebraic function), FLAME (giving the conductive heat feedback from gas to burning surface), PYROL (relating surface temperature to burning rate), RTMI (finding the root of the algebraic equation by a bisection procedure of a prefixed temperature interval), and SSTATE (where the most significant steady quantities are printed). Next, the initial overall thermal profile in the solid phase is computed in the main routine. For the simple case of constant thermal properties and unreacting solid phase, the profile is immediately computed (being analytically known) and printed on a prefixed number of points. When the problem is of a more complex nature, the iterative procedure described in Sec. 5.5 is activated; in this case the analytical profile is assumed as a false initial condition. The computation of the initial steady state terminates by printing the value of the pre-exponential factor $A_c(P)$. At this point, it is possible to simulate a combustion transient by selecting the wanted forcing functions (subroutine DELAW) or calculate the static restoring function (Eq. 4.2.9) related to the available steady configuration.

Appropriate error messages are printed in the case of abnormal termination of the run.

5.7 - NUMERICAL SIMULATION OF DYNAMIC EXTINCTION

Extensive checks of the dynamic extinction boundary were reported in Refs. 9, 12-13, 36 both for depressurization and deradiation driven combustion transients. Numerical simulation tests, performed under a very wide variety of operating conditions, successfully validated the analytical predictions. In particular, the dynamic extinction boundary was proved, as predicted in Sec. 2.5, to be:

1. independent on the nature of the implemented monotonical law (linear, parabolic, exponential, bilinear, ecc.).
2. independent on the rate of change of the implemented monotonical law.
3. valid both for depressurization and deradiation tests.
4. valid for optically opaque or transparent condensed phase.
5. strictly dependent on the final set of operating conditions.
6. meaningful for MTS and KTSSN flames only; no dynamic extinction limit exists for linearized flames (KTSS, KZ, and LC).
7. valid for simultaneous or consecutive monotonical forcing laws, even of different nature; see Figs. 44-45.
8. valid for pulsed forcing laws.

Further numerical experimentation confirmed the validity of the analytical approach for $\bar{\epsilon}_\lambda \neq 0$, $C_G \neq 1$, $C_C(\theta) \neq 1$, $K_C(\theta) \neq 1$ and over a wide interval of operating pressures. The best agreement, between analytical predictions and numerical results, is found for n ranging from 2.5 to 3 for both polynomial and exponential approximating profiles (see Chapter 4). In any event, it should be clear that, while the dynamic extinction boundary is a property of the burning material evaluated at the final set of operating conditions, reaching or not this critical boundary depends on the whole combustion transient history.

Some new results will now be illustrated. Since the dynamic extinction boundary corresponds to the (statically) unstable B-root at the end of a burning transient, it cannot be observed directly either experimentally or numerically. In this investigation (see Ref. 9, e.g.) a go/no-go technique was implemented. An example is shown in Fig. 46, where a deradiation test was computed to check the dependence of the dynamic extinction boundary on the E_s value. It can be seen that, once the trajectory in time goes near the boundary ($I_0 = 103.2772 \text{ cal/cm}^2\text{s}$), a very slight increase of the distur-

bance (in this case the initial condition was increased to $I_0=103.2773$ cal/cm²s) is enough to yield dynamic extinction. The results obtained as to the \tilde{E}_s dependence of the B-root are summarized in Fig. 47. One can observe that: (1) the agreement between analytical predictions and numerical results is good; (2) B-root increases quickly with \tilde{E}_s in the range 15,000-25,000 cal/gmole

Further results are reported in Figs. 48-49, showing respectively a deradiation and a depressurization driven combustion transient of a propellant with chemical reactions distributed in the condensed phase. Even under these circumstances, the agreement between analytical predictions and numerical results is good.

Numerical simulation of experimental depressurization tests is discussed next chapter.

5.8 - NUMERICAL VALIDATION OF THE BIFURCATION DIAGRAMS

The bifurcation diagrams can be validated numerically and experimentally. Numerically, one has to check whether the final steady combustion configuration of an hypothetical transient, evaluated by numerical integration of the governing set of equations (see Chapter 3), is that analytically predicted by the bifurcation diagrams based on the burning stability analysis (see Chapter 4). Experimental validations will be discussed next chapter.

The bifurcation parameter $Q_{s,ref}$ is considered first. The numerical tests reported in Figs. 50-51 was intended to validate respectively the bifurcation diagrams shown in Figs. 18-19. MTS flame with $C_g=1$ or 1.12 was implemented; $C_c(\theta)=K_c(\theta)=1$, $\epsilon_c=\bar{\epsilon}_\lambda=F_0=0$. The exponential and linear pressurizations from 10 to 30 atm of Figs. 50-51 successfully verify that: the final steady combustion configuration is time-independent reacting (root A) for $Q_{s,ref}$ small enough, self-sustained oscillatory (between D and E roots) for $Q_{s,ref}(A \equiv D) < Q_{s,ref} < Q_{s,ref}(B \equiv D)$, and time-independent extinguished (root C) for $Q_{s,ref}$ large enough.

The bifurcation parameter Q_c is considered next. The numerical tests reported in Fig. 52 were intended to validate the bifurcation diagram shown in Fig. 22. KTSSN flame with $C_g=1.67$ was implemented; $C_c(\theta)=K_c(\theta)=1+0.2\theta$, $\bar{\epsilon}_\lambda=0.75$, $F_0=0$, $\tilde{E}_c=30$ kcal/mole. The exponential pressurizations from 40 to 50 atm of Fig. 52 successfully verify that: the final steady combustion configuration is time-independent reacting (root A of Fig. 22) for Q_c small enough, self-sustained oscillatory

(between D and E roots) for $Q_c(A \equiv D) < Q_c < Q(B \equiv D)$, and time-independent extinguished (root C) for Q_c large enough.

The bifurcation parameter p is considered next. The numerical tests reported in Fig. 53 are intended to validate the bifurcation diagram shown in Fig. 31. KTSSN flame with $C_g = 1.67$ was implemented; $C_c(\theta) = K_c(\theta) = 1 + 0.2\theta$, $\bar{\epsilon}_\lambda = 0.75$, $F_o = 0$, $E_c = 30$ kcal/mole. The exponential pressurizations from p_i to p_f atm of Fig. 53 successfully verify that: the final steady combustion configuration is time-independent reacting (root A of Fig. 31) for p large enough, self-sustained oscillatory (between D and E roots) for $p(A \equiv D) > p > p(B \equiv D)$, and time-independent extinguished (root C) for p small enough.

Remember that in Chapter 4 the pressure deflagration limit was defined as $PDL \equiv p(B \equiv D)$. The bifurcation diagram shown in Fig. 31 predicts, for the indicated data set, PDL slightly below 2 atm; this is confirmed by the numerical integrations reported in Fig. 53. Numerical integrations were repeated for a quite different set of operating conditions: MTS flame with $C_g = 1.12$, $C_c(\theta) = K_c(\theta) = 1$, $\bar{\epsilon}_\lambda = F_o = K_c = 0$; the results obtained by linear pressurizations from 1 to p_f atm are shown in Fig. 54. It is confirmed that p is a bifurcation parameter (cf. Fig. 53), but PDL is again slightly below 2 atm. It is well known that PDL of AP-based, unmetallized composite propellants is much lower (see Sec. 2.4). The reason for the large PDL value found in the numerical exercises of Fig. 53 ($Q_{s,ref} = 125$ cal/g and $Q_c = 50$ cal/g) and Fig. 54 ($Q_{s,ref} = 158.2$ cal/g but zero Q_c) is the exaggerated values of heat release at the burning surface and in the condensed phase ($Q_{s,ref} + Q_c$): this is strongly destabilizing, as shown in Figs. 50-52. If $Q_{s,ref}$ is reduced to 125 cal/g, the predicted PDL is of the order of 0.05 atm for a wide range of operating conditions (see Figs. 32-37). Experimental checks are discussed next chapter.

The bifurcation parameter \tilde{E}_c and the non-bifurcating parameter \tilde{E}_s are verified in Fig. 55 and 56 respectively. Comments similar to those made above can be repeated. The non-bifurcating parameter w behaves just like \tilde{E}_s .

5.9 - NUMERICAL SIMULATION OF RADIATION PULSES

Computer simulated burning transients, driven by pressure or radiation pulses, were performed to check the validity of the analytical predictions in the case of forcing functions of arbitrary shape but levelling off in time. A wide variety of computer tests, collected under different sets of operating conditions, confirmed that the concepts of static restoring function and bifurcation diagram (see Chapter 4) hold true for trapezoidal pulses of forcing function as well. The only difference concerns the dynamic extinction boundary: this is valid instantaneously for forcing functions monotonically decreasing in time, after the external disturbance ($\tau > \tau_{ext}$) for forcing functions of arbitrary shape but levelling off in time. For details, go back to Sec. 4.5.

In this section only numerical simulation of radiation pulses is discussed; numerical simulation of pressure pulses will be presented in Chapter 6, since it is directly connected with shock tube experiments. The results obtained during the previous contract period are reported in Ref. 8 and 22; they can be summarized by the burning transient computations of Fig. 57. Trapezoidal radiation pulses impinging on steadily burning propellants were considered. Results show that, for a propellant not yet adjusted to radiation, extinction or burning follows the radiative pulse cut-off in a difficult to predict fashion depending on dynamic burning (Ref. 22). On the other hand, the results reported in Fig. 57 show that dynamic extinction can be obtained, for steadily radiation overdriven propellants, by monotonically increasing either the radiant flux intensity or the pulse cut-off rate. Moreover, the dynamic extinction boundary analytically predicted in Sec. 4.5 is well verified. MTS flame was implemented at 10 atm with $C_g=1$.

Since radiation pulses can be easily performed experimentally, attention was dedicated to the detailed structure of the combustion wave when driven by radiation pulses. In particular, those variables which can be observed experimentally without excessive difficulties (perhaps on a relative scale) are tracked in time in Figs. 58-60; they are the surface temperature θ_s , flame temperature θ_f , and flame thickness X_f . In all figures KTSSN was implemented at 10 atm with $C_g=1$. Two detailed solutions, related to a trapezoidal radiation pulse with sharp cut-off of the radiation sources, are shown in Fig. 58 (radiation time $\tau_{ext}=1.9$; continued burning) and Fig. 59 (radiation time $\tau_{ext}=2.0$; dynamic extinction). Notice: that in Figs. 58a and 59a the dynamic extinction limit is

respected (minimum surface temperature occurring for $\tau \approx 2 \text{ ext}$ in Fig. 58a); in Fig. 58b and 59b the pronounced sensitivity of X_f to both pulse start and pulse end (already verified in preliminary experimental tests); in Fig. 58b the prolonged undershoot of Θ_f (down to about 1/3 of the initial value) following the pulse cut-off in contrast with its moderate overshoot when radiation starts.

The computer run reported in Fig. 60 illustrates how the steady solution changes when the propellant is subjected to a radiation pulse of illimited duration (i.e., a radiation step). Depending on the enforced set of operating conditions, the final steady state may be self-sustained oscillatory even though the initial steady state is time-independent. This is exactly the case shown in Fig. 60, where a radiant flux less than half of that used in Figs. 58-59 was implemented (40 against 90 cal/cm²s). Remark that the burning oscillations of Fig. 60 have been tracked by computer far a time about triple that shown in the figure and no appreciable damping could be perceived.

5.10 - CONCLUDING REMARKS

Numerical checks of upper dynamic instability, self-sustained oscillatory burning, ignition transients were extensively performed in the previous Final Technical Report (Ref. 9); for a matter of space, they are not discussed in this report. However, several results implicitly contained in the numerical validations of the bifurcation diagrams (Figs. 50-56) and numerical simulations of the radiation pulses (Fig. 57-60) confirm the analytical predictions as to the upper dynamic instability and self-sustained oscillatory burning. Ignition dynamics, being more complex, will be the object of a specific research program.

While the Final Technical Report 1980 (Ref. 9) was focused on the static restoring function and its numerical validation, this report is focused on the bifurcation diagram and its numerical as well as experimental validation. It should be clear that the analytical predictions (in terms of static restoring function or bifurcation diagram) are absolutely decoupled from the numerical integration of the governing set of equations. Moreover, being any experimental activity of significance much more time and money consuming than numerical work, so far the strategy has been followed to check first all analytical predictions by numerical integration. This implies that often, and sometimes on purpose, the imple-

mented data set were not realistic as compared to currently used solid rocket propellants. Obviously, a great care has to be exerted when trying to reproduce and/or predict experimental trends.

Radiation pulses were discussed in this chapter, because so far numerical results only are available in this area. But an experimental rig is being set up, with the intent to verify the theoretical results; particular attention will be given to the transition of the steady state configuration from time-independent to self-sustained oscillatory when a radiation step is applied (see Fig. 60). Pressure pulses will be discussed next chapter, being strictly connected with the shock tube experiments.

The numerical code, implemented to obtain the results presented throughout this chapter, was illustrated in detail in Secs. 5.1-5.6. Usually, the finite difference scheme on three time levels is resorted to, because of its superior properties in terms of stability and of capability to follow fast changes of the burning wave. In general, the numerical code proved reliable and flexible. Under special circumstances, typically oscillatory solutions, faster algorithms are desirable though. This was realized by means of appropriate scale changes in the condensed phase, but it is not discussed in this report for sake of brevity.

CHAPTER 6 - EXPERIMENTAL RESULTS

Experimental results, collected with the intent to validate the analytical predictions (ODE formulation of the problem, see Chapter 4) and/or the numerical code (PDE formulation of the problem, see Chapter 5), are reported in this chapter. Most experiments were performed with AP-based composite propellants. The experimental rigs used are: 1) fast depressurization strand burners (see Sec. 6.1), 2) shock tube and piston tube (see Sec. 6.2), 3) standard strand burners (see Sec. 6.3), 4) subatmospheric or low pressure strand burners (see Sec. 6.4). Results from low temperature strand burners and a laser assisted strand burner are not reported because of their preliminary nature.

Details of the experimental investigations are given in several master's theses presented at the Politecnico di Milano: Refs. 149-150 for the fast depressurization tests, Refs. 151-157 for the shock tube and piston tube tests, Refs. 158-168 for the strand burner tests. Papers of experimental nature published are listed in Refs. 28-32.

6.1 - FAST DEPRESSURIZATION EXPERIMENTS

Up to the present four series of depressurization tests, corresponding to four different experimental rigs, were performed. All of the depressurization tests were realized, at ambient temperature and in a nitrogen atmosphere, in a pressurizable laboratory strand burner. A first series of runs was performed with a relatively large (12.7 mm orifice diameter) ball valve manually operated. A second series of runs was performed combining several solenoid valves (orifice diameter ranging from 1.2 to 4.0 mm) simultaneously operated. The third series of runs was performed with the same combination of solenoid valves, but in addition a closed loop circuit was implemented to keep the combustion pressure constant prior to the abrupt opening of the solenoid valves. These first 3 series of runs were performed by exhausting the combustion chamber always to atmospheric pressure. The results obtained were already discussed in Ref. 9 (see pp. 79-80) and Ref. 28.

A fourth and, for the time being, last series of depressurization runs was performed by enforcing a parametrically variable final pressure. This was realized with the strand burner apparatus schematically shown in Fig. 61. The combustion chamber is connected to a much larger dump tank (to regulate the exhaust pressure), by means of a double burst diaphragm system

acting as exhausting device. Before depressurization, the exhausting device is kept close, but the small chamber (about 3 cm^3 volume) between the two diaphragms is maintained at a pressure about half that of the combustion chamber. In this way neither diaphragms have to support the whole differential pressure between the combustion chamber and the dump tank. The burning of the last fuse wire commands depressurization of the small chamber, between the two diaphragms, by means of an appropriate solenoid valve. In a quick succession the two diaphragms fail and cause fast depressurization of the whole combustion chamber. The burning pressure will then decay, from its initial value, to a final value depending on the initial pressure levels of both the combustion chamber and dump tank. For details, cf. Ref. 31.

The same combustion chamber was used in the four series of depressurization tests just described. This was a stainless steel vessel of about 350 cm^3 internal volume, containing: the ignition device (an electrically heated nichrome wire of 0.8 mm diameter), a fuse wire system to measure the steady burning rate of the propellant strand prior to depressurization, two plexiglass windows for visual observation of the relevant phenomena. The propellant samples were cylinders, about 50 mm length and 6 mm diameter, cut from a relatively large solid grain. The lateral surface is inhibited to combustion by overlapping coatings of teflon spray and butyrate slope (usually). Extinguished samples showed a very flat burning surface.

The first two series of data were collected by testing a composite propellant with low oxidizer loading (AP70/PVC30). The last two series of data were collected by testing a composite propellant with large oxidizer loading (AP84/CTPB16); notice that this basic formulation was available in several modified versions containing different but small amounts ($\leq 1\%$) of alumina Al_2O_3 . For all compositions, particle sizes of AP were polydispersed in the range 10 to 200 μm about.

The experimental procedure for the four series of depressurization tests, was kept identical as much as possible. After pressurizing the combustion chamber (up to about 40 atm in the results to be presented here) and igniting the propellant sample, enough time is waited for the deflagration wave to assume a stationary state. The steady burning rate is then measured by means of several (typically, three) fuse wires. This allows to check the steadiness of the deflagration wave at the initial pressure p_1 and assures the consistency of the data set (propellant ageing or ill conditioned may cause lack of reproducibility, even though steady state is

observed). When the last fuse wire burns, the combustion chamber is suddenly exhausted (on manual command or automatically as in the apparatus of Fig. 61). The pressure drop results of exponential nature when exhausting is performed through solenoid valves or burst diaphragms, more gradual for ball valves (see sketch in Fig. 62).

For each run the first result to be observed, important albeit only qualitative, is the overall fate of the depressurization transient: extinction or continued burning. As a matter of fact, due to the known difficulties in measuring instantaneous values of burning parameters (cf. Sec. 2.1.2), the usual experimental technique of a go/no-go testing was adopted. However, in order to probe the nonlinear burning stability theory presented in Chapter 4, the strategy followed was to resort to a wide range of closely related experimental as well as numerical go/no-go. For each run and during the whole run, the following quantities were recorded by means of a multichannel (UV sensitive paper) galvanometric recorder with flat frequency response up to 1 KHz: ignition current and time, light emission, combustion chamber pressure, fuse wire currents. The galvanometric recording of a typical depressurization test is shown in Fig. 63. In addition, for each run but during the depressurization transient only, the combustion chamber pressure and light emission were recorded by means of a digital memory. Typically, 4000 points with a sampling time of 10 μ s were stored for each trace (see Fig. 64). The digital recording of a typical depressurization test is shown in Fig. 65; digital recording was effected only for the fourth series of tests. The burning pressure was measured by a piezoelectric, quartz transducer of 60 KHz resonant frequency and mounted flush with the combustion chamber wall. The light emitted from the burning sample was detected by means of a photodiode featuring a view angle of 30° and spectral sensitivity in the range 0.5 to 1.1 μ m (with maximum response at 0.9 μ m). The photodiode is placed in front of the combustion chamber window at a distance of about 50 mm from the propellant. Both the photodiode and pressure transducer point the propellant zone where depressurization is commanded, i.e. immediately under the last fuse wire (see Fig. 61). Further details are given in Refs. 149-150, 28 and 31.

Differently from other approaches, only the permanent extinguishment of the combustion process is considered as extinction criterion. However, reignition phenomena were not observed during the experimental runs. This is probably due to the combustion chamber configuration adopted: it does not approximate an actual motor but was designed to obtain a monodimensional combustion behavior of the propellant sample.

The sample lateral surface is not in contact with the chamber wall or other metallic structures, so that no external energy source can reignite the propellant. The phototransistor signal permits to follow qualitatively the behavior of the propellant flame during the pressure transient. During the experimental runs with maximum depressurization rate values near the go/no-go boundary, a characteristic behavior of the phototransistor signal was detected: at the beginning of the pressure drop the signal drops rapidly toward very low values but, before the end of the pressure transient, a recovery of luminosity can be observed. A drop to zero follows in the case of extinction runs. For continuous burning runs, the recovery is followed by a drop to near zero values and then a gradual increasing of the signal can be observed. The recovery of luminosity during the pressure drop is likely to correspond to the development of a flame due to a different combustion mechanism. The phenomenon of a redeveloped flame was already observed by other researchers, e.g. Steinz and Selzer (Ref.71) and Baer et al. (Ref.73), and was explained with a change of the oxidizer/fuel mixture ratio during the transient (because this flame burns preferentially AP particles). Indeed, holes in correspondence of AP particles position can be observed on the surface of the extinguished samples.

Experimental results obtained from depressurization tests of AP70/PVC30 samples, from some initial pressure to atmospheric pressure, are summarized in Fig. 66. This is a $[\text{dp}(t)/\text{dt}]_{\text{max}}$ vs p_i plot, as already done by several investigators in the past (see Sec. 2.1). However, according to our nonlinear burning stability theory, no special meaning whatsoever is attached to the maximum depressurization rate. The fate of a depressurization test, extinction vs continued burning, is rather the integrated result of the whole history of the burning propellant (initial conditions, depressurization law, etc.). The critical boundary, as defined in Sec. 4.5.1, is a property of the burning propellant; but whether it will be reached or not depends on the previous history of the burning propellant. Obviously, high $[\text{dp}(t)/\text{dt}]_{\text{max}}$ for exponential depressurization implies that the whole transient is faster and this favors dynamic extinction. Experimentally, different depressurization transients were obtained by changing the total exhaust orifice area. On a linear $[\text{dp}(t)/\text{dt}]_{\text{max}}$ vs p_i plot, a straight boundary is found to separate quite neatly the extinction region from the continued burning region.

In agreement with Ciepluch (Refs. 41-43) and Merkle et al. (Ref. 44), the experimental results reported in Fig. 66

suggest a straight boundary between the region of extinction and that of continued burning for go/no-go testing. However, this does not exclude bending upwards of the go/no-go extinction boundary, when the final and initial pressures of the depressurization transients are closed enough, as found in the experimental tests with AP84/CTPB16 (see Fig. 67). Fast depressurization, from some initial pressure to atmospheric or 3.25 atm final pressure, was performed with the strand burner apparatus of Fig. 61. The experimental results suggest for $p_f=1$ atm the usual straight boundary between extinction and continued burning in the $(dp/dt)_{\max}$ vs p_i plot. However, a novel effect is the behavior of the boundary when the initial pressure approaches the final pressure for $p_f=3.25$ atm (see Fig. 67). The boundary, for decreasing initial pressure (but fixed final pressure), is first seen to decrease linearly as usual but later goes through a minimum and turns upward. Nevertheless, this result should not surprise; indeed the smaller is the pressure drop the larger has to be the required depressurization rate for extinction. Obviously, no dynamic extinction can occur when initial and final pressures coincide; therefore, a vertical asymptote to the go/no-go extinction boundary is somewhere expected when p_i approaches p_f .

A summary of the experimental results obtained by Merkle et al. (Ref. 44), by Von Elbe and McHale (Ref. 49), and in this investigation by Ceriotti (Ref. 149) and Dondé et al. (Refs. 150, 28, 31) is shown in Fig. 68. Remark that the maximum depressurization rate occurs at mid depressurization for manual ball valves, but at the very beginning of the depressurization history for solenoid valves. Depressurization rates were measured by considering the time required for pressure to drop from (p_i-1) atm to (p_f+1) atm for manual ball valves. For a fair comparison one should consider depressurization rates about 3 times lower. Even so, the two plots found in this work do not correspond. With the same maximum depressurization rate, the depressurization history of Fig. 62b is more effective than the exponential depressurization of Fig. 62a in extinguishing the sample. This spectrum of results is not surprising from our viewpoint, rather is welcome because it offers a more stringent constraint to the theoretical approach while confirming the fact that maximum depressurization rate is not the controlling factor.

The numerical code, solving the PDE formulation of the problem, is fully capable to reproduce depressurization transients. For several aspects the numerical solution provides details much beyond the currently available experimental

information. A host of such numerical solutions was reported in Refs. 9 and 12-13. Obviously, the most wanted piece of information is the burning rate history during depressurization. Although progress has been made (see Refs. 78-80), no reliable experimental technique is operative yet. This makes impossible a straightforward validation of the numerical solution, which on the other hand was shown to confirm the analytical predictions (ODE formulation of the problem) in Chapter 5. However, the qualitative aspects of the numerical solution are found to agree with the corresponding experimental information, collected in this laboratory (by high speed movies and recordings of the type shown in Figs. 63 and 65) and/or available from the open literature (e.g., see Refs. 41-44 and 70-78). Quantitatively, the go/no-go extinction boundaries of the type shown in Figs. 66-68 can easily be constructed numerically. Attention was therefore focused on this task. The results obtained by implementing the MTS flame are shown as dashed lines in Fig. 66 (AP70/PVC30 propellant) and Fig. 67 (AP84/CTPB16 propellant).

A typical computed depressurization test for AP84/CTPB16 propellant is shown in Fig. 69; the fast depressurization rate enforced was not enough to extinguish the combustion wave for $p_f=3.25$ atm and the indicated set of parameters. By repeating this kind of computation for different depressurization rates, the go/no-go extinction boundaries of Figs. 66-67 are obtained. Computations of this nature are quite easy and fast; in any event they were performed according to the guidelines discussed in Chapter 5. Remark that in the numerical runs extinction was assumed to occur when unbounded decrease of the burning rate towards zero value was observed; this in turn occurs when the analytically predicted dynamic extinction boundary is crossed (see Fig. 69). In Fig. 66 the computed go/no-go extinction boundary is found to be strictly linear and shows a good agreement with the experimental boundary. Numerical predictions are slightly less satisfactory (not shown for graphical reasons) if variable thermal conductivity in the condensed phase is allowed, for example, according to the linear law $K_c(\theta)=1 + b\theta$ with $b = 0.4$. Note, on the contrary, that the agreement is improved if variable thermal conductivity and specific heat in the condensed phase are simultaneously allowed, for example, according to the linear law $K_c(\theta)=C_c(\theta) = 1+b\theta$ with $b=0.4$. However, since the thermal properties of the AP70/PVC30 propellant were not measured, the exercise was not pursued. Indeed, the theoretical results are very satisfactory and it was judged more meaningful to test the numerical code by further experimental data sets. In Fig. 67 the computed go/no-go extinction boundaries are found to follow the experimental trends for both 1 and 3.25 atm final

pressure. The numerical tests were performed with constant thermal properties. The bending upwards of the go/no-go extinction boundary for p_1 approaching p_f is clearly reproduced, even if quantitatively in a less satisfactory manner than the straight portion of the boundary. More faithful fitting of the experimental results could have been attempted by a proper choice of the less known parameters. But, again, this was judged pointless because the experimental information is not enough accurate (further data could not be collected for lack of propellant!), while the theoretical results already successfully reproduce the experimental trends over a relatively large range of the operating parameters and for more than one order of magnitude span of the maximum depressurization rate (see Fig. 67).

It is our opinion that a good agreement exists between analytical, numerical, and experimental results for AP-based composite propellants subjected to depressurization tests. This bids well for the whole nonlinear burning stability theory being developed in this research study. Future work in this area will focus on the collection of experimental data in the range of operating conditions where fast depressurization extinction and low pressure extinction overlap. This should critically probe the capability of the theoretical approach to discriminate and reproduce the two phenomena.

6.2 - SHOCK TUBE EXPERIMENTS

Shock tubes have been extensively employed in solid propellant burning for ignition studies, less commonly for unsteady combustion driven by pressure pulses. The shock tube is a unique tool, in that it provides very high pressures and especially temperatures without great difficulties. Unfortunately, testing times are usually too short compared to most of the tests of interest in heterogeneous combustion. Therefore, one is obliged either to deal with pressure pulses of exceedingly complicate structure (see Sec. 6.2.1) or to modify somehow the shock tube into something more manageable (see Sec. 6.2.2).

6.2.1 - Shock Tube Configuration

At the very beginning of this research study, the shock tube apparatus available at our laboratories for standard gasdynamic research was converted to be used for ignition experiments (Fig. 70a). A catalyzed DB propellant was tested, but the collected data were too scarce for significant conclusions to be reached (Ref. 151). However, the practical

expertise gained during this task proved very useful for the successive developments. On the other hand, analytical predictions of ignition transients, in particular of catalyzed DB compositions, revealed too difficult to obtain; of course, this does not exclude the possibility to simulate an ignition transient by computer.

It was, therefore, considered more fruitful to use the shock tube for fast pressurization tests on propellant samples initially burning under steady state conditions (Ref. 152). Since the propellant sample had to be placed at the end wall of the shock tube (Fig. 70b), where low pressure initially prevails, a preliminary step was to evaluate the PDL of the propellants under investigation. Tests were performed for different propellants (AP-based composite, catalyzed DB, noncatalyzed DB), different geometries of the sample (cylinders of 8 or 15 mm diameter and 10 mm height), different pressurizing gases (nitrogen, air, oxygen). Strands of propellants were placed in the test section of the shock tube and carefully ignited by several electrically heated wires. Ignition was considered successful only when a self-sustained flame would develop. As to the possible shortcomings of this experimental technique, consult Sec. 2.4. The results obtained are reported in detail in Ref. 152 and partly in Ref. 9 (Fig. 82); they are not discussed here because more accurate experimental investigations on the same subject were later developed and will be presented in Sec. 6.4. In any event, the PDL knowledge allowed to go on with the second part of the project. Samples of the selected propellants were placed at the same location of the shock tube where PDL was evaluated, ignited and, after reaching a steady burning configuration, subjected to shock waves of appropriate strength (see Fig. 70). The light emitted by the burning propellant was detected by two photodiodes directionally selective and sensitive in the visible as well as near infrared (spectral response peaks at 0.8 and 0.9 μm). Several tests with different propellants, ignition pressures, pressurizing gases, and shock speeds failed unfortunately to show conclusive trends as to the dynamic burning rate behavior (as revealed by the light emission). The basic difficulty was the too fast succession of shock waves and expansion fans impinging on the surface of the burning propellant during the same test. For details see Ref. 152. In this series of tests, complete extinguishment of the propellant was never achieved. The duration of the pressure pulse (actually of the depressurization tail, being the pressure rise extremely fast) was typically of 10 ms.

6.2.2 - Piston Tube Configuration

To overcome the experimental difficulty just mentioned, the shock tube was slightly modified into a piston tube configuration (Ref. 153). Usually, a teflon piston (Fig. 71) of 150 g weight was used; a small magnet was inserted in the piston body to measure its speed by means of four coils wrapped around the tube walls. Each coil was made of 300 turns of 0.17 mm copper wire. An electronic circuit could properly handle the signal and provide directly the piston speed. With this operating configuration, a longer testing time was obtained and, more generally, a better control and flexibility of the whole experimental apparatus was made possible. Typically, the pressure pulse duration could reach 50 ms, including 20 ms of pressure rise. The pressure history was measured by a piezoelectric pressure transducer (Kistler 603B, resonant frequency 0.4 MHz) mounted very close to the burning propellant (see Fig. 70b). A series of experiments was performed to study the effects of compression waves on steadily burning propellants, with the intent in particular to verify the overstability and dynamic extinction phenomena expected from the nonlinear burning stability theory (cf. Chapter 4). Two different propellants were tested: an AP-based composite (AP70/PVC30) and a noncatalyzed DB. Cylindrical pellets (15 mm diameter and 10 mm height) were located on the end wall of the piston tube, ignited and, after a steady burning configuration was reached, subjected to pressure pulses of the wanted shape by properly varying the piston speed. Tests were carried out with different initial pressures (ranging from 0.5 to 1 atm) and different ambient gases (nitrogen, air, oxygen). The signals coming from two photodiodes (detecting the light emission from the burning propellant) and the pressure transducer were monitored and recorded by means of two oscilloscope, triggered by a pick-up sensing the breakage of the tube diaphragm (see Fig. 70b).

The results of a systematic experimental campaign of runs were reported in detail in Ref. 153, more concisely in Refs. 9 and 30. It was shown that solid propellant burning stability is strongly influenced by rapid pressure changes, especially in the presence of oxygen. On the contrary, the initial pressure level did not manifest dramatic effects, probably thanks to the stabilizing mechanism provided by the relatively slow beginning of the pressure rise. Permanent extinction of the burning sample was observed, for both the AP70/PVC30 and the noncatalyzed DB propellants, in all tested ambient gases. Reignition was also observed, but did not

receive much attention (due also to instrumental inadequacy). The computer simulated runs of Ref. 153 were the first to be performed, but lack of consistency. The results of Refs. 30 and 153 are presently superseded; therefore, the details are omitted.

The work described (Refs. 151-153 and 30) was very valuable as a preliminary exploration. Some of the evidenced experimental deficiencies were taken care of in Refs. 154-155. The piston tube test section and the piston geometry were modified as shown in Fig. 72. In particular, pistons properly designed were tested to obtain less friction with the tube walls, less gas leakage between piston and tube walls, better mechanical resistance (than those observed with the teflon piston of Fig. 71). Pistons of different material were also tested, of weight ranging from 100 to 200 g. It was experimentally verified that the maximum piston speed is well represented by the theoretical results of Fig. 73, in function of the initial pressure of the piston tube high pressure section and for biatomic gases (Ref. 155). A good control of the piston performances allows, within reasonable limits, to produce pressure pulses of the wanted shape. Long time recording, suitable to study reignition events, was provided by a transient recorder. High speed cinematography was set up, making use of a Hitachi HD-16 camera capable of 8000 pps and Kodak Ektachrome 7250 color films. Moreover, a technique, based on the detection of the ionisation level in the gas phase near the propellant surface, was set up with the purpose of revealing near burning surface flames. Indeed, both photodiodes and high speed camera do not clearly show what happens near the burning surface, because they see the light emission of the hot gases from the whole volume of the test chamber. A schematic layout of the experimental arrangement is shown in Fig. 74 (where the propellant was placed on the side walls for assembling convenience). Two thin copper wires of 0.2 mm diameter were inserted through the propellant sample, separated by a gap of 3 mm and protruding about 0.5 mm from the surface. Changes of electrical resistance through the gap, due to flame ionisation, were measured in terms of voltage changes and recorded during the combustion tests. Results from this technique were given in Ref. 154, but also summarized in Ref. 9 (Figs. 90-92).

Most of these experimental improvements were implemented in a second series of burning tests, essentially of qualitative nature, performed at the piston tube with the simultaneous use of the high speed camera. Only an AP-based composite

propellant (AP84/CTPB16) was tested. Cylindrical samples (15 mm diameter and 10 mm height) were experimented with the same procedure described above. Using pistons around 100 g weight, pressure peaks of the order of 130 atm and pressure rise times of 15-20 ms were enforced. Tests were carried out for the same initial pressure (1 atm) in the test section, but with different ambient gases (nitrogen, air, oxygen). Luminosity and pressure histories were measured respectively by a photodiode (Hewlett-Packard HP 5082-4205, spectral response peak at 0,8 μm) and a piezoelectric pressure transducer (Piezotronic PCB 113A, resonant frequency 0.5 MHz and rise time 1 μs). High speed color movies were taken in the range 3000 to 7000 pps. The detailed results were given in Ref. 154, but a typical sequence of photograms was also reported in Fig. 86 of Ref. 9. The simultaneous information, collected from both high speed movies and traces of pressure and luminosity, clearly illustrate the combustion dynamics during the pressure transient. One could distinguish a rapid burning increase during the pressurization period (revealed by luminosity increases), a maximum luminosity reached while the pressure is still increasing, flame detachment and finally extinction. Usually, after the (luminosity) extinction, the sample reignites under the effect of the oncoming pressure pulses. However, in some instances (about 5% of the performed tests) permanent extinction occurred, in that the propellant samples could be recovered after the experimental run. A distinctive feature of the combustion dynamics during the pressure transient is the sharp decrease of the flame luminosity however occurring during the pressurization period. This behavior was found for all testing conditions and repeated the trends previously observed (Ref. 153).

Likewise, the ionization probe of Fig. 74 revealed, for burning tests conducted in air, a sharp increase of ionisation in correspondance with the first pressure step arrival, followed by a fall down to zero while the pressure is still increasing. This seems to confirm the occurrence of flame extinction at the propellant surface. Indeed, by comparison with simultaneous luminosity recordings, ionisation falling down to zero just precedes the luminosity disappearance. High speed movies suggest that this is due to flame detachment from the burning surface and later flame extinction. The chance that ionisation and luminosity being not in phase may depend on transient ionisation phenomena seems discarded by further results, showing the ionisation probe to respond in phase to multiple pressure pulses impinging on the burning surface until reignition occurs. On the other hand, steady burning featured a steady, albeit noisy, ionisation level.

However, the response of the ionisation probe to ignition transient was not investigated in detail.

A third series of burning tests (Refs. 156-157) was performed at the piston tube under the usual experimental procedure. Most runs were realized with a noncatalyzed DB propellant; only a few runs were realized with an AP-based composite propellant (AP84/CTPB16) for a regretful lack of samples. Cylindrical pellets were used of 15 mm diameter and 15 mm height. Further improvements of the experimental apparatus (with respect to the one employed in Ref. 153) were obtained by realizing a double diaphragm system, allowing the exact time command of the events, and using pistons of special material, allowing to tailor the wanted pressure pulse shape and succession. The best results were obtained with different versions of teflon and doped teflon; these materials offer an optimum combination of low friction, low density, high mechanical resistance over a large range of pressure, easiness of machining. Pistons of weight ranging from 100 to 150 g were used. A block diagram of the experimental apparatus implemented is shown in Fig. 75. Tests were carried out at 1 atm initial pressure of nitrogen or air; attempts to run in oxygen yielded confusing results due to the exceedingly vigorous burning (combustion was however little affected by the pressure pulses).

Testing of the noncatalyzed DB propellant in nitrogen was performed with peak pressure in the range 30 to 150 atm and duration of the first pressure pulse in the range 15 to 35 ms. The nonlinear combustion dynamics is well excited by the complicate shape and strong intensity of the pressure pulse. Overstability at low pressure and lack of synchronization (between different parts of the heterogeneous combustion wave as well as between the combustion wave and the compression waves) yield attempts of extinction, as revealed by luminosity undershoots, even during the pressurization period of the pressure pulse. Obviously, the fast increase of pressure toward large values always overcomes these attempts (by reignition, if necessary). But following the pressure peak, the fast fall of pressure toward low values (although larger than PDL) often causes dynamic extinction of the burning sample. An example is shown in the pressure and luminosity recording of Fig. 76, where the photodiode was saturated for some portions of the recording time. Notice in Fig. 76 the damped oscillations of luminosity between the tail of the first pressure pulse and the rise of the second pressure pulse generated by the piston motion. In this case the first pressure pulse provoked complete extinction

of the initially burning propellant. Out of 20 tests in nitrogen, the noncatalyzed DB propellant extinguished in 15 ms and manifested damped oscillations in 9 runs. Of course, being this kind of extinction of dynamic nature, it is expected that low pressure peaks and prolonged duration pulses (more exactly prolonged depressurization times) favor the continued burning through the process dynamics. An example of continued burning is shown in Fig. 77, where as a matter of fact the first pressure peak was only of 31 atm and not much happened during the depressurization tail and the successive weak pressure pulse. Although the photodiode was saturated for a portion of the first pressure rise, notice the low burning level (but of oscillatory character) during the crest of the pressure pulse. The rather regular damped oscillatory combustion, revealed by the luminosity trace in Fig. 76, was observed quite commonly. According to the nonlinear burning stability theory developed in Chapter 4, damped oscillatory combustion can be of dynamic (near extinction limit or upper dynamic instability or sheer fully unsteadiness) or static (low pressure) origin. It is difficult and perhaps impossible to discriminate. It is however of interest that the luminosity disappearance was abrupt when dynamic extinction requirements were more sharply enforced (e.g., pressure peak of 140 atm and pressure fall down in 5 ms). An overlapping phenomenon, which sometimes creates some confusion in the data interpretation, is reignition. This was clearly observed in 2 out of the 5 instances of continued burning. An example is shown in Fig. 78, where the first pressure peak was above 70 atm and fell down in 7 ms: the luminosity seems nil for a long time span, the second pressure pulse at 65 ms travels through without perceivable effects, but then the third pressure pulse at 110 ms reignites the sample, which slowly redevelops a full flame and following a prolonged oscillatory pattern burns completely. Reignition is favored by the succession of pressure pulses and/or the presence of hot spots on samples, whose dynamic extinction has not been abrupt. Reignition can be recognized by the relatively long induction times required to restart and complete the burning process.

Testing of the noncatalyzed DB propellant in air was performed with peak pressure in the range 20 to 160 atm and duration of the first pressure pulse in the range 15 to 40 ms. Several comments made above, concerning the results in nitrogen, could be repeated. The attempts to extinguish, as revealed by the luminosity undershoots, during the first pressure rise are now more effectively counteracted by the vigorous burning

in air. The fast fall down of pressure after the peak always causes a dramatic decrease of luminosity (more substantial than the corresponding runs in nitrogen). However, dynamic extinction was not frequently obtained due to the easily occurring reignition. Out of 17 runs, 7 showed dynamic extinction while 10 manifested burning oscillations clearly forced by the succession of pressure pulses. An example is shown in Fig. 79, where the first pressure peak reached 95 atm: the sensible luminosity decrease following each pressure pulse (attempts of dynamic extinction?) is counteracted by the succeeding pressure pulse until full combustion develops. The photodiode in Fig. 79 was saturated at the luminosity peaks by the intense burning in air. The presence of oxygen creates a diffusion flame which vigorously assist the propellant flame, makes hot spots likely to form, and causes 3D effects on the burning sample supporting flame propagation. For these reasons, reignition was frequently observed in air whereas dynamic extinction was frequently observed in nitrogen. Remark that, in several cases of testing in air, extinction followed unsuccessful reignition (probably triggered by hot spots rather than oncoming pressure pulses).

Computer simulated runs were also performed. Besides the usual limitation of thin flame (i.e., quasi-steady gas phase) enforced throughout this report, the validity of these computations requires also negligible effects of the pressure pulses and associated temperature pulses on the chemical kinetics of the overall combustion wave. These requirements are impossible to meet with shock tube operations, difficult but not impossible with piston tube operations. As a matter of fact, by a proper selection of the initial operating conditions, pressure pulses of the order of some 10 ms can be produced at the piston tube. This is enough to virtually ensure quasi-steady gas phase at large pressure levels, while at low pressure levels pressures steps are so weak and prolonged in time that no dramatic effect is however expected. Temperature pulses are intrinsically less important in piston tube operations; in any event hot temperatures of the environmental atmosphere are known to be little influent on solid propellant burning rates. Therefore, if the chemical kinetics of the propellant is not sensibly affected by the pressure pulses (but this is not likely to occur for under-oxidized compositions tested in air or oxygen), the computations performed make sense. Examples are shown in Fig. 80 (AP70/PVC30) and Fig. 81 (AP84/CTPB16). A wide variety of computations are reported in Ref. 156, where the effects of thermal properties, flame models, pyrolysis

laws, surface heat release, ecc., were systematically studied for AP-based composite propellants. Notice in Fig. 81 the "instantaneous" response of flame temperature to pressure changes, in contrast with the sluggish response of surface temperature. On purpose the computations of Fig. 81 are shown for two different, but very close, values of \tilde{E}_s of a reasonable size: remark that dynamic extinction may be yielded very easily and the predicted dynamic extinction limit is well respected.

6.3 - RESULTS FROM STEADY BURNING EXPERIMENTS

Several strand burners were designed, built, tested, and properly assembled during the whole time span of this research study (from 1976 to date). The first experimental information of interest is the steady burning rate dependence on pressure, $\bar{r}_b = r_b(\bar{p})$. Some standard strand burners are operative to this end, covering the range of pressure from subatmospheric to 100 atm (the pressure interval of interest for the theoretical developments). These burners are standard Crawford bombs (essentially, a fuse wire technique is used to measure the burning rate), with some minor modifications. For example, a pneumatic closed loop circuit is implemented in order to keep the burner pressure constant during the experimental run. Details on the overall experimental procedure and data processing are given in Refs. 158-162. A sensible improvement of this standard procedure is required, if one wishes to eliminate the small but perceivable influence on the physical processes due to the presence of the fuse wires. Such a wish may arise when either the burning process is near the propagation limits (typically, for pressures close the PDL) or the simultaneous employment of other intrusive techniques (typically, thermocouples) makes problematic the presence of several wires on the same propellant sample.

A nonintrusive, laser-based optical technique was therefore developed (Refs. 163-164 and 35); a schematic sketch is shown in Fig. 82. The laser beam, after being expanded is intercepted by the propellant strand; the burning surface, during its regression, discovers a larger and larger fraction of the laser beam; the receiving optics is a vector of photodiodes collecting the light impinging from the combustion

zone through an interferential filter. This technique was successfully tested, and is presently operational over a large pressure range and for different classes of solid propellants. Typical results, obtained with the fuse wire technique and/or the optical technique, are reported in Fig. 83 (a noncatalyzed DB propellant) and Fig. 84 (AP84/CTPB16 composite propellant).

A wide range of complementary techniques was also tested and sometimes successfully used: low and high speed movies, motorized cameras, thin films of mylar, color TV, linear photodiodes. They are mentioned in Refs. 161-164, but are far from the simplicity and reliability of the diagnostic technique sketched in Fig. 82. In particular movie cameras give a good qualitative picture of the burning phenomena; however smoke in the chamber, cost, and delays due to film processing make this a less than ideal tool to obtain quantitative data. Measurements of steady burning rate vs pressure were also performed at parametrically variable ambient temperature (Refs. 165-166), in order to evaluate the temperature sensitivity of the tested propellants.

Another information of great interest in solid propellant burning are the steady surface temperature and, more generally, the steady temperature profile through the entire deflagration wave. The standard technique used to this end resorts to microthermocouples; other diagnostic techniques mentioned in the competent literature are far less reliable, although sometimes appealing because of their nonintrusive nature. In the tests conducted during this research study (Refs. 167-168), different kinds of thermocouples with lead size down to 5 μm were inserted in the propellant strands. A schematic sketch of the experimental set up is shown in Fig. 85, where a simplified version of the laser - based technique to measure simultaneously the burning rate is represented too. A typical temperature profile recording is shown in Fig. 86 (AP84/CTPB16 composite propellant burning steadily at 0.09 atm). Evaluating the surface temperature is not easy; if the usual method of the broken slope surface temperature is adopted, the results shown in Fig. 87 are found (AP84/CTPB16 composite propellant).

Why to perform steady state experiments in the framework of the nonlinear burning stability theory? The purpose is not to validate the theory, but only to provide data for the analytical predictions and/or numerical simulations to be quantified. In particular, one curve $\bar{r}_b(p)$, for a given ambient temperature and diabaticity, is required to "identify" the propellant (see Sec. 3.1), while one or more $\bar{T}_s(r_b, p)$ dependency are required to evaluate \bar{E}_s (or w) and n_s of the pyrolysis law (see Eqn. 3.1.6). Of course, the experiments mentioned in this

section are also meant to provide quantities such as: $r_{b,ref}$, n , $T_{s,ref}$, α_{ref} . After measuring the density ρ_c , it is then possible to evaluate

$$(6.3.1) \quad k_{ref}/c_{ref} = \rho_c \alpha_{ref} \quad .$$

At least for the simple case of constant thermal properties, one can go further and obtain from thermocouple measurements:

$$(6.3.2) \quad k = \left[\left(k \frac{dT}{dx} \right)_{c,s} + \rho_{out} (\bar{T}) - c_{p,b} \bar{T} \right] / \left(\frac{dT}{dx} \right)_{\alpha,s}$$

where φ_{out} can be neglected without any appreciable consequence.

6.4 - SUBATMOSPHERIC BURNING EXPERIMENTS

The objectives of the experiments were to measure the PDL of the tested propellants and check the existence of the self-sustained oscillatory burning regime predicted in Sec. 4.6. Further, both experimental results are used to verify and tune the numerical code.

6.4.1 - Pressure Deflagration Limit Measurements

Most of the runs were performed in the combustion chamber schematically reported in Fig. 88. It consists of a test section, where the propellant sample burns, and an oscillation damping tank. The total internal volume is about 6335 cm³. The ignition system consists in a nichrome wire that can be electrically heated.

Pressure is measured by means of a Kistler 412 quartz transducer (range from 0 to 11 atm and natural frequency 7.5 kHz) facing the propellant in the test section, and at the same time by a mercury manometer. The luminous emission from the burning propellant is measured by means of two different phototransistors facing the propellant from two different points of view. The first one (Fairchild FPT 120, with a view angle of about 100° and spectral response from 0.4 to 1 μm with maximum at 0.8 μm) is placed in front of a glass window of the combustion chamber at a distance of 80 mm from the propellant and sees the side of the propellant sample and the flame. The second phototransistor (Texas Instrument TIL 81, view angle of about 20°, spectral response from 0.5 to 1.1 μm and maximum at 0.9 μm) is placed on top of the combustion chamber and sees the burning surface across

the flame. Pressure and phototransistors signals were recorded by means of a multichannel galvanometric recorder (flat frequency response up to 1 kHz) and a Nicolet digital transient recorder.

Before each run the combustion chamber is evacuated and purged with the test gas. Pressure is then set at the desired value by regulating the test gas and vacuum pump flow rates. When pressure is stabilized, the propellant sample is ignited. For very low pressure tests the procedure is generally performed at higher pressure in order to achieve a successful ignition, following which the pressure is slowly lowered to the desired value. The recording of signals begins after the burning of about 20 mm of propellant sample, when pressure in the combustion chamber is stabilized. During the whole run no pressure oscillation was observed even in the case of pressure near PDL, when oscillatory burning occurs.

To find the PDL after ignition is achieved, the chamber pressure is lowered very slowly until the propellant stops burning. Because of the very low burning rate due to the low pressure, complete combustion takes several minutes. For most experimental runs, the propellant samples were strands about 60 mm long with a 5x5 mm square cross section. Experiments were performed in nitrogen with two AP-based composite propellants: the usual AP84/CTPB16 taken as a datum case and a metallized composition containing 16% Al. The nonmetallized AP84/CTPB16 was also tested in a slightly oxygenated gas mixture (95% N₂+5% O₂). Experiments were performed in the burner of Fig. 88 and in two more burners of quite different geometry. In most cases the lateral surface was not inhibited to combustion. For all tested configurations, the measured PDL was found to be of the order of 0.06-0.09 atm.

6.4.2 - Self-Sustained Oscillatory Burning

It was impossible to distinguish steady self-sustained oscillations from time-independent steady burning above, say, 0.5 atm (due to the background, small amplitude fluctuations of the flame). Therefore, attention was focused on the pressure range immediately above PDL: in this region burning is self-sustained oscillatory, as shown in Figs. 88-90. The combustion oscillations can be detected by the naked eye; the results of Figs. 89-90 were obtained by collecting the light emitted from the burning surface with one of the phototransistors (spectral response from visible to near IR with peak

at $0.9 \mu\text{m}$ and view angle of 20°) mentioned in the previous section. Other phototransistors and a Langmuir probe, differently located, gave similar results. For all tested configurations, the burning frequency increases with increasing pressure starting from the experimental PDL (see Figs. 91-92). Notice in particular that Fig. 91 shows the oscillation frequency, as a function of pressure, for two different lateral surface finishes (uninhibited and inhibited) and two different atmospheres (100% N_2 or 5% O_2 + 95% N_2). The data points for the 100% N_2 case were obtained from tests with two different combustion chambers (1000 cm^3 and 6350 cm^3 volume). No steady burning regime was observed below $p=0.06 \text{ atm}$. The frequency dependence on pressure is fairly well represented by an exponential whose constant is itself a weak function of pressure, i.e. $f=a \exp(np)$ where, for 100% N_2 , $a=14.69 \text{ s}^{-1}$ and $n=0.323 \text{ atm}^{-1}$. For the aluminized propellant (Fig. 92) both the burning frequency and its rate of increase with pressure are less than the values obtained for the nonaluminized propellant; indeed, at such low pressure, aluminum behaves essentially as a heat sink.

For the nonaluminized propellant, only limited testing could be performed with 5% O_2 without flame inhibitor: for $p>0.13 \text{ atm}$ one-dimensionality was in fact lost. If the burning oscillations are due to the condensed phase thermal wave relaxation, results should not be affected by the presence of oxygen. Actually, it can be seen from Fig. 91 that the curve obtained with 5% O_2 is displaced slightly upwards as compared to the curve obtained with no oxygen. However, measuring the average burning rate vs pressure (over hundreds of combustion oscillations) revealed that the presence of oxygen slightly augmented the average burning rate. Comparing the oscillations frequency at the same average burning rate, instead of at the same pressure, eliminates the small discrepancy.

Some of the runs were performed in a smaller (1000 cm^3) chamber, equipped with a laser beam perpendicular to the strand and grazing the burning surface. A photodiode array receives the beam and senses the instantaneous motion of the surface, that is pushed upwards by a stepping motor so that its position relative to the observer stays constant. A Nicolet recorder follows the surface in time (Fig. 93). Color high speed movies and TV camera recordings were taken of the combustion wave while the burning rate was oscillating. The measured frequency of the oscillations was found independent on which one of the two chambers was used, a sign that a 1000 cm^3 volume was large enough to damp the potential pressure

waves induced by the unsteady burning regimes. Further experiments in a third combustion chamber, of quite different geometry and with the propellant sample placed horizontally rather than vertically, yielded essentially the same results (within the limits of the remark made above on the burning rate effect). Therefore, it can be concluded that: (1) a self sustained oscillatory burning regime exists for $p > PDL$, exactly as predicted by the nonlinear burning stability theory; (2) no significant effect of the combustion chamber volume could be detected (except minor changes of the propellant burning rate, which in turn affects the combustion frequency). Further experimental details are reported in Refs. 32 and 35.

Analytical predictions of the PDL are in good agreement with the experimentally observed values (cf. Fig. 33-37). The numerical validation of the analytical predictions was also successful; for example, see Fig. 94, where the bifurcation diagram of Fig. 33 has been validated by smooth pressurization runs from some initial pressure to the wanted final pressure of interest. The combustion frequency numerically obtained in Fig. 94 is also plotted in Fig. 91. The numerical values are lower than those measured, while their trend, i.e. the increase with pressure, is well verified. Reasons for the discrepancy may lie in the approximation used in the model. For instance, in these tests c_g , c_c and k_c were assumed temperature-independent, an approximation of consequence. Also, at the low pressures near PDL, the thin surface flame model is probably not very good any longer: in fact, movies of the flame show a sharp distinction between the decomposition flame anchored to the surface, and the diffusion flame that undergoes large elongations and even detaches itself during the oscillations. Further tests will focus on resolving the possible causes (finite thickness of the condensed phase reacting layer?). To complete the picture, Fig. 94 shows numerical solutions of the surface temperature vs time for four pressure ranges. Going from lower p to higher p the amplitude decreases just as predicted by the bifurcation diagram, while the frequency increases, just as observed experimentally. No comparison was attempted between predicted and measured amplitudes; from the phototransistor luminosity traces at $p = 0.12$ atm (Figs. 91-92) it is clear that residual fumes in the chamber intercept some of the light, making amplitude not very reproducible. Besides this random error, luminosity does not yield easily surface temperature. The frequency of the emission peaks is instead nearly constant. The upper and lower limits of the oscillation (dashed lines E and D) are reported in Fig. 94 for the same

case of $p=0.12$ atm. Reasonable agreement exists between the analytical predictions and the actual numerical solutions. When $p = 0.06$ atm no oscillations are numerically observed, and the surface temperature drops to zero: the pressure is lower than the PDL.

The results of this section point to the stability nature of extinction corresponding to the PDL, at least for AP-based composite solid propellants and for the experimental conditions used. Contrary to most of the intuitive explanations supplied so far, the PDL does not strongly depend on heat losses or a particular heat loss, as shown experimentally by Cookson and Fenn (Ref. 124) and also by the fact that radiative heat losses corresponding to emissivity $\bar{\epsilon}_\lambda$ ranging from 0 to 0.75 did not have any effect on the analytical predictions and numerical results as well.

Rather unsatisfactory instead is the prediction of the oscillations frequency near PDL. Among the possible causes are: uncomplete AP combustion (not accounted for in the present treatment); the flame model used (unlikely, as at low pressure the heat feedback from the gas has been found negligible compared to the other terms); thermal properties varying with temperature differently than assumed; or some other (unsuspected) burning rate behavior at low pressure. For example, it remains to investigate the influence of condensed phase kinetics (included in the model) which is, however, usually negligible for AP propellants.

As for the PDL itself, the evidence indicates this is the inevitable consequence of the weaker and weaker coupling between solid and gas when the pressure is reduced, that increases the amplitude of the burning rate excursions until the surface temperature falls below the value that allows recovery. The novel feature of this investigation consists in a simultaneous analytical, numerical, and experimental verification of the PDL without recourse to either external (unknown) heat losses or additional new physical phenomena.

6.5 - CONCLUDING REMARKS

The experimental results collected so far fully confirm the theoretical picture (stability analysis and numerical simulations). In considering this statement, recall that a wide variety of experimental results can be predicted and reproduced within the framework of this theoretical approach.

Attempts to reproduce the PDL of the nonmetallized propellant burning in nitrogen were straightforward. By using the data corresponding to the properties of the tested material (AP/CTPB), in particular the appropriate values of \tilde{E}_s and n_s , the experimental value of PDL=0.06 atm could easily be reproduced both with constant and variable thermal properties. Likewise, analytical prediction and numerical reproduction of the go/no-go extinction boundaries for fast depressurization were straightforward. The qualitative agreement (the only presently possible), with the complicate pressure pulse tests at the piston tube, is also extremely encouraging. The qualitative, but not quantitative, agreement with the pressure dependence of self-sustained oscillatory burning is just a challenge for further progress; the explanation has probably already been detected. In any event, one should consider very positively the fact that parallel analytical, numerical, and experimental work could shed light on so many (apparently unconnected) physical phenomena, with no string attached to the fundamental nonlinear burning stability theory.

CHAPTER 7 - CONCLUSIONS AND FUTURE WORK

Activities connected with this research study have been developed for almost ten years along analytical, numerical, and experimental guidelines (Refs. 10-40, 149-168). The authors feel that no comparable theory exists in the relevant literature of nonlinear burning stability (see Chapter 2). However, the authors also consider that further developments are in order to complete the picture. Therefore, in this final chapter, first the state of the art of the overall research study is presented, then the unifying concepts so far ascertained will be underlined, finally the present and future directions of investigation will be illustrated.

7.1 - STATE OF THE ART OF THE RESEARCH STUDY

The problem of solid propellant burning has been dealt with in a rather general form, but within the restrictions of monodimensional heterogeneous thin flames of thermal nature (see Chapter 1). This yields a complicated set of equations, based on the PDE describing the thermal field of the propellant condensed phase (see Chapter 3). This nonlinear model, as any other model of similar nature, can be solved by numerical means only (see Chapter 5). The basic novelty of this research study is an attempt to predict the fundamental stability laws of the nonlinear model by analytical means (see Chapter 4). In order to retain the nonlinearity of the problem, an approximate formulation in terms of an ODE was written. This was done by means of an integral approach, limited to situations in which no inflection point in the history of the condensed phase thermal profiles would occur. It is shown that the important facts (see below) of heterogeneous combustion may be ascertained. The two fundamental regimes of the static (intrinsic random perturbations) and dynamic (externally assigned changes of the controlling parameters) stability of heterogeneous flames are examined, allowing for finite size disturbances.

The following facts emerge from the nonlinear static stability analysis. For a given set of parameters:

1. A stable stationary nonreacting configuration (trivial solution) is always found.
2. A stable stationary, time-independent or self-sustained oscillatory, reacting configuration is usually found.
3. The stable stationary time-independent reacting configuration is found before A-D roots coalescence occurs.

4. The stable stationary self-sustained oscillations are found between A-D roots coalescence and B-D roots coalescence.
5. After B-D roots coalescence, no stable stationary reacting solution is found; this originates the PDL when pressure is changed.
6. The static burning boundary, for small but finite size random intrinsic disturbances, is the locus of the A-B roots coalescence at fixed pressure.
7. The static stability of the steady state configurations can be measured by the slope of the static restoring function vs the surface temperature at the point $\bar{\theta}_s$ of interest.
8. The effect of the relevant parameters can be easily evaluated by considering the corresponding static restoring function and bifurcation diagrams.
9. The quantities p , $Q_{s,ref}$, Q_c , \tilde{E}_c are bifurcation parameters; \tilde{E}_s and w are not.

The following facts emerge from the nonlinear dynamic stability analysis. For a given monotonic or pulsed law of time-wise decrease of the controlling parameters:

1. Extinction may occur even though the final point of the transition is statically stable.
2. The lower dynamic stability boundary, or dynamic extinction boundary, for finite size disturbances consequent to timewise monotonical changes of the controlling parameters, is the locus of the statically unstable roots (B-type) associated with the final operating conditions. The dynamic extinction boundary holds true instantaneously for monotonic forcing functions, after the disturbance for pulsed forcing functions.
3. The dynamic extinction boundary holds true for both deradiation and/or depressurization driven transients, since it does not depend on the forcing law.
4. Upper dynamic instability is related to D-root and may cause vigorous acceleration of the combustion wave followed by attempts of dynamic extinction.

The following facts emerge by comparing several flame models:

1. The linearized flame models (KTSS, KZ, and LC) are of no value for burning rates less than about 90% of the corresponding steady value.
2. The KTSSN nonlinear flame model is physically questionable for burning rates near zero, otherwise it

displays results similar to those obtained by MTS.

3. The MTS flame model is a principle acceptable over the whole range of burning rates, since it accounts also for chemical kinetics, but requires two constants to be evaluated by an appropriate fitting procedure.

The following facts emerge by changing the order n and nature of the approximating disturbance thermal profile in the condensed phase:

1. The shape of the restoring function and bifurcation diagram is qualitatively the same.
2. C and A-roots are never affected.
3. B, D and E-root are affected by n , while the nature of the approximating profile influences only if volumetrically distributed terms are important.
4. The static burning boundary can be predicted independently of n .
5. The pressure deflagration limit prediction depends on n .
6. The prediction of dynamic stability boundaries (both lower and upper) depends on n .
7. The best results are found for approximating profiles of polynomial nature and order n ranging from 2.5 to 3.

The addition in the condensed phase of temperature dependent thermal properties and volumetrically distributed chemical reactions does not sensibly affect the fundamental burning stability properties. Likewise, the presence of polychromatic external radiation impinging on a (possibly) optically transparent condensed phase does not sensibly affect the fundamental burning stability properties. The extension of the model to more sophisticated pyrolysis laws allows a better fitting of experimentally determined steady ballistic properties, but again no sensible effect on the fundamental burning stability properties can be detected.

In particular, the nonlinear stability theory of heterogeneous thin flames developed in this research study shows that:

1. pressure deflagration limit can be predicted even for adiabatic combustion waves.
2. self-sustained oscillatory burning is found for both increasing $Q_{s,ref} + Q_c$ (at a fixed pressure) and decreasing pressure (with a fixed chemical composition).
3. damped oscillatory burning is found for both increasing $Q_{s,ref} + Q_c$ (at a fixed pressure) and decreasing pressure (with a fixed chemical composition) before the self-sustained

- oscillatory burning.
4. The effect of $C_g \neq 1$ is appreciable in reducing the amplitude and region of occurrence of the self-sustained oscillatory burning.
 5. the effect of radiative heat loss from the burning surface is negligible.
 6. the effect of large values of \tilde{E}_s is to increase appreciably the amplitude and region of occurrence of the self-sustained oscillatory burning.
 7. the effect of $K_c(\theta)$ increasing with temperature is to reduce the amplitude of the self-sustained oscillatory burning.
 8. the effect of $C_c(\theta)$ increasing with temperature is to reduce sensibly the amplitude and region of occurrence of the self-sustained oscillatory burning.
 9. ignition transients in general cannot be fully predicted (for the time being).
 10. all findings have a clear interpretation in the standard pressure vs burning rate plot.

Notice that numerical values were given only for two composite propellants (AP/PBAA No. 941 and AP84/CTPB16). This was done simply because properties and good flame models were readily available for those particular propellants. It is felt however, that all analyses were conducted from a broad point of view, and in no way were they dependent on the particular type of propellant chosen as datum case. Therefore, the conceptual results are expected to hold, although in different ranges of the relevant parameters, for a wide variety of solid propellants.

7.2 - CONCLUSIONS

A nonlinear stability analysis of solid propellant burning was carried out, within the framework of a thermal theory and for thin flame (quasi-steady gas phase) allowing for finite size disturbances. This required an integral method reducing the partial differential equation for the condensed phase heat transfer to an approximate ordinary differential equation. It is shown that a nonlinear algebraic function, called restoring function, can be defined that contains all basic properties of equilibrium and stability of burning solid propellants. This function does not depend on time, but only on the nature of the solid propellant (including its flame) and the operating conditions (pressure, ambient temperature, and diabaticity). Analysis of the nonlinear algebraic restoring function and associated bifurcation diagrams reveals that two well defined burning regimes exist, each limited by stability boundaries:

the static and the dynamic regimes. Of these two, the region of dynamic burning is wider, in that under dynamic conditions the propellant may momentarily burn also in a region which is statically forbidden.

The static regime can be observed experimentally and therefore can be studied also in the framework of Zeldovich approach. The statically stable reacting steady solution is either stationary or self-sustained oscillating. The static burning boundary is defined as that ultimate burning condition, at constant pressure and for a given set of operating conditions, below which steady solutions are no longer found. Pressure deflagration limit is defined as the minimum pressure, for a given set of operating conditions, below which steady solutions are no longer statically stable. Methods are suggested as to the prediction of both static boundaries.

The dynamic regime cannot be observed experimentally in a stationary mode and can only be studied in the framework of a flame model. In general, a lower (burning rate below the steady value) dynamic stability boundary is always found, except for large enough ambient temperature and/or (external) radiant flux. Moreover, for each propellant an appropriate combination of pressure and surface heat release exists for which lower and upper (burning rate above the steady value) dynamic stability boundaries are found. The lower dynamic stability boundary or dynamic extinction boundary is defined as that ultimate burning condition beyond which extinction necessarily follows during a burning transient. The upper dynamic stability boundary implies a vigorous accelerations of the combustion wave, possibly followed by attempts of dynamic extinction.

It is shown that the lower dynamic stability boundary holds true both for deradiation and/or depressurization, for opaque as well as transparent condensed phase, for fast deceleration of the combustion wave (e.g., by depressurization) as well as for fast acceleration (e.g., by pressurization) if an excessively large burning rate overshoot is attained. The dynamic extinction boundary was determined for arbitrary but levelling off external controlling parameters or monotonically decreasing external controlling parameters. If no change in time of the external controlling parameters occurs, the propellant is only subjected to random intrinsic disturbances and the static stability analysis apply. If the effect of the time change of the external controlling parameters (nonautonomous function) is negligible compared to the restoring function, the lower dynamic stability boundary collapses to the range of

influence of the statically stable equilibrium configuration and therefore holds true at any instant and for any external law (even non monotonic or levelling off).

The validity of this nonlinear stability theory was verified by computer simulated transients. In general, excellent agreement was found between the analytical predictions and the numerical results obtained by integration of the governing partial differential equation. For example, the numerical integration of the basic set of equations in terms of the PDE suggests the existence of a no-return point for fast transients and defines its value by a trial and error procedure. Incidentally, it was observed that changes in the decay rate are most effective in affecting the overall fate of the dynamic history if realized in the early portion of the transition. The values obtained in several different configurations are in excellent agreement with the predictions made from an analysis of the approximate ODE describing the system. This also confirms that the static stability boundary, as determined for example in the Zeldovich approach, has no relevance in dynamic disturbances of finite size. Moreover, the analytical predictions of the PDL is well verified numerically. Likewise, the bifurcation diagrams are well verified numerically under a wide variety of operating conditions.

The theoretical work (analytical predictions and numerical simulations) was successfully validated by fast depressurization and low pressure (PDL and self-sustained oscillatory burning) experiments. Qualitative agreement was also found with the complicate phenomena induced by pressure pulses at the piston tube. The only point to improve, for the time being, is the frequency prediction of the self-sustained oscillatory burning; several routes are being tested in this direction.

It is felt that conclusive evidence was offered for: (1) the existence of several static burning regimes (stationary time-independent burning, stationary self-sustained oscillatory burning, extinction); (2) the capability of the proposed theory to predict pressure deflagration limit even for adiabatic combustion waves; (3) the capability of the proposed theory to predict dynamic extinction limits. In conclusion, the nonlinear static restoring function and the associated bifurcation diagram contain all basic properties of equilibrium and asymptotic (both static and dynamic) stability of burning solid propellants, even for finite size disturbances, provided that the external forcing terms are monotonic or level off in time. The most important conclusion is perhaps the fact that one theory exists which predicts, within a unique framework,

such apparently unrelated phenomena as depressurization or deradiation extinction, low pressure extinction, oscillatory burning, ecc., without any string attached (i.e., ad hoc assumption).

7.3 - FUTURE WORK

The most urgently needed task is the collection of a wide range of experimental results obtained under well known and controlled operating conditions. For this purpose, a laser driven combustion apparatus is being set up and is expected to be operative within a short time. A continuous wave CO₂ laser, emitting at 10.6 μ m in the far infrared, was already received and tested; the selected laser tube can also be used in the pulsed mode and permits several waveforms to be implemented. The laser driven combustion apparatus is planned to provide ignition and extinction maps, radiation augmented or assisted steady burning rate data, radiation augmented or assisted self-sustained oscillatory burning information. These results will allow to test critical predictions of the nonlinear burning stability theory for both the static and dynamic regimes. Of course, other conventional experimental rigs will be maintained productive and possibly improved: in particular, the fast depressurization strand burner and piston tube apparatus are meant to provide pressure driven tests complementary to the radiation driven tests of the laser apparatus. Special attention will be kept on the subatmospheric pressure range and pressure deflagration limit phenomena. Extensive data collections by microthermocouples will be performed. Systematic data collections of steady burning rate at different ambient temperatures and different pressures will be realized, in order to evaluate experimentally the temperature sensitivity coefficients to be compared with the theoretically predicted values. Finally, the flame structure in the gas phase will be studied by means of color movies, TV recordings, light emission, laser doppler velocimetry.

As to the theoretical side of the overall research study, the authors feel that the theory is already quite mature and exploitable. However, the following points deserve further attention: (1) the influence of the specific integral technique, implemented to transform the PDE problem into an ODE one, on the fundamental stability properties established during this investigation; (2) the relationship of this theory with the Zeldovich approach as well as other burning stability theories available from the relevant literature; (3) prediction of ignition dynamics; (4) completion of the bifurcation maps. Two specific theoretical problems will require more in-depth

analyses: the exact prediction of frequency for self-sustained oscillatory burning regimes and the inclusion of condensed phase heterogeneity in the nonlinear burning stability theory.

REFERENCES

- (1) Williams F.A., "Combustion Theory", Addison-Wesley Publ. Reading, Mass., 1965.
- (2) Williams F.A., Barrère M., and Huang N.C., "Fundamental Aspects of Solid Propellant Rockets", AGARDograph No.116. Technivision Series, Slough, England, October 1969.
- (3) Price E.W. and Culick F.E.C., "Combustion of Solid Rocket Propellants", AIAA Professional Study Series, preliminary manuscript, 1970.
- (4) Novozhilov B.V., "Nonstationary Combustion of Solid Rocket Fuels", Nauka, Moscow, 1973. Translation AFSC No. FTD-MT-24-317-74.
- (5) Zeldovich Ya.B., Leypunskiy O.I., and Librovich V.B., "The Theory of the Unsteady Combustion of Powder", Nauka, Moscow, 1975.
- (6) Librovich V.B., "Theory of Nonsteady Flames", Manuscript based on the lectures presented at Princeton University in December 1969 - January 1970. Revised Draft on 9 May 1970.
- (7) Boggs T.L. and Zinn B.T. editors, "Experimental Diagnostics in Combustion of Solids", AIAA Progress in Astronautics and Aeronautics, Vol. 63, 1978.
- (8) Kuo K.K. and Summerfield M. editors, "Fundamentals of Solid Propellant Combustion", AIAA Progress in Astronautics and Aeronautics, Volume on print.
- (9) De Luca L., Coghe A., and Reggiori A., "The Dynamics of Solid Propellant Combustion", Final Technical Report to European Research Office (Grant No. DA-ERO 78-G-029), Istituto di Macchine, Politecnico di Milano, December 1980.
- (10) De Luca L., "Nonlinear Stability Analysis of Solid Propellant Combustion", II International Symposium on Dynamics of Chemical Reactions, University of Padova, Italy, 15-17 December 1975. Proceedings, pp.245-256, 1975.
- (11) De Luca L., "Instability of Heterogeneous Deflagration Waves", VI International Symposium on Detonation, San Diego, California, USA, 24-27 August 1976. Proceedings, pp. 281-289, 1976.
- (12) De Luca L., "Solid Propellant Ignition and Other Unsteady Combustion Phenomena Induced by Radiation", Ph. D. Thesis,

Department of Aerospace and Mechanical Sciences, Princeton University, AMS Report No. 1192-T, November 1976.

- (13) De Luca L., Galfetti L., and Zanotti C., "Dynamic Extinction of Composite Solid Propellant", XIX Israel Conference on Aviation and Astronautics, Technion, Haifa, Israel, 2-3 March 1977. Israel Journal of Technology, Vol. 16, No. 16, pp. 159-168, 1978.
- (14) De Luca L., "Theoretical Studies on Heterogeneous Deflagration Waves: I. A Partial Differential Equation Formulation of the Problem", Meccanica, Vol. 13, No. 1, pp. 16-27, 1978.
- (15) De Luca L., "Theoretical Studies on Heterogeneous Deflagration Waves: II. An Approximate Ordinary Differential Equation Formulation of the Problem", Meccanica, Vol. 13, No. 2, pp. 71-77, 1978.
- (16) De Luca L., Galfetti L., and Zanotti C., "Comparison of Two Flame Models Used in Solid Rocket Propellant Unsteady Combustion", XXVI Convegno Nazionale delle Comunicazioni, Genova, Italy, 5-7 October 1978. Proceedings, pp. 442-453, 1978.
- (17) De Luca L., "Self-sustained Oscillatory Combustion of Solid Rocket Propellants", The Propulsion and Energetics Panel of AGARD, 53rd Meeting on Solid Rocket Motor Technology, Oslo, Norway, 2-5 April 1979. AGARD Conference Proceedings No. 259, pp. 24/1-24/14, July 1979.
- (18) De Luca L., Galfetti L., and Zanotti C., "Ignition and Extinction of Solid Rocket Propellants", The Propulsion and Energetics Panel of AGARD, 53rd Meeting on Solid Rocket Motor Technology, Oslo, Norway, 2-5 April 1979. AGARD Conference Proceedings No. 259, pp. 4/1-4/14, July 1979.
- (19) De Luca L., Coghe A., Ferrari G.C., Galfetti L., Martinnelli L., Volpi A., Zanotti C., Basso A., and Casci C., "Recent Research on Unsteady Combustion at CNPM", VI International Symposium on Combustion Processes, Karpacz, Poland, 26-30 August 1979. Archivum Combustionis, Vol. 1, No. 3/4, pp. 301-328, 1981.
- (20) De Luca L., "Frequency Response Function of Burning Solid Propellants", V Congresso Nazionale dell'Associazione Italiana di Aeronautica e Astronautica (AIDAA), Milano, Italy, 22-26 October 1979. Meccanica, Vol. 15, No. 4, pp. 195-205, 1980.

- (21) De Luca L., Riva G., Galfetti L., and Tabacco U., "Unstable Burning of Thin Solid Propellant Flames", XVI AIAA/SAE/ASME Joint Propulsion Conference, Hartford, Connecticut, USA, 30 June - 2 July 1980. AIAA Paper 80-1126.
- (22) De Luca L., "Nonlinear Burning Stability Theory of Heterogeneous Thin Flames", XVIII International Symposium on Combustion, University of Waterloo, Canada, 17-22 August 1980. Proceedings, pp.1439-1450, 1981.
- (23) De Luca L., Riva G., Galfetti L., and Zanotti C., "Theoretical and Experimental Nonlinear Dynamics of Heterogeneous Deflagration Waves", VI Heat and Mass Transfer Conference, Byelorussian Academy of Science, Minsk, USSR, 10-12 September 1980. Proceedings, Vol. III, pp. 83-91, 1980.
- (24) De Luca L., Riva G., and Tanturli I., "Numerical Solution of Solid Propellant Unsteady Burning", VI Congresso Nazionale dell'Associazione Italiana di Aeronautica e Astronautica (AIDAA), Roma, Italy 15-19 June 1981. Proceedings, pp. 177-191, 1981. Aerotecnica Missili e Spazio, Vol. 61, No. 2, pp. 61-68, 1982.
- (25) De Luca L., "A Generalized Nonlinear Stability Theory of Solid Propellant Combustion", XXXII International Astronautical Federation Congress, Roma, Italy, 4-12 September 1981. IAF Paper 81-358. Acta Astronautica, Vol. 9, No. 9, pp. 579-580, 1982.
- (26) De Luca L., Dondé R., and Riva G., "Effects of Distributed Condensed Phase Reactions on Heterogeneous Deflagration Waves", Second International Specialists Meeting of the Combustion Institute on Oxidation, Budapest, Hungary, 18-22 August 1982. Oxidation Communications, on print.
- (27) De Luca L., Riva G., and Bruno C., "Bifurcation in Heterogeneous Combustion", NATO Advanced Study Institute on Non-Equilibrium Cooperative Phenomena in Physics and Related Fields, Madrid, Spain, 1-11 August 1983. Proceedings, on print.
- (28) De Luca L., Dondè R., and Zanotti C., "Experimental Dynamic Extinction by Depressurization of a Composite Solid Rocket Propellant", XXXIV Congresso Nazionale Associazione Termotecnica Italiana (ATI), Palermo, 8-12 October 1979. Proceedings, Vol. 2, pp. 51-78, 1979.

- (29) Coghe A., De Luca L., Sensalari G.L., and Volpi A., "Gas Phase Velocity Measurements in Solid Rocket Propellants by Laser-Doppler Anemometry", The Propulsion and Energetics Panel of AGARD, 53rd Meeting on Solid Rocket Motor Technology, Oslo, Norway, 2-5 April 1979, AGARD Conference Proceedings No. 259, pp. 31/1-31/14, July 1979.
- (30) Reggiori A., De Luca L., and Geremi R., "Experimental Investigation on Solid Rocket Propellant Burning Instability by Shock Tube". Aerotecnica Missili e Spazio, Vol. 58, No. 2/3 pp. 158-166, 1979.
- (31) Dondé R., Riva G., and De Luca L., "Experimental and Theoretical Extinction of Solid Rocket Propellants by Fast Depressurization", XXXIII International Astronautical Federation Congress, Paris, France, 26 September-3 October 1982. IAF Paper 82-361. Acta Astronautica, on print.
- (32) Bruno C., Riva G., Zanotti C., Dondè R., Grimaldi C., and De Luca L., "Experimental and Theoretical Burning of Solid Rocket Propellants Near the Pressure Deflagration Limit", XXXIV International Astronautical Federation Congress, Budapest, Hungary, 10-15 October 1983. IAF Paper 83-367. Acta Astronautica, on print.
- (33) Raimondi V., "Analisi Nonlineare della Stabilità di Combustione di Propellenti Solidi Compositi per Endoreattori", Master's Thesis in Aeronautical Engineering, Dipartimento di Energetica, Politecnico di Milano, April 1977.
- (34) Magugliani F., "Analisi Teorica della Struttura di Onde Eterogenee Stazionarie di Deflagrazione", Master's Thesis in Aeronautical Engineering, Dipartimento di Energetica, Politecnico di Milano, October 1983.
- (35) Grimaldi C., "Combustione di Propellenti Solidi per Endoreattori in Prossimità della Pressione Limite di Deflagrazione", Master's Thesis in Mechanical Engineering, Dipartimento di Energetica, Politecnico di Milano, July 1983.
- (36) Riva G., "Modellistica della Combustione di Sostanze Solide", Doctoral Thesis in Energetics, Dipartimento di Energetica, Politecnico di Milano, April 1984.

- (37) Casci C. e De Luca L. "La Vitesse Linéaire de Regression du Perchlorate d'Ammonium dans un Ecoulement Gazeux Combustible", XXIV Meeting of AGARD, Dayton, Ohio, USA, 13-17 October 1969. AGARD Conference Proceedings No. 52, pp. 35/1 - 35/30, 1969. CNPM NT-119.
- (38) Ohlemiller T.J., Caveny L.H., De Luca L., and Summerfield M., "Dynamics Effects on Ignitability Limits of Solid Propellants Subjected to Radiative Heating", XIV International Symposium on Combustion, Pennsylvania State University, Pennsylvania, USA 20-25 August 1972. Proceedings, pp. 1297-1307, 1973.
- (39) De Luca L., Caveny L.H., Ohlemiller T.J. and Summerfield M., "Radiative Ignition of Double-Base Propellants: I. Some Formulation Effects", AIAA J., Vol. 14, No. 8, pp. 940-946, 1976.
- (40) De Luca L., Ohlemiller T.J., Caveny L.H. and Summerfield M., "Radiative Ignition of Double Base Propellants: II. Pre-Ignition Events and Source Effects", AIAA J., Vol. 14, No. 8, pp. 1111-1117, 1976.
- (41) Ciepluch C.C., "Effect of Rapid Pressure Decay on Solid Propellant Combustion", ARS J., Vol. 31, November 1961, pp. 1584-1586, 1961.
- (42) Ciepluch C.C., "Effect of Composition on Combustion of Solid Propellants During a Rapid Pressure Decrease", NASA TN D-1559, 1962.
- (43) Ciepluch C.C., "Spontaneous Reignition of Previously Extinguished Solid Propellants", NASA TN D-2167, 1964.
- (44a) Merkle C.L., Turk S.L., and Summerfield M., "Extinguishment of Solid Propellant by Rapid Depressurization", Princeton University, AMS Report No. 880, 1969.
- (44b) Merkle C.L., Turk S.L., and Summerfield M., "Extinguishment of Solid Propellant by Depressurization: Effects of Propellant Parameters", AIAA Paper No. 69-176, 1969.
- (44c) Merkle C.L. and Summerfield M., "Extinguishment of Solid Propellant Flames: a Theory Based on a New Feedback Law", Princeton University, AMS Report No. 838, Presentation Version, 1968.
- (45) Krier H., "Solid Propellant Burning Rate During a Pressure Transient", Combustion Science and Technology, Vol. 5, pp. 69-73, 1972. See also: "Comments", Combustion Science and Technology, Vol. 9, p. 195, 1974.

- (46) Paul B.E., Levine R.L., and Fong L.Y., "A Ballistic Explanation of the Ignition Pressure Peak", AIAA Paper No. 64-121, 1964.
- (47) Parker K.H. and Summerfield M., "The Ignition Transient in Solid Propellants Rocket Motors", Department of Aerospace and Mechanical Sciences, Princeton University, AMS Report, No. 769, 1966. See Appendix II.
- (48) Von Elbe G., "Solid Propellant Ignition and Response of Combustion to Pressure Transients", AIAA Paper No. 66-668, 1966.
- (49) Von Elbe G. and McHale E.T., "Extinguishment of Solid Propellants by Rapid Depressurization", AIAA J., Vol. 6, No. 7, pp. 1417-1419, 1968.
- (50) T'ien J.S., "A Theoretical Criterion for Dynamic Extinction of Solid Propellants by Fast Depressurization", Combustion Science and Technology, Vol. 9, pp. 37-39, 1974.
- (51) T'ien J.S., "The Effects of Perturbations on the Flammability Limits", Combustion Science and Technology, Vol. 7, No. 4, pp. 185-188, 1973.
- (52) Horton M.D., Bruno P.S. and Graesser E.C. "Depressurization Induced Extinction of Burning Solid Propellant", AIAA J., Vol. 6, No. 2, pp. 292-297, 1968. See also ICRPG/AIAA 2nd Solid Propulsion Conference, pp. 232-239, 1967.
- (53) Marxman G.A. and Wooldridge C.E., "Effect of Surface Reactions on the Solid Propellant Response Function", AIAA J., Vol. 6, No. 3, pp. 471-478, 1968.
- (54a) Wooldridge C.E. and Marxman G.A., "Nonlinear Solid Propellant Burning Rate Behavior During Abrupt Pressure Excursion", AIAA Paper No. 69-172, 1969.
- (54b) Wooldridge C.E. and Marxman G.A., "A Comparison between Theoretical and Experimental Behavior of Solid Propellants", AIAA Paper No. 70-666, 1970.
- (55) Mongia H.C. and Ambs L.L., "A Model for the Combustion and Extinction of Composite Solid Propellants During Depressurization", Combustion and Flame, Vol. 22, pp. 59-69, 1974. See also: "Comments", Combustion and Flame, Vol. 23, pp. 401-402, 1974.
- (56) Suhas H.K. and Bose T.K., "A Mathematical Model to Predict Transient Burning Rate and Pressure Decay Rates for Extinction of Composite Propellants", Combustion and

- Flame, Vol. 28, pp. 145-153, 1977. See also: "Comments", Combustion and Flame, Vol. 31, pp. 329-332, 1978; "Comments", Combustion and Flame, Vol. 35, pp. 213-218, 1979.
- (57) Suhas H.K. and Bose T.K., "Nonsteady Combustion of Composite Propellants Subjected to Rapid Depressurization", Combustion Science and Technology, Vol. 28, pp. 55-68, 1982.
- (58) Zeldovich Ya.B., "On the Theory of Combustion of Powder and Explosives", Journal of Experimental and Theoretical Physics, Vol. 12, No. 11-12, pp. 498-524, 1942.
- (59) Zeldovich Ya. N., "The Burning Velocity of Powder under Variable Pressure", Journal of Applied Mechanics and Theoretical Physics, Vol. 5, No. 3, pp. 126-130, 1964.
- (60) Istratov A.G., Librovich V.B., and Novozhilov B.V., "An Approximate Method in the Theory of Unsteady Burning Velocity of Powder", Journal of Applied Mechanics and Technical Physics, Vol. 5, No. 3, p. 139, 1964.
- (61) Marshakov V.N. and Leipunskiy O.I., "Burning and Quenching of a Powder in the Presence of a Rapid Pressure Drop", FGV, Vol. 3, No. 2, pp. 144-146, 1967.
- (62) Novozhilov B.V., "Nonstationary Burning of Powder Having a Variable Surface Temperature", Journal of Applied Mechanics and Technical Physics, Vol. 8, No. 1, pp. 54-63, 1967.
- (63) Summerfield M., Caveny L.H., Battista R.A., Kubota N., Gostintsev Yu. A., and Isoda H., "Theory of Dynamic Extinguishment of Solid Propellants with Special Reference to Non-steady Heat Feedback", JSR, Vol. 8, No. 3, pp. 251-258, 1971. See also AIAA Paper No. 70-667, 1970.
- (64) Battista R.A., Caveny L.H. and Summerfield M., "Nonsteady Combustion of Solid Propellants", Department of Aerospace and Mechanical Sciences, Princeton University, AMS Report No. 1049, October 1972.
- (65) Frost V.A., "Extinction of a Powder with a Change in Pressure", Journal of Applied Mechanics and Technical Physics, Vol. 13, No. 5, pp. 113-118, 1972.
- (66) Frost V.A. and Yumashev V.L., "Study of the Extinction of Gunpowder in the Combustion Model with a Variable Surface Temperature", Journal of Applied Mechanics and Technical Physics, Vol. 14, No. 3, pp. 92-100, 1973.
- (67) Frost V.A. and Yumashev V.L., "Extinction of a Solid Propellant Accompanying a Fall in Pressure as a Loss

- of Combustion Stability", Combustion Explosion and Shock Waves, Vol. 2, No. 4, pp. 548-555, 1976.
- (68) Assovskiy I.G., Istratov A.G., and Leypunskiy O.I., "Extinction of a Propellant with a Pressure Drop", Combustion Explosion and Shock Waves, Vol. 13, No. 2, pp. 200-205, 1977.
- (69) Librovich V., "Non-steady Burning Processes for Powder and Solid Propellants", XII International Symposium on Space Technology and Science, Tokyo, pp. 585-590, 1977.
- (70) Steinz J.A. and Selzer H., "Depressurization Extinguishment of Composite Solid Propellants: Flame Structure, Surface Characteristics, and Restart Capability", Combustion Science and Technology, Vol. 3, pp. 25-36, 1971.
- (71) Steinz J.A. and Selzer H., "Depressurization Extinguishment for Various Starting Pressures and Solid Propellant Types", AIAA Paper No. 71-631, 1971.
- (72) Selzer H., "Depressurization Extinguishment of Composite Solid Propellants: Influence of Composition and Catalysts", AIAA J., Vol. 11, No. 9, pp. 1221-1222, 1973.
- (73) Baer A.D., Ryan N.W., and Schulz E.B., "Spectra and Temperature of Propellant Flames during Depressurization", AIAA J. Vol. 9, No. 5, pp. 869-875, 1971. See also: AIAA Paper No. 70-663, 1970.
- (74) Park C.P., Ryan N.W. and Baer A.D., "Extinguishment of Composite Propellants at Low Pressures", AIAA Paper No. 73-175, 1973.
- (75a) Jensen G.E. and Brown R.S., "An Experimental Investigation of Rapid Depressurization Extinguishment", AIAA J., Vol. 9, No. 9, pp. 1667-1673, 1971.
- (75b) Jensen G.E. and Brown R.S., "An Experimental Investigation of Rapid Depressurization Extinguishment", 6th ICRPG Combustion Conference, CPIA Publication No. 192, pp. 411-423, 1969.
- (76) Zemskikh V.I., Istratov A.G., Leypunskiy O.I. and Marshakov V.N., "Three Characteristic Ballistic Powder Combustion Modes with a Pressure Drop", Combustion Explosion and Shock Waves, Vol. 13, No. 1, pp. 14-19, 1977.
- (77) Ivashchenko Y.S. and Komarov A.S., "Extinction of a Ballasted Powder due to Pressure Drop", Combustion Explosion and Shock Waves, Vol. 14, No. 1, pp. 151-153, 1978.

- (78) Strand L.D., Schultz A.L., and Reedy G.K. "Microwave Doppler Shift Technique for Determining Solid Propellant Transient Regression Rates", Journal of Spacecraft and Rockets, Vol. 11, No. 2, pp. 75-83, 1974.
- (79) Strand L.D., Magiawala K.R., and McNamara R.P., "Microwave Measurement of the Solid Propellant Pressure Coupled Response Function", Journal of Spacecraft and Rockets, Vol. 17, Vol. 6, pp. 483-488, 1980.
- (80) Levine J.N. and Andrepont W.C., "Measurement Methods of Transient Combustion Response Characteristics of Solid Propellant - An Assessment", AIAA Paper No. 79-1209, 1979.
- (81) Klevnoi S.S., "Quenching of Explosive Following Interruption of the Ignition Light Flux", Combustion Explosion and Shock Waves, Vol. 7, No. 2, pp. 178-188, 1971.
- (82) Mikheev V.F. and Levashov Yu. V., "Experimental Study of Critical Conditions during the Ignition and Combustion of Powders", Combustion Explosion and Shock Waves, Vol. 9, No. 4, pp. 506-510, 1973.
- (83) Assovskiy I.G., "Transient Combustion of Powder Subjected to Intense Light", Combustion Explosion and Shock Waves, Vol. 9, No. 6, pp. 874-883, 1973.
- (84) Gostintsev Yu.A., "Extinction of a Steady State Burning Powder by a Pulse of Thermal Radiation", Combustion Explosion and Shock Waves, Vol. 10, No. 5, pp. 764-767, 1974.
- (85) Zarko V.E. and Kiskin A.B., "Numerical Modeling of Non-steady Powder Combustion Under the Action of a Light Flux", FGV, Vol. 16, No. 6, pp. 650-654, 1980.
- (86) Kiskin A.B. "Stability of Stationary Powder Combustion Acted on by a Constant Light Flux", FGV, Vol. 19, No. 3, pp. 295-297, 1983.
- (87) Zarko V.E., Simonenko V.N. and Kiskin A.B., "Unsteady Burning of Double-Base Propellants", VIII International Colloquium of Gasdynamics of Explosions and Reactive Systems, Byelorussian Academy of Sciences, USSR, 23-26 August 1981.
- (88) Huffington J.D., "The Burning and Structure of Cordite", Trans. Faraday Soc., Vol. 47, pp. 864-876, 1951.
- (89) Huffington J.D., "The Unsteady Burning of Cordite", Trans. Faraday Soc., Vol. 50, pp. 942-952, 1954.
- (90) Clemmow D.M. and Huffington J.D., "An Extension of the Theory of Thermal Explosion and its Application to the Oscillatory Burning of Explosives", Trans. Faraday Soc., Vol. 52, pp. 385-396, 1956.

- (91) Frank-Kamenetskii D.A., "Diffusion and Heat Exchange in Chemical Kinetics", Princeton University Press, 1955, Chapters 6-9.
- (92) Huggett C., Bartley C.E., and Mills M.M., "Solid Propellant Rockets", Princeton Aeronautical Paperbacks No. 2, Princeton University Press, 1960.
- (93) Inami Y.H. and Shanfield H., "Nonacoustic Combustion Pulsations of Ammonium Perchlorate Containing Aluminum", AIAA Journal Vol. 2, No. 7, pp. 1314-1318, 1964.
- (94) Eisel J.L., Horton M.D., Price E.W. and Rice D.W., "Preferred Frequency Oscillatory Combustion of Solid Propellants", AIAA Journal, Vol. 2, No. 7, pp. 1319-1323, 1964.
- (95a) Angelus T.A., "Unstable Burning Phenomenon in Double-Base Propellants", AIAA Progress in Astronautics and Rocketry, M. Summerfield editor, Vol. 1, pp. 527-559, 1960.
- (95b) Angelus T.A., "Solid Propellant Combustion Instability", VIII Symposium (International) on Combustion pp.921-924, 1962.
- (96) Yount R.A. and Angelus T.A., "Chuffing and Nonacoustic Instability Phenomena in Solid Propellant Rockets", AIAA Journal, Vol. 2, No. 7, pp. 1307-1313, 1964.
- (97) Price E.W., "Recent Advances in Solid Propellant Combustion Instability", XII Symposium (International) on Combustion, pp. 101-113, 1969.
- (98) Shkadinskii K.G., Khaikin B.I., and Merzhanov A.G., "Propagation of a Pulsating Exothermic Reaction Front in the Condensed Phase", FGV, Vol. 7, No. 1, pp.19-28, 1971.
- (99) Librovich V.B. and Makhviladze G.M., "One Limiting Scheme for the Propagation of a Pulsating Exothermic Reaction Front in a Condensed Medium", JPMTF, Vol. 15, No. 6, pp. 107-116, 1974.
- (100) Svetlichnyi I.B., Margolin A.D., and Pokhil P.F., "Low Frequency Self-Oscillatory Processes in Propellant Combustion", FGV, Vol. 7, No. 2, pp. 188-194, 1971.
- (101) Ilyukhin V.S., Mysov V.G., and Novikov S.S., "Low Frequency Nonacoustic Fluctuations During Combustion of Nitroglycerine Powder", FGV, Vol. 10, No. 3, pp. 334-337, 1974.
- (102) Ilyukhin V.S., Margolin A.D., Mysov V.G., and Novikov S.S., "Role of Heterogeneity of Composite Solid Fuels in the Mechanism of Pulsating Burning", FGV, Vol. 11, No. 3, pp. 498-501, 1975.

- (103) Kooker D.E. and Nelson C.W., "Numerical Solution of Solid Propellant Transient Combustion", J. Heat Transfer, Vol. 101, pp. 359-364, 1979.
- (104) T'ien J.S., "Oscillatory Burning of Solid Propellants Including Gas Phase Time Lag", CST, Vol. 5, No. 2, pp. 47-54, 1972.
- (105) Peters N., "Theory of Heterogeneous Combustion Instabilities of Spherical Particles", XV Symposium (International) on Combustion, pp. 363-375, 1975.
- (106) Matkowski B.J. and Sivashinky G.I., "Propagation of a Pulsating Reaction Front in Solid Fuel Combustion", SIAM J. Appl. Math., Vol. 35, No. 3, pp. 465-478, 1978.
- (107) Delfosse L., Baillet C., and Lucquin M., "Pulsating Combustion of Liquid Hydrocarbons", Combustion and Flame, Vol. 54, pp. 203-207, 1983.
- (108) Friedman R., Nugent R.G., Rumbel K.E., and Scurlock A.G., "Deflagration of Ammonium Perchlorate", 6th Symposium (International) on Combustion, Reinhold Publ.Corp., New York, pp. 612-618, 1957.
- (109) Levy J.B. and Friedman R., "Further Studies of Pure Ammonium Perchlorate Deflagration" 8th Symposium (International) on Combustion, pp. 663-672, 1962.
- (110) Horton M.D. and Price E.W., "Deflagration of Pressed Ammonium Perchlorate", ARS Journal, p. 1745, November 1962.
- (111) Hightower J.D. and Price E.W., "Combustion of Ammonium Perchlorate", 11th Symposium (International) on Combustion pp. 463 - 472, 1967.
- (112) Watt D.M. and Petersen E.E., "Relationship between the Limiting Pressure and the Solid Temperature for the Deflagration of Ammonium Perchlorate", Journal of Chemical Physics, Vol. 50, No. 5, pp. 2196-2198, 1969.
- (113) Watt D.M. and Petersen E.E., "The Deflagration of Single Crystals of Ammonium Perchlorate", Combustion and Flame, Vol. 14, pp. 297-302, 1970.
- (114) Johnson W.E. and Nachbar W., "Deflagration Limits in the Steady Linear Burning of a Monopropellant with application to Ammonium Perchlorate", 8th Symposium (International) on Combustion, The Williams and Wilkins Co., Baltimore, pp. 678-689, 1962.
- (115) Guirao C. and Williams F.A., "A Model for Ammonium Perchlorate Deflagration between 20 and 100 atm", AIAA Journal, Vol. 9, No. 7, pp. 1345-1356, 1971.

- (116) Lieberherr J.R., "High Temperature Pyrolysis of Ammonium Perchlorate", 20th Symposium (International) on Combustion, p. 533, 1969.
- (117) Boggs T.L., "Deflagration Rate, Surface Structure and Subsurface Profile of Self Deflagration Single Crystals of Ammonium Perchlorate", AIAA Journal, Vol. 8, No. 5, pp. 867-873, 1970.
- (118) Shadman-Yazdi F. and Petersen E.E., "The Effect of Catalysts on the Deflagration Limits of Ammonium Perchlorate", Combustion Science and Technology, Vol. 5, p. 61, 1972.
- (119) Cohen Nir E., "An Experimental Study of the Low Pressure Limit for Steady Deflagration of Ammonium Perchlorate", Combustion and Flame, Vol. 14, pp. 419-435, 1973.
- (120) Cohen Nir E., "Effet de la Température Initiale sur la Vitesse de Combustion et sur la Pression Limite de Déflagration de Perchlorate d'Ammonium", La Recherche Aérospatiale, No. 1972-2 (mars-avril), pp.75-84, 1972.
- (121) Sohn H.Y., "A Unified Theory of Ammonium Perchlorate Deflagration and the Low Pressure Deflagration Limit", Combustion Science and Technology, Vol. 10, pp. 137-154, 1975.
- (122) Godon J.C., "Modèle de Combustion du Perchlorate d'Ammonium", La Recherche Aérospatiale, No. 1982-2 (mars-avril), pp. 101-107, 1982.
- (123a) Steinz J.A., Stang P.L., and Summerfield M. "The Burning Mechanism of Ammonium Perchlorate Based Composite Propellants", Princeton University, AMS Report No.830 February 1969.
- (123b) Steinz J.A. and Summerfield M., "Low Pressure Burning of Composite Solid Propellants", Reprinted from Advances in Chemistry Series No. 88, 1969.
- (123c) Steinz J.A. and Stang P.L., "The Burning Mechanism of Ammonium Perchlorate Based Composite Solid Propellant", AIAA Paper No. 68-658, June 1968.
- (123d) Steinz J.A., Stang P.L., and Summerfield M., "Effects of Oxidizer Particle Size on Composite Solid Propellant Burning: Normal Burning, Plateau Burning and Intermediate Pressure Extinction", AMS Report No. 810, Princeton University, Presentation Version, October 1967.
- (124) Cookson R.E. and Fenn J.B., "Strand Size and Low Pressure Deflagration Limit in a Composite Propellant", Project Squid Technical Report PR-116-PU, Purdue University, December 1968.

- (125) Silla H., "Burning Rates of Composite Solid Propellants at Subatmospheric Pressure", ARS Journal, pp.1277-1278, September 1961.
- (126) Northam G.B., Pellet C.L., and Cofer III W.R., "Effects of Low Temperature Ammonium Perchlorate Decomposition on the Ballistic Properties of a CTPB Propellant", AIAA Journal, Vol. 10, No. 8, pp. 1068-1072, 1972.
- (127) Peterson J.A., Reed Jr. R., and Mc Donald A.J., "Control of Pressure Deflagration Limits of Composite Solid Propellants", AIAA Journal, Vol. 5, No. 4, pp.764-770, 1970.
- (128a) Baliga B.R. and T'ien J.S., "Unsteady Effects of Low Pressure Extinction Limit of Solid Propellants", AIAA Journal, Vol. 13, No. 12, pp. 1653-1656, 1975.
- (128b) Baliga B.R. and T'ien J.S., "Flammability Limits and the Oscillatory Burning of Solid Propellants at Low Pressure", Case Western Reserve University Report, FTAS/TR-74-100, 1974.
- (129) Zenin A.A. and Nefedova O.I., "Burning of Ballistic Powder over a Broad Range of Initial Temperatures", Combustion, Explosion and Shock Waves, Vol. 3, No. 1, pp. 26-31, 1967.
- (130) Zenin A.A., "Burning of Nitroglycerine Powder in Vacuum and at Subatmospheric Pressure", Combustion, Explosion and Shock Waves, Vol. 2, No. 1, pp. 42-44, 1966.
- (131) Kydd P.H. and Foss W.I., "A Comparison of the Influence of Heat Losses and Three-Dimensional Effects on Flammability Limits", Combustion and Flame, vol. 14, pp.267-274, 1964.
- (132) Chan W.Y. and T'ien J.S., "An Experiment on Spontaneous Flame Oscillation Prior to Extinction", Combustion Science and Technology, Vol. 18, pp. 139-143, 1978.
- (133) Imber M., "Thermal Conductivity: A Parameter in Solid Propellant Burning", AIAA Journal, Vol. 4, No. 9, pp. 1610-1614, 1966.
- (133b) Cohen M.L. and Imber M. "Variation of the Thermal Conductivity of Solid Propellants in an Acoustic Field", AIAA Journal, Vol. 5, No. 7, pp. 1295-1299, 1967.
- (134) Williams F.A. and Lengellé G., "Simplified Model for Effect of Solid Heterogeneity on Oscillatory Combustion", Astronautica Acta, Vol. 14, No. 2, pp. 97-118, 1969.
- (135) Nelson C.W., "Calculated Transient Combustion of Solid Propellants", Internationale Jahrestagung 1979, Karlsruhe, Germany, pp. 153-167, 1979.

- (136a) Krier H., T'ien J.S., Sirignano W.A., and Summerfield M., "Nonsteady Burning Phenomena of Solid Propellants": Theory and Experiments", AIAA J., Vol. 6, No. 2, pp. 278-285, 1968.
- (136b) Summerfield M., Krier H., T'ien J.S., and Sirignano W.A., "Non steady Burning Phenomena of Solid Propellants": Theory and Experiment (U)", AMS Report No. 793, Princeton University, July 1967.
- (136c) Krier H., "Solid Propellant Burning in Nonsteady Pressure Fields", Ph.D. Thesis, Princeton University, September 1968.
- (137) Kooker D.E. and Zinn B.T., "Numerical Investigation of Nonlinear Axial Instabilities in Solid Rocket Motors", BRL Contract Report No. 141, March 1974.
- (138) Levine J.N. and Culick F.E.C., "Nonlinear Analysis of Solid Rocket Combustion Instability", AFRPL TR-74-75, October 1974.
- (139) Goodman T.R., "Application of Integral Methods to Transient Nonlinear Heat Transfer", Advances in Heat Transfer, Vol. 1, Academic Press, pp. 51-122, 1964.
- (140) Andronov A.A., Vitt A.A., and Khaikin S.E., "Theory of Oscillators", English Edition by Pergamon Press Ltd., London; U.S.A. Edition distributed by Addison-Wesley, Mass., 1966.
- (141) Kuo K.K., "Theory of Flame Front Propagation in Porous Propellant Charges Under Confinement", Ph.D. Thesis, Princeton University, AMS Dept., 1971.
- (142) Peretz A., Caveny L.H., Kuo K.K., and Summerfield M., "The Starting Transient of Solid Propellant Rocket Motors with High Internal Gas Velocities", Princeton University, AMS Dept. Report No. 1100, April 1973.
- (143) Gostintsev Yu. A., "Method of Reduction to Ordinary Differential Equations in Problems of the Nonstationary Burning Solid Propellants", FGV, Vol. 3, No. 3, pp. 218-220, 1967.
- (144) Nogotov E.F., "Application of Numerical Heat Transfer", Hemisphere Publ. Corp., 1978.
- (145) Ozisk M.N., "Heat Conduction", J. Wiley and Sons, 1980.
- (146) Patankar S.V., "Numerical Heat Transfer and Fluid Flow", Hemisphere Publ. Corp., 1980.

- (147) Richtmyer R.D. and Morton K.W., "Difference Methods for Initial Value Problems", Interscience Publishers, II Edition, 1967.
- (148) Ames W.F., "Numerical Methods for Partial Differential Equations, Computer Sciences and Applied Mathematic Series, II Edition, 1977.
- (149) Ceriotti A., "Estinzione per Depressurizzazione di Propellenti Solidi Compositi", Master's Thesis Aeronautical Engineering, Dipartimento di Energetica, Politecnico di Milano, July 1978.
- (150) Dondé R., "Teoria e Sperimentazione dell'Estinzione Dinamica per Depressurizzazione dei Propellenti Solidi Compositi", Master's Thesis in Engineering, Dipartimento di Energetica, Politecnico di Milano, October 1979.
- (151) Giobbio G., "Studio dell'Ignizione dei Propellenti Solidi Compositi al Tubo d'Urto", Master's Thesis in Aeronautical Engineering, Dipartimento di Energetica, Politecnico di Milano, July 1977.
- (152) Falzoni C., "Instabilità di Combustione di Propellenti Solidi al Tubo d'Urto", Master's Thesis in Aeronautical Engineering, Dipartimento di Energetica, Politecnico di Milano, December 1977.
- (153) Germi R., "Verifica di Tubo d'Urto con Pistone della Instabilità di Combustione di Propellenti Solidi per Endoreattori", Master's Thesis in Engineering, Dipartimento di Energetica, Politecnico di Milano, April 1979.
- (154) Reggiori A. and Parigi G.P., "Experimental Study of Solid Rocket Propellant Combustion with High Speed Cinematography", VI Congresso Nazionale della Associazione Italiana di Aeronautica e Astronautica (AIDAA), Roma, Italy, 15-19 June 1981. Proceedings, pp. 159-176, June 1981.
- (155) Reggiori A. and Carlevaro R., "Studio e Sviluppo di un Tubo d'Urto a Pistoni per Prove Dinamiche ad Alte Pressioni", XXXVI Congresso Nazionale dell'Associazione Termotecnica Italiana (ATI), Viareggio, Italy 5-9 ottobre 1981. Proceedings, pp. 91-104, October 1981.

- (156) Poli A., "Rilievo delle Caratteristiche di Combustione di un Propellente a Doppia Base mediante Tubo d'Urto a Pistone", Master's Thesis in Aeronautical Engineering, Dipartimento di Energetica, Politecnico di Milano, June 1982.
- (157) Reggiori A., Carlevaro R., and Poli A., "Studio Sperimentale delle Caratteristiche di Combustione di un Propellente Solido a Doppia Base in Regime Non Stazionario", XXXVII Congresso della Associazione Termotecnica Italiana (ATI), Padova, Italy, 27 September-1 October 1982. Proceedings, pp. 751-762. October 1982.
- (158) Zanotti C. and Galfatti L., "Combustione di Propellenti Solidi per Endoreattori", Master's Thesis in Aeronautical Engineering, Dipartimento di Energetica, Politecnico di Milano, December 1976.
- (159) De Luca L. and Zanotti C., "Measurement of Steady Solid Propellant Burning Rate and Data Processing", XXXII Congresso Nazionale della Associazione Termotecnica Italiana (ATI), Roma, 20-23 September 1977. Proceedings pp. 278-301, 1977.
- (160) De Luca L., Galfatti L., and Zanotti C., "Evaluating the Kinetic and Diffusion Time Constants in the MTS Flame Model", XXXII Congresso Nazionale della Associazione Termotecnica Italiana (ATI), Roma, 20-23 September 1977. Proceedings, pp. 278-301, 1977.
- (161) De Luca L., Casarini M., Pastore G., Portaro A., Tanturli I., and Zanotti C., "Experimental results on the Steady Burning of Solid Rocket Propellants", XXXIV Congresso Nazionale della Associazione Termotecnica Italiana (ATI), Palermo, 8-12 October 1979. Proceedings Vol. 2, pp. 79-106, 1979.
- (162) Pastore G., "Misura della Velocità Stazionaria di Combustione di Propellenti Solidi per Endoreattori", Master's Thesis in Aeronautical Engineering, Dipartimento di Energetica, Politecnico di Milano, Ottobre 1978.
- (163) Portaro A., "Metodi Sperimentali per il Rilievo della Velocità di Combustione per Propellenti a Doppia Base", Master's Thesis in Aeronautical Engineering, Dipartimento di Energetica, Politecnico di Milano, April 1984.
- (164) Molinari A., "Misure della Velocità Stazionaria di Regressione per Propellenti Solidi mediante Tecnica Ottica Laser", Master's Thesis in Mechanical Engineering, Dipartimento di Energetica, Politecnico di Milano, July 1984.

- (165) Vimercati G., "Velocità Stazionaria di Combustione di Propellenti Solidi in funzione della Temperatura Ambiente", Master's Thesis in Aeronautical Engineering, Dipartimento di Energetica, Politecnico di Milano, April 1978.
- (166) Piccolo A., "Velocità Stazionaria di Combustione di un Propellente Solido Alluminato in funzione di Pressione e Temperatura", Master's Thesis in Aeronautical Engineering, Dipartimento di Energetica, Politecnico di Milano, July 1983.
- (167) Tanturli I., "Rilievo Sperimentale del Profilo Termico Stazionario nell'Onda di Combustione di Propellenti Solidi", Master's Thesis in Aeronautical Engineering, Dipartimento di Energetica, Politecnico di Milano, July 1977.
- (168) Lapegna V., "Rilievo del Profilo Termico in Propellenti Solidi per Endoreattori", Master's Thesis in Aeronautical Engineering, Dipartimento di Energetica, Politecnico di Milano, July 1983.
- (169) Price C., Boggs T., and Derr R., "Modeling of Solid Monopropellant Deflagration", AIAA paper No. 78-219, 1978.
- (170) Price C., Boggs T., and Derr R., "The Steady State Combustion Behavior of Ammonium Perchlorate and HMX", AIAA paper No. 79-0164, 1979.
- (171) Rosser W. A. Jr., Inami S. H., and Wise H., "Thermal Diffusivity of Ammonium Perchlorate", AIAA J., Vol. 4, No. 4, pp. 663-666, 1966.

NOMENCLATURE

a	= constant used in nondimensional specific heat law
a_{λ}	= volumetric optical absorption coefficient, cm^{-1}
A_j	= coefficient of the PDE in finite difference form
A_m	= kinetic constant used in the MTS flame model
b	= constant used in nondimensional thermal conductivity law
B_j	= coefficient of the PDE in finite difference form
B_m	= diffusion constant used in the MTS flame model
B_p	= nondimensional pressurization rate coefficient
B_r	= nondimensional radiation rate coefficient
c	= specific heat, cal/g K
C	= c/c_{ref} , nondimensional specific heat
C_j	= coefficient of the PDE in finite difference form
d	= layer thickness, cm
d_{ref}	= $\alpha_c/r_{b,\text{ref}}$, reference distance, cm
D_j	= coefficient of the PDE in finite difference form
$E(\cdot)$	= $\tilde{E}/R/T(\cdot)_{,\text{ref}}$, nondimensional activation energy
E	= activation energy, cal/mole
$f(\theta_s - \bar{\theta}_s)$	= nondimensional static restoring function (see Chapter 4)
$f_1(X, \lambda)$	= nondimensional function depending on the optical properties of condensed phase and external radiation source
F_o	= I_o/φ_{ref} , nondimensional external radiant flux intensity
$g(\tau, \theta_s - \bar{\theta}_s)$	= nondimensional nonautonomous function (see Chapter 4)
$G(x)$	= nondimensional function depending on the disturbance profile type (see Chapter 4)
$H(\cdot)$	= $Q(\cdot)/Q_{\text{ref}}$, nondimensional heat release
I_o	= external radiant flux intensity, $\text{cal/cm}^2 \text{s}$
JF	= total number of nodes in the space net
k	= thermal conductivity, cal/cm s K
K	= k/k_{ref} , nondimensional thermal conductivity

m	= mass flow rate, $\text{g/cm}^2\text{s}$
n	= exponent in ballistic burning rate law; also: order of the approximating temperature disturbance profile (see Chapter 4)
n_s	= pressure exponent in the pyrolysis law
p	= pressure, atm
p_{ref}	= 68 atm, reference pressure, atm
P	= p/p_{ref} , nondimensional pressure
q	= $\varphi/\varphi_{\text{ref}}$, nondimensional energy flux
Q	= heat release (positive if exothermic), cal/g
Q_{ref}	= $c_{\text{ref}}(T_{s,\text{ref}} - T_{\text{ref}})$, reference heat release, cal/g
r_b	= burning rate, cm/s
$r_{b,\text{ref}}$	= $r_b(p_{\text{ref}})$, reference burning rate, cm/s
r_λ	= optical reflectivity of the burning surface, %
R	= $r_b/r_{b,\text{ref}}$, nondimensional burning rate
\mathcal{R}	= 1.987 cal/mole K, universal gas constant, cal/mole K
t	= time, s
t_{ref}	= $\alpha_c/r_{b,\text{ref}}^2$, reference time, s
T	= temperature, K
T_{ref}	= 300 K, reference temperature, K
$T_{s,\text{ref}}$	= $T_s(p_{\text{ref}})$, reference surface temperature, K
$T_{f,\text{ref}}$	= $T_f(p_{\text{ref}})$, reference flame temperature, K
u	= nondimensional finite size disturbance of temperature (see Chapter 4)
u_g	= gas velocity, cm/s
u_x	= nondimensional finite size disturbance of thermal gradient (see Chapter 4)
U	= nondimensional gas velocity
w	= $\rho_g \tilde{\epsilon}_g$, mass reaction rate used in LC flame models; also: power of KTSS pyrolysis law
x	= space variable, cm
X	= x/d_{ref} , nondimensional space variable

GREEK SYMBOLS

α	= thermal diffusivity, cm^2/s
β	= reaction order of KZ flame model
δ	= d/d_{ref} , nondimensional layer thickness
$\delta(x-x_f)$	= Dirac delta function located at the flame position $x=x_f$
ϵ	= nondimensional reaction rate
ϵ_λ	= surface optical emissivity, %
θ	= $(T-T_{\text{ref}})/(T_{\text{s,ref}}-T_{\text{ref}})$, nondimensional temperature
θ_k	= matching temperature for surface pyrolysis laws
θ_m	= minimum temperature for occurrence of chemical reactions in the condensed phase
ϑ	= nondimensional temperature used in the analytical solution of steady temperature profiles, $\vartheta = \int_0^{\theta} \epsilon(\theta) d\theta$ (see Chapter 4).
$T(\)$	= $T(\)/T(\),_{\text{ref}}$, nondimensional temperature
ξ	= nondimensional thickness of disturbance thermal layer
λ	= wavelength, μm
ρ	= density, g/cm^3
σ	= $1.37 \times 10^{-12} \text{ cal}/\text{cm}^2 \text{ s K}^4$, Stefan-Boltzmann constant, $\text{cal}/\text{cm}^2 \text{ s K}^4$
τ	= t/t_{ref} , nondimensional time
τ'	= nondimensional characteristic time parameter used in flame models, $(C_g/Kg) (\rho_c/\bar{\epsilon}g) \tau$
φ	= energy flux, $\text{cal}/\text{cm}^2 \text{ s}$
φ_{ref}	= $\rho_c c_{\text{ref}} r_{\text{b,ref}} (T_{\text{s,ref}}-T_{\text{ref}})$, reference energy flux, $\text{cal}/\text{cm}^2 \text{ s}$
Φ	= nondimensional function used in KTSS flame model
ψ	= constant used in Voon Elbe's expression describing depressurization transients
Ψ	= AP loading, %
ω	= frequency, Hz

SUBSCRIPTS AND SUPERSCRIPTS

a	= optical absorption layer
b	= burning
c	= condensed phase
cr	= crystalline
c,s	= surface, condensed phase side
di	= diffusion
f	= flame; also: final
g	= gas phase
g,s	= surface, gas phase side
i	= initial
j	= space counter in the finite difference mesh (see Chapter 5)
ki	= kinetic
n	= time counter in the finite difference mesh (see Chapter 5)
out	= lost from the propellant
p	= pressure
re	= reaction
ref	= reference
s	= surface
ST	= static
th	= thermal
v	= vaporization
ξ	= penetration depth
λ	= spectral
=	= average value
-	= steady state value
o	= at the burning surface
$+\infty$	= far upstream
$-\infty$	= far downstream
\sim	= dimensional value

ABBREVIATIONS

A	= Ammonia (NH_3)
AFSC	= Air Force System Command
AGARD	= Advisory Group for Aerospace Research and Developments
AIAA	= American Institute of Aeronautics and Astronautics
AIDAA	= Associazione Italiana di Aeronautica e Astronautica
AIMETA	= Associazione Italiana di Meccanica Teorica ed Applicata
AMS	= Aerospace and Mechanical Sciences Department
AP	= Ammonium Perchlorate (NH_4ClO_4)
ASME	= American Society of Mechanical Engineers
ATI	= Associazione Termotecnica Italiana
BC	= Boundary Condition
BC1	= Boundary Condition at $x = 0$
BC2	= Boundary Condition at $x = -\infty$
BRL	= Ballistic Research Laboratory
CF	= Combustion and Flame
CNPM	= Centro di Studio per Ricerche sulla Propulsione e sull'Energetica
CPIA	= Chemical Propulsion Information Agency
CST	= Combustion Science and Technology
CTPB	= Carboxyl Terminated PolyButadiene
CTPIB	= Carboxyl Terminated PolyIsoButylene
DB	= Double Base
FGV	= Combustion, Explosion and Shock Waves
GDF	= Granular Diffusion Flame (a model of steady state burning)
HTBP	= Hydroxyl Terminated PolyButadiene
IAF	= International Astronautical Federation
IC	= Initial Condition

JETF = Journal of Experimental and Theoretical Physics
JPMTF = Journal of Applied Mechanics and Theoretical Physics
JSR = Journal of Spacecraft and Rockets
KTSS = Krier-T'ien-Sirignano-Summerfield
KTSSN = KTSS Nonlinear
KZ = Kooker-Zinn
LC = Levine-Culick
MTS = Merkle-Turk-Summerfield
NC = Nitrocellulose
NG = Nitroglycerine
NOTS = Naval Ordnance Test Station
NWC = Naval Weapons Center
ODE = Ordinary Differential Equation
ONERA = Office National d'Etudes et de Recherches
Aérospatiales
PA = Perchloric Acid (HClO_4)
PBAA = PolyButadiene Acrylic Acid
PDE = Partial Differential Equation
PDL = Pressure Deflagration Limit
PS = PolySulfide
PU = PolyUrethane
PVS = PolyVinylChloride
SAE = Society of Automative Engineers
SRI = Stanford Research Institute
TDI = Toluene DiIsocyanate
UTC = United Technology Center

LIST OF TABLES

- Tab. 1 - Properties of solid composite propellant AP/PBAA No. 941. Surface heat release positive if exothermic. Optical properties evaluated at 10.6 μm . Values taken from Refs. 44, 123, 137, 138.
- Tab. 2 - Properties of solid composite propellant AP84/CTPB16. Surface heat release positive if exothermic.
- Tab. 3 - Influence of temperature dependent specific heat in condensed phase on the kinetic (A_n) and diffusion (B_n) characteristic time parameters used in the MTS flame model.
- Tab. 4 - Stabilizing effect of large radiant flux and destabilizing effects of large surface heat release or ambient temperature on stability strength of steady reacting solutions. Nonlinear static restoring function evaluated from MTS flame with $n=3$ at standard conditions of $p=30$ atm.

LIST OF FIGURES CAPTIONS

- Fig. 1 - a) Schematic diagram of the physical problem.
b) Energy balance at the burning surface.
- Fig. 2 - Steady temperature profiles in the condensed phase computed for variable thermal properties.
- Fig. 3 - Heat feedback law computed according to KTSSN flame: influence of pressure and variable specific heat in the condensed phase. The different trend (at low burning rates) of the linearized version is drawn.
- Fig. 4 - Temperature profiles in the gas phase computed according to KTSSN flame: influence of pressure and variable specific heat in the condensed phase.
- Fig. 5 - Working map (burning rate vs heat feedback) for the propellant AP/CTPB No. 02 according to KTSSN flame: effects of diabaticity, ambient temperature and pressure.
- Fig. 6 - Qualitative sketch of the nonlinear static restoring function, illustrating the existence of several potential equilibrium roots: C and A are solutions of the steady energy equation, while B D and E are solutions of the perturbed energy equation.
- Fig. 7 - Nonlinear static restoring function: stabilizing effect of pressure on both reacting modes (roots A and B). AP/PBAA No. 941, MTS flame, $C_g=1$, $n=3$.
- Fig. 8 - Nonlinear static restoring function: stabilizing effect of external radiant flux on the dynamic extinction boundary. AP/PBAA No. 941, MTS flame, $C_g=1$, $n=3$.
- Fig. 9 - Nonlinear static restoring function: stabilizing effect of pressure on both reacting modes (roots A and B). AP/PBAA No. 941, KTSSN flame, $C_g=1$, $n=3$.
- Fig. 10 - Compared nonlinear static restoring functions for MTS, KTSS nonlinear and KTSS linear (or KZ or LC) flames. The linearized flame models are of limited value. AP/PBAA No. 941, $C_g=1$, $n=3$.

- Fig. 11 - Nonlinear static restoring function: effect of the order of the polynomial temperature disturbance profile. AP/PBAA No. 941, MTS flame, $C_g=1$, $p=20$ atm.
- Fig. 12 - Evaluating the static burning limit for different pressure levels. AP/PBAA No. 941, MTS flame, $C_g=1$.
- Fig. 13 - Evaluating the static burning limit through the static restoring function at 20 atm of pressure. AP/PBAA No. 941, MTS flame, $C_g=1$, $n=3$.
- Fig. 14 - The stability of the dynamic burning regime is limited by the no-return point B_f (the unstable root associated to the static restoring function for $\tau \rightarrow \infty$).
- Fig. 15 - Static Burning and dynamics stability boundaries on a burning rate vs heat feedback plot. AP/PBAA No.941, MTS flame, $C_g=1$, $n=3$.
- Fig. 16 - Bifurcation diagram plotting nontrivial roots A,B, D and E vs surface heat release. AP/PBAA No. 941, MTS flame, $C_g=1$, $p=10$ atm, $n=3$.
- Fig. 17 - Bifurcation diagram plotting nontrivial roots A,B,D, and E vs surface heat release. AP/PBAA No. 941, MTS flame, $C_g=1$, $p=20$ atm, $n=3$.
- Fig. 18 - Bifurcation diagram plotting nontrivial roots A,B, D and E vs surface heat release. AP/PBAA No. 941, MTS flame, $C_g=1$, $p=30$ atm, $n=3$.
- Fig. 19 - Bifurcation diagram plotting nontrivial roots A,B, D and E vs surface heat release. AP/PBAA No. 941, MTS flame, $C_g=1$, $p=40$ atm, $n=3$.
- Fig. 20 - Bifurcation diagram plotting nontrivial roots A,B, D and E vs surface heat release. AP/PBAA No. 941, MTS flame, $C_g=1$, $p=50$ atm, $n=3$.
- Fig. 21 - Bifurcation diagram plotting nontrivial roots A,B, D and E vs surface heat release. AP/PBAA No. 941, MTS flame, $C_g=1$, $p=60$ atm, $n=3$.
- Fig. 22 - Bifurcation diagram plotting nontrivial roots A,B, D and E vs condensed phase heat release. AP/PBAA No. 941, KTSSN flame, $C_g=1.67$, $Q_{s,ref}=125$ cal/g, $E_c=30$ Kcal/mole, $p=50$ atm, $n=3$.

- Fig. 23 - Bifurcation diagram plotting nontrivial roots A,B, D and E vs condensed phase heat release. AP/PBAA No. 941, KTSSN flame, $C_g=1.67$, $a=b=0.2$, $Q_{s,ref}=125$ cal/g, $\tilde{E}_c=30$ Kcal/mole, $p=20$ atm, $n=3$.
- Fig. 24 - Bifurcation diagram plotting nontrivial roots A,B, D and E vs condensed phase heat release. AP/PBAA No. 941, KTSSN flame, $C_g=1.67$, $a=b=0.2$, $Q_{s,ref}=125$ cal/g, $\tilde{E}_c=15$ Kcal/mole, $p=50$ atm, $n=3$.
- Fig. 25 - Bifurcation diagram plotting nontrivial roots A,B, D and E vs condensed phase heat release. AP/PBAA No. 941, KTSSN flame, $C_g=1.67$, $a=b=0.2$, $Q_{s,ref}=145$ cal/g, $\tilde{E}_c=30$ Kcal/mole, $p=50$ atm, $n=3$.
- Fig. 26 - Bifurcation diagram plotting nontrivial roots A,B, D and E vs condensed phase activation energy. AP/PBAA No. 941, KTSSN flame, $C_g=1.67$, $a=b=0.2$, $Q_{s,ref}=125$ cal/g, $Q_c=50$ cal/g, $p=50$ atm, $n=3$.
- Fig. 27 - Bifurcation diagram plotting nontrivial roots A,B, D and E vs condensed phase activation energy. AP/PBAA No. 941, KTSSN flame, $C_g=1.67$, $a=b=0.2$, $Q_{s,ref}=125$ cal/g, $Q_c=100$ cal/g, $p=50$ atm, $n=3$.
- Fig. 28 - Bifurcation diagram plotting nontrivial roots A,B, D and E vs condensed phase activation energy. AP/CTPB No.02, $Q_{s,ref} + Q_c=125$ cal/g, $p=10$ atm, $n=3$.
- Fig. 29 - Bifurcation diagram plotting nontrivial roots A,B, D and E vs burning surface activation energy. This parameter does not originate marked bifurcation of the solution. AP/CTPB No. 02, $Q_{s,ref}=160$ cal/g, $n=0$, $p=11$ atm, $n=3$.
- Fig. 30a- Bifurcation diagram plotting nontrivial roots A,B, D and E vs KTSS pyrolysis power. This parameter does not originate bifurcation of the solution. AP/PBAA No. 941, KTSSN flame, KTSS pyrolysis, $C_g=1.12$, $Q_{s,ref}=158.2$ Cal/g, $p=40$ atm, $n=3$.
- Fig. 30b- Bifurcation diagram plotting nontrivial roots A,B, D and E vs KTSS pyrolysis power. This parameter does not originate bifurcation of the solution. AP/PBAA No. 941, KTSSN flame, KTSS pyrolysis, $C_g=1.12$, $Q_{s,ref}=158.2$ cal/g, $p=50$ atm, $n=3$.

- Fig. 31 - Bifurcation diagram plotting nontrivial roots A,B, D and E vs pressure PDL (B-D coalescence) and bifurcation (A-D crossing) occur at high parameters due to the large energy release in condensed phase and at the burning surface. AP/PBAA No. 941, KTSSN flame, Arrhenius pyrolysis, $C_g=1.67$, $a=b=0.2$, $Q_{s,ref}=125$ cal/g, $Q_c=50$ cal/g, $\tilde{E}_c=30$ Kcal/mole, $n=3$.
- Fig. 32 - Bifurcation diagram plotting nontrivial roots A,B, D and E vs pressure. By decreasing the energy release in the condensed phase, both the PDL and bifurcation move toward lower values of pressure. AP/PBAA No.941 KTSSN flame, Arrhenius pyrolysis, $C_g=1.67$, $Q_{s,ref}=125$ cal/g, $Q_c=0$ cal/g, $n=3$.
- Fig. 32b- Magnification of the subatmospheric region of Fig. 32a, showing realistic predictions of PDL (B-D coalescence) and bifurcation (A-D crossing).
- Fig. 33 - Bifurcation diagram plotting nontrivial roots A,B, D and E vs pressure . PDL is realistic, while the self-sustained oscillatory burning regions is too wide (bifurcation near the atmospheric pressure). AP84/CTPB16 propellant, KTSSN flame, $C_g=1.48$, $Q_{s,ref}=125$ cal/g, $n=3$.
- Fig. 34 - Bifurcation diagram plotting nontrivial roots A,B, D and E vs pressure. Both PDL and bifurcation are realistic. AP84/CTPB16 propellant, KTSSN flame, $C_g=1.12$, $Q_{s,ref}=125$ cal/g, $\tilde{E}_s=19$ Kcal/mole, $n_s=0.551-2.67 \times 10^{-5}$, $\tilde{E}_s=0.043$ (from best fitting of experimental data), $\tilde{n}=3$.
- Fig. 35 - Bifurcation diagram plotting nontrivial roots A,B and E vs pressure. Both PDL and bifurcation are realistic. Upper instability combustion reduced by lowering the burning surface activation energy. AP84/CTPB16 propellant, KTSSN flame, $C_g=1.12$, $Q_{s,ref}=125$ cal/g, $\tilde{E}_s=16$ Kcal/mole, $n_s=0.551 \times 2.67 \times 10^{-5}$, $\tilde{E}_s=0.123$ (from best fitting of experimental data), $n=30$.
- Fig. 36 - Bifurcation diagram plotting nontrivial roots A,B, D and E vs pressure. Both PDL and bifurcation are realistic. AP/CTPB No. 01, $\tilde{E}_s=19$ Kcal/mole, $n_s=0.044$ (optimized from experimental data), $n=3$.

- Fig. 37 - Bifurcation diagram plotting nontrivial roots A,B, D and E vs pressure. Both PDL and bifurcation are realistic. The stabilizing effect of lower (with respect to the pressure figure); burning surface activation energy is put in evidence. AP/CTPB No. 02, $E_s = 16$ Kcal/mole, $n_s = 1.22$ (optimized from experimental data), $n=3$.
- Fig. 38 - Bifurcation diagram plotting nontrivial roots A,B, D and E vs net surface heat release. AP/PBAA No. 941 propellant, $C_g=1.12$, MTS flame, $p=30$ atm, $n=3$.
- Fig. 39 - Bifurcation diagram plotting nontrivial roots A,B, D and E vs net surface heat release. Variable condensed phase thermal conductivity ($K_c(0)=1+bC$, $b=1$) and increasing C_g reduce the amplitude of the self-sustained oscillations. AP/PBAA No. 941 propellant, KTSSN flame, $p=30$ atm, $n=3$, exponential disturbance.
- Fig. 40 - Diagram plotting the condensed phase characteristic layer thicknesses (thermal and chemical vs pressure. The chemical layer thickness increases when condensed phase heat release increases and/or condensed phase activation energy decreases. The thermal thickness is not significantly affected by the presence of distributed chemical reactions, at least for the tested range of pressure and parameters. The influence of variable thermal conductivity ($K_c(0)+b$) on the chemical layer thickness is sensible.
- Fig. 41 - Burning rate vs pressure plot predicting static burning, PDL, bifurcation and dynamic extinction boundaries. AP/CTPB No. 02, KTSSN flame, $n=3$.
- Fig. 42 - Numerical molecules implemented for the numerical solution.
- Fig. 43 - Flow chart of overall computer code.
- Fig. 44 - Computed combustion transient following simultaneous deradiation (opaque condensed phase) and depressurization. The dynamic extinction limit (analytically predicted) separates extinction vs continued burning regions. AP/PBAA No. 941, MTS flame, $C_g=1$.
- Fig. 45 - Computed combustion transient following consecutive deradiation (opaque condensed phase) and depressurization. The dynamic extinction limit (analytically predicted) separates extinction vs continued burning regions. AP/PBAA No. 941, MTS flame, $C_g=1$.

- Fig. 46 - Computed combustion transient following linear deradiation. The dynamic extinction limit (analytically predicted) separates extinction vs continued burning regions. AP/PBAA No. 941, KTSSN flame, $C_g=1.12$.
- Fig. 47 - Comparison between analytically predicted and numerically computed values of the dynamic extinction limit (the unstable root B of the static restoring function) for values of the surface activation energy ranging from 1.5 to 35 Kcal/mole. AP/PBAA No.941, KTSSN flame, $C_g=1.12$.
- Fig. 48 - Computed combustion transient following linear deradiation. Volumetrically distributed heat release in the condensed phase is considered. AP/PBAA No. 941 propellant KTSSN flame, $Q_{s,ref}=140$ cal/g, $Q_c=18.2$ cal/g, $C_g=1.12$.
- Fig. 49 - Computed combustion transient following linear depressurization. Volumetrically distributed heat release in the condensed phase is considered. AP/PBAA No.941, propellant, KTSSN flame, $Q_{s,ref}=140$ cal/g, $Q_c=18.2$ cal/g, $C_g=1.12$.
- Fig. 50 - Numerical validation of the bifurcation diagram of Fig. 18. The predicted combustion regimes were numerically tested for three values of the surface heat release, corresponding to steady time-independent, steady self-sustained oscillatory, and unreacting modes. AP/PBAA propellant, MTS flames, $C_g=1$, $p_f=30$ atm.
- Fig. 51 - Numerical validation of the bifurcation diagram of Fig. 38. The predicted combustion regimes were numerically tested for three values of the surface heat release, corresponding to steady time-independent, steady self-sustained oscillatory, and unreacting modes. AP/PBAA propellant, MTS flame, $C_g=1.12$, $p_f=30$ atm.
- Fig. 52 - Numerical validation of the bifurcation diagram of Fig. 22. The predicted combustion regime were numerically tested for three values of the condensed phase heat release, corresponding to steady time-independent, steady self-sustained oscillatory, and unreacting modes. AP/PBAA propellant, KTSSN flame, $C_g=1.67$, $a=b=0.2$, $Q_{s,ref}=125$, $E_c=30$ Kcal/mole, $p=50$ atm.

- Fig. 53 - Numerical validation of the bifurcation diagram of Fig. 31. The predicted combustion regimes were numerically tested for three values of the pressure corresponding to steady time-independent, steady self-sustained oscillatory, and unreacting modes. PA/PBAA propellant, KTSSN flame, Arrhenius pyrolysis, $C_g=1.67$, $a=b=0.2$, $Q_{s,ref}=125$ cal/g, $Q_c=50$ cal/g, $E_c=30$ Kcal/mole.
- Fig. 54 - Computed pressurization transients showing three possible static regimes (stationary after damped oscillations for $p_f=8$ atm, self-sustained oscillating for $p_f=3$ atm, extinguished for $p_f=1.9$ atm). AP/PBAA No. 941, MTS flame, $C_g=1.12$.
- Fig. 55 - Numerical validation of the bifurcation diagram of Fig. 28. The predicted behavior of the combustion were numerically tested for three values of the condensed phase activation energy. AP/CTPB No. 02, $Q_{s,ref}+Q_c=125$ cal/g, $p=10$ atm, KTSSN flame.
- Fig. 56 - Numerical validation of the diagram of Fig. 29. The predicted behavior of the combustion were numerically tested for three values of the burning surface activation energy. AP/CTPB No.02, $n_s=0$, KTSSN flame.
- Fig. 57 - Computed combustion transients driven by radiation pulses. Extinction or continued burning are obtained depending on the radiation cutoff time and rate. AP/PBAA No. 941, MTS flame, $C_g=1$, $p=10$ atm.
- Fig. 58 - Computed combustion transient driven by radiation pulse leading to a final reacting combustion state ($\tau_e=1.9$). The time histories are radiant flux intensity and surface temperature (Fig. 58a), flame temperature and flame thickness (Fig. 58b) are plotted. AP/PBAA No. 941, KTSSN flame, $C_g=1.12$, $p=10$ atm.
- Fig. 59 - Computed combustion transient driven by radiation pulse leading to extinction ($\tau_e=2$). The time histories of radiant flux intensity and surface temperature (Fig. 59a), flame temperature and flame thickness (Fig. 59b) are plotted. AP/PBAA No. 941, KTSSN flame, $C_g=1.12$, $p=10$ atm.

- Fig. 60 - Computed oscillatory combustion regime induced by an external radiation pulse ($\tau_e \rightarrow \infty$). The behavior of radiant flux intensity and surface temperature (Fig. 60 a), flame temperature and flame thickness (Fig. 60b) are plotted. Both amplitude and frequency become constant few cycles after the initial combustion transient. AP/PBAA No. 941, KTSSN flame, $C_g=1.12$, $p=10$ atm.
- Fig. 61 - Schematic of the depressurization strand burner (IV version)
- Fig. 62 - Sketch illustrating the experimental pressure decay of depressurization strand burners when solenoid valves (top) or manual ball valves (bottom) are used.
- Fig. 63 - Typical recording from galvanometric recorder.
- Fig. 64 - Sketch of the combustion chamber and associated recording devices.
- Fig. 65 - Typical recording from digital memory.
- Fig. 66 - Experimental vs computed go/no-go extinction boundaries for AP70.PVN30 propellant.
- Fig. 67 - Experimental go/no-go extinction boundaries obtained from different investigations.
- Fig. 68 - Experimental vs computed go/no-go extinction boundaries for AP84/CTPB16 propellant.
- Fig. 69 - Computed burning transient following fast depressurization.
- Fig. 70a- Schematic of shock tube apparatus.
70b- Schematic of shock tube test section.
- Fig. 71 - Piston (I version) used in the piston tube apparatus.
- Fig. 72 - Piston (II version) used in the piston tube apparatus.
- Fig. 73 - Computed maximum piston speed vs initial pressure of the high pressure section.
- Fig. 74 - Experimental set-up for ionization measurements near the propellant burning surface.

- Fig. 75 - Block diagram of the instrumented piston tube apparatus.
- Fig. 76 - Extinction of noncatalyzed DB propellant tested in nitrogen.
- Fig. 77 - Continued burning of noncatalyzed DB propellant tested in nitrogen.
- Fig. 78 - Reignition of noncatalyzed DB propellant tested in nitrogen.
- Fig. 79 - Reignition of noncatalyzed DB propellant tested in nitrogen.
- Fig. 80 - Computed response of burning AP70/PVC30 propellant to piston tube pressurization. MTS flame, $C_g=1$, $a=b=0$.
- Fig. 81 - Computed response of burning AP84/CTPB16 propellant to piston tube pressurization. KTSSN flame, $C_g=1.33$, $a=b=0$.
- Fig. 82 - Schematic of laser-based technique to measure steady burning rate.
- Fig. 83 - Measured steady burning rate of noncatalyzed DB propellant.
- Fig. 84 - Measured steady burning rate of AP84/CTPB16 propellant.
- Fig. 85 - Schematic of the instrumented steady strand burner used to measure burning rate and temperature profiles.
- Fig. 86 - Typical temperature profile obtained with a 5 μ m Pt/Pt-Rh bead.
- Fig. 87 - Measured steady surface temperatures vs pressure for AP84/CTPB16 propellant.
- Fig. 88 - Schematic of the low pressure strand burner.
- Fig. 89 - Measured burning oscillations of AP84/CTPB16 at 0.12 atm N_2 and 0.12 atm (95% N_2 +5% O_2).
- Fig. 90 - Measured burning oscillations of AP84/CTPB16 at 0.12 atm N_2 and 0.08 atm (95% N_2 +5% O_2).

Fig. 91 - Measured burning frequency vs pressure of AP 84/CTPB16 propellant.

Fig. 92 - Measured burning frequency vs pressure of alumined AP propellant.

Fig. 93 - Experimental burning oscillations and stepping motor feeding velocity.

Fig. 94 - Computed burning rate oscillations near the PDL.

TABLE 1

Properties of solid composite propellant AP/PBAA
 No. 941 used as datum case in this study.
 Surface heat release positive if endothermic.
 Optical properties evaluated at 10.6 μm .
 Values taken from Refs.29, 82, 86-87.

ASSUMED OR MEASURED PROPERTIES

AP crystal transition heat, $Q_{cr,AP}$	2.000 E+01 cal/g
AP vaporization heat, $Q_{v,AP}$	5.260 E+02 cal/g
AP decomposition heat, $Q_{A/PA}$	-8.000 E+02 cal/g
Binder vaporization heat, $Q_{v,Binder}$	2.250 E+02 cal/g
AP weight fraction, p	8.000 E+01 %
Ballistic burn rate exponent, n	4.600 E-01
Pyrolysis law pressure power, n_s	0
KTSS pyrolysis law power, w	6.000
Surface activation temperature, \tilde{E}_s/a	8.081 E+03 K
Flame activation temperature, \tilde{E}_f/a	1.010 E+04 K
KZ flame reaction order, β	1.7
Condensed density, ρ_c	1.540 g/cm ³
Condensed specific heat, C_c	3.300 E-01 cal/g K
Condensed thermal diffusivity, α_c	1.400 E-03 cm ² /s
Gas thermal conductivity, k_g	1.000 E-04 cal/cm K s
Average product molecular weight, \bar{w}	2.600 E+01 g/mole
Optical surface reflectivity, \bar{r}_λ	3.800 %
Optical volumetric scattering, s_λ	0 cm ⁻¹
Minimum temperature for reactions, T_m	3.000 E+02 K
Matching temperature for pyrolysis, T_k	4.050 E+02 K

COMPUTED PROPERTIES

Net surface heat release, $Q_{s,ref}$	-1.582 E+02 cal/g
Condensed thermal conductivity, k_c	7.115 E-04 cal/cm K s
MTS chemical time constant, A_M	3.380 E-01
MTS diffusion time constant, B_M	2.350
Adiabatic flame temperature, $\bar{T}_f(P)$	$T_{f,ref} - (50/68) \cdot (P_{ref} - \bar{P})$

REFERENCE PROPERTIES

Pressure, P_{ref}	6.800 E+01 atm
Temperature, T_{ref}	3.000 E+02 K
Burning Rate, $\dot{r}_{ref} = \dot{r}(P_{ref})$	8.370 E-01 cm/s
Surface temperature, $T_{s,ref} = T_s(P_{ref})$	1.000 E+03 K
Flame temperature, $T_{f,ref} = T_f(P_{ref})$	2.430 E+03 K
Distance, $x_{ref} = \alpha_c / \dot{r}_{ref}$	1.673 E-03 cm
Time, $t_{ref} = \alpha_c / \dot{r}_{ref}^2$	1.998 E-03 s
Heat, $Q_{ref} = C_c(T_{s,ref} - T_{ref})$	2.310 E+02 cal/g
Energy flux, $I_{ref} = \rho_c C_c \dot{r}_{ref}(T_{s,ref} - T_{ref})$	2.978 E+02 cal/cm ² s

TABLE 2

=====
 Properties of solid propellant AP/CTPB No. 02.
 Surface heat release positive if exothermic.
 =====

ASSUMED OR MEASURED PROPERTIES

Net surface heat release, $Q_{s,ref}$	1.250 E+02 cal/g
AP weight fraction, ψ	8.400 E+01 %
Ballistic burning rate exponent, n	5.510 E-01
Surface activation energy, \tilde{E}_s	1.600 E+04 cal/mole
Pyrolysis law pressure power, n_s	1.220 E-01
Flame activation energy, \tilde{E}_f	2.000 E+04 cal/mole
Condensed phase density, ρ_c	1.600 E+00 g/cm ³
Ref. specific heat, c_{ref}	2.930 E-01 cal/g K
Ref. thermal diffusivity, α_{ref}	1.400 E-03 cm ² /s
Nondim. $C_c(\theta) = c_c(\theta)/c_{ref}$,	$C_c(\theta) = 1+0.28\theta$
Nondim. thermal conductivity, K_c	1.000 E+00
Gas phase thermal conductivity, $K_{g,w}$	1.000 E-04 cal/cm s K
Average product molecular weight, \bar{w}	2.600 E+01 g/mole
Optical surface reflectivity, \bar{r}_λ	0
Optical volumetric scattering, s_λ	0

COMPUTED PROPERTIES

Ref. thermal conductivity, k_{ref}	6.563 E-04 cal/cm s K
MTS chemical time constant, A_m	3.800 E-01
MTS diffusion time constant, B_m	2.650 E+00
Adiabatic flame temperature ($T = 300$ K),	2519.557 p ^{0.551} K

REFERENCE PROPERTIES

Pressure, P_{ref}	6.800 E+01 atm
Temperature, T_{ref}	3.000 E+02 K
Burning rate, $r_{b,ref}$	1.260 E+00 cm/s
Surface temperature, $T_{s,ref}$	9.880 E+02 K
Flame temperature, $T_{f,ref}$	2.683 E+00 K
Distance, d_{ref}	1.111 E-03 cm
Time, t_{ref}	8.818 E-04 s
Heat, Q_{ref}	2.016 E+02 cal/g
Energy flux, ψ_{ref}	4.064 E+02 cal/cm ² s

=====

TABLE 3

=====

Influence of temperature dependent specific heat
in condensed phase on the kinetic (A_m) and diffu-
sion characteristic time parameters used in the
MTS flame model. AP/PBAA No.951; $C_c=1+a\theta$; $c_g=0.5$ cal/g K.

=====

pressure range (atm)	a	A_m	B_m
8 - 20 ($\Delta p=2$)	-0.02	0.82	1.68
"	0	0.74	1.95
"	0.1	0.47	2.52
"	0.2	0.33	2.62
"	0.3	0.24	2.67
"	0.5	0.16	2.52
20 - 70 ($\Delta p=10$)	-0.1	1.00	1.87
"	0	0.73	2.10
"	0.1	0.54	2.14
"	0.2	0.43	2.25
"	0.3	0.36	2.22
"	0.5	0.26	2.15

=====

TABLE 4

Stabilizing effect of large radiant flux and destabilizing effect of large surface heat release or ambient temperature on stability strength of steady reacting solutions. Nonlinear static restoring function evaluated from MTS flame with $n=3$ at standard conditions
 ($p=30$ atm, $T_a=300$ K), $C_g=1$, $\epsilon_\lambda=0$

$I_o, \text{cal/cm}^2 \text{ s}$	$Q_{s, \text{ref}}, \text{cal/g}$	T_a, K	$(df/d\theta_s)_{\theta_s}$
0	158.2	300	-3.53
10	158.2	300	-3.89
20	158.2	300	-4.03
30	158.2	300	-4.27
40	158.2	300	-4.50
60	158.2	300	-5.18
80	158.2	300	-6.01
100	158.2	300	-7.05
120	158.2	300	-8.29
-10	158.2	300	-3.33
-20	158.2	300	-3.14
-30	158.2	300	-2.78
-40	158.2	300	-2.33
-50	158.2	300	-1.85
-60	158.2	300	-1.50
-70	158.2	300	-1.35
-80	158.2	300	-0.52
0	110	300	-0.71
0	120	300	-2.10
0	130	300	-3.02
0	135	300	-3.30
0	140	300	-3.55
0	145	300	-3.73
0	150	300	-3.74
0	155	300	-3.62
0	160	300	-3.51
0	165	300	-3.24
0	170	300	-2.86
0	180	300	-1.75
0	190	300	-0.05
0	200	300	+2.41
0	210	300	+5.85
0	220	300	+10.60
0	230	300	+17.17
0	240	300	26.23
0	158.2	250	-3.84
0	158.2	200	-3.57
0	158.2	350	-3.38
0	158.2	400	-2.73
0	158.2	500	-1.05

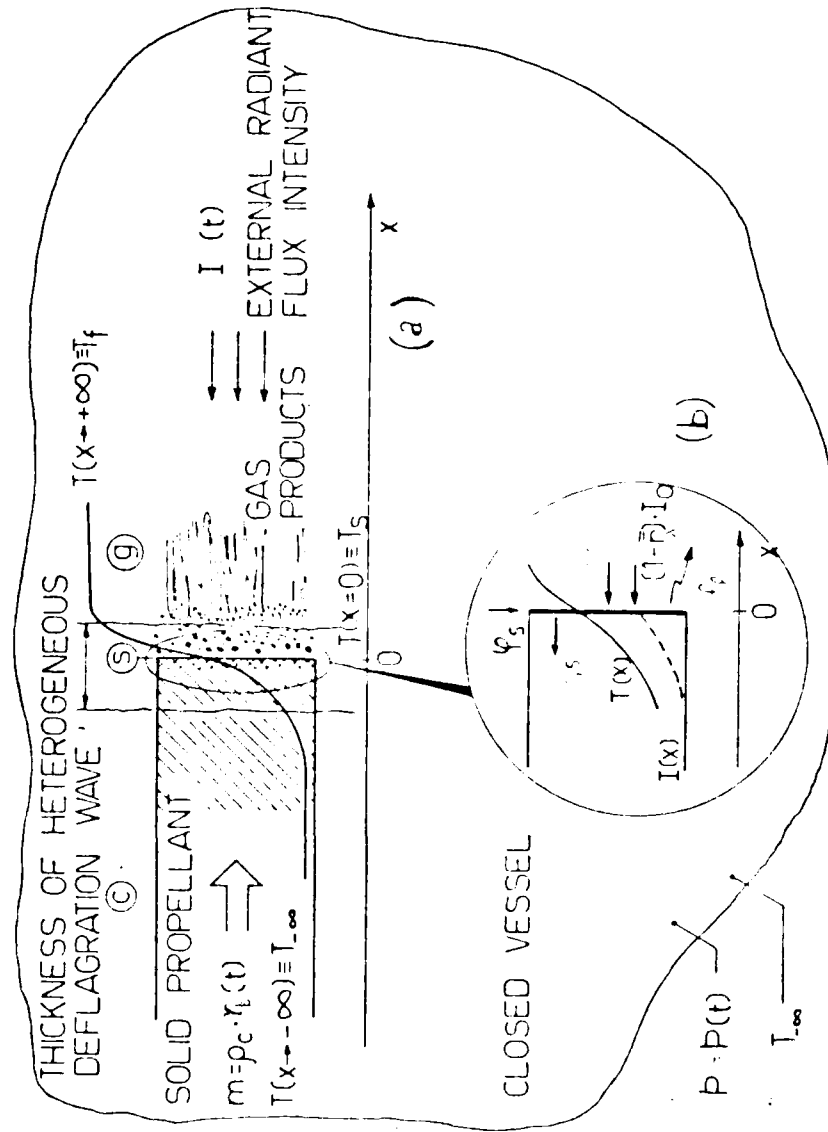


FIG. 1

AP/PBAA No 941

P = 25 atm

$(1-\frac{1}{2}) I_0 = 0 \text{ cal/cm}^2$

$K_0(T)/K_0, \text{ref} = 1 + b\theta \quad C_0(T)/C_0, \text{ref} = 1 + d\theta$

— $b = 5 \quad d = 0.5$

- - - $b = 2 \quad d = 0.5$

— · — $b = 1 \quad d = 0.5$

SURFACE TEMPERATURE, K

1100
1000
900
800
700
600
500
400
300

0

-40

-80

-120

-160

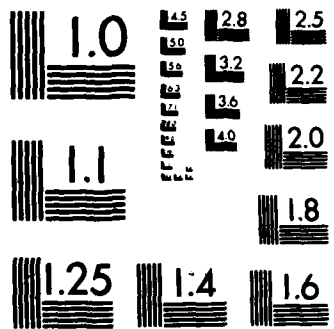
-200

-240

-280

DIMENSIONAL SPACE, micron

FIG. 2



MICROCOPY RESOLUTION TEST CHART
NATIONAL BUREAU OF STANDARDS-1963-A

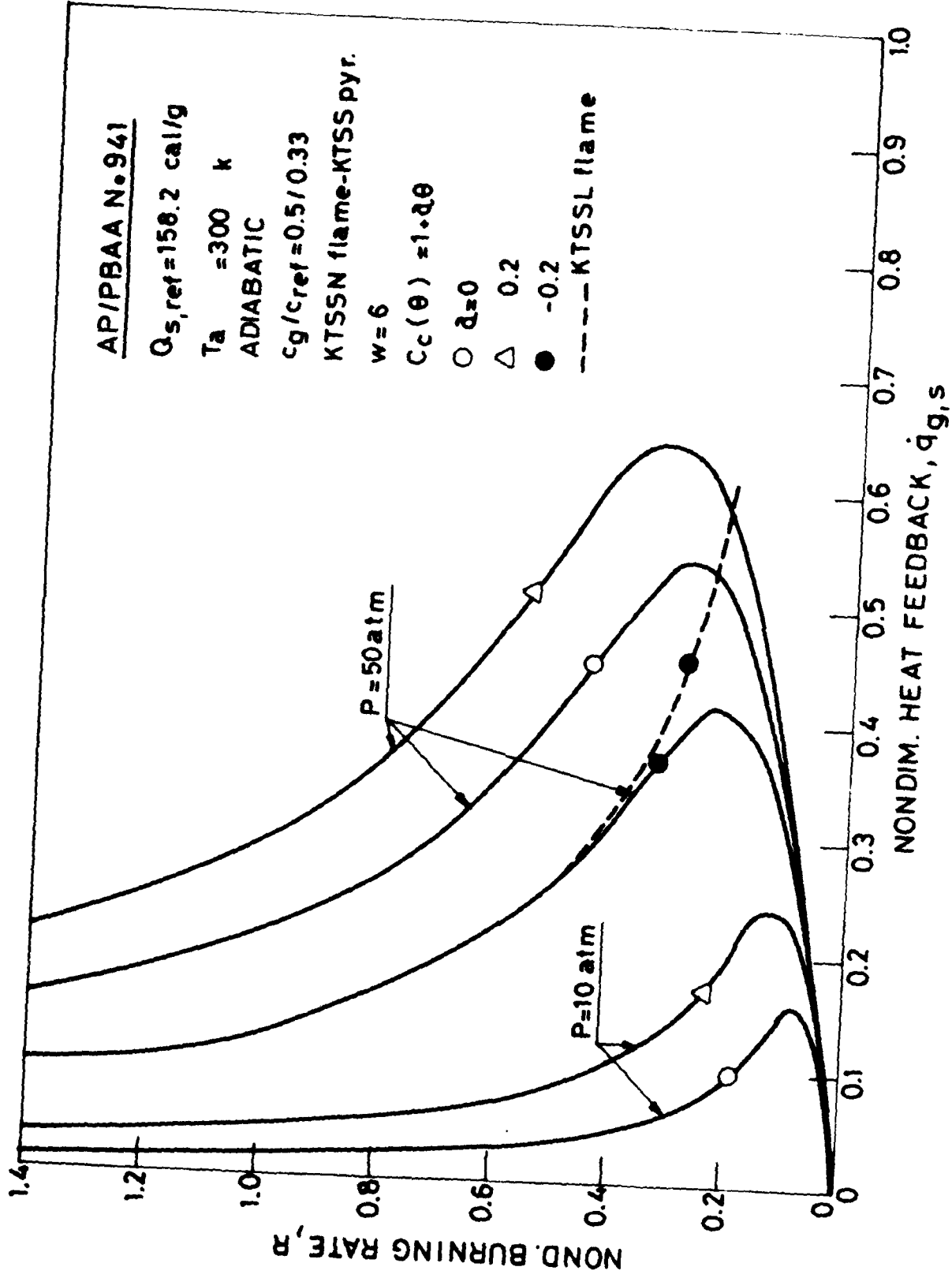


FIG. 3

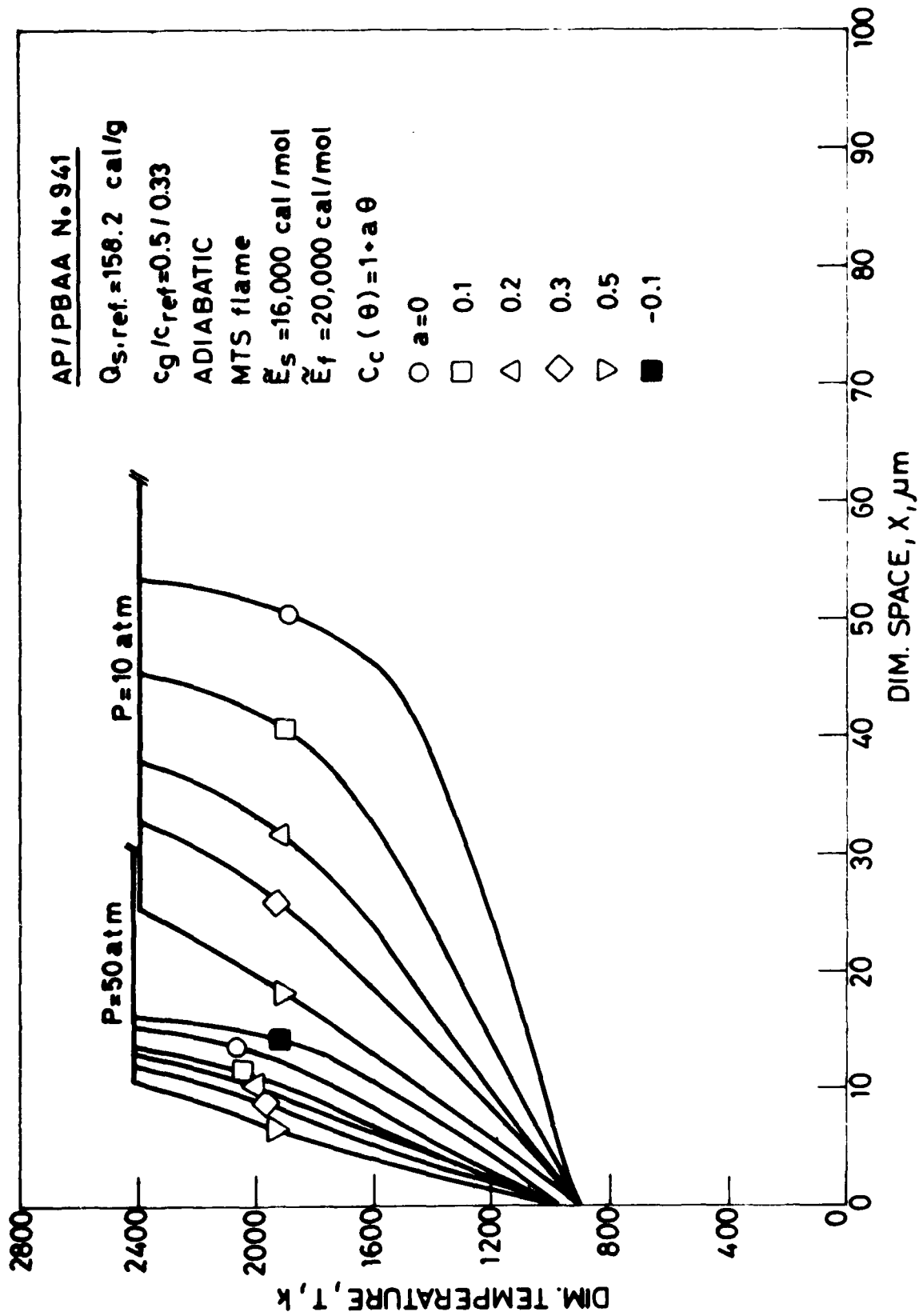
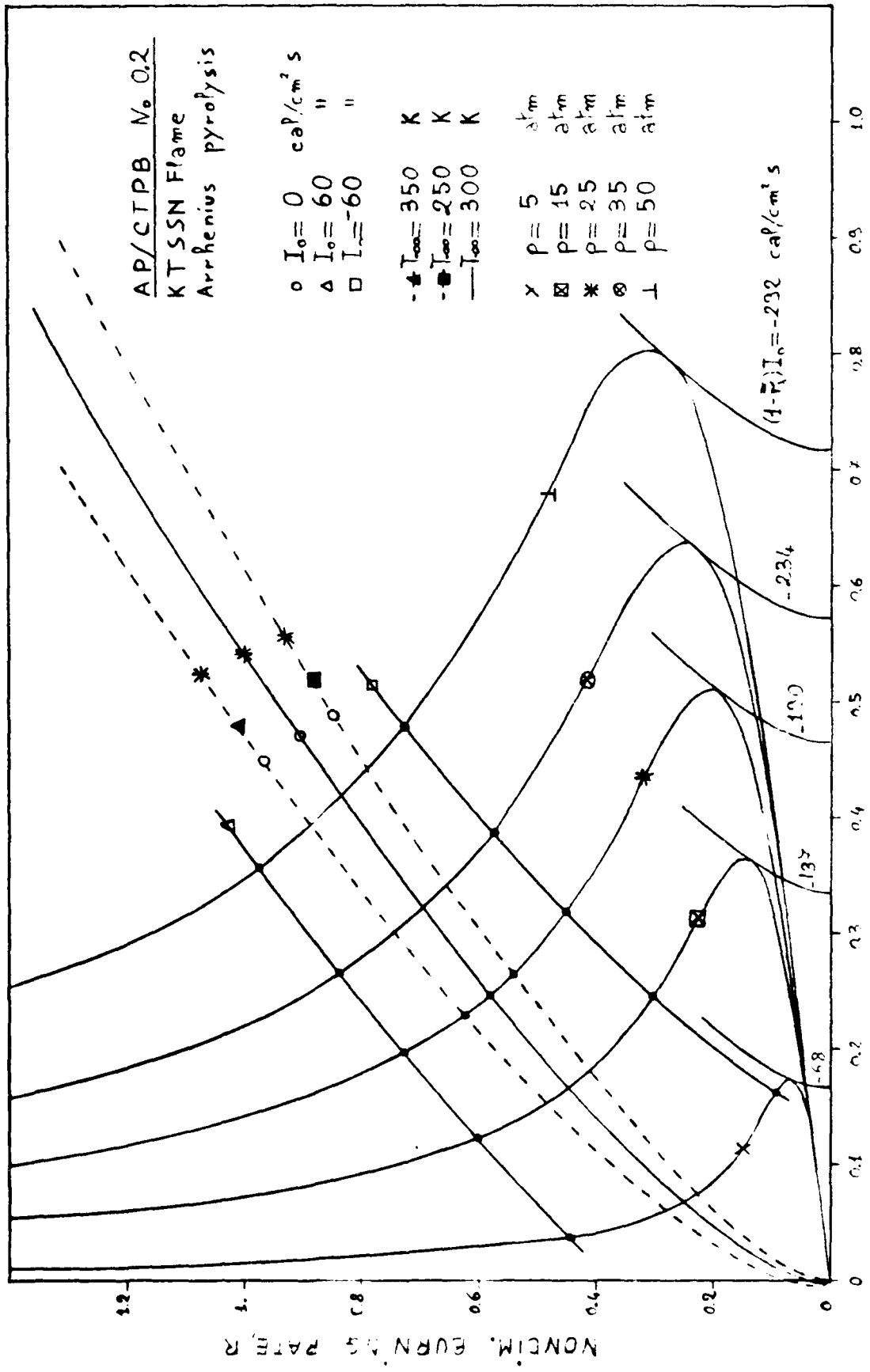


FIG. 4



NONDIM. HEAT FEEDBACK, $\eta_{2.5}$
FIG. 5

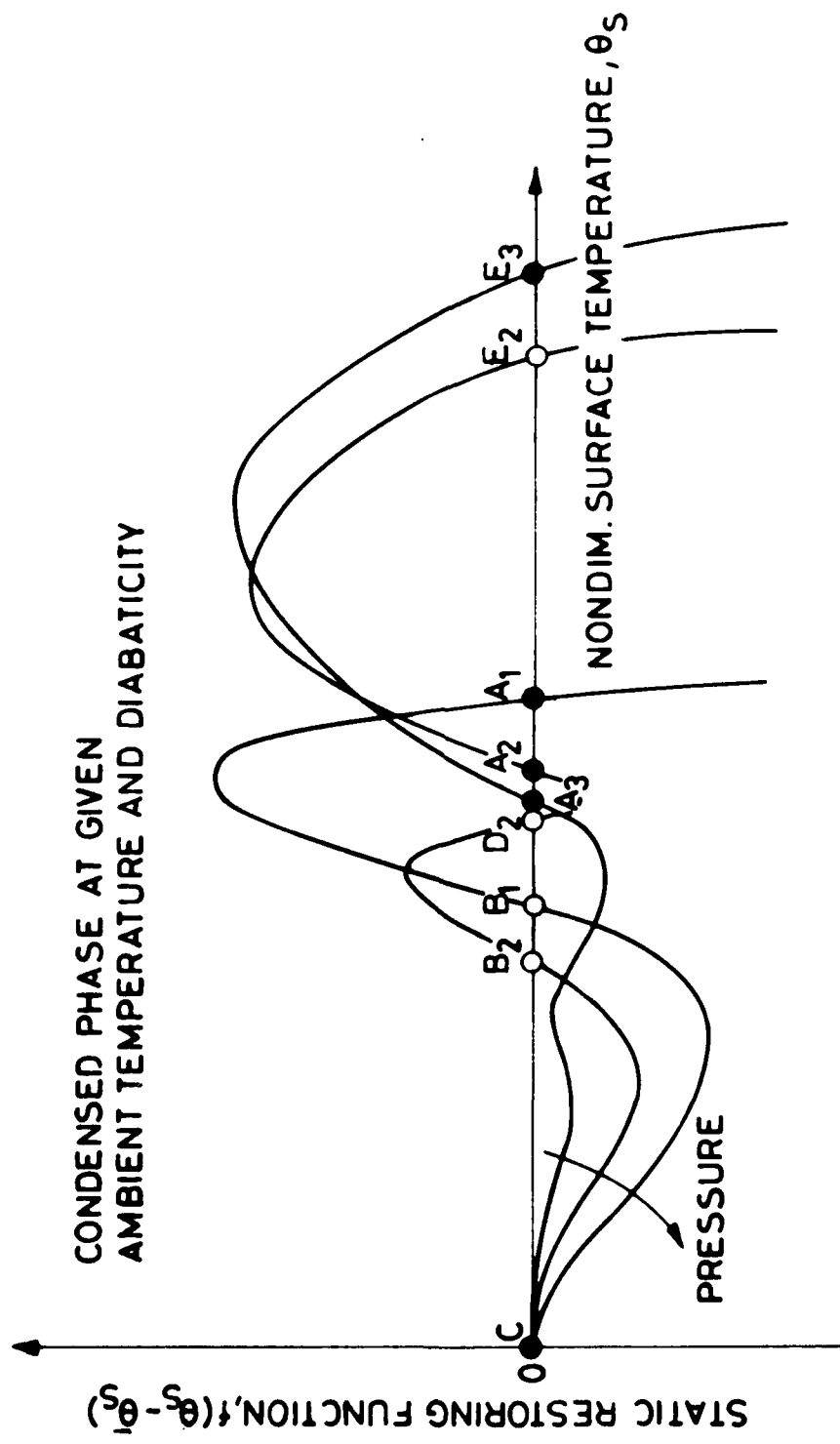


FIG. 6

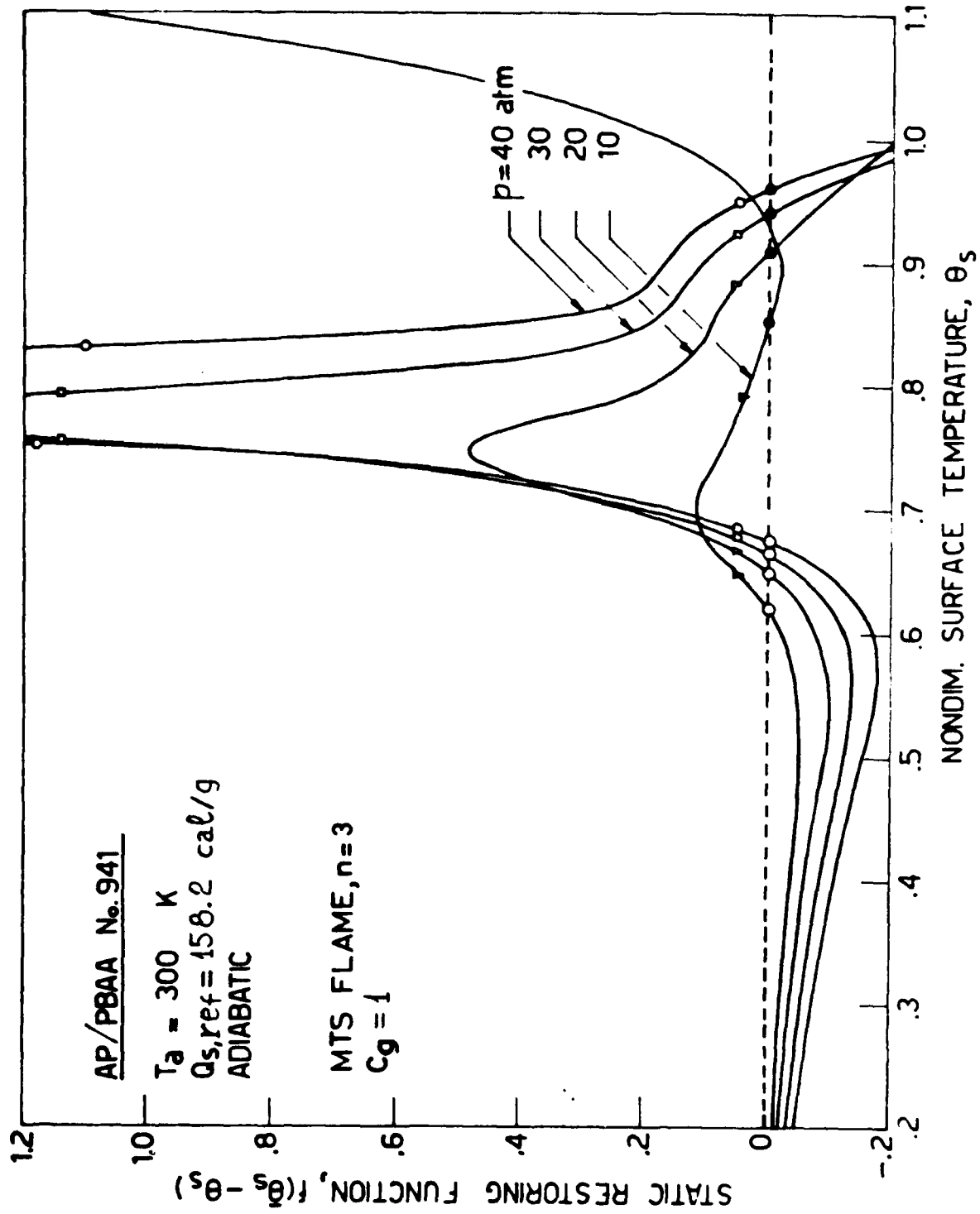


FIG 7

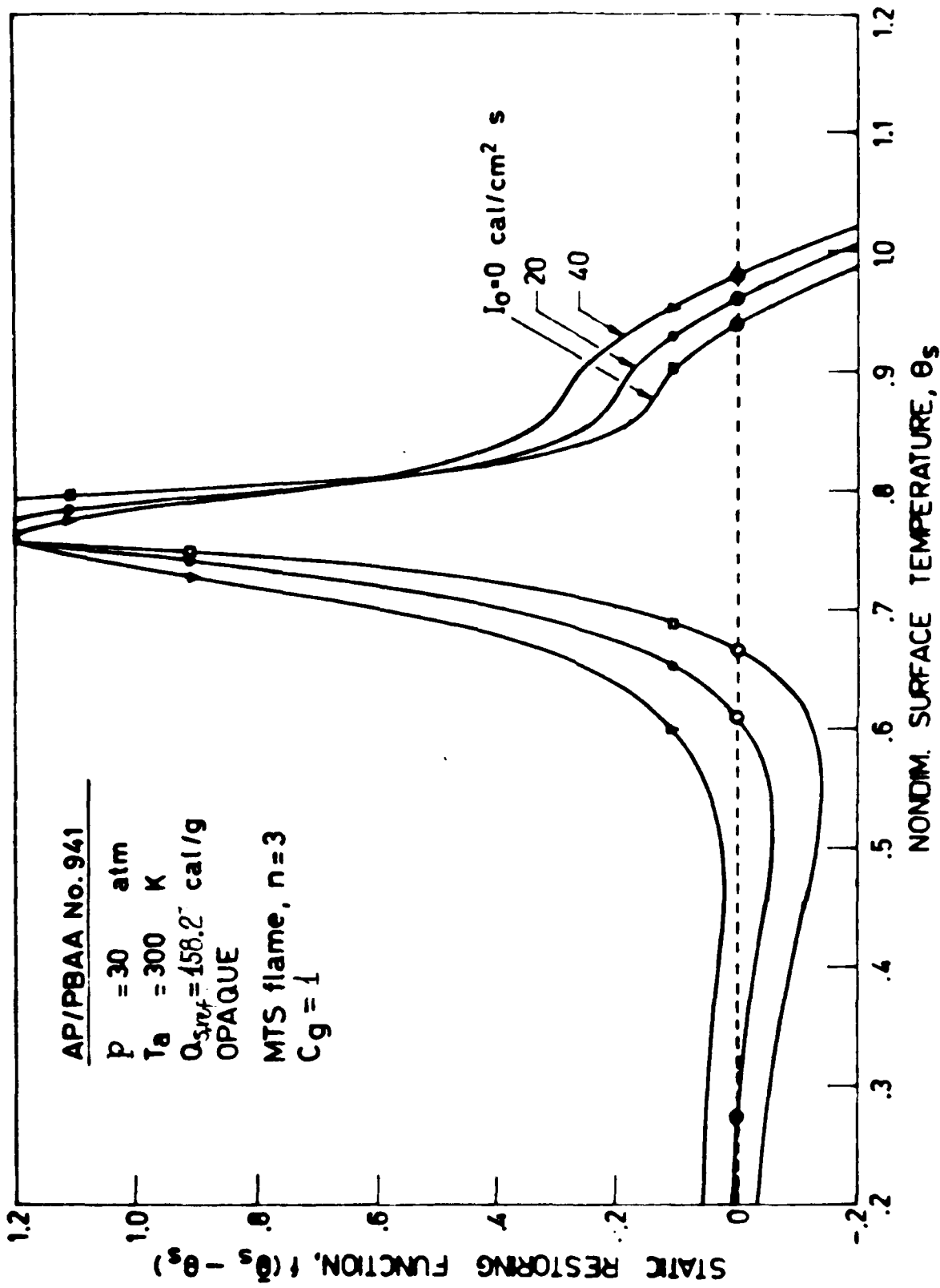


FIG. 8

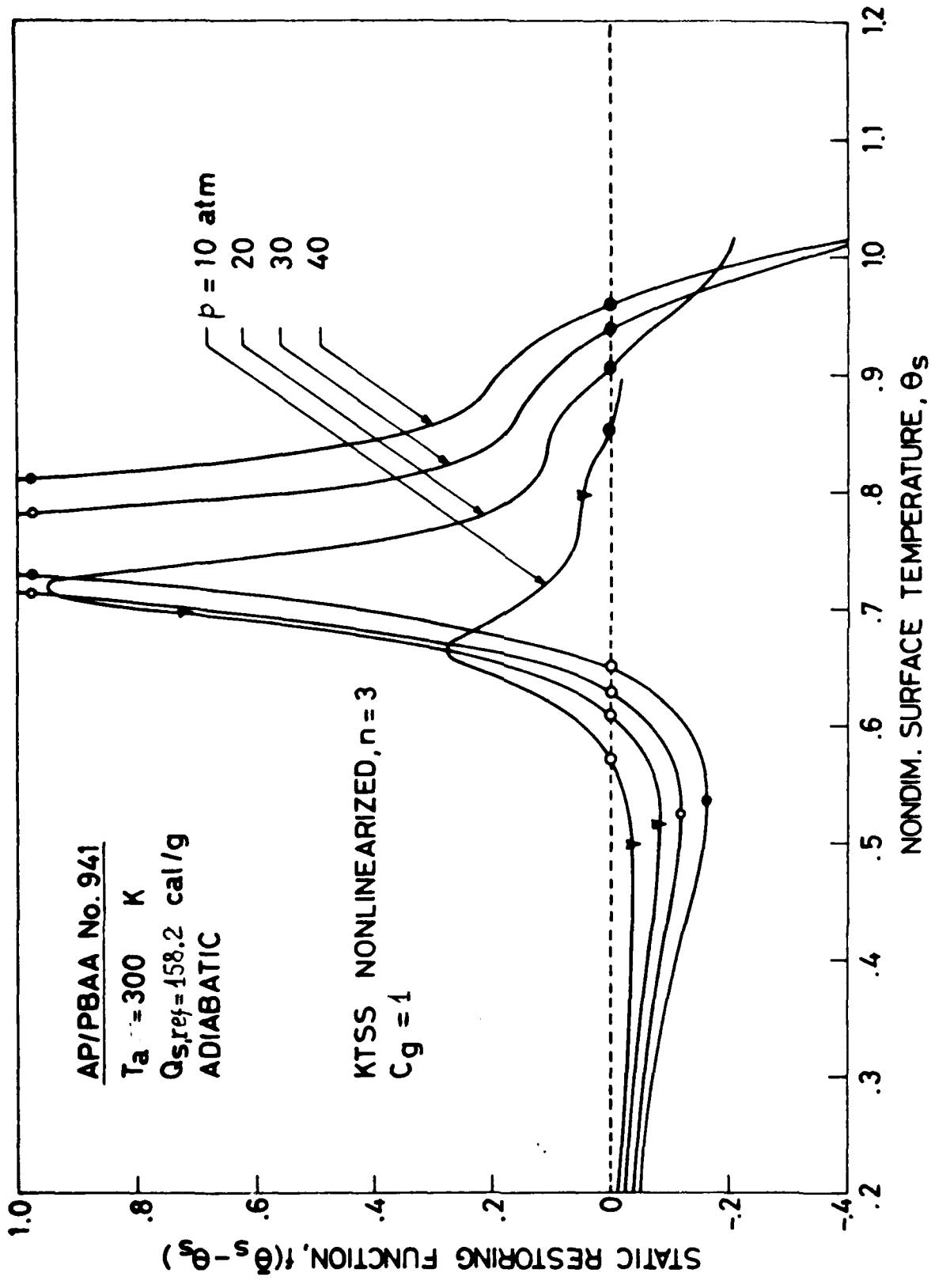


FIG. 9

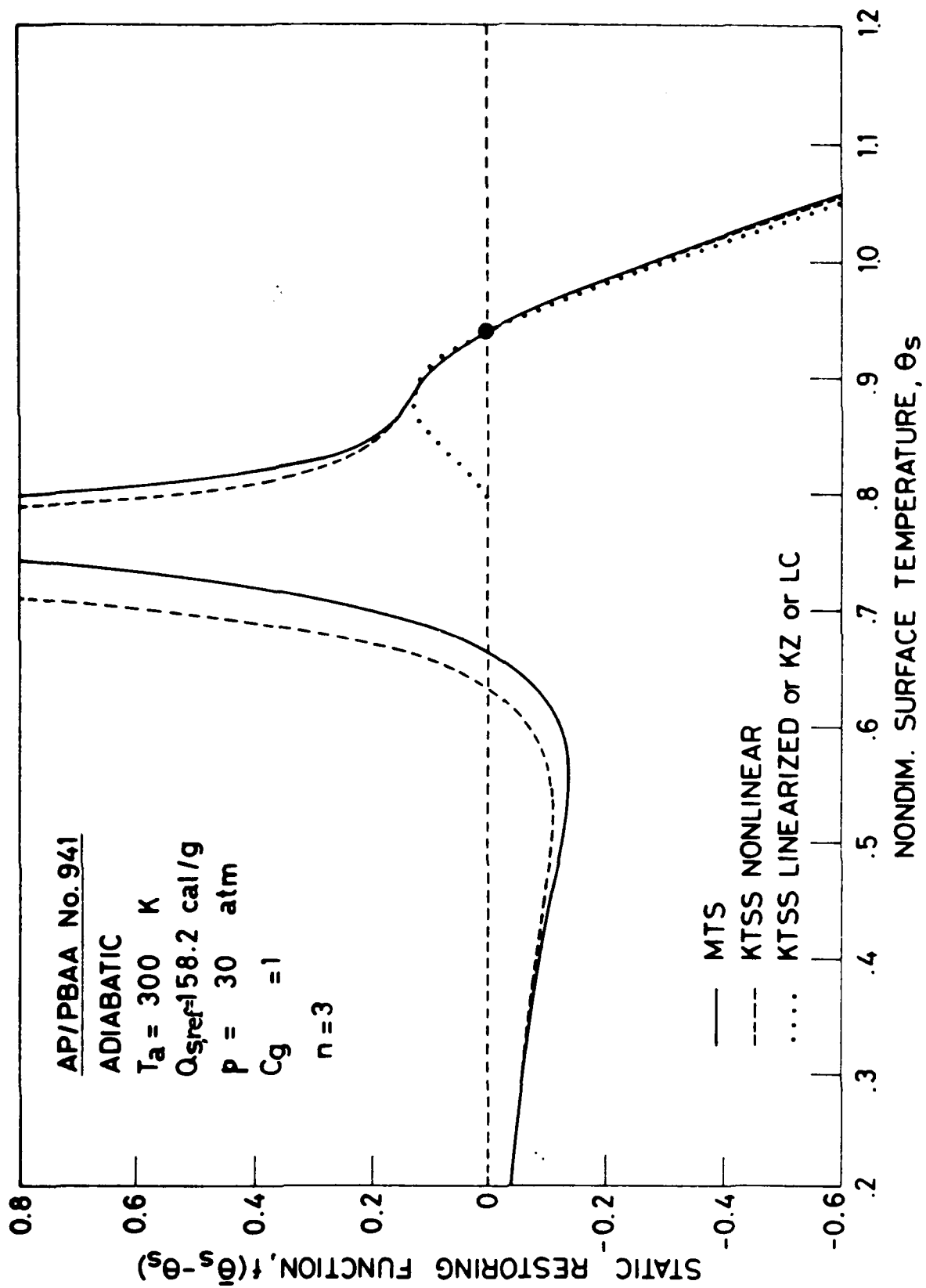


FIG 10

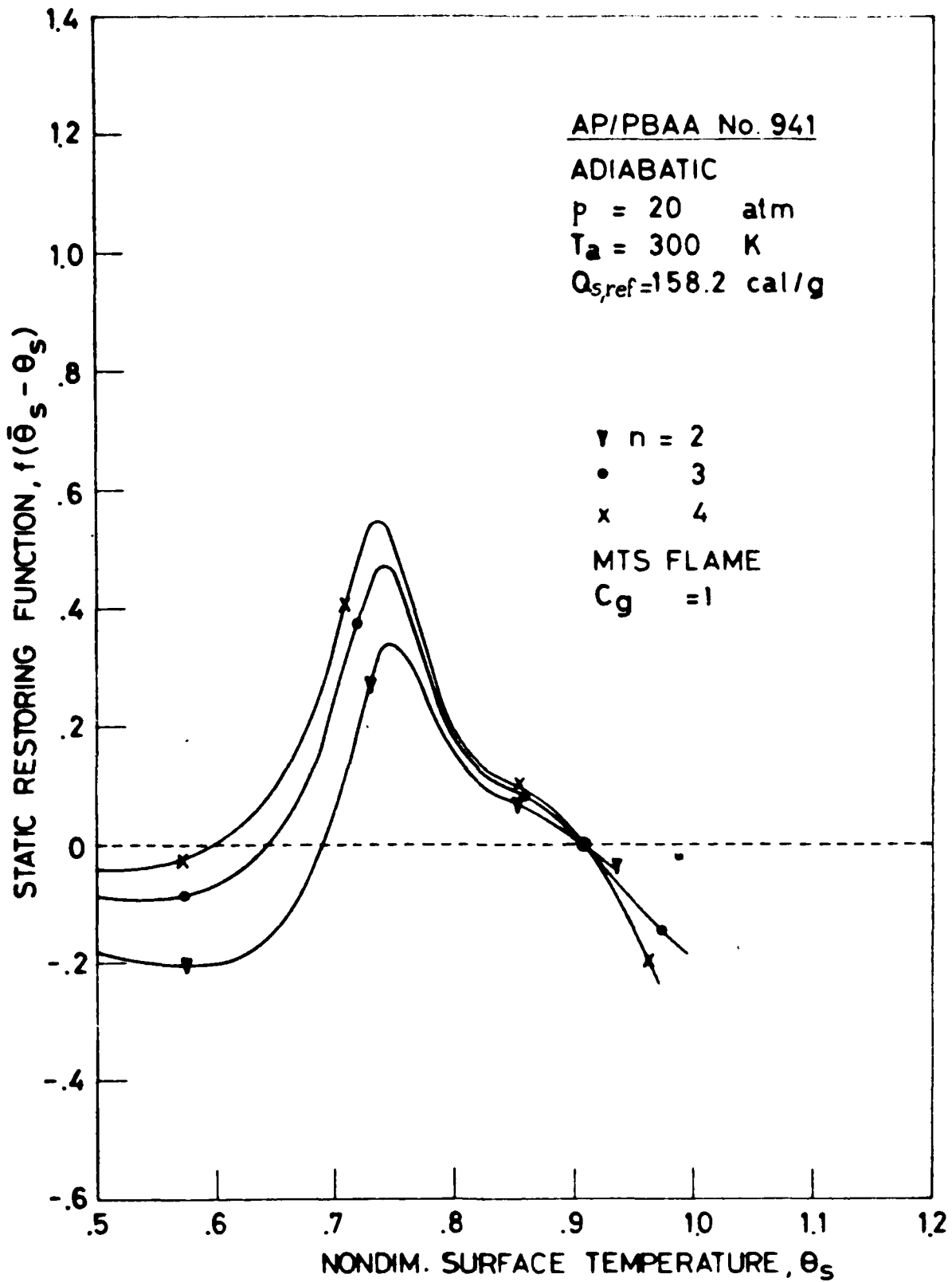


FIG. 11

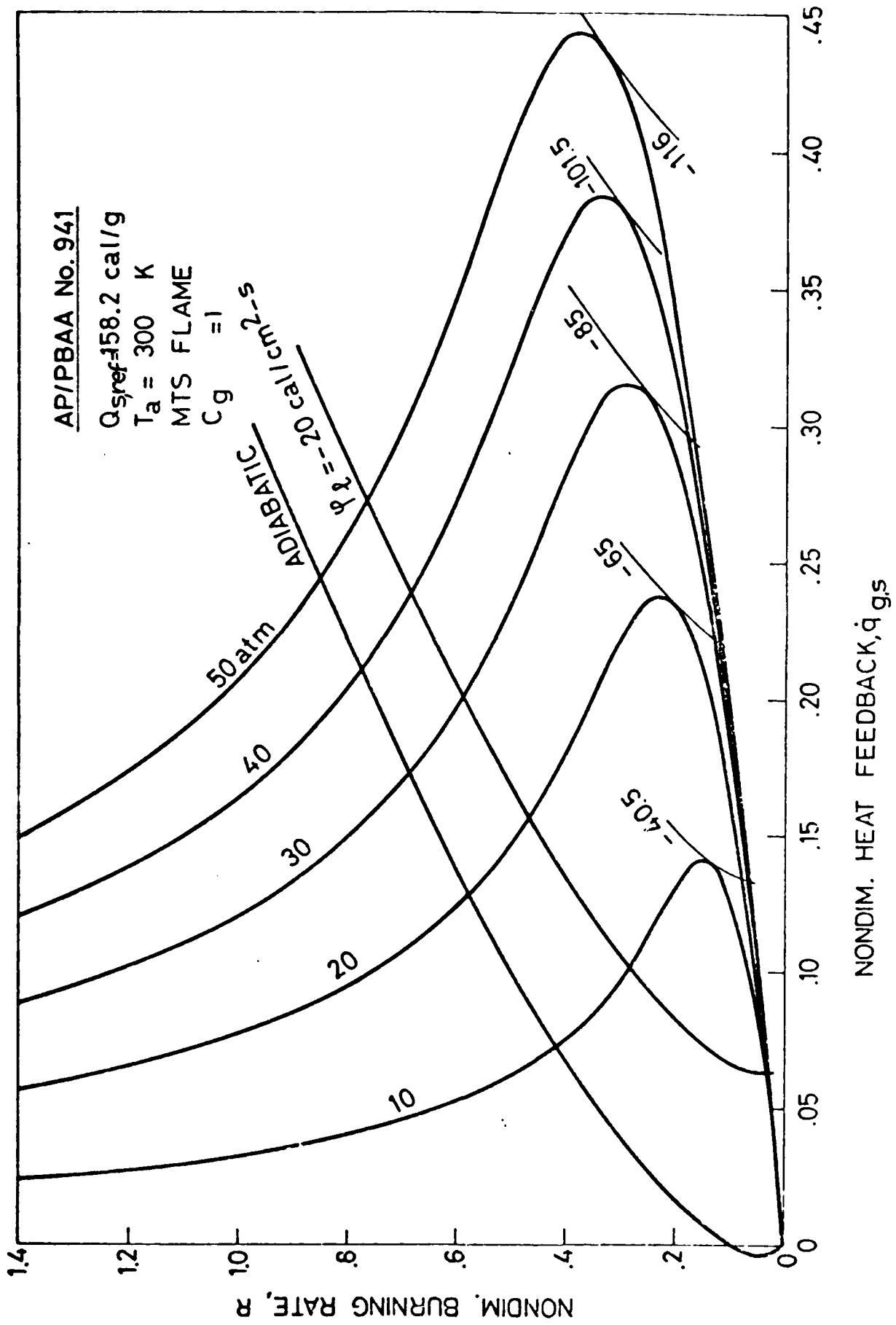


FIG. 12

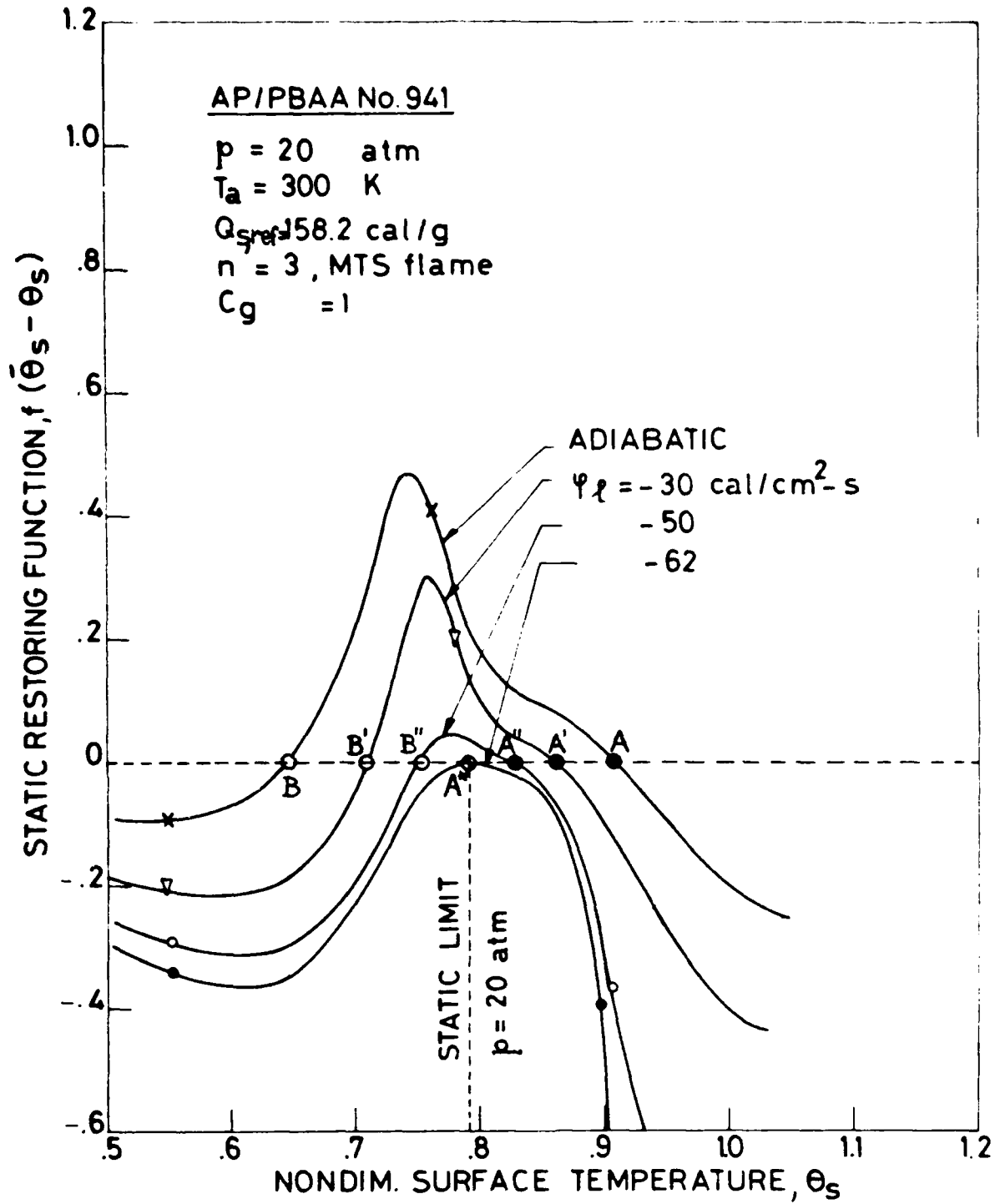


FIG. 13

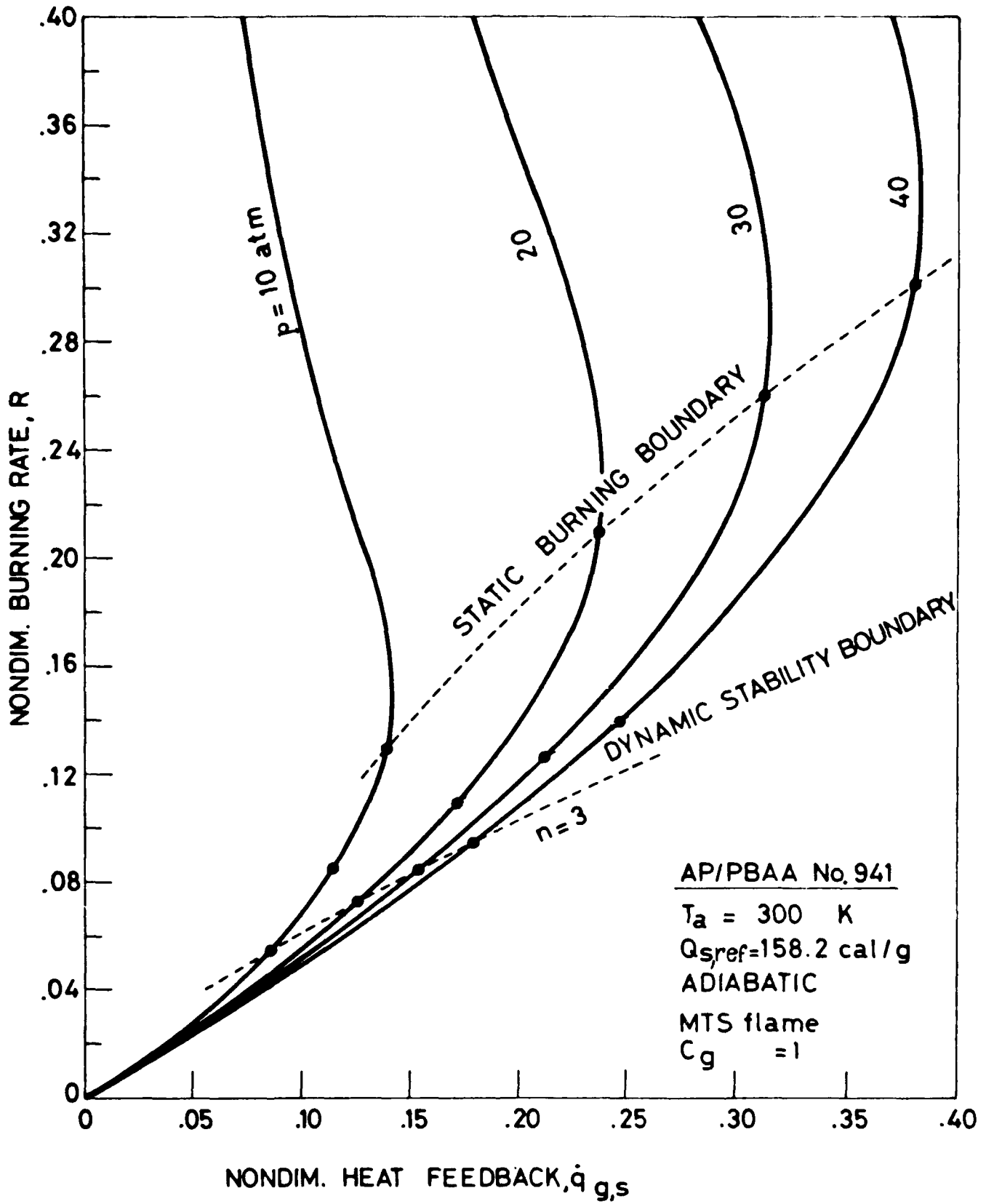


FIG. 15

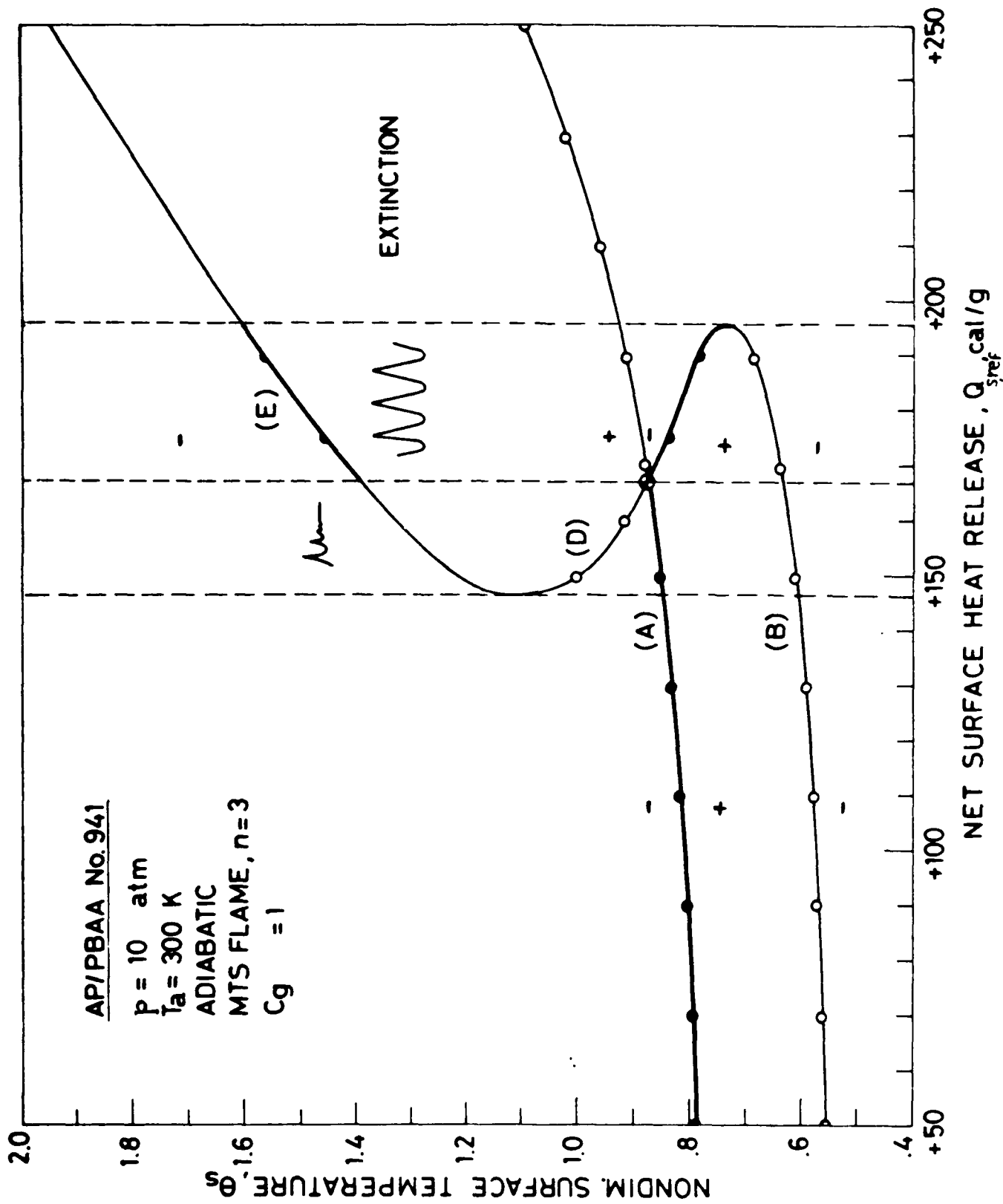


FIG. 16

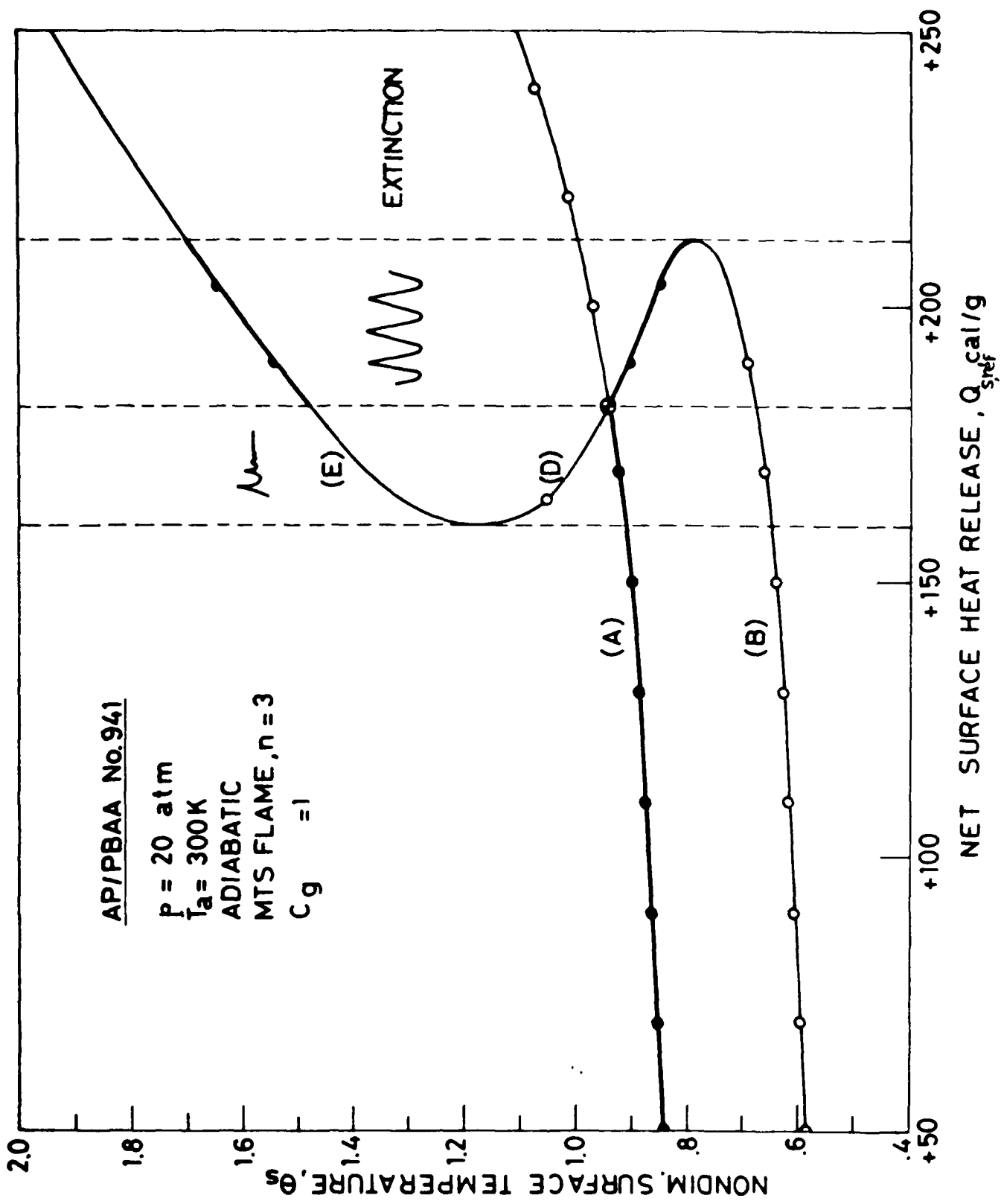


FIG 17

AP/PBAA No. 941

P = 30 atm

T_a = 300 K

ADIABATIC

MTS FLAME, n=3

C_g = 1

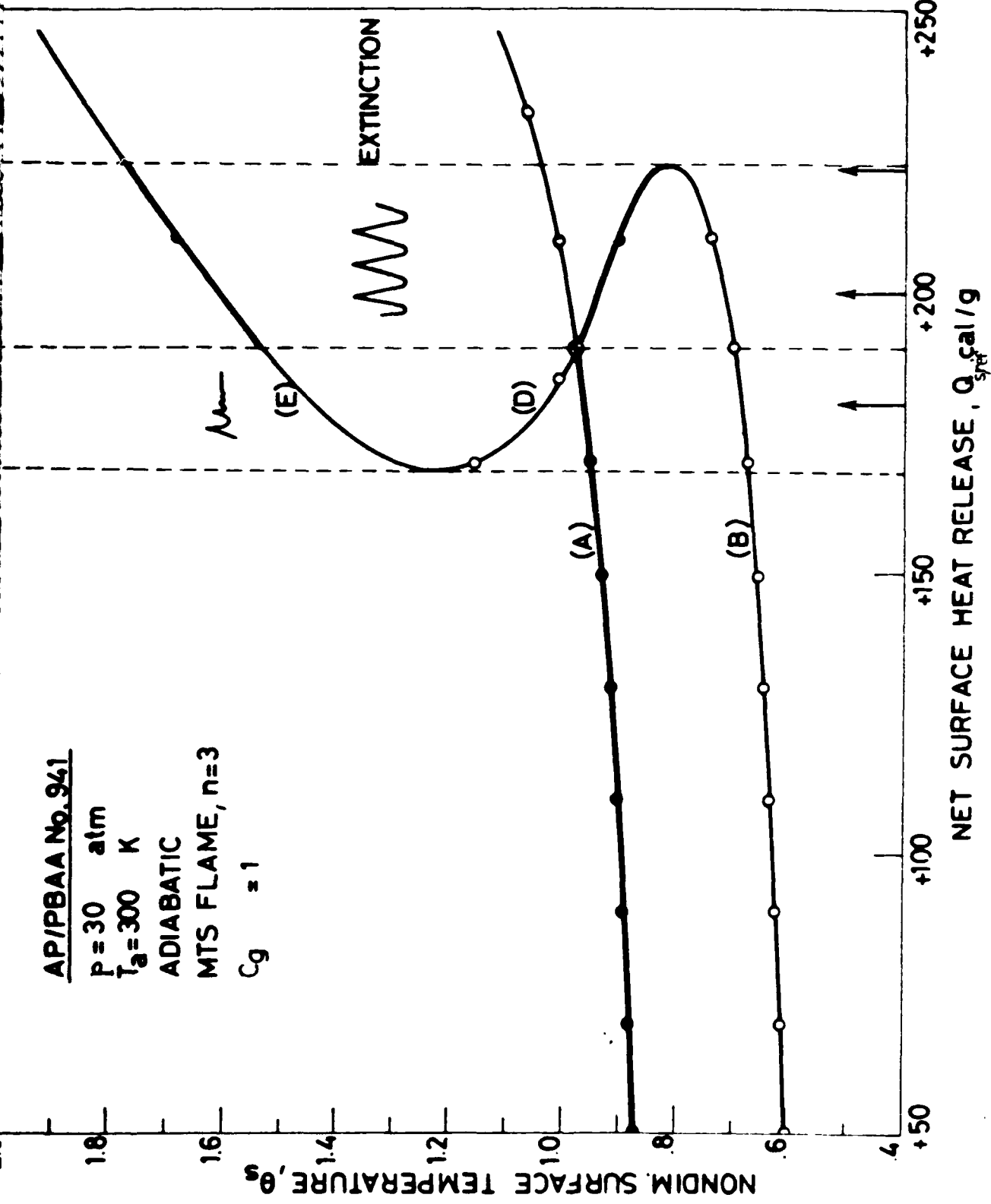


FIG. 18.

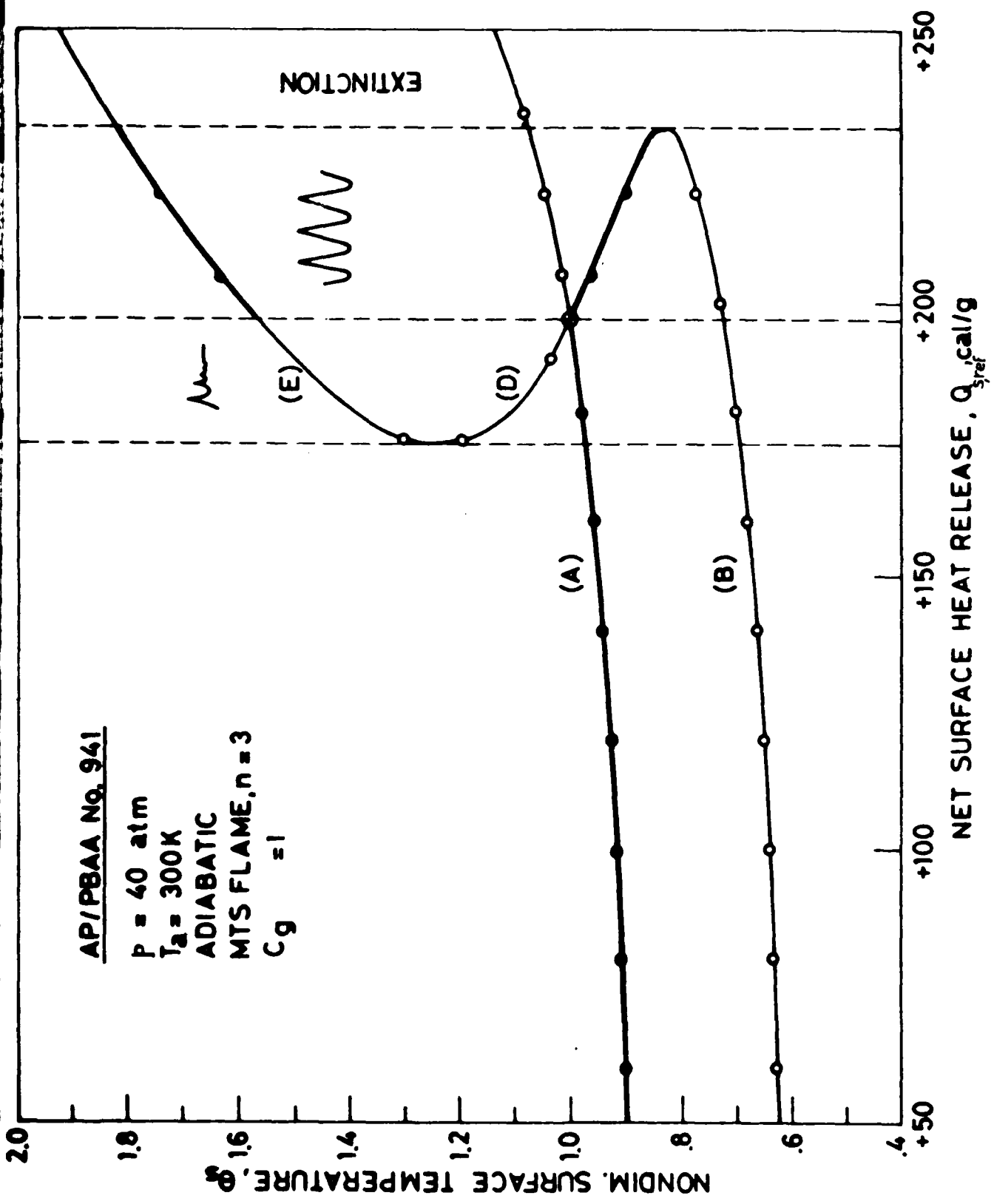


FIG. 19

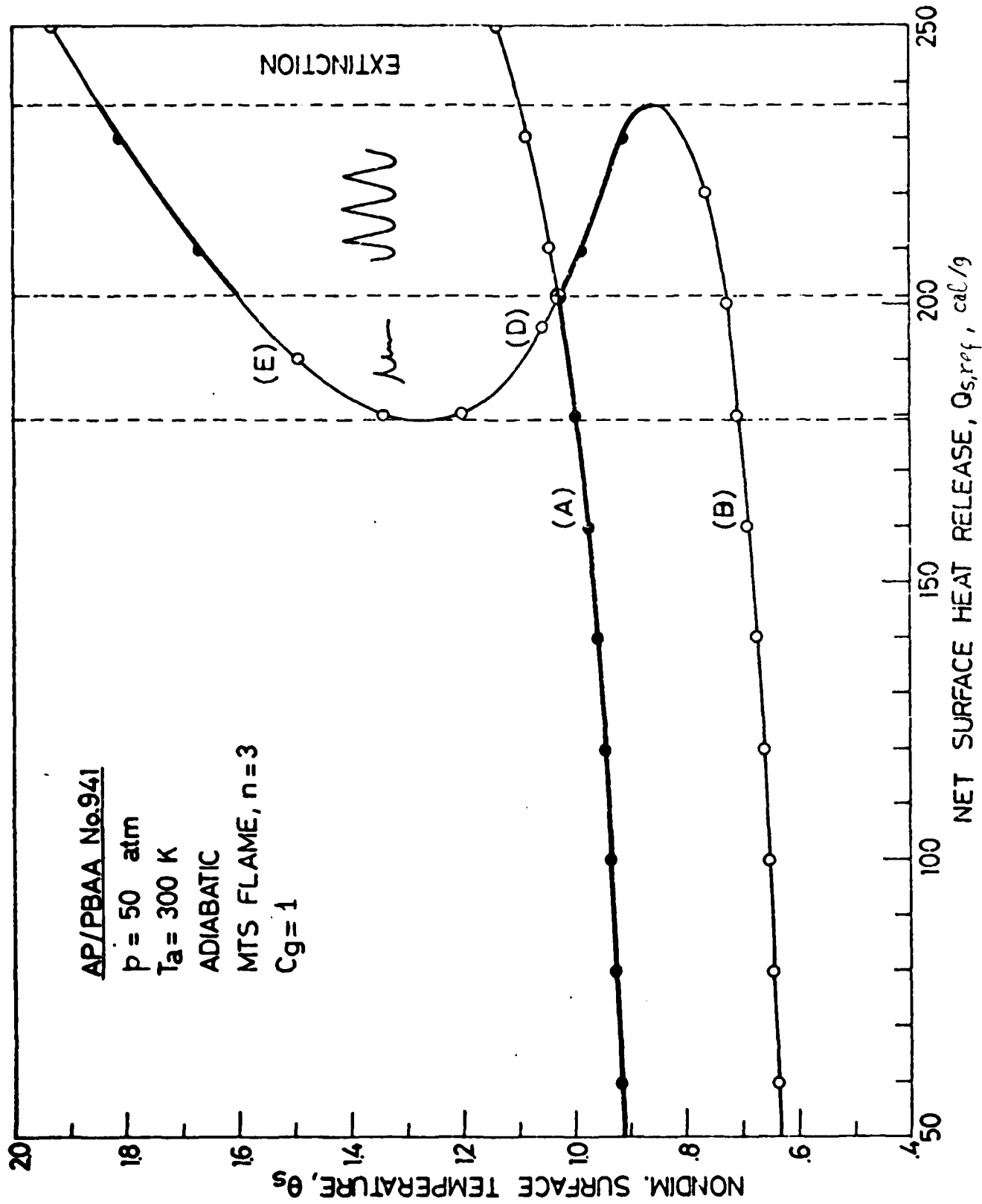
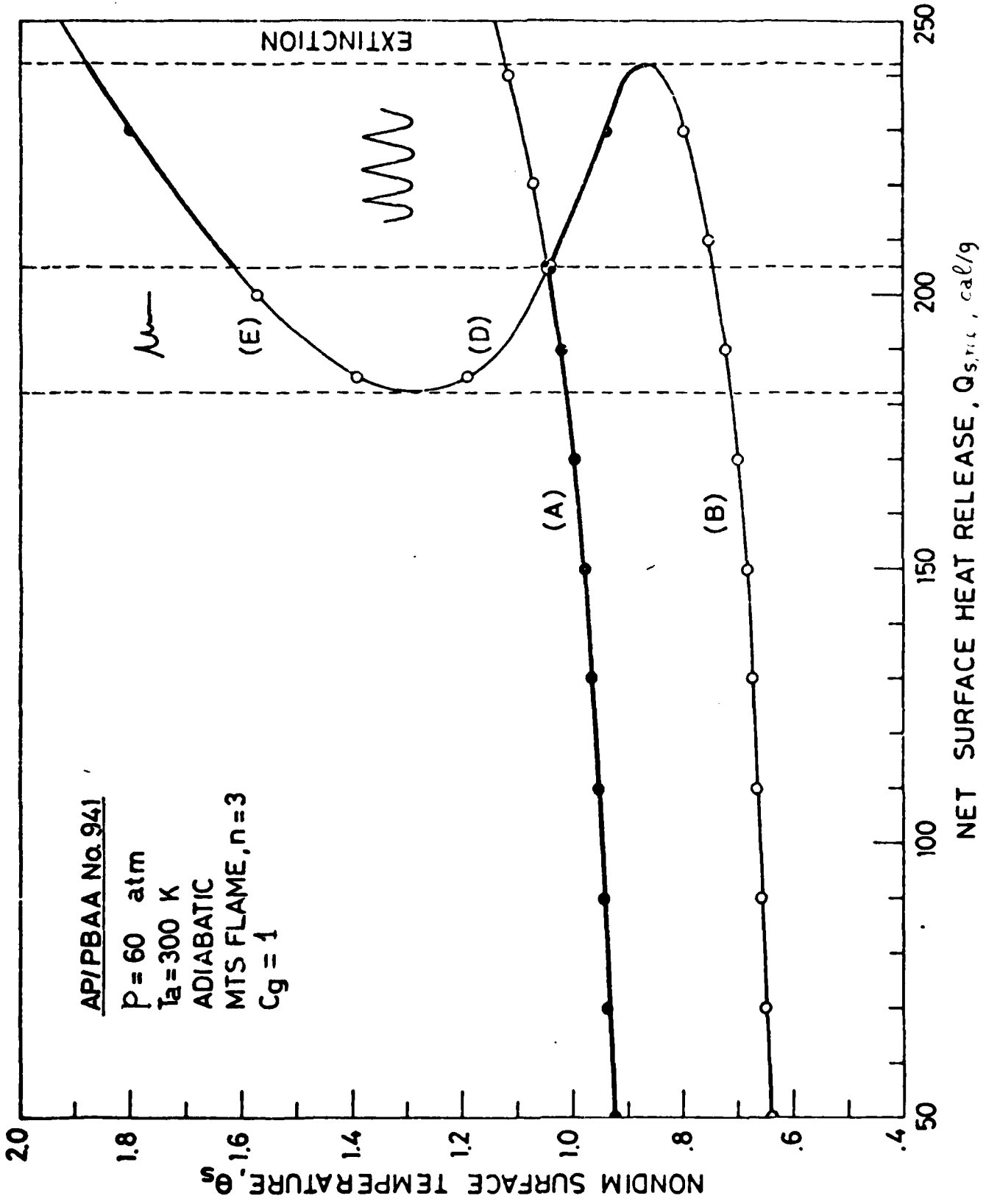


FIG. 20



AP/PFAA No. 341

$Q_{\text{cond}} = 125 \text{ cal/s}$
 $C_1 = 1.67$
 $b = 9$
 $E_A = 175$
 $E_c = 30 \text{ kcal/mole}$

STACK PLANE
 Ammonius Pyrolysis
 $E_s = 24 \text{ Kcal/mole}$
 $P = 50 \text{ atm}$
 $n = 3$, pyrolysis

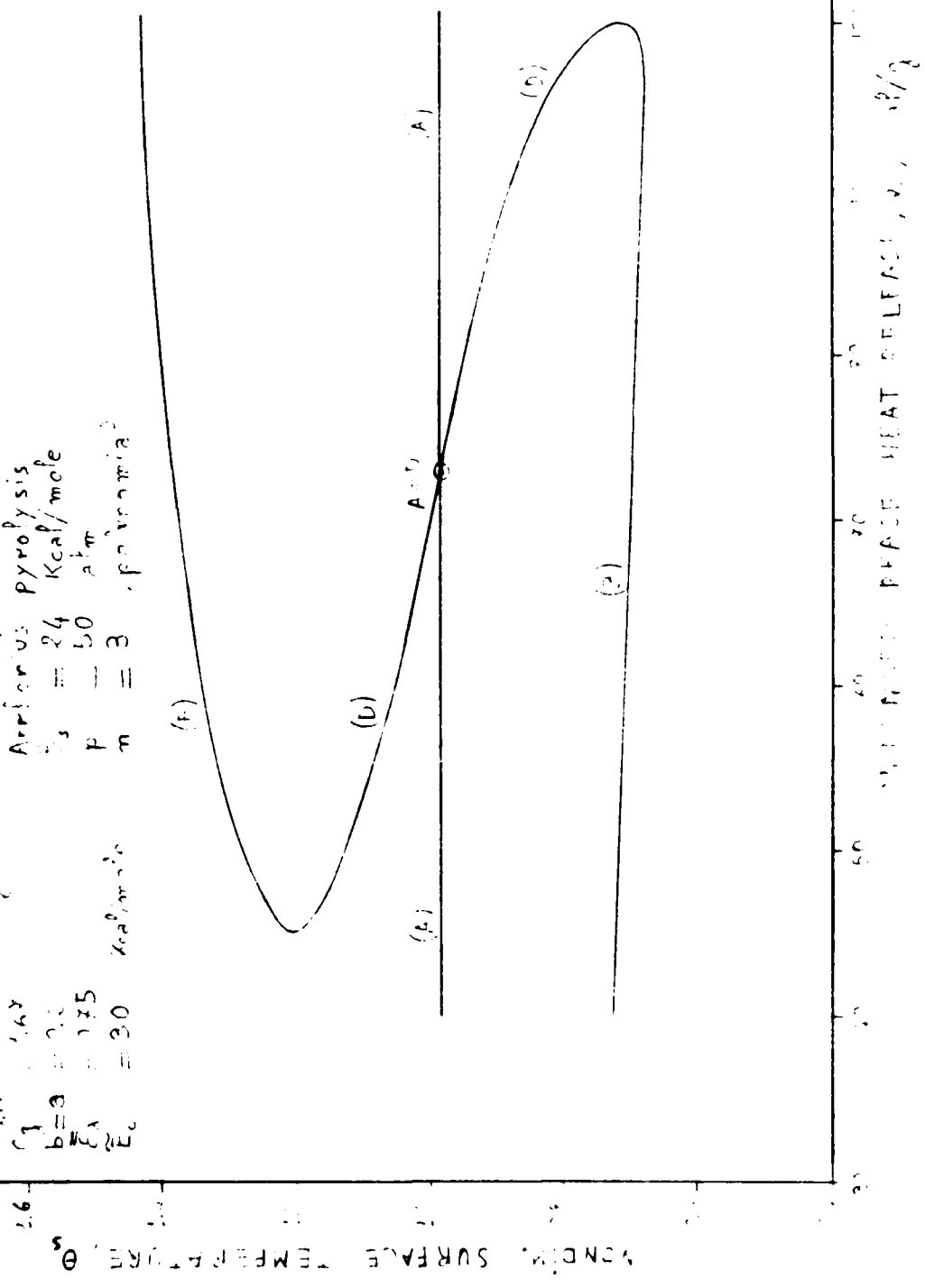


Fig. 29

AF/PEAA 1/0.3/1

$Q_{ref} = 125 \text{ cal/g}$
 $C_p = 1.07$
 $b = a \cdot O_2$
 $E_c = 30 \text{ kcal/mole}$

KTSSM flame
 KTSS pyrolysis
 $E_s = 34 \text{ kcal/mole}$
 $F = 20 \text{ atm}$
 $m = 2, \text{ polynomial}$

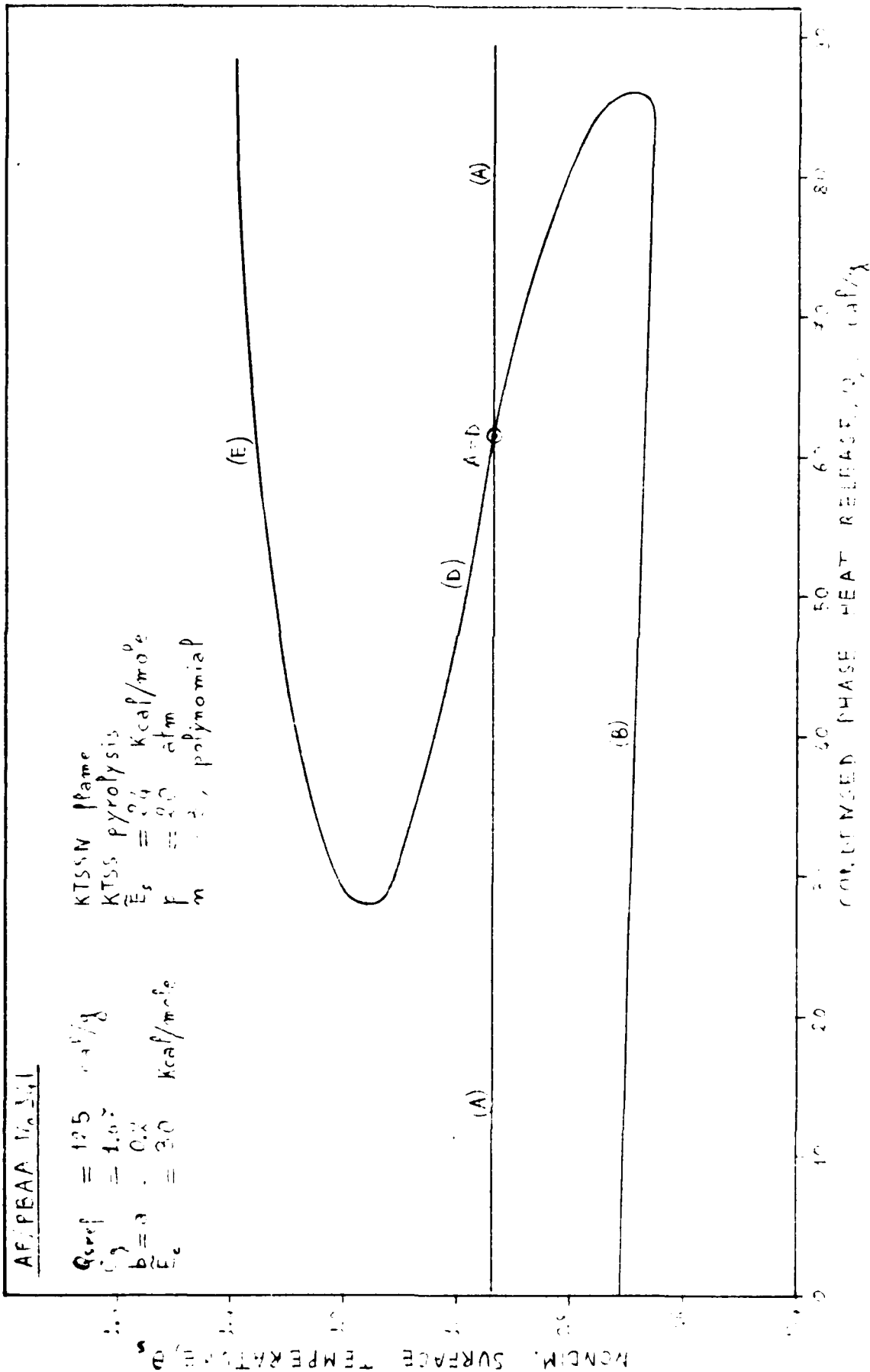


FIG. 23

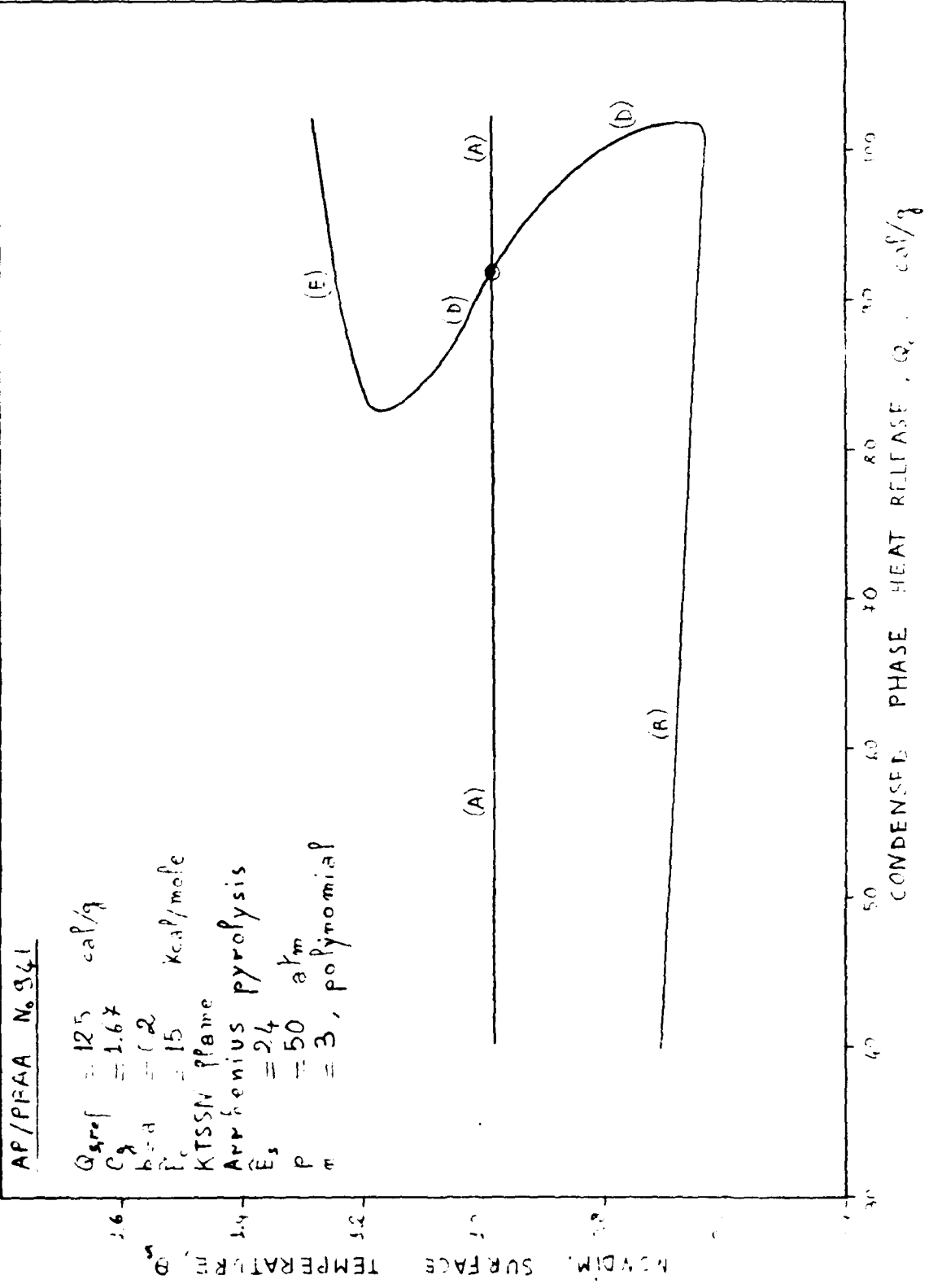


Fig. 24

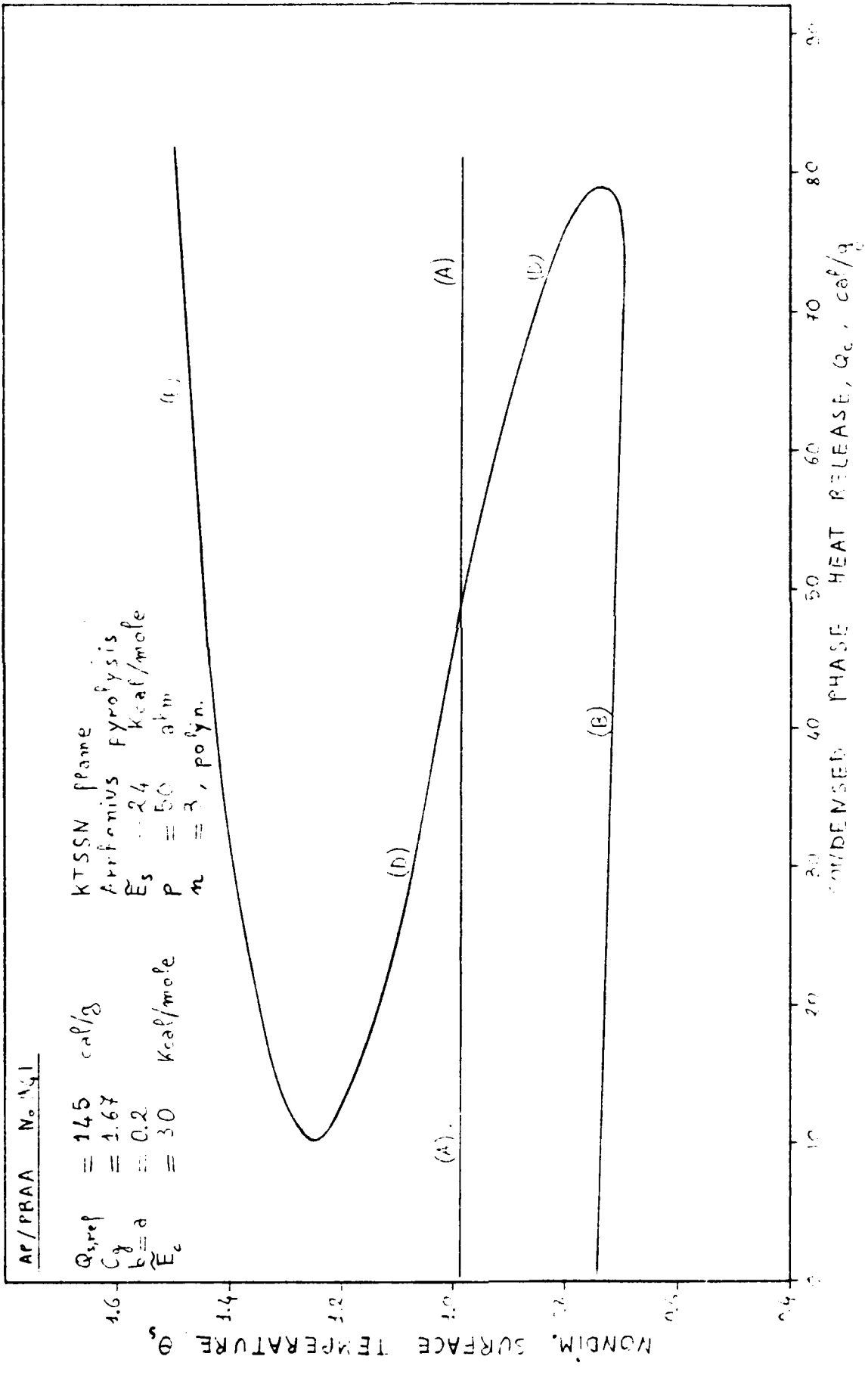


FIG. 25

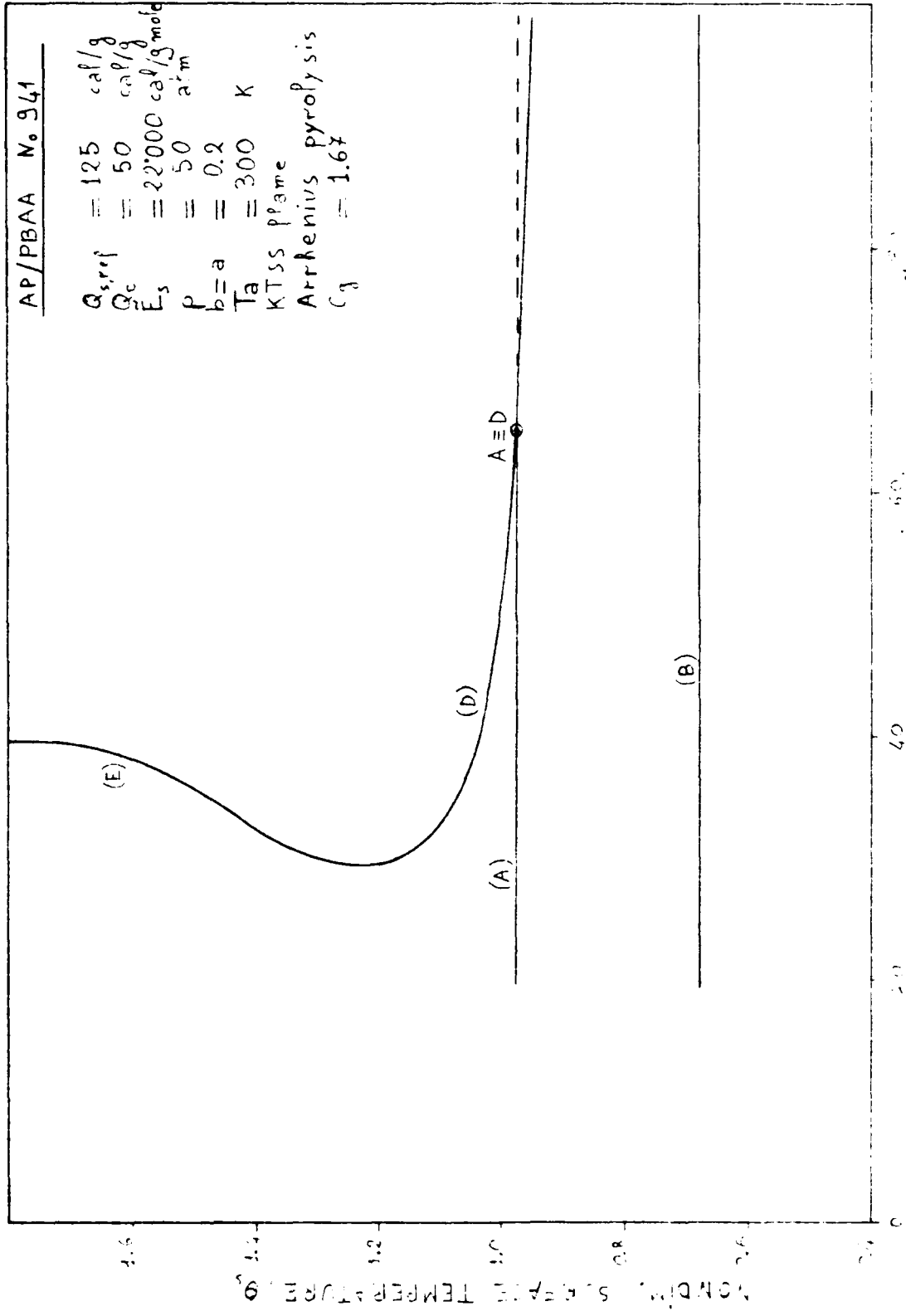
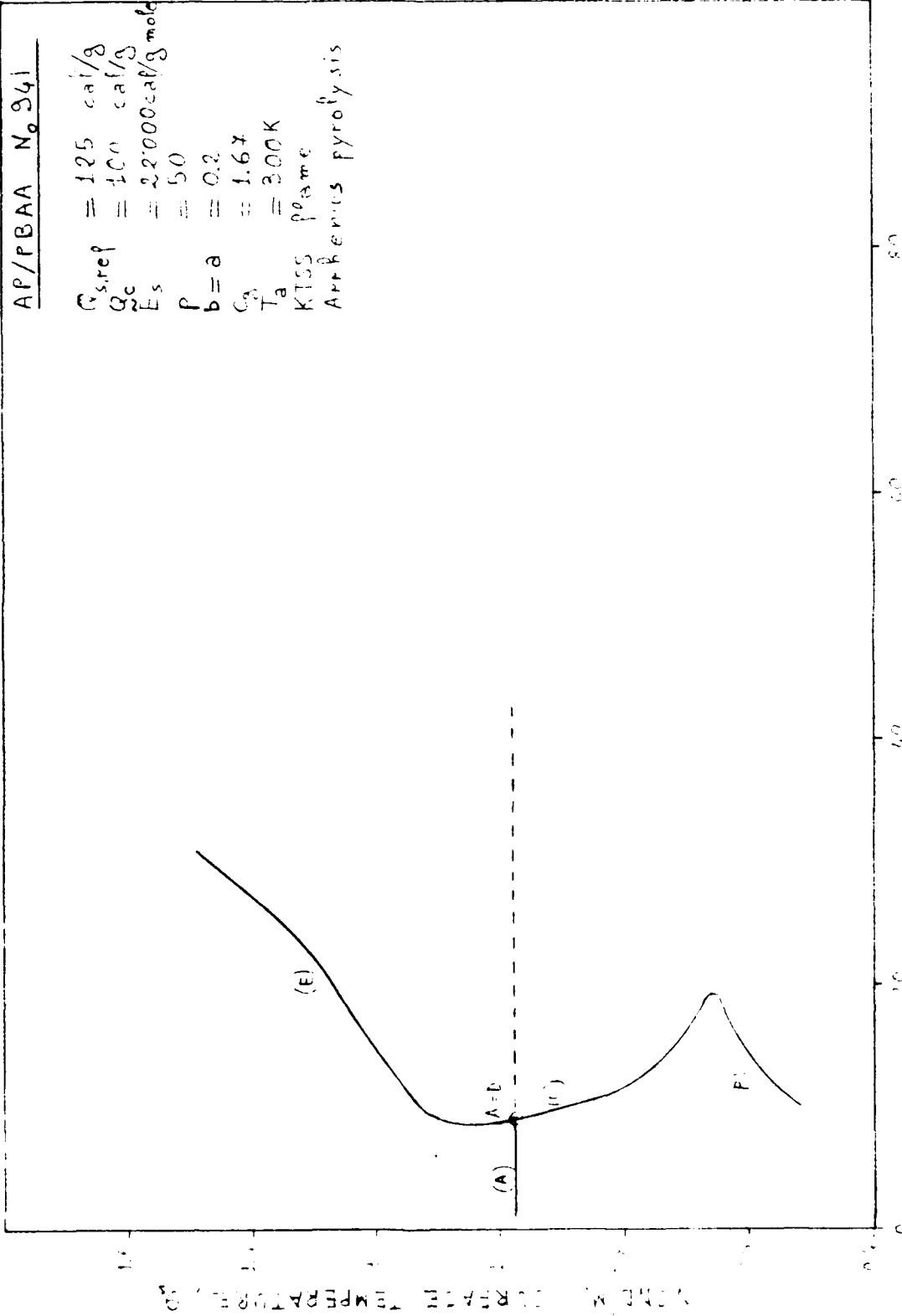


FIG. 26

AP/PBAA No. 941

$C_{s,ref} = 125 \text{ cal/g}$
 $Q_c = 100 \text{ cal/g}$
 $E_s = 22,000 \text{ cal/g mole}$
 $P = 50$
 $b = a = 0.2$
 $C_a = 1.67$
 $T_a = 300 \text{ K}$
KTSS same
Arrhenius pyrolysis



CONDENSED PHASE ACTIVATION ENERGY, T_s , P , C_a , E_s , Q_c , $C_{s,ref}$

FIG. 27

AP/CTPB No. 02

$Q_{\text{lim}} = 0$ cal/g
 $Q_c = 125$ cal/g
 $P = 10$ atm
KISSI flame
polynomial, $n=3$

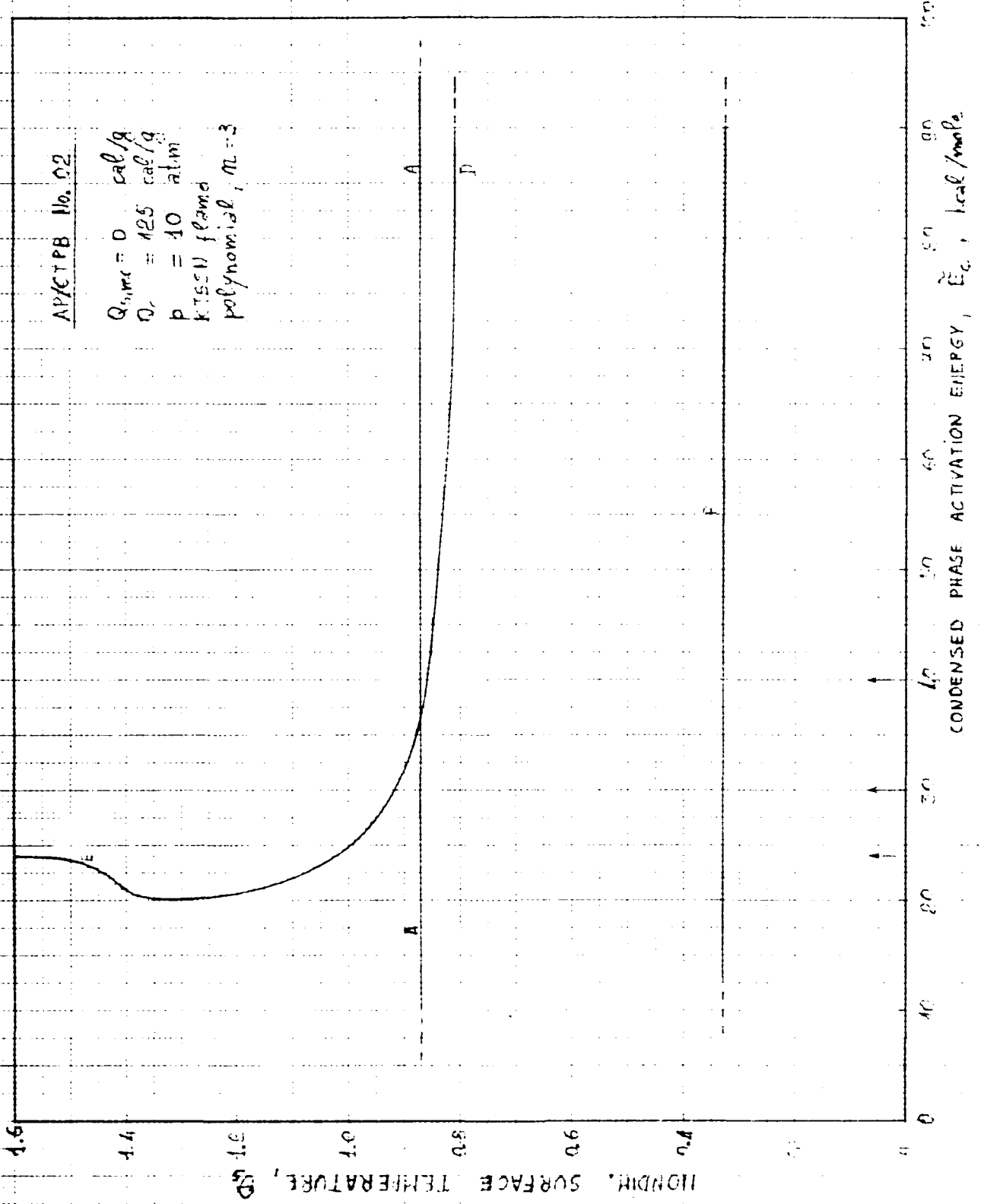


FIG. 28

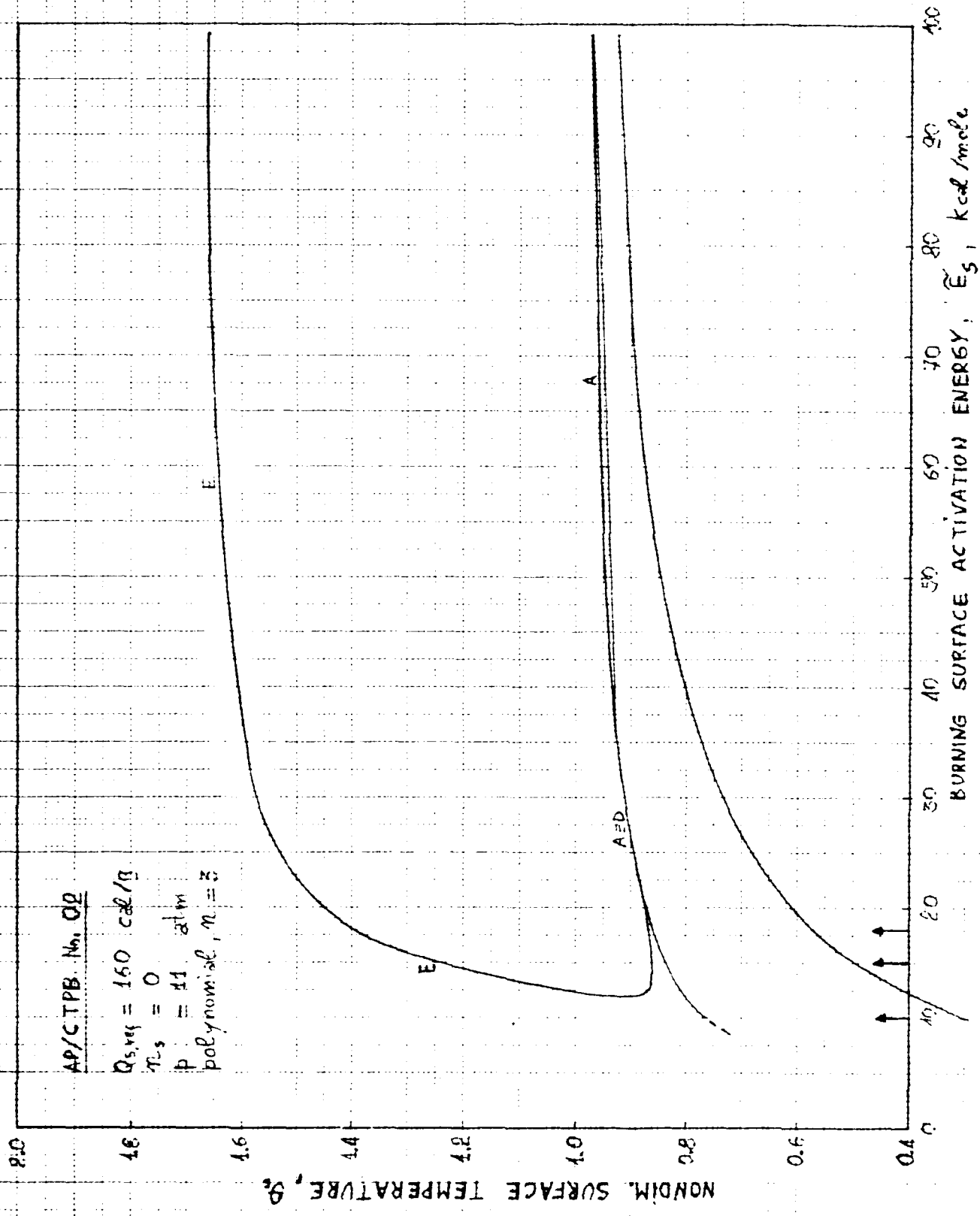


FIG. 29

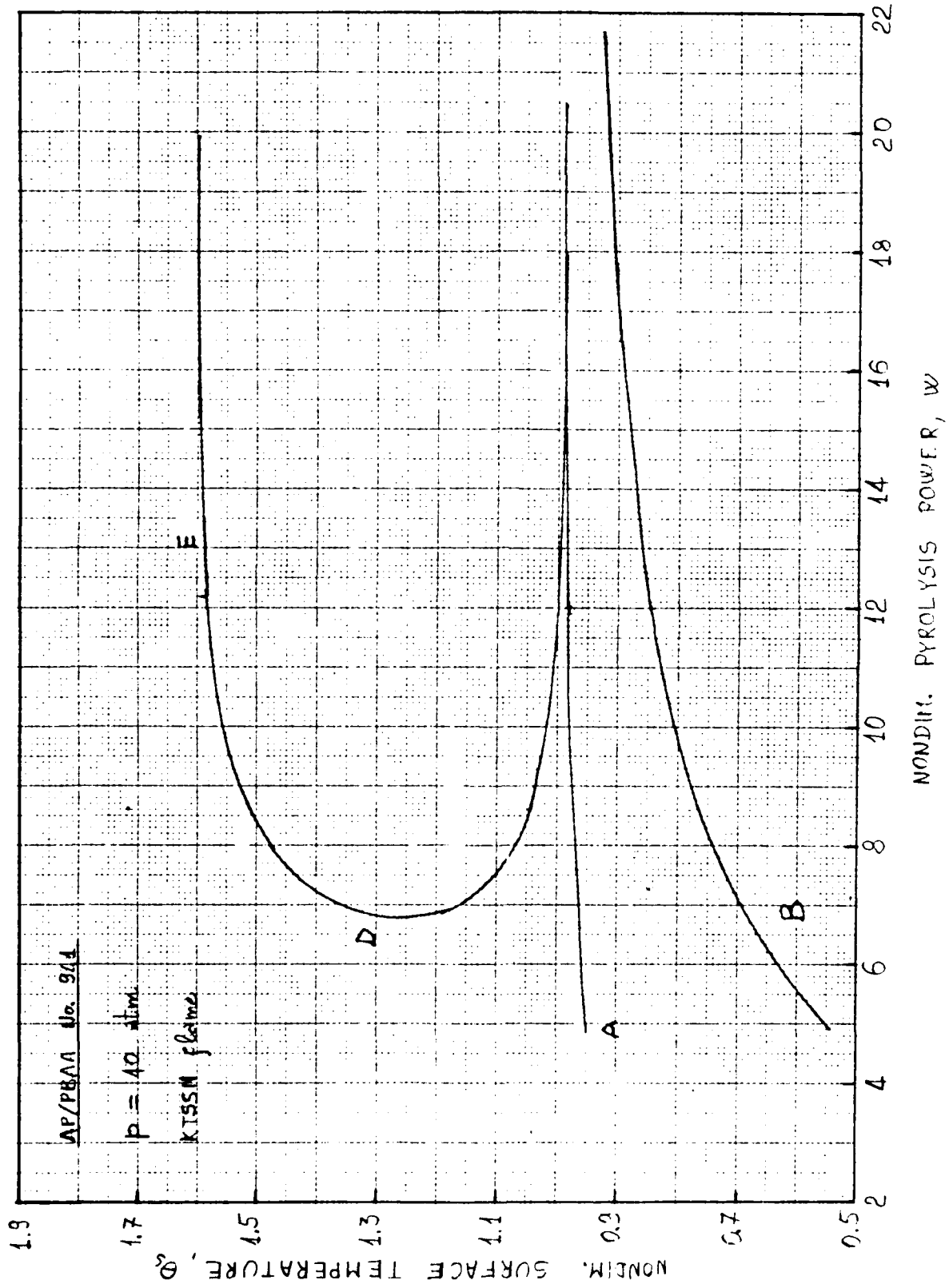


FIG. 30 a

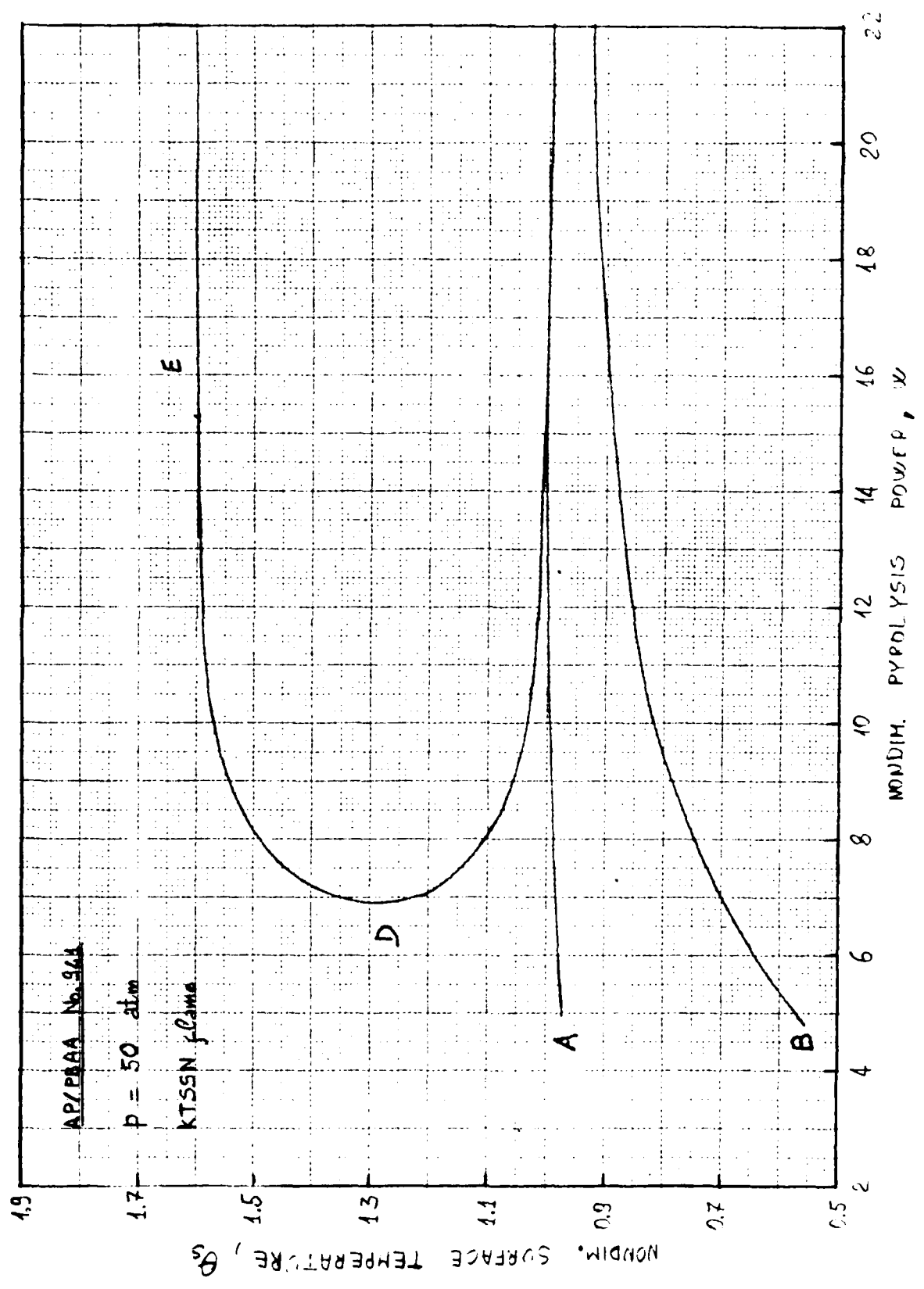


FIG. 30b

AP/FBAA No. 941

$Q_{s,ref} = 125$ cal/g
 $Q_c = 50$ cal/g
 $E_c = 30$ Kcal/mole
 $C_g = 1.67$
 $b = a = 0.2$

KTSSM Name
Arrhenius Pyrolysis
 $\hat{\lambda} = 0.75$
 $E_s = 24$ Kcal/mole
 $n = 3$, polynomial

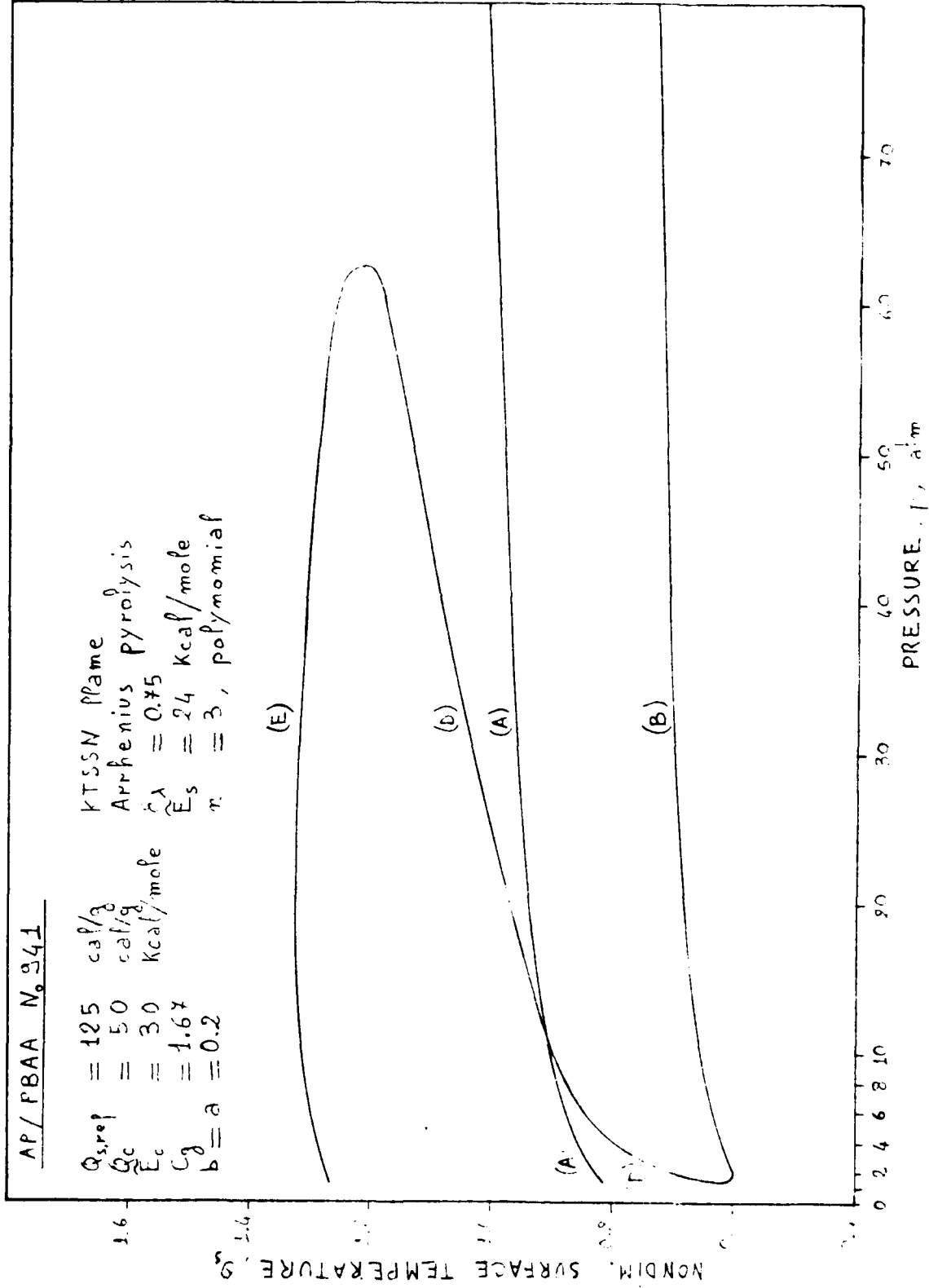


FIG. 21

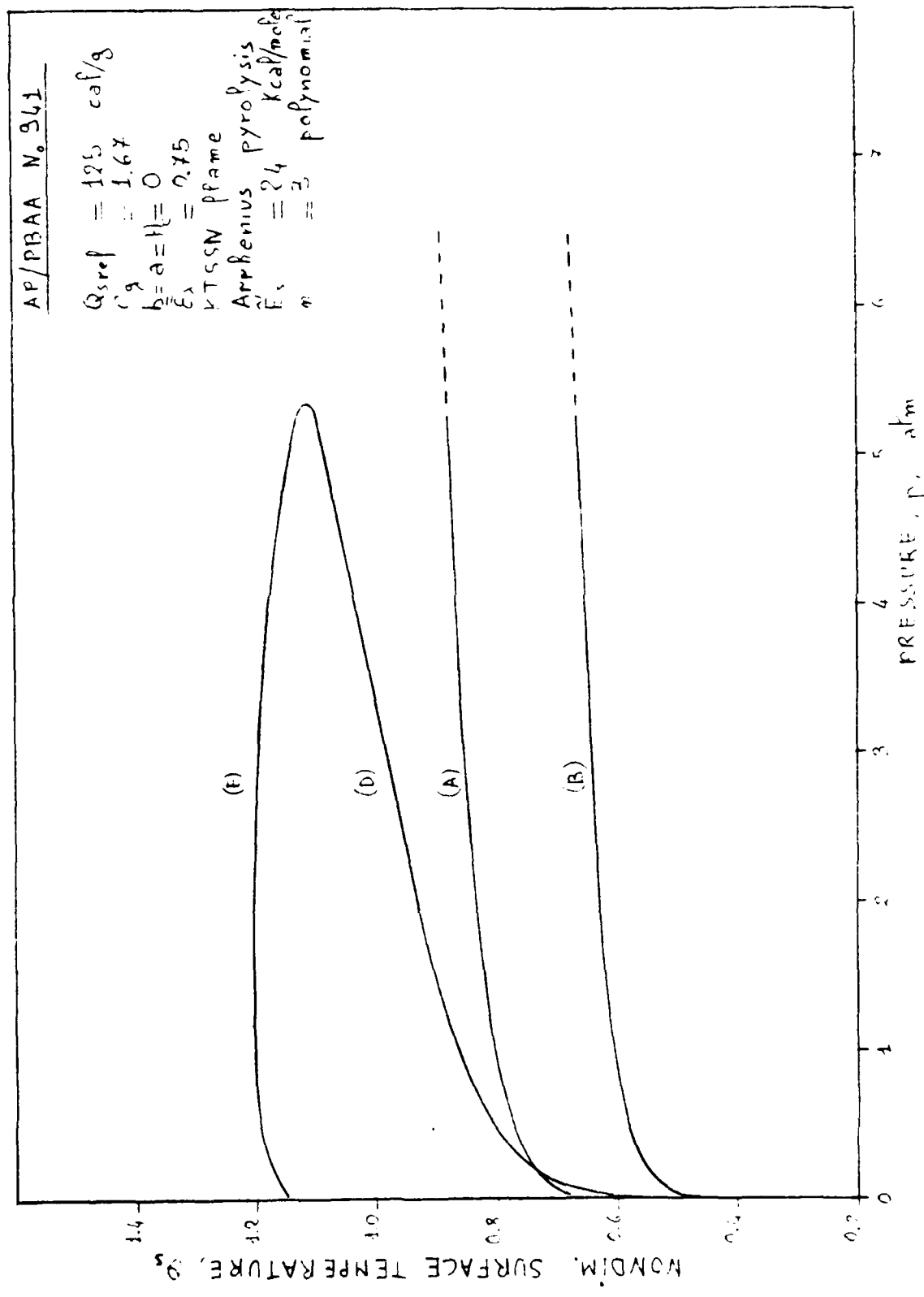


FIG. 32a

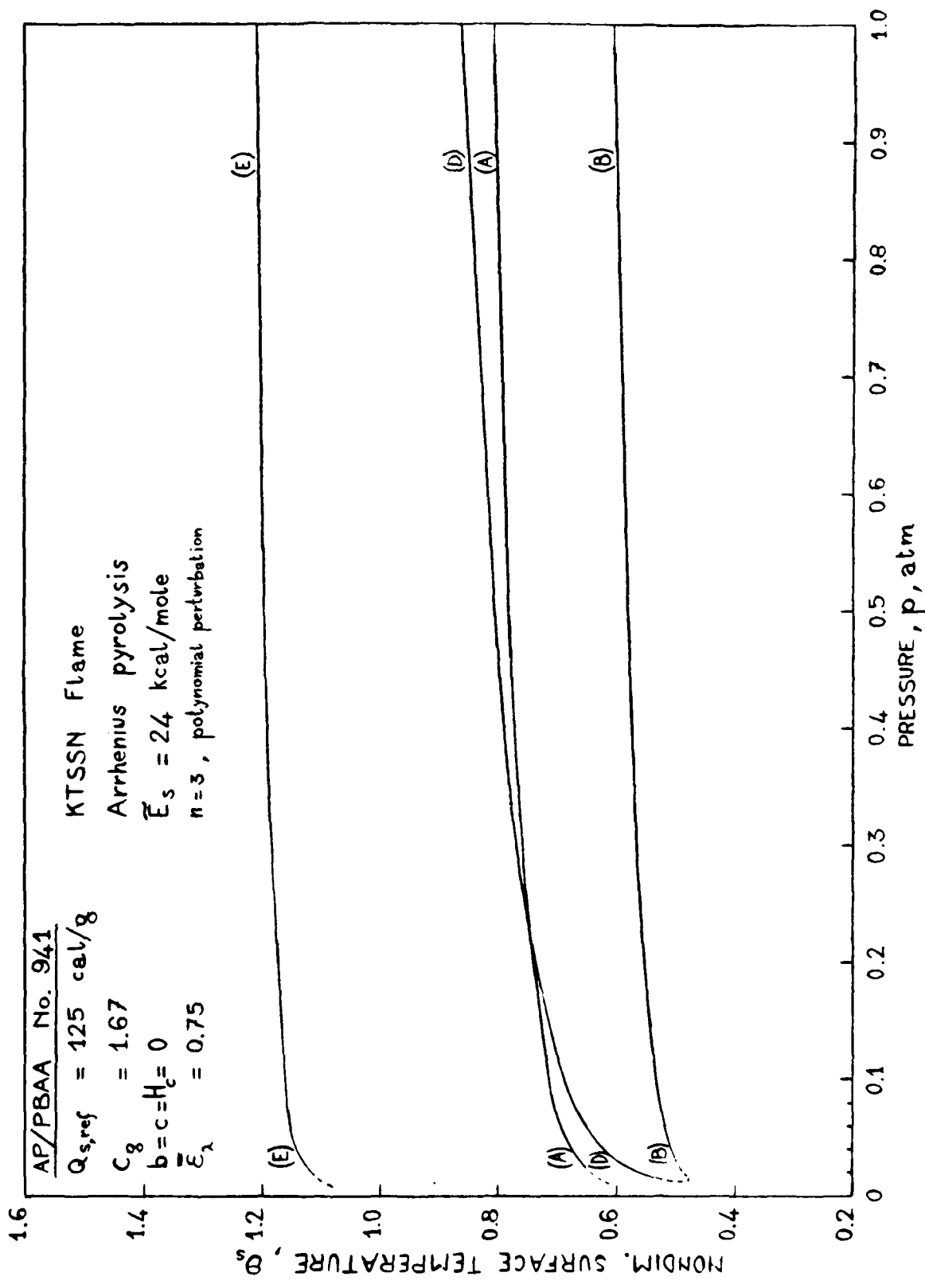


FIG. 32b

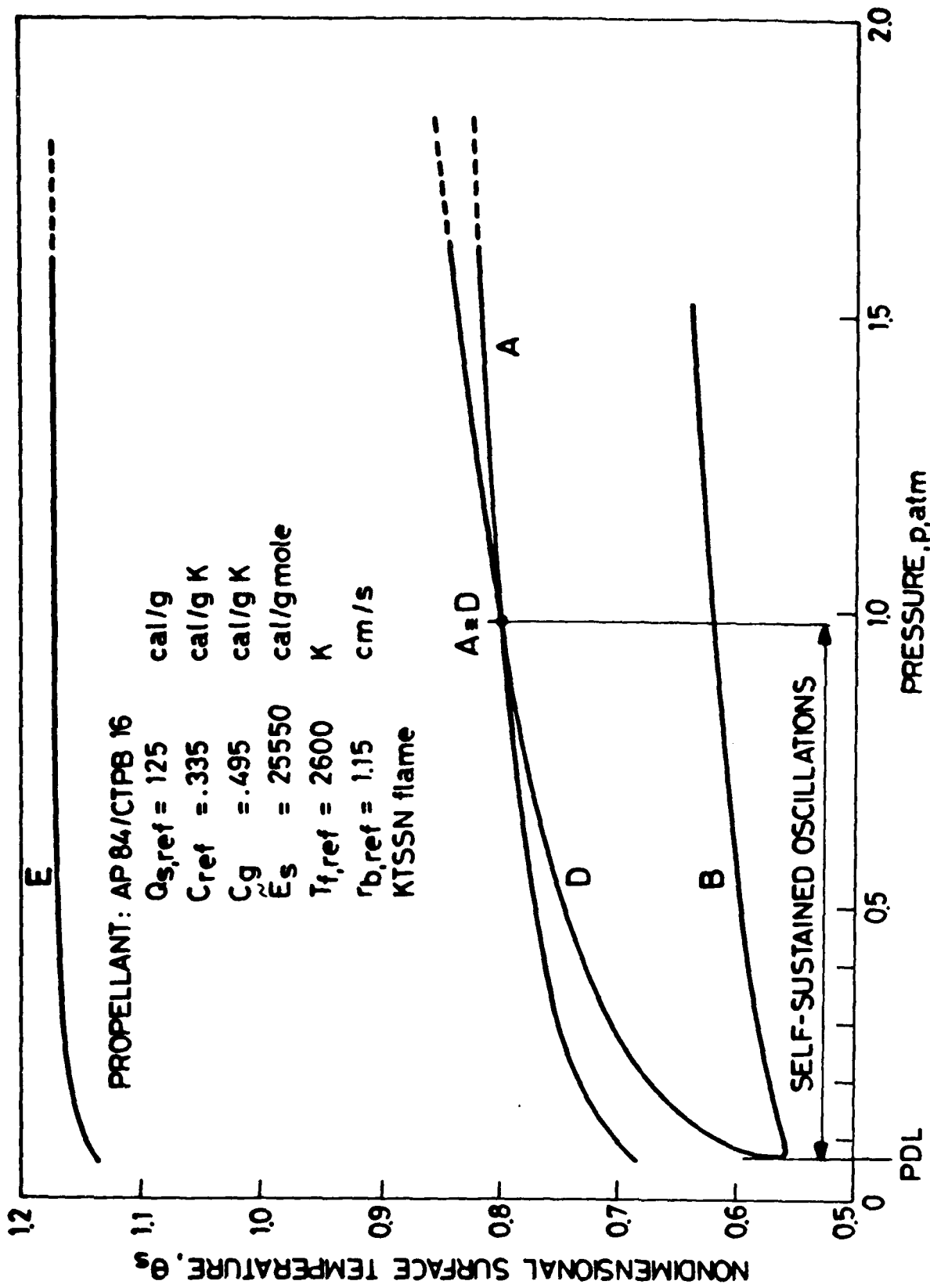


FIG. 33

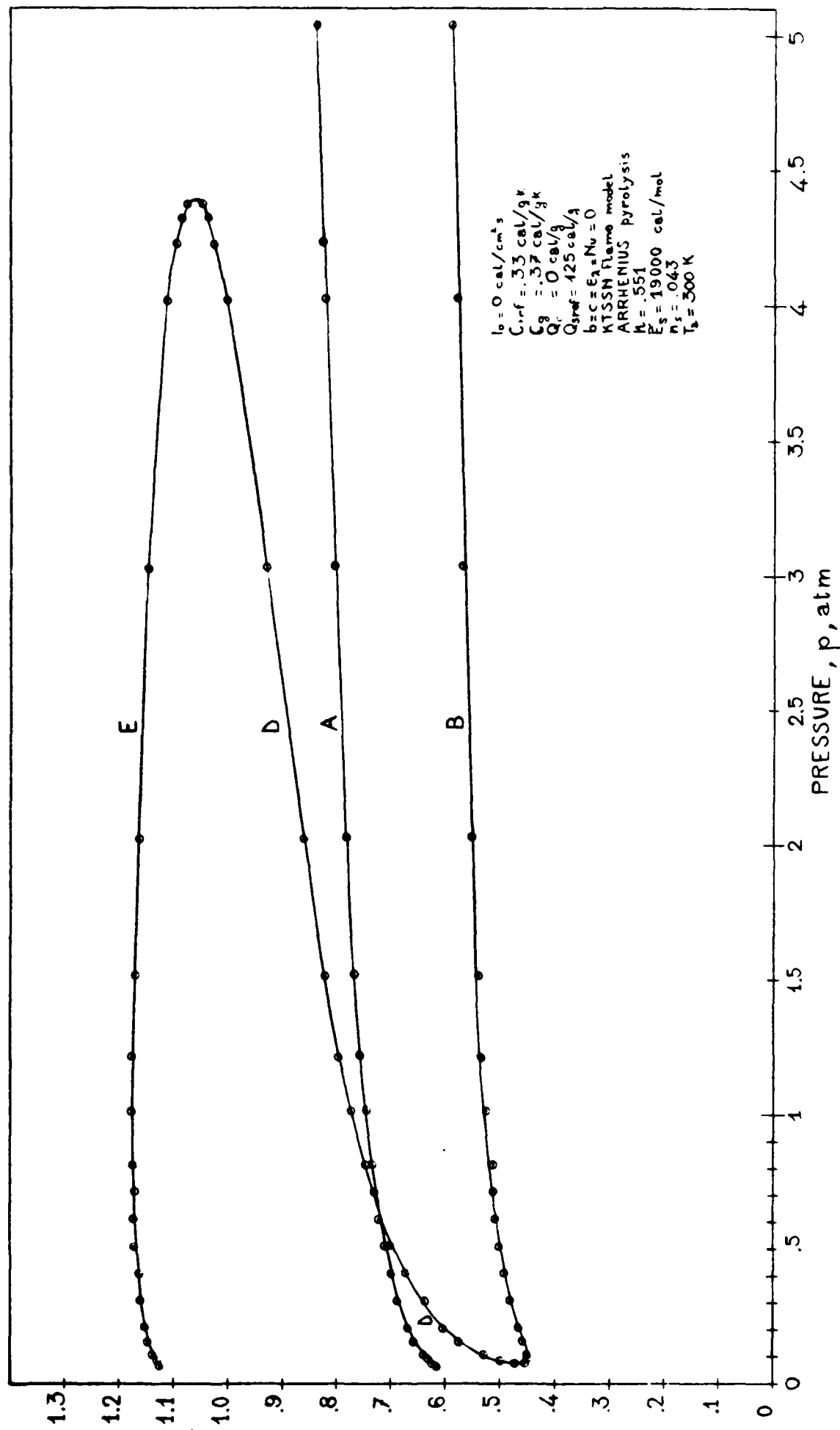


FIG. 34

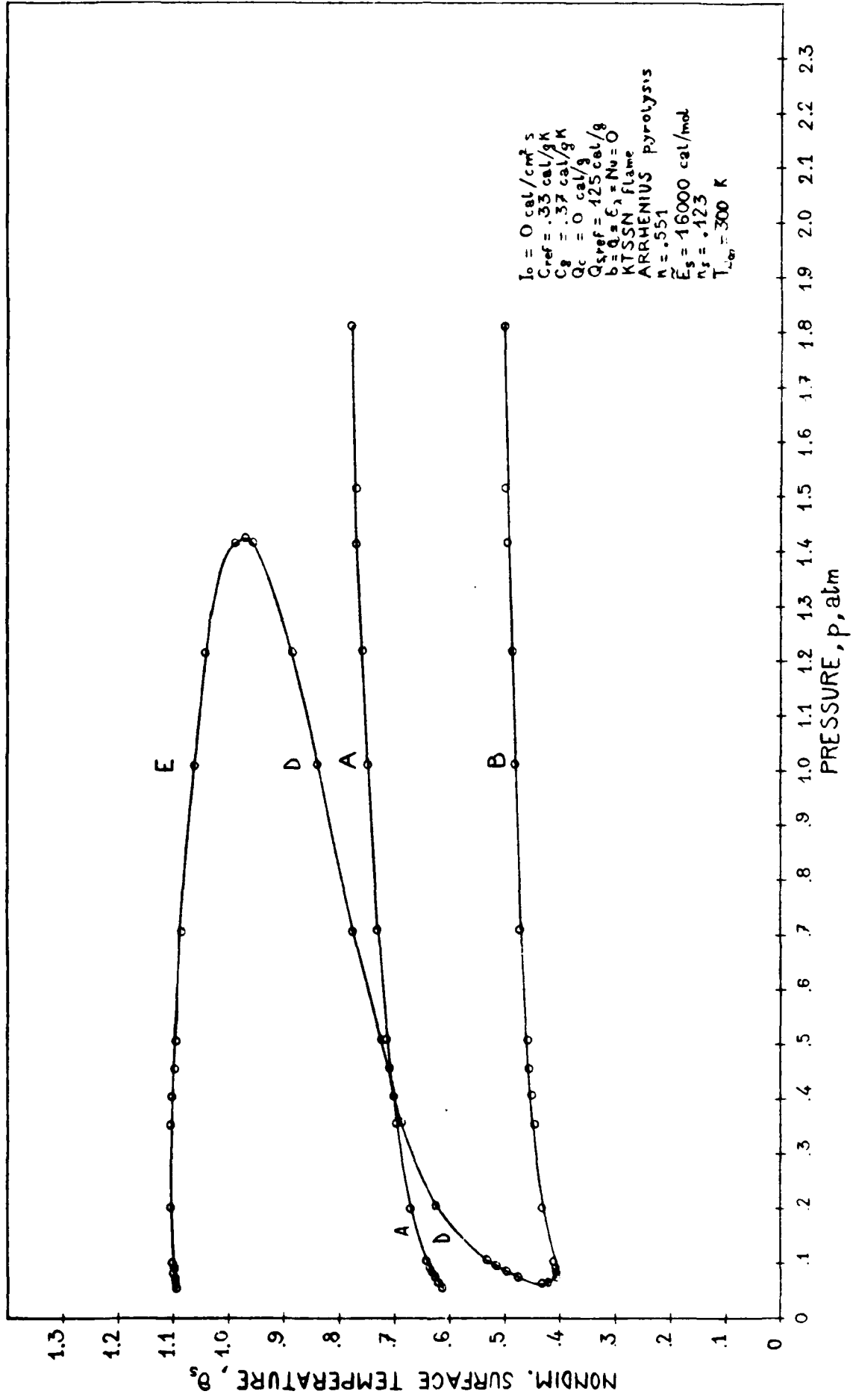


FIG. 35

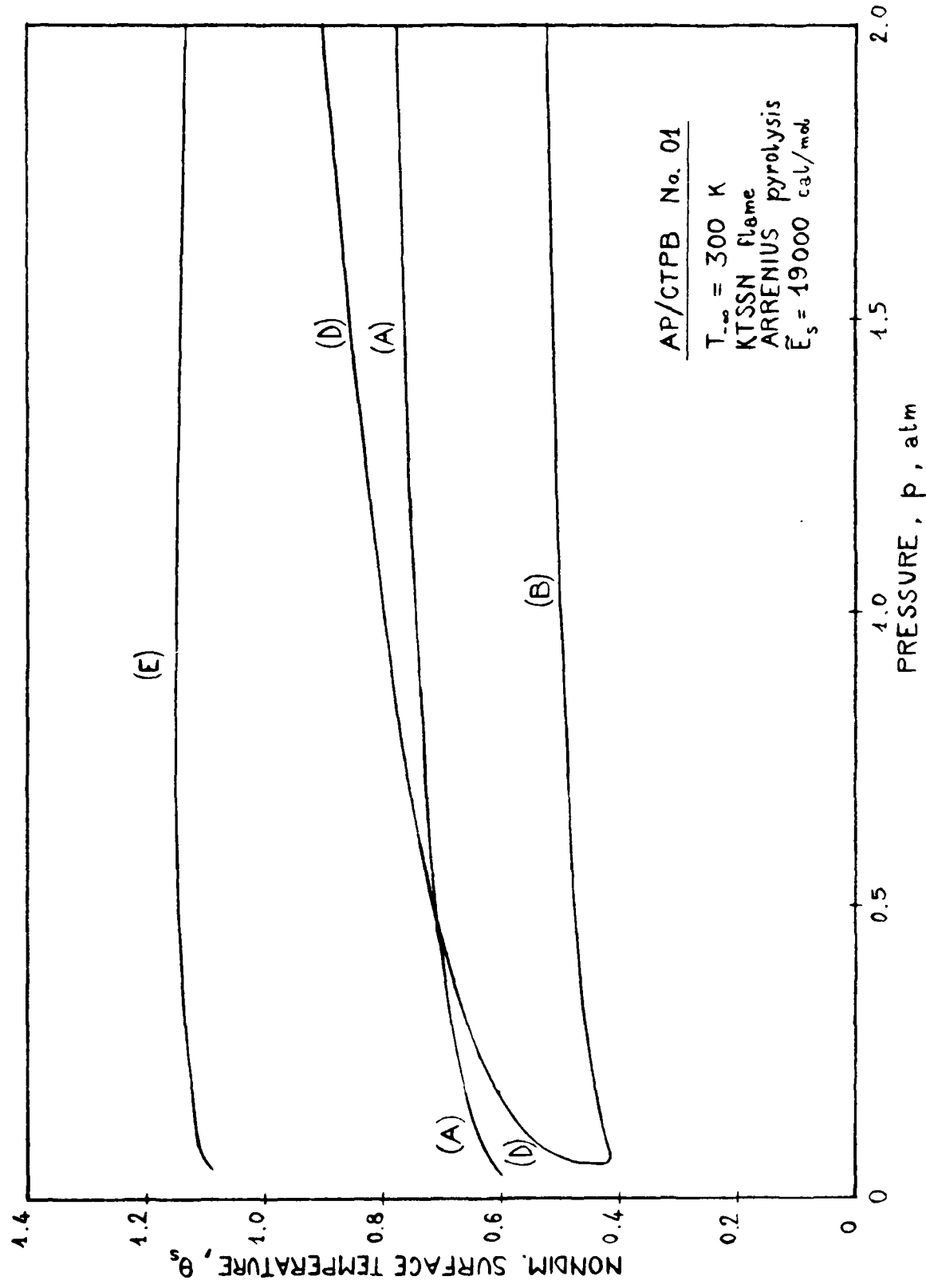


FIG. 36

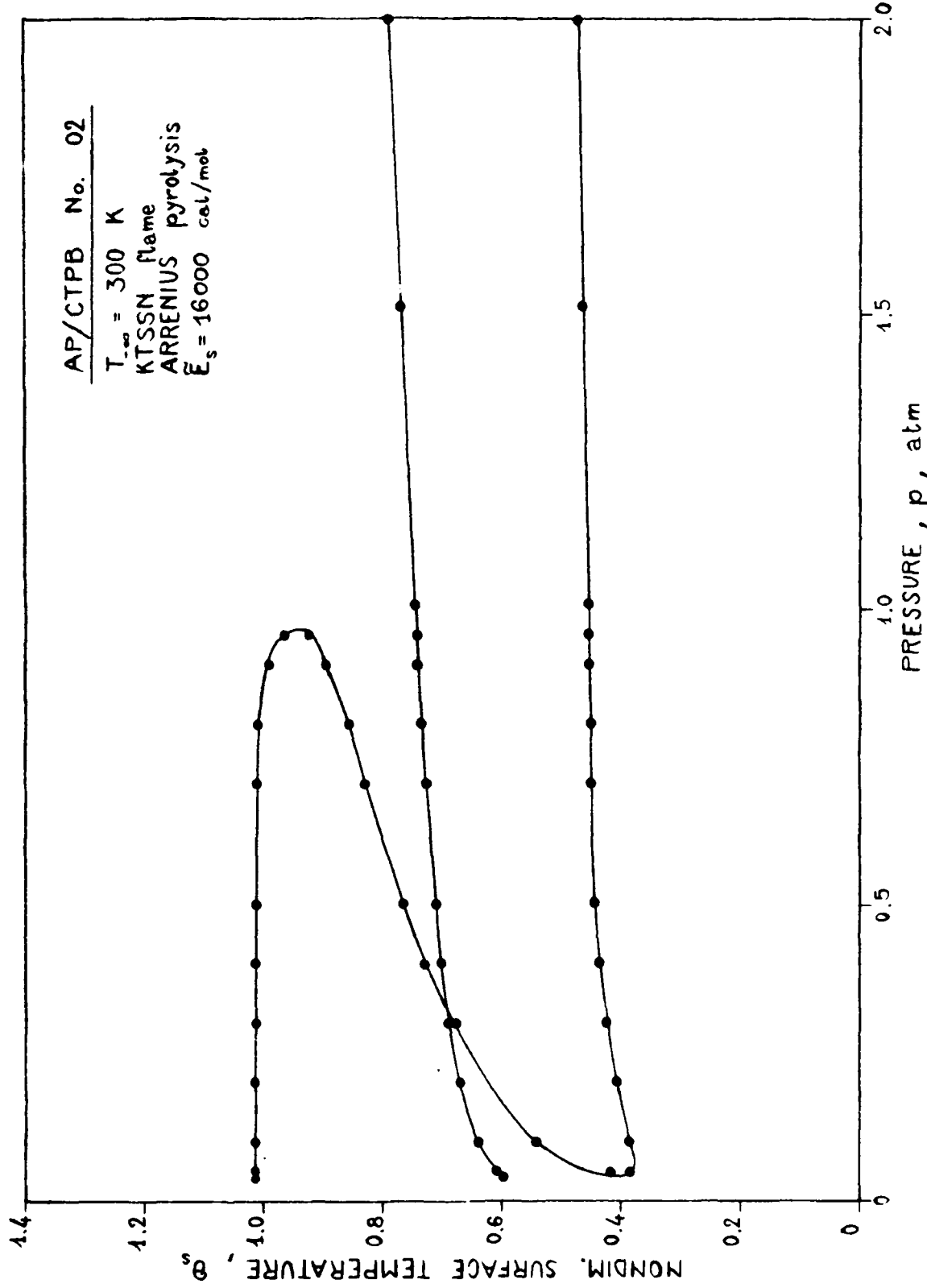


FIG. 37

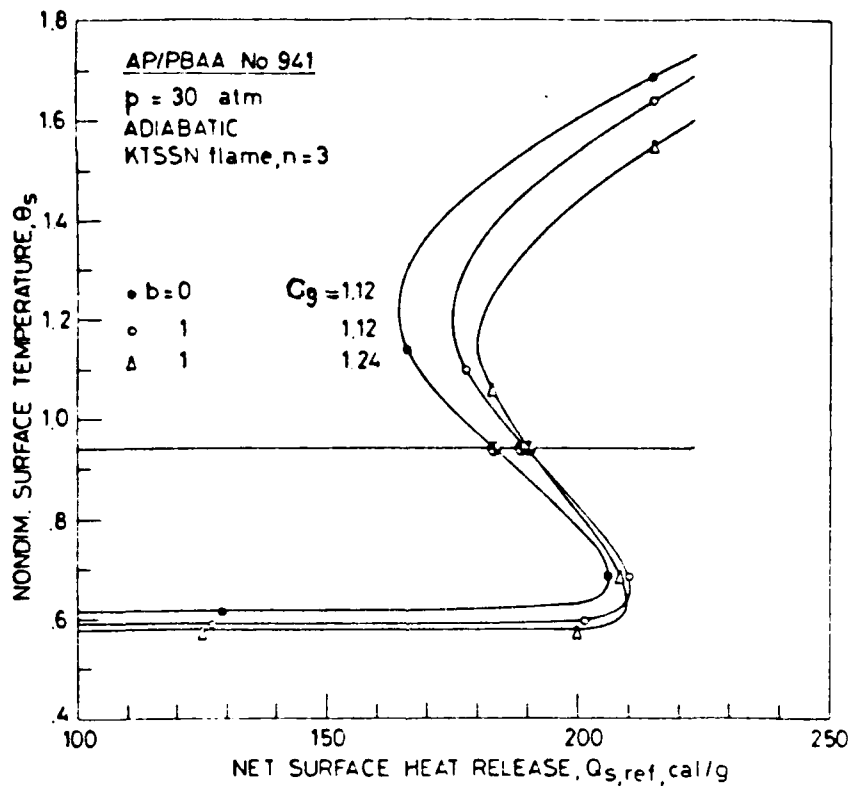


FIG. 39

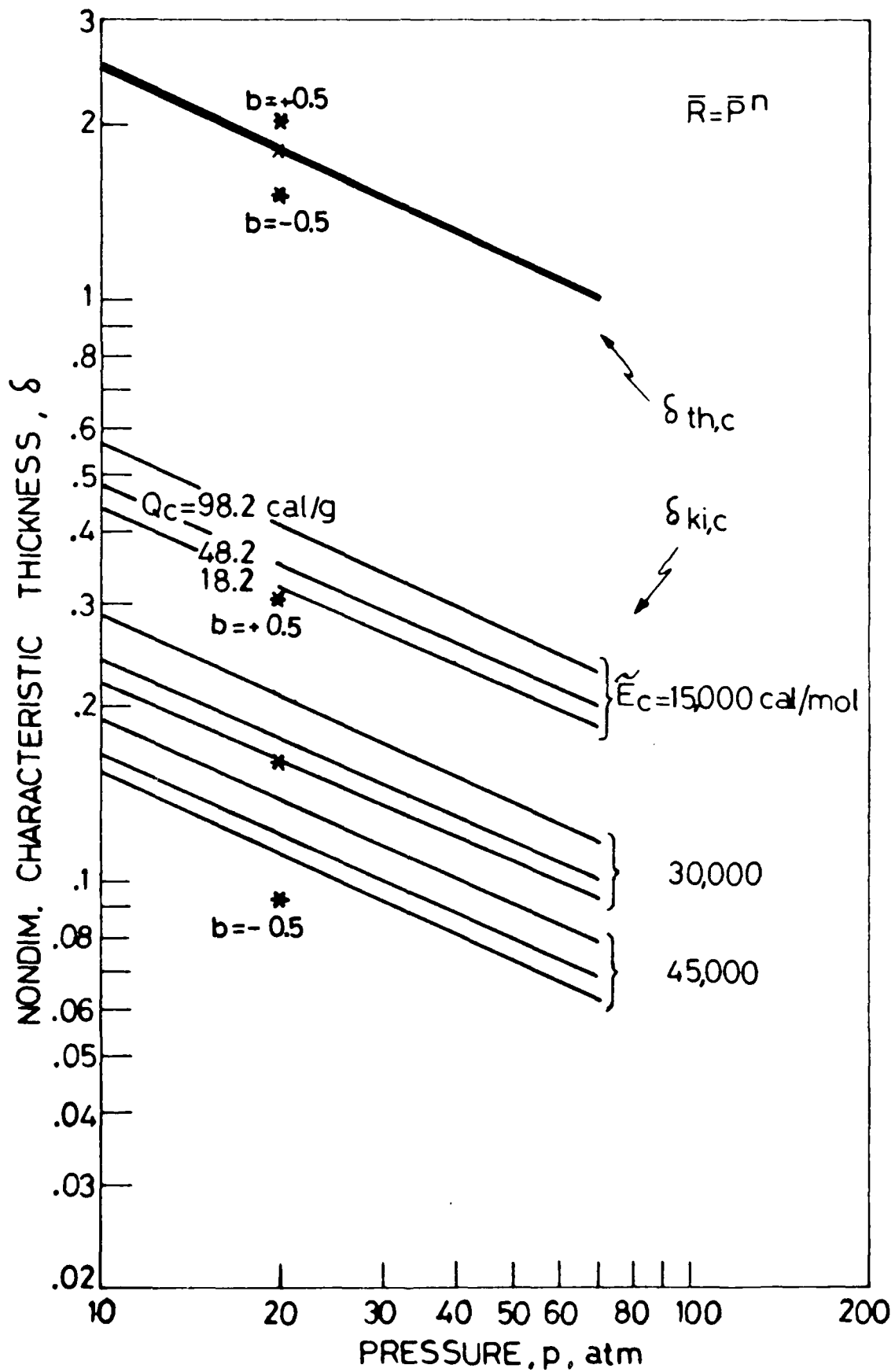


FIG. 40

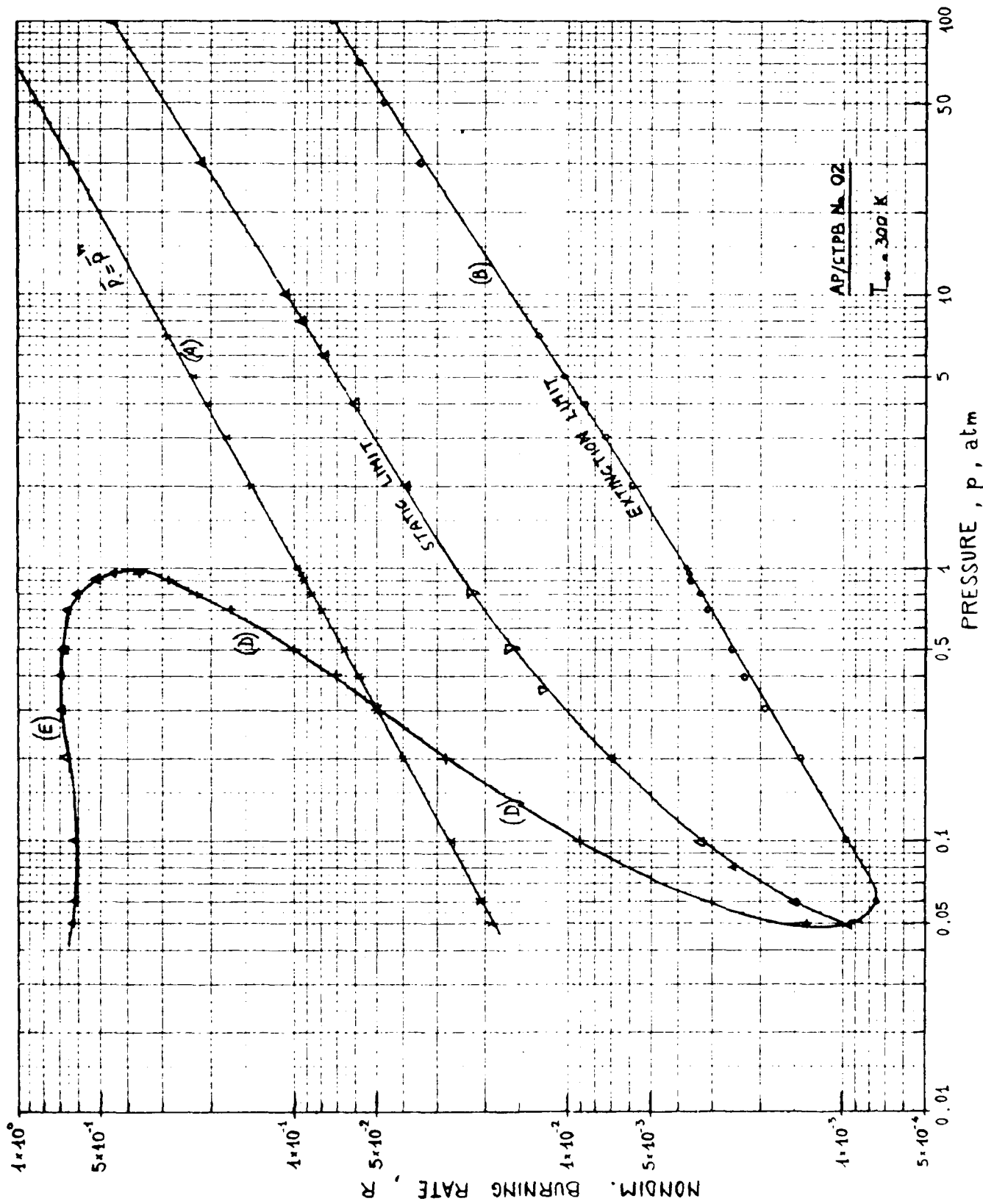
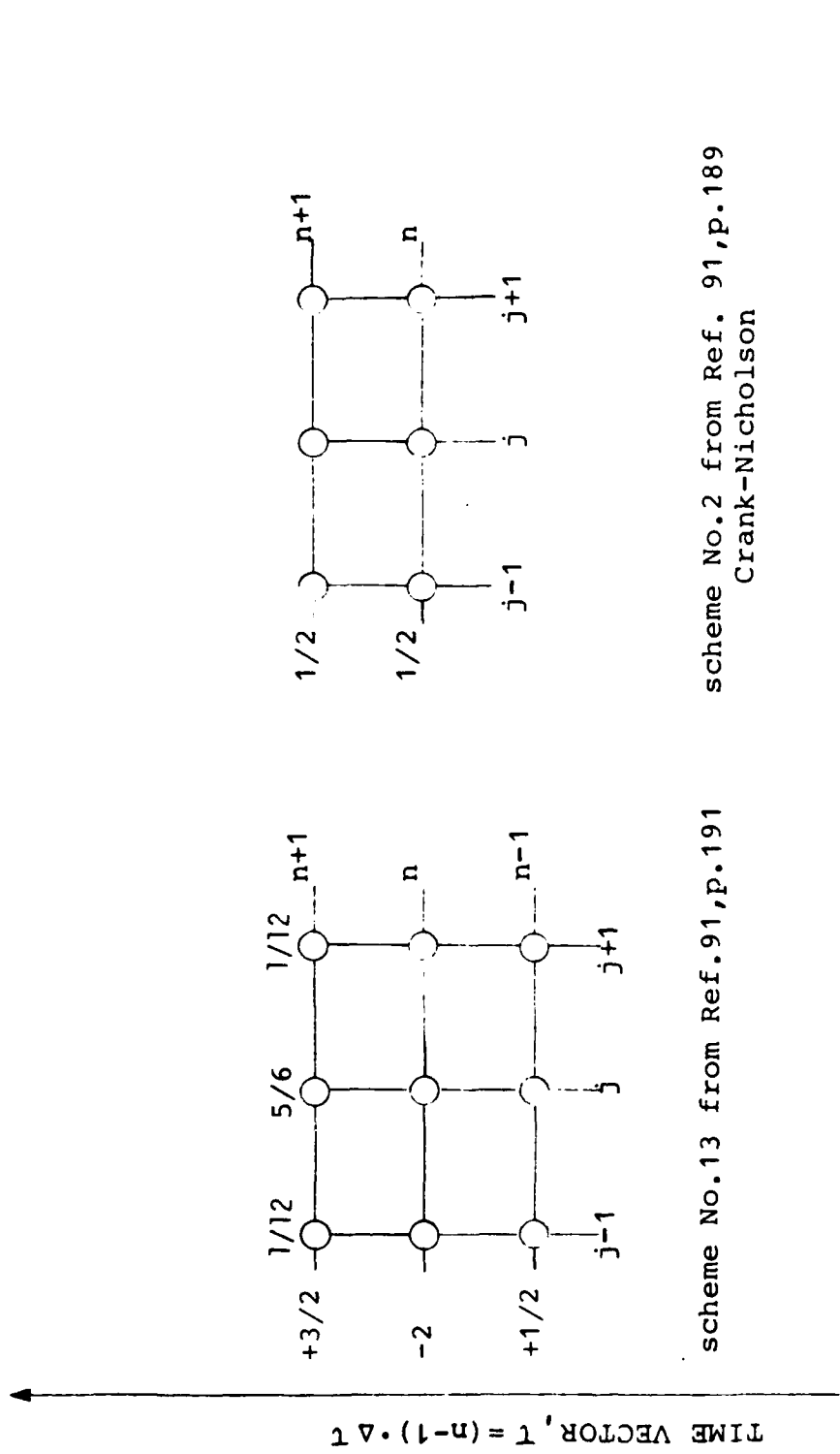


FIG. 41



scheme No.13 from Ref.91,p.191

scheme No.2 from Ref. 91,p.189
Crank-Nicholson

Implicit, always stable
error=0 $[(\Delta\tau)^2] + o [(\Delta X)^4]$

Implicit, always stable
error=0 $[(\Delta\tau)^2] + o [(\Delta X)^2]$

FIG. 42

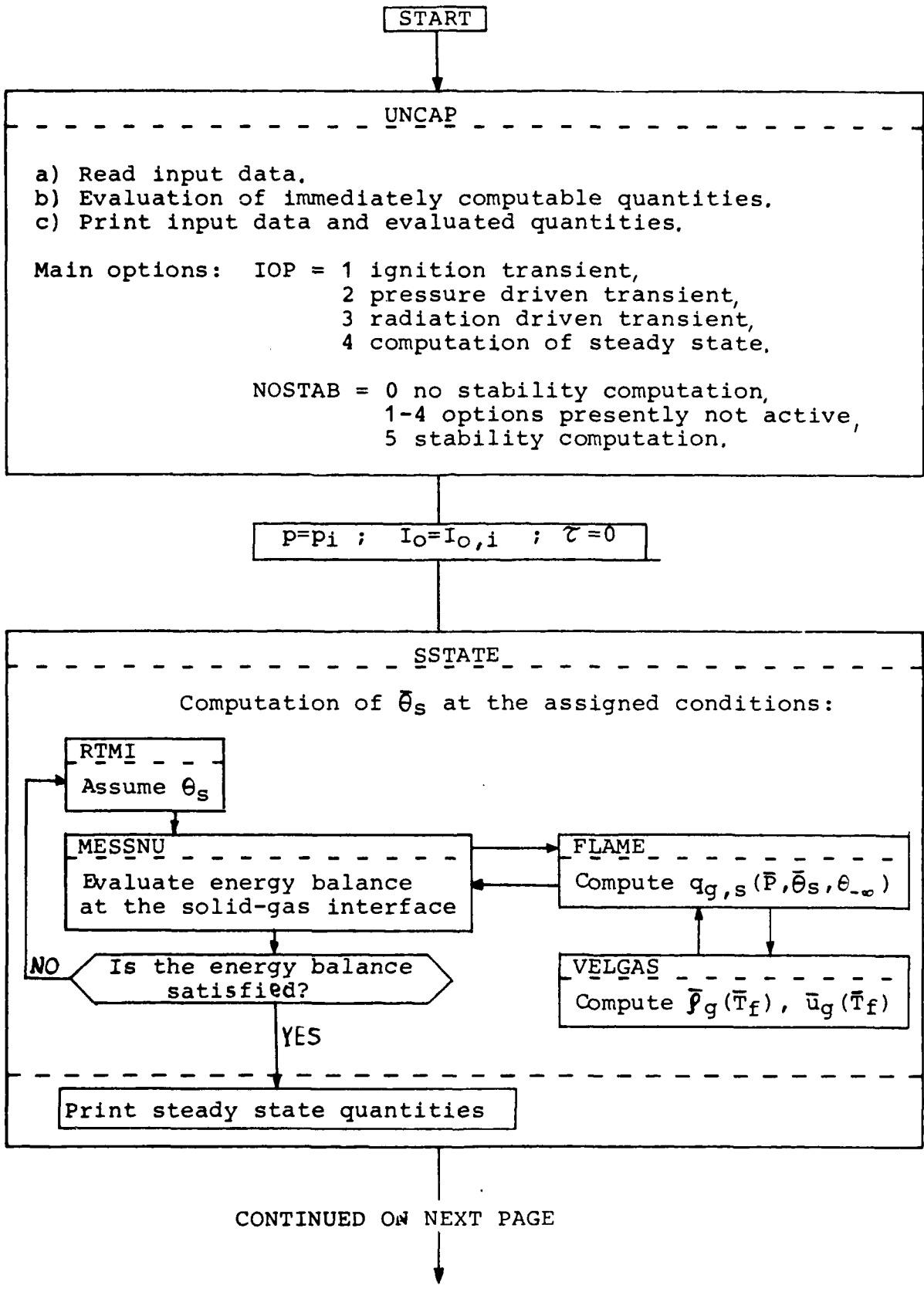


FIG. 43a

CONTINUED FROM PREVIOUS PAGE

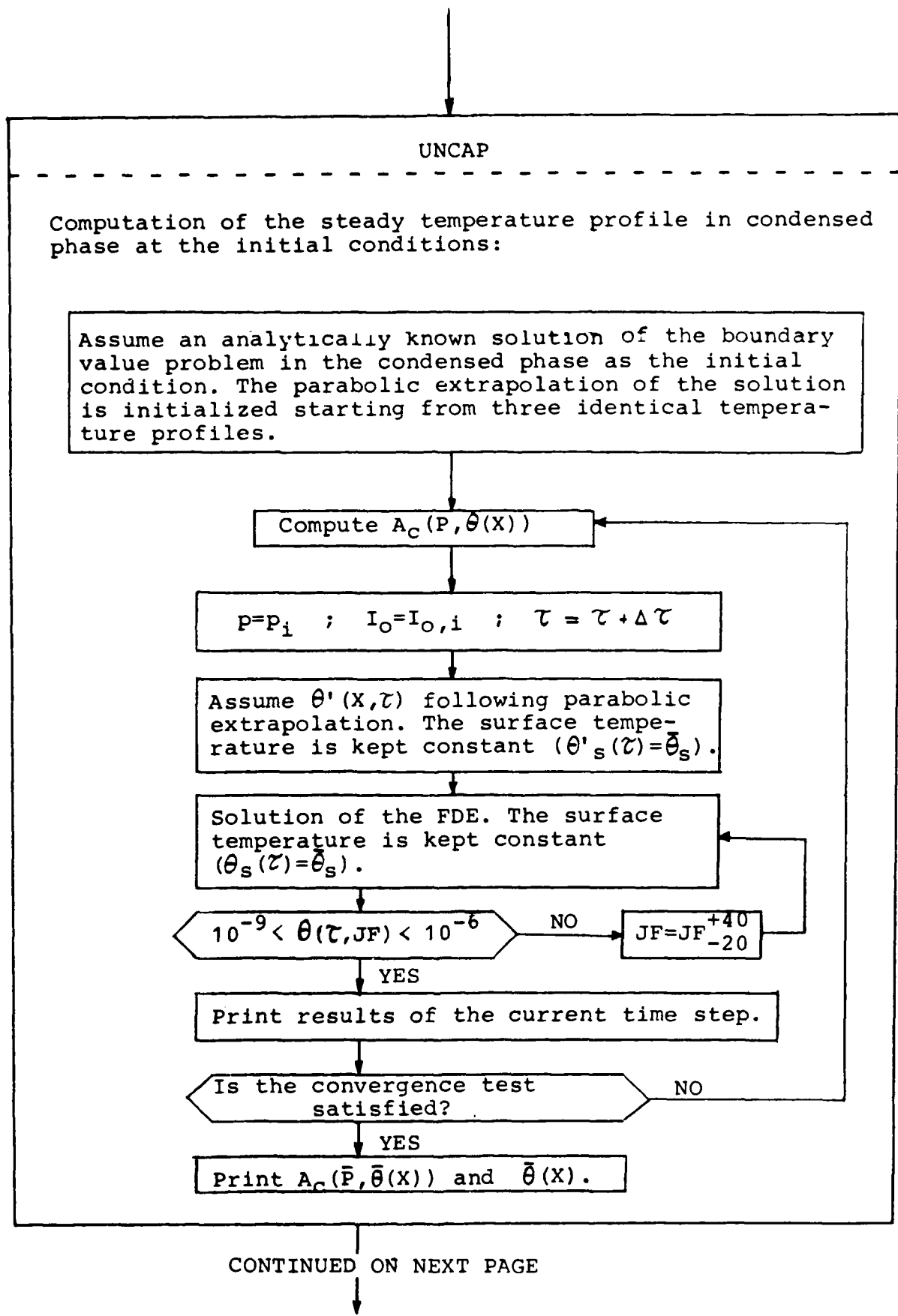


FIG. 43b

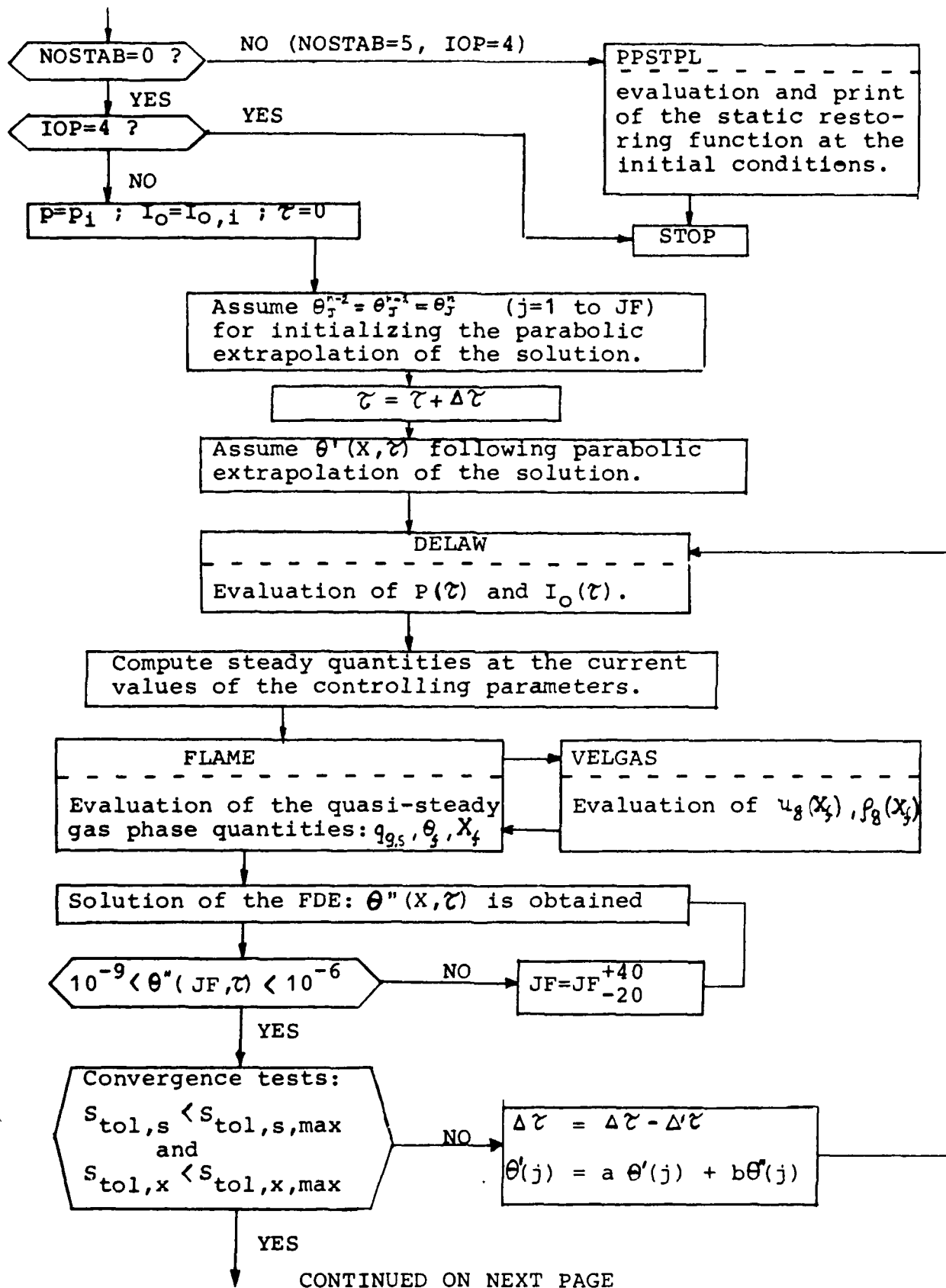


FIG. 43c

CONTINUED FROM PREVIOUS PAGE

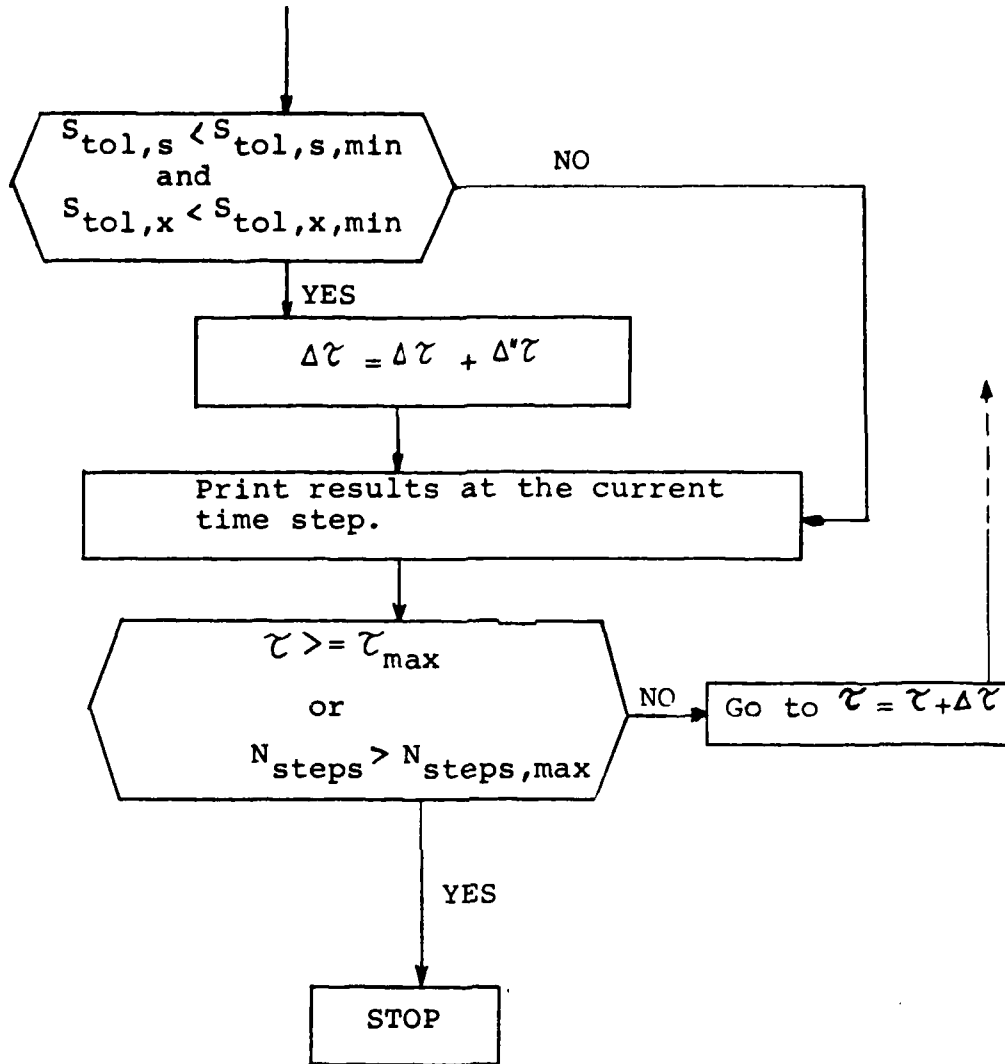


FIG. 43d

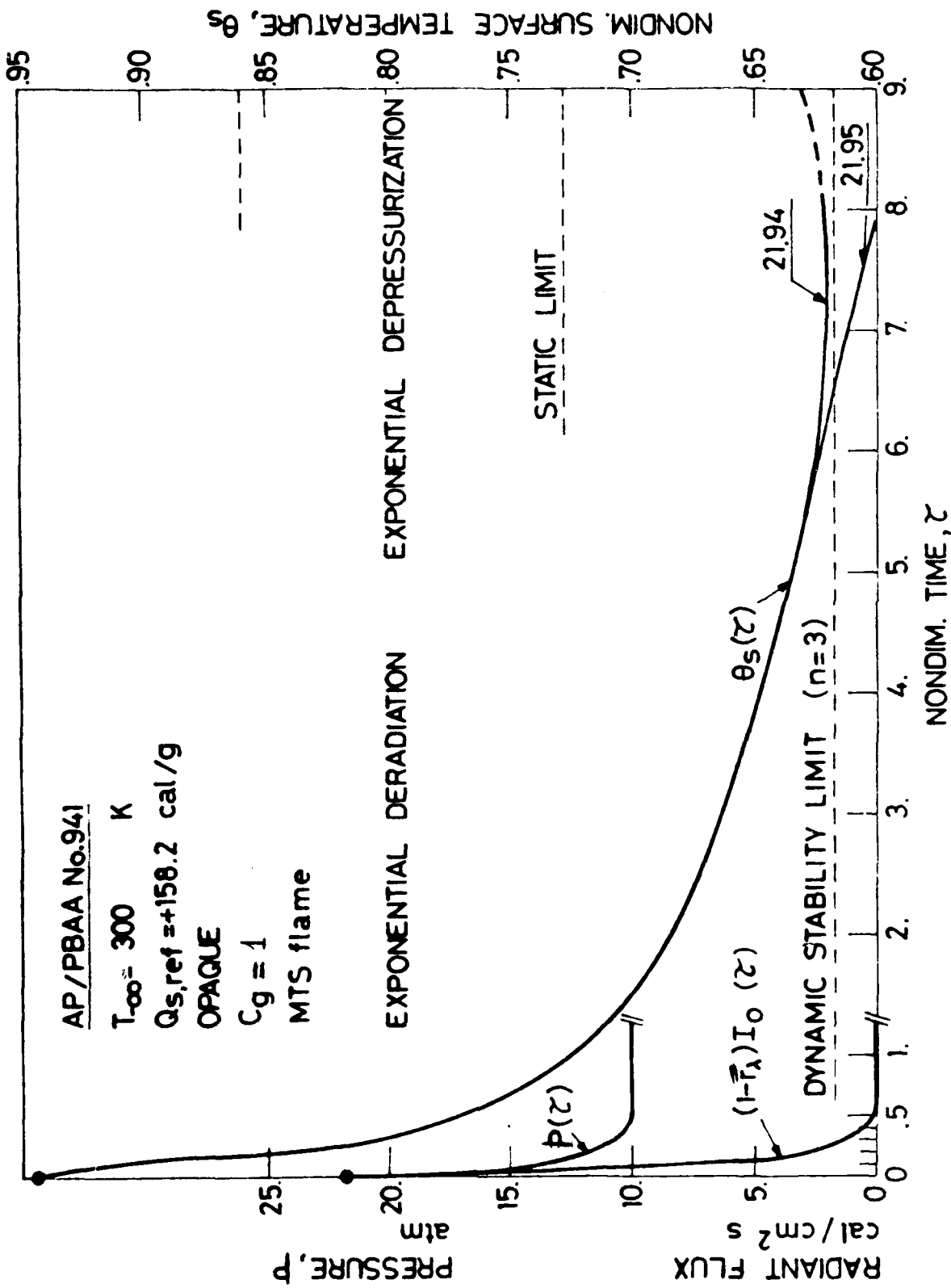


FIG. 44

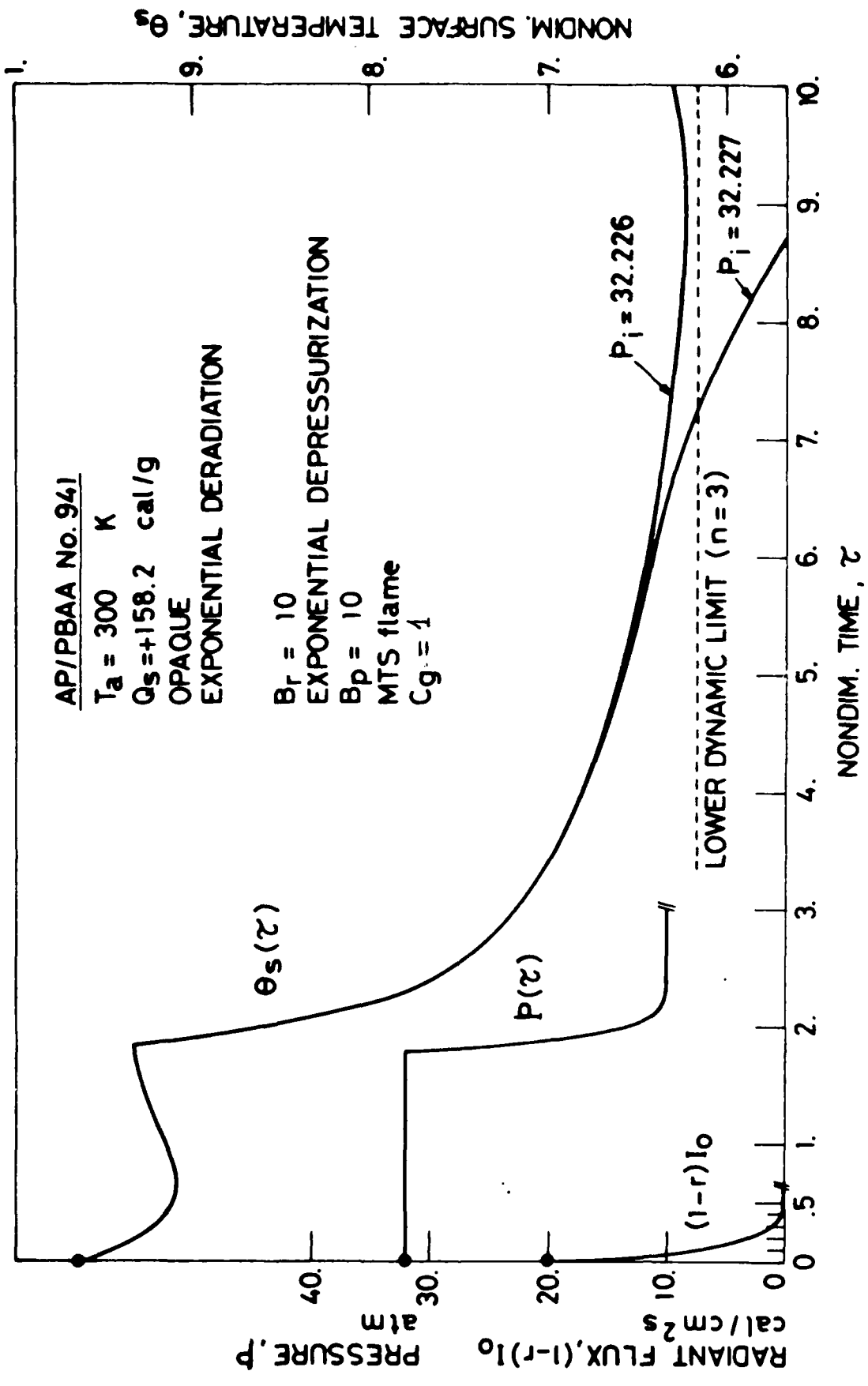


FIG. 45

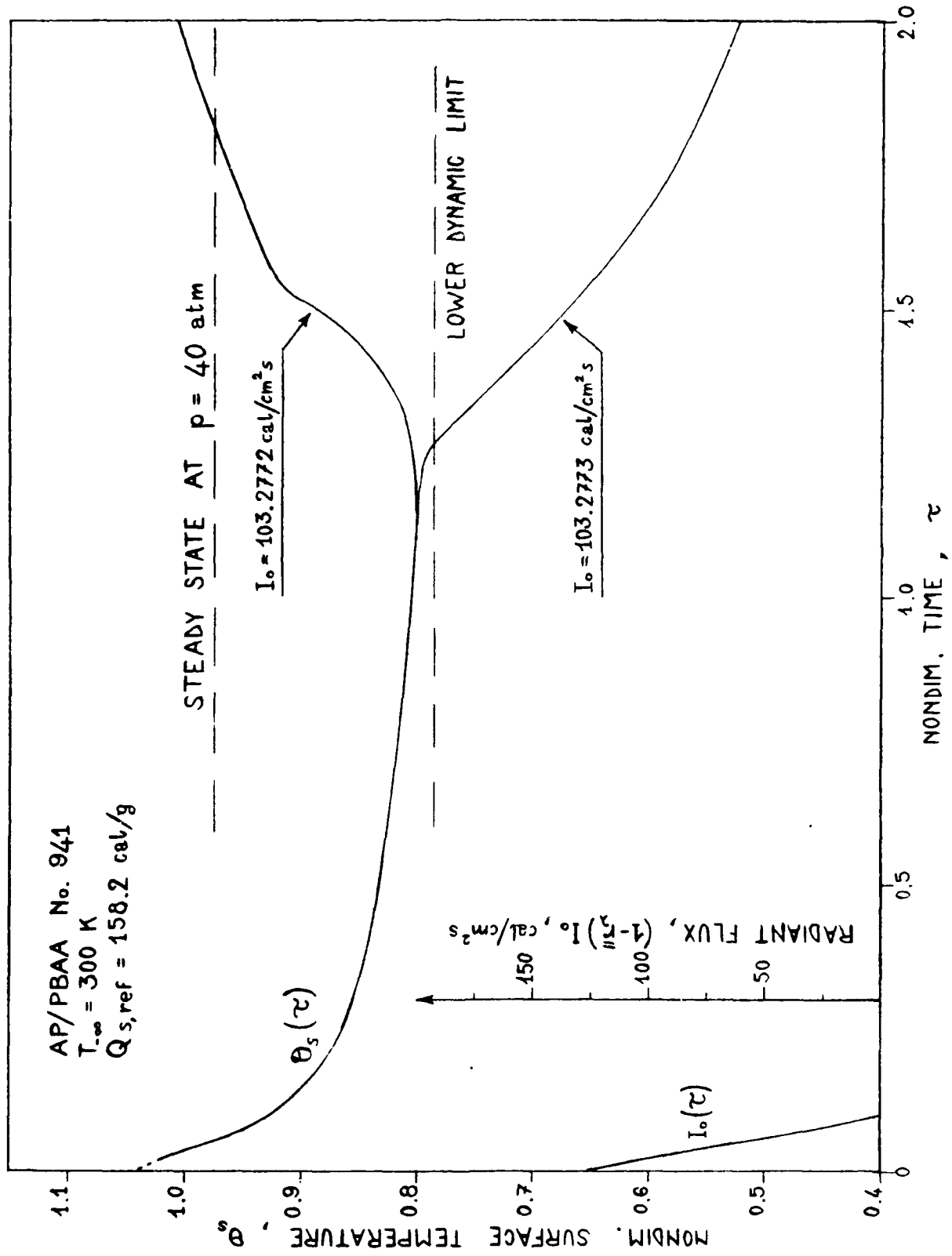


FIG. 46

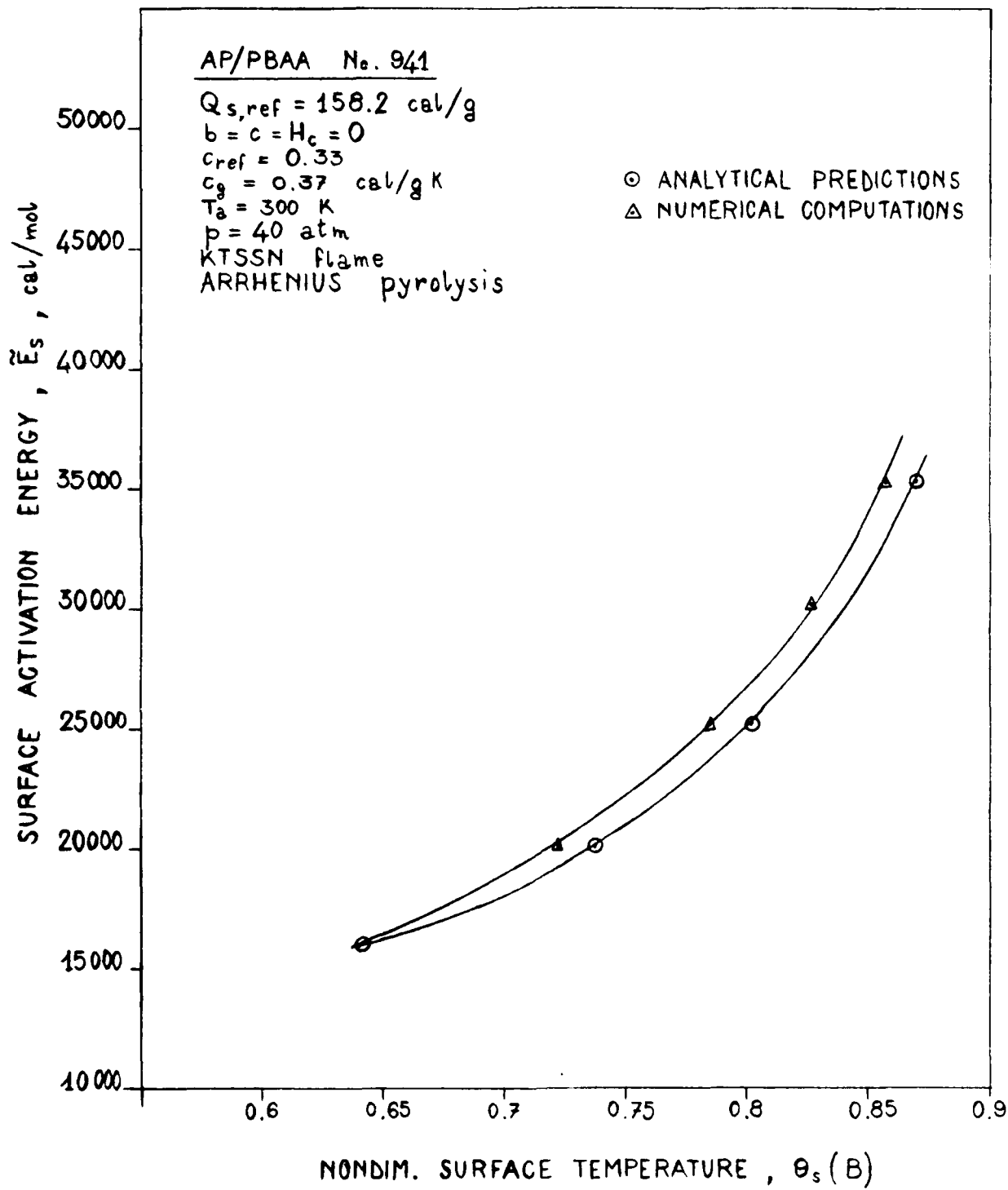


FIG. 47

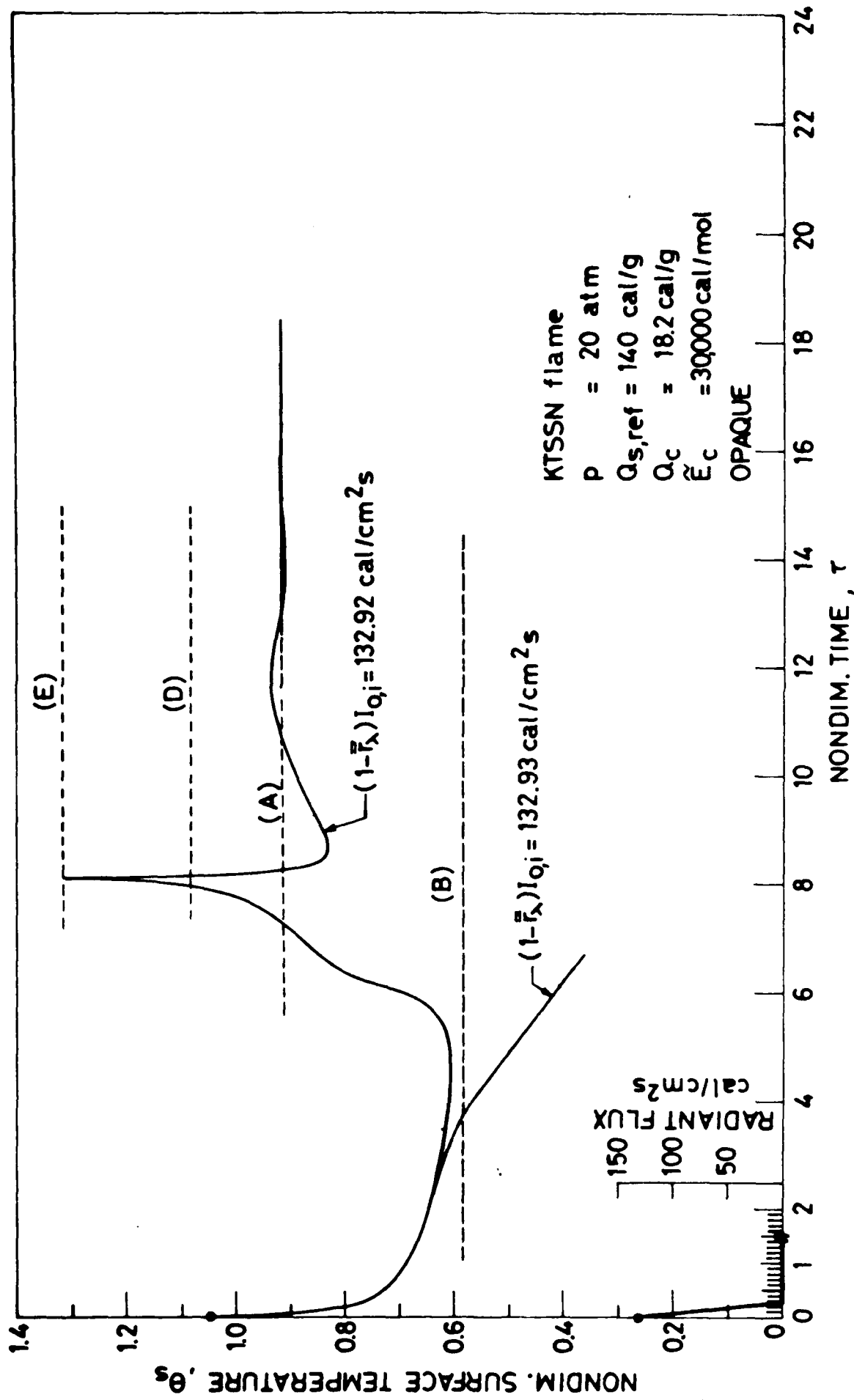


FIG. 48

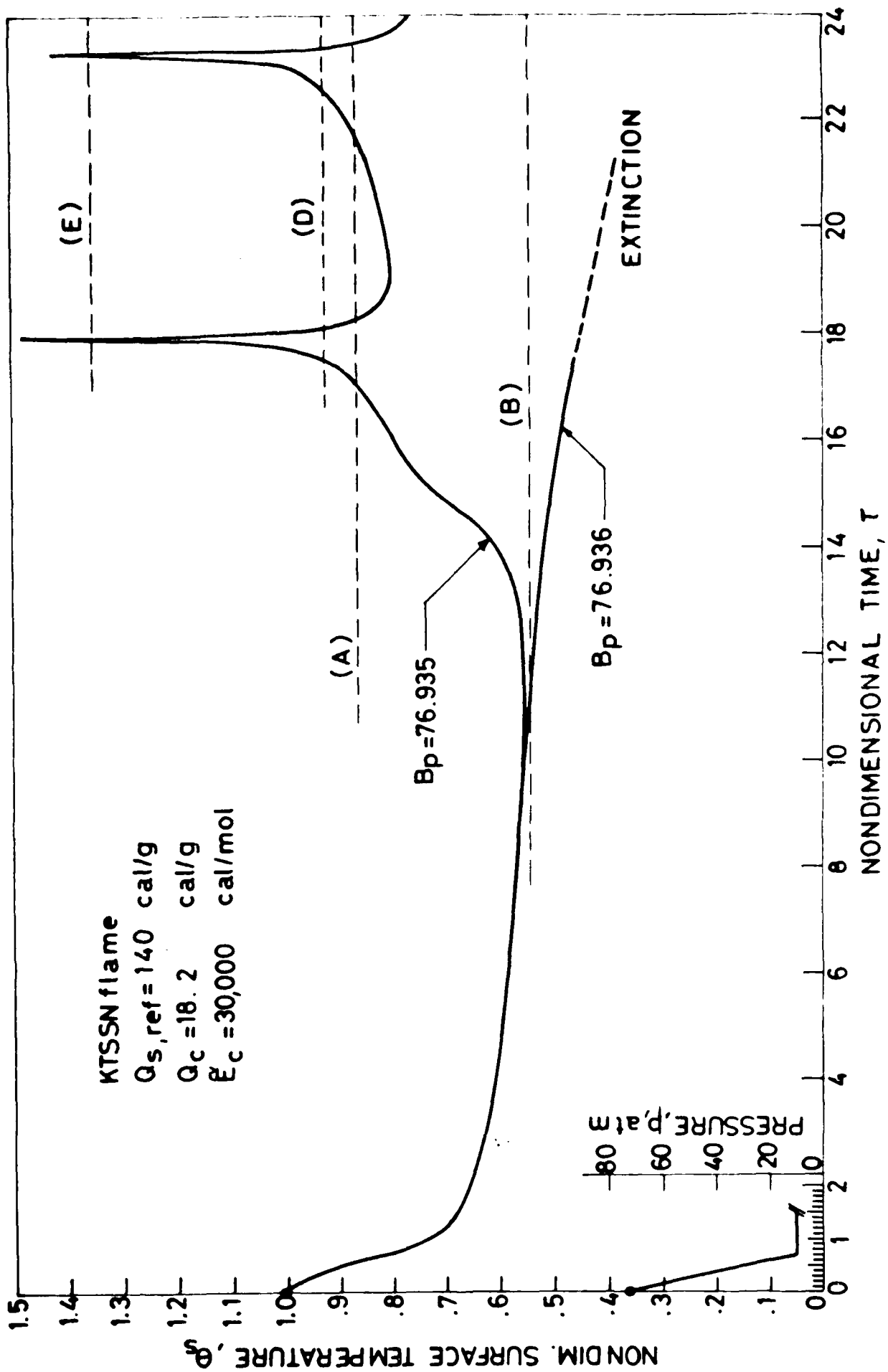


FIG. 49

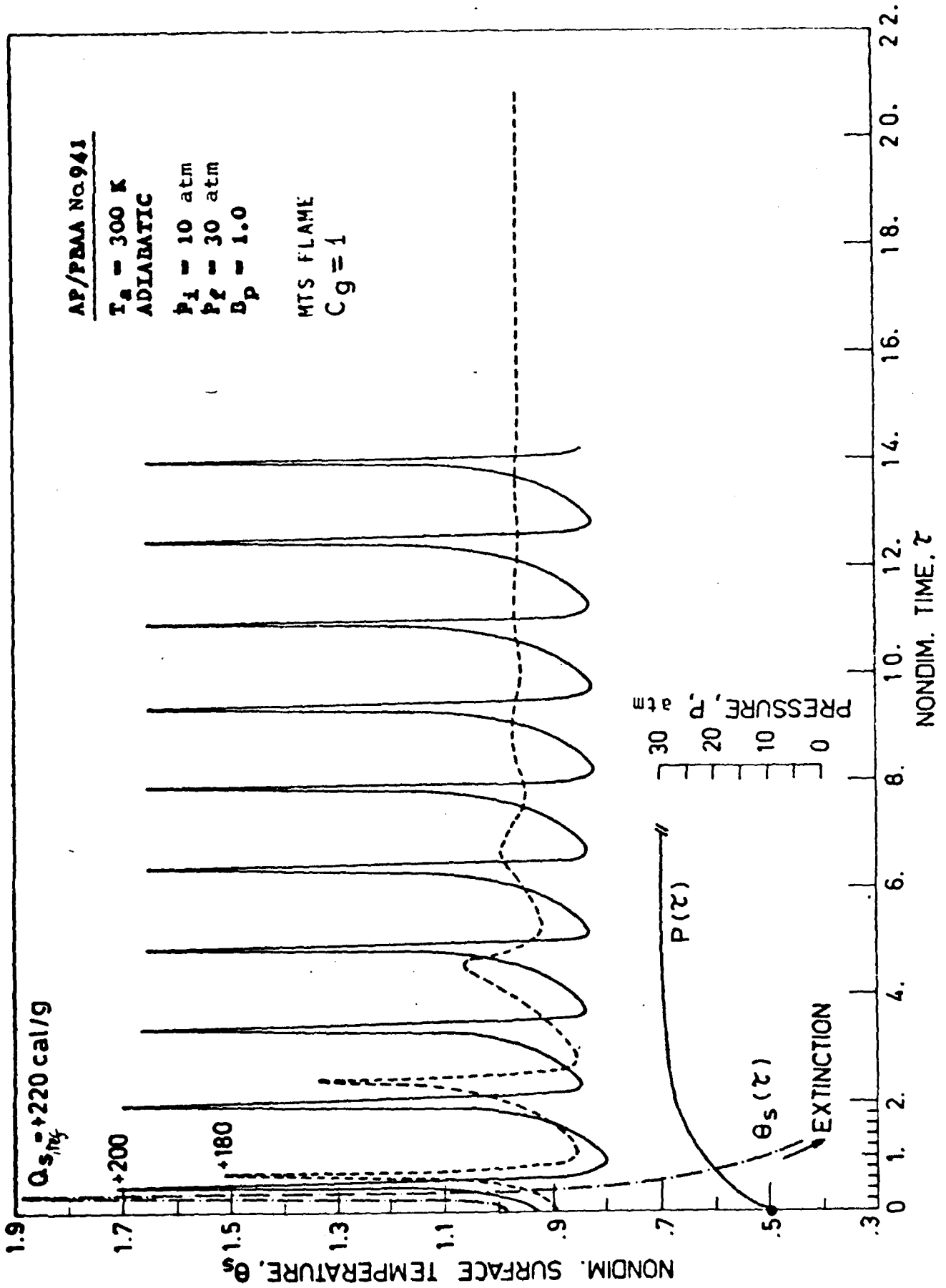


FIG. 50

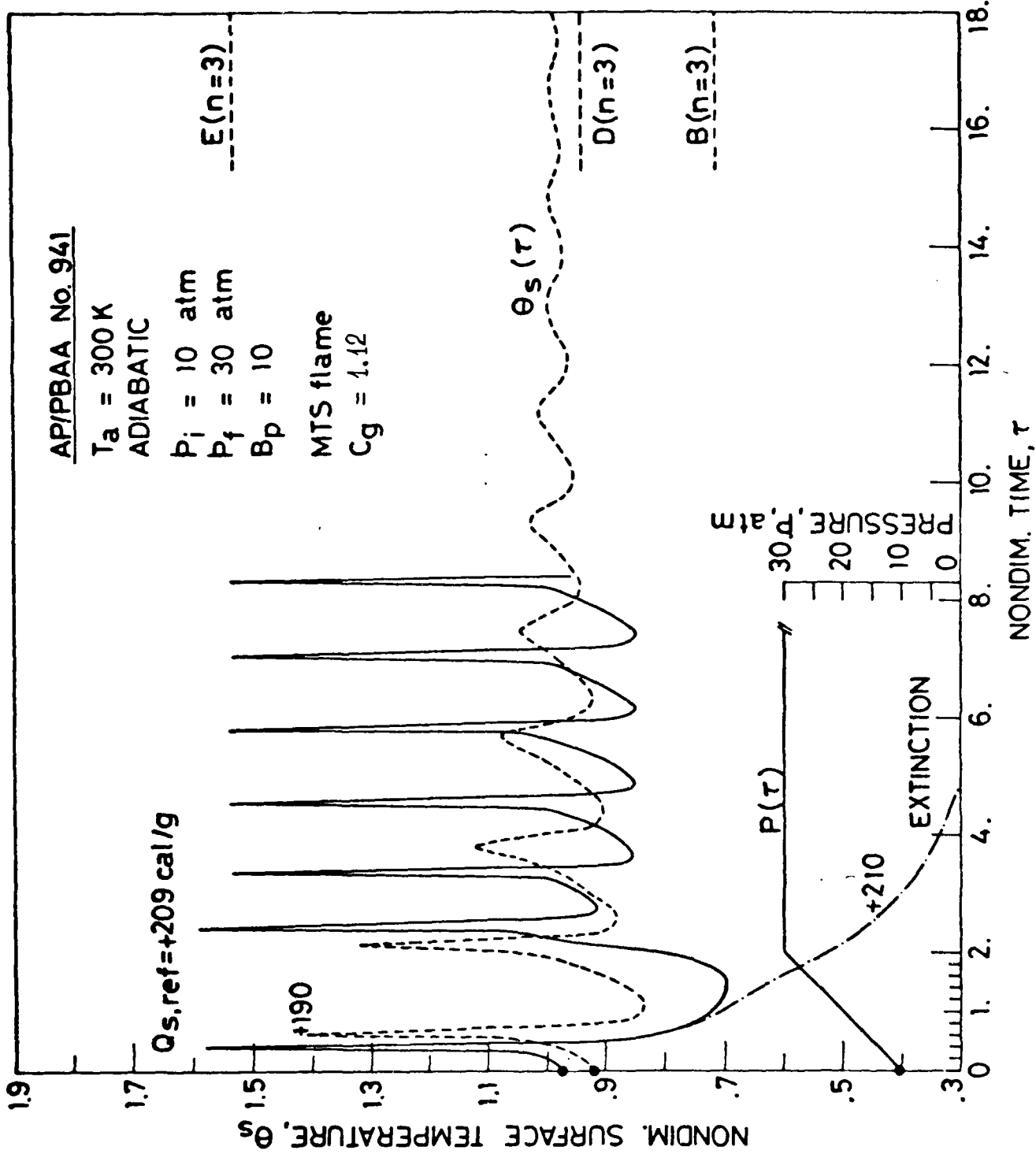


FIG. 51

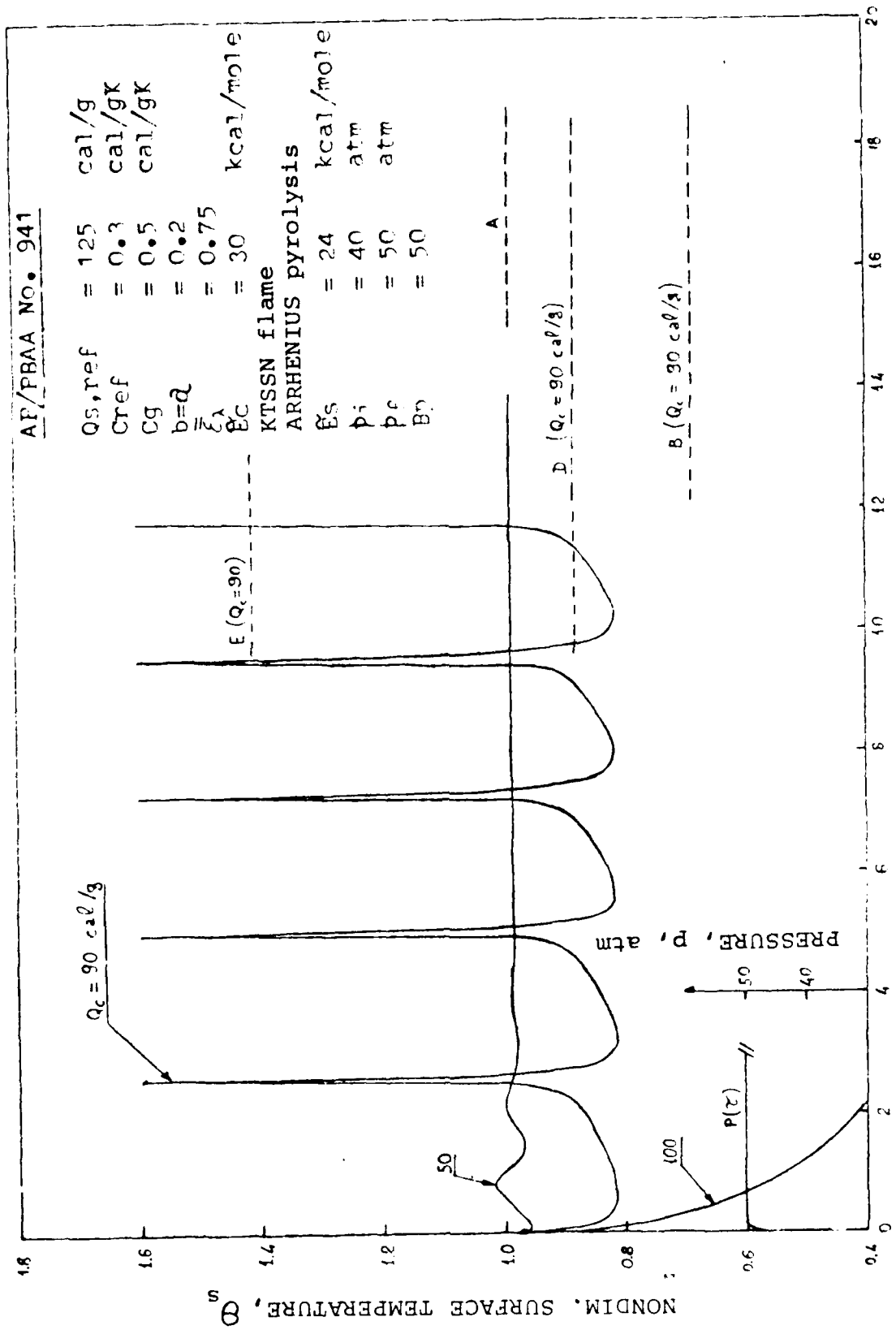
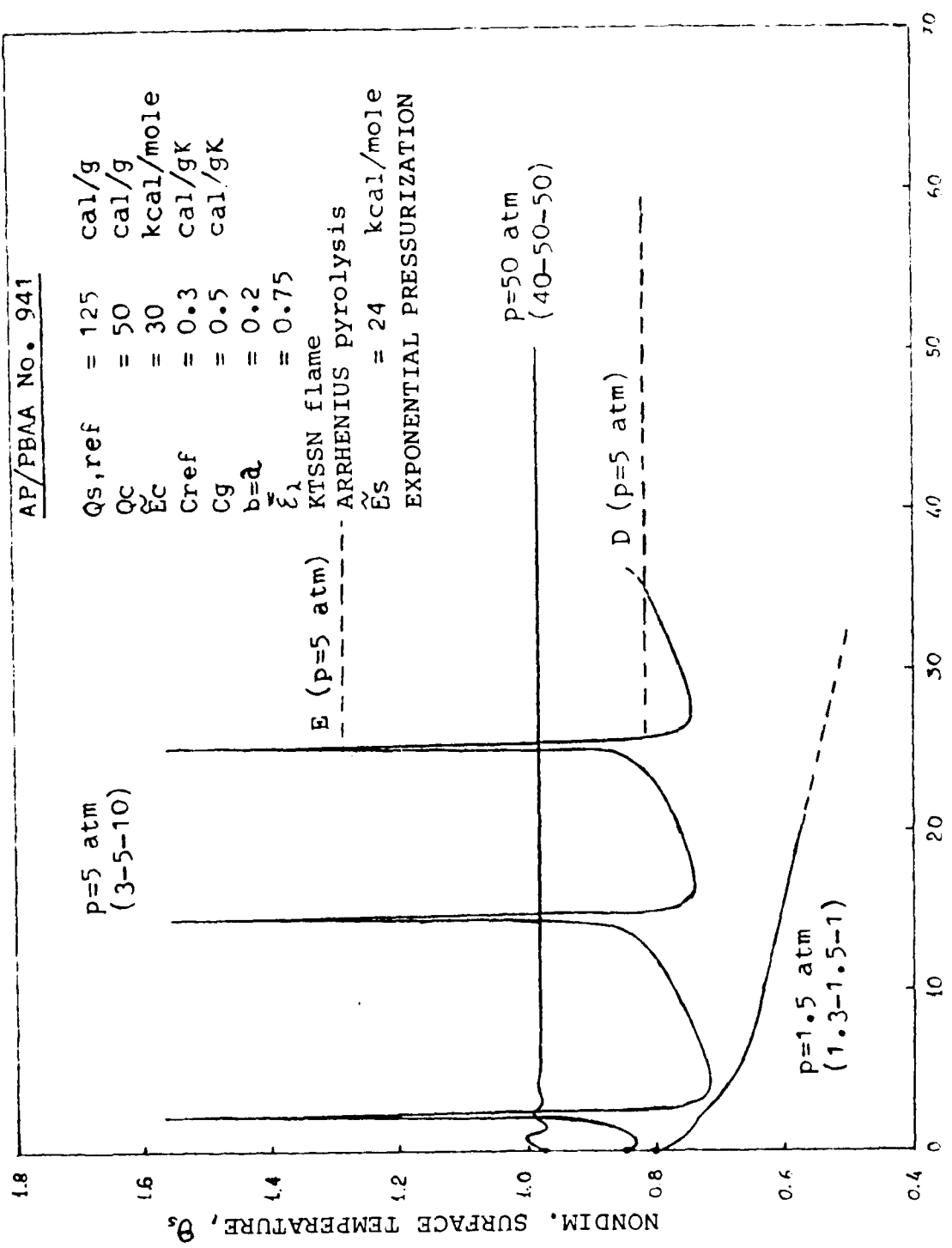


FIG. 52



NONDIM. TIME, τ

FIG. 53

API/PBAA No. 941

$Q_{s,ref} = +158.2 \text{ cal/g}$

$T_a = 300 \text{ K}$

ADIABATIC

MTS flame

$C_g = 1.12$

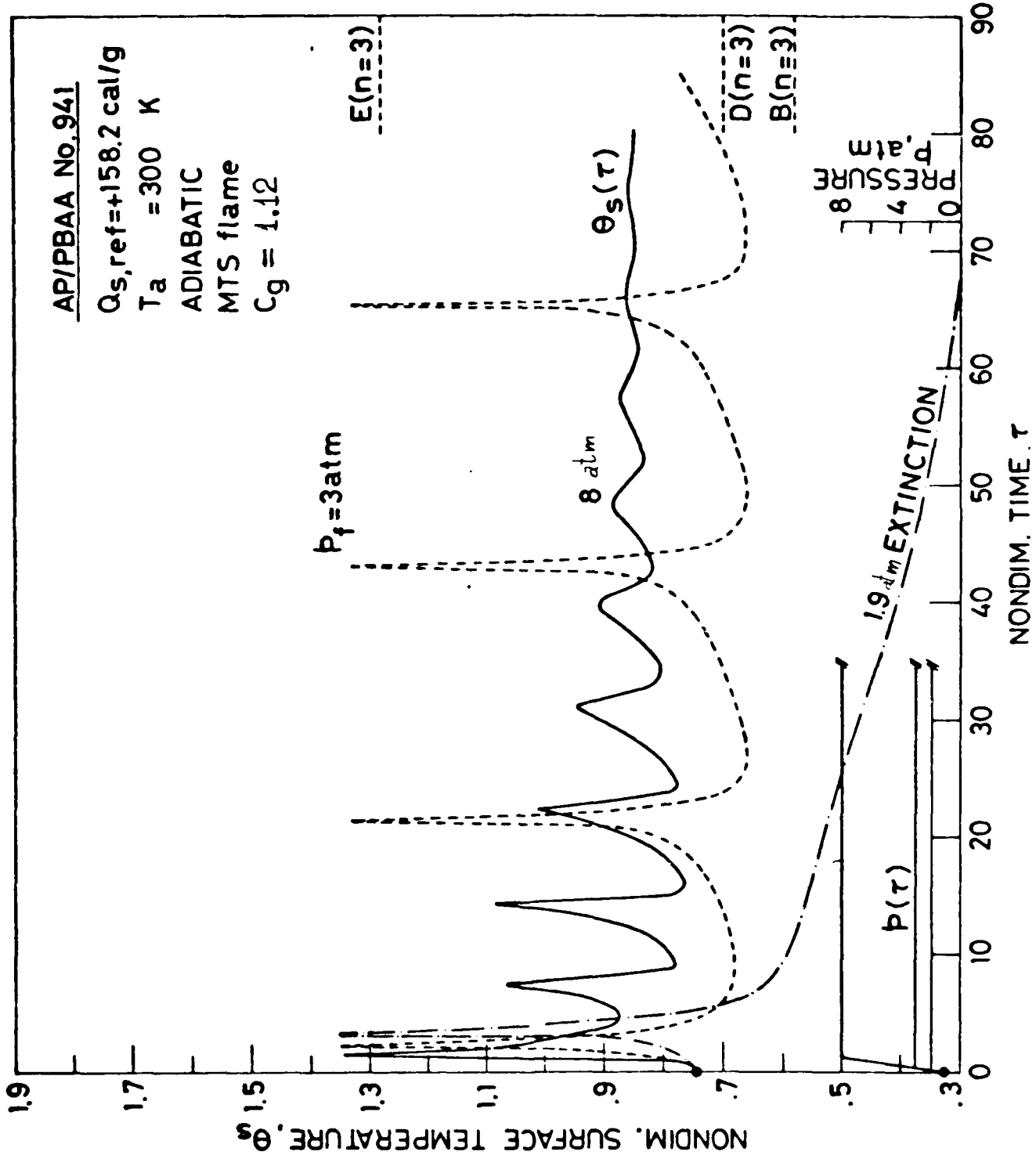


FIG. 54

AP/CTPB No 02

$Q_{s,ref} = 0 \text{ cal/g}$
 $Q_c = 125 \text{ cal/g}$
 $p = 10 \text{ atm}$
KTSSN flame

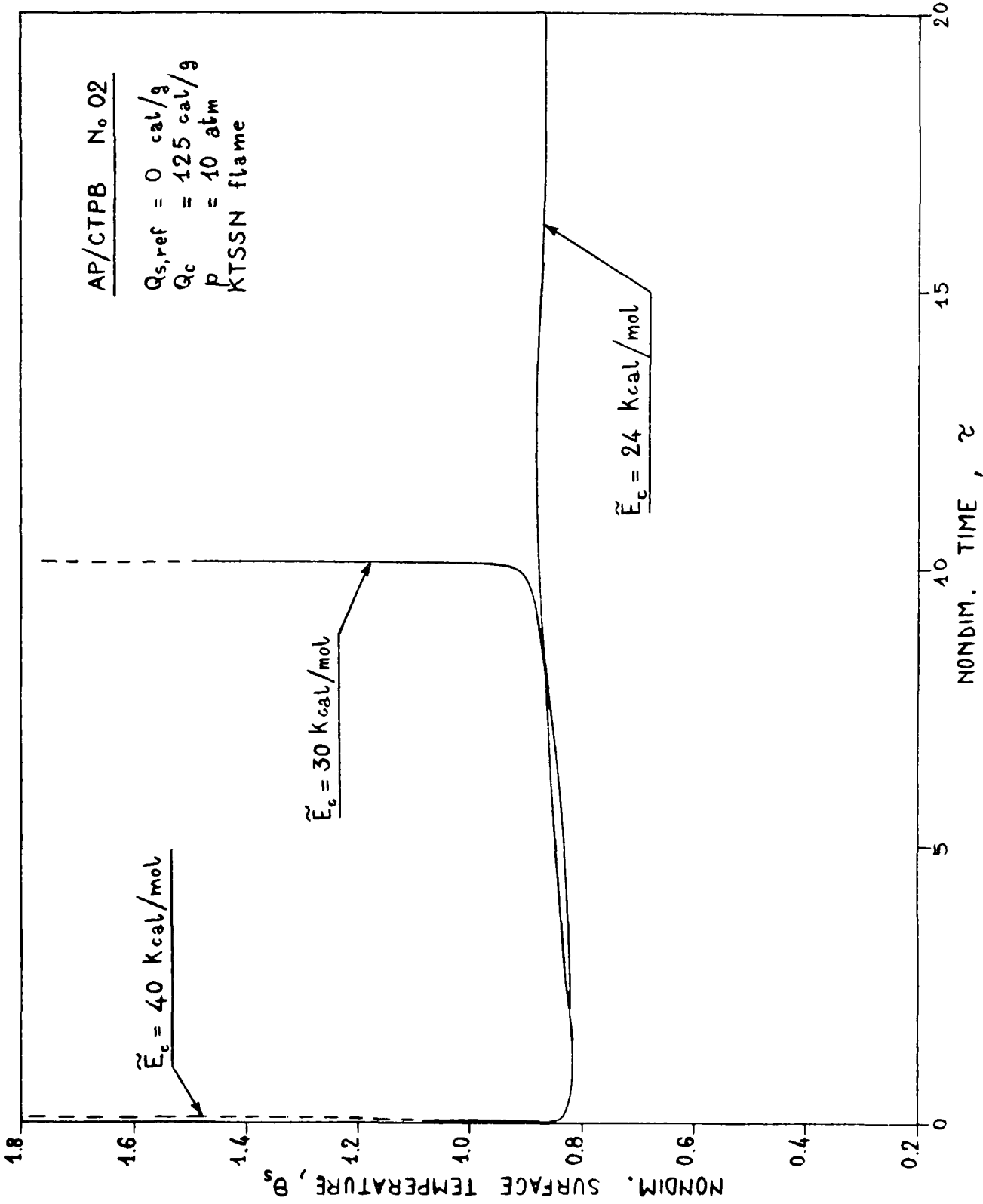


FIG. 55

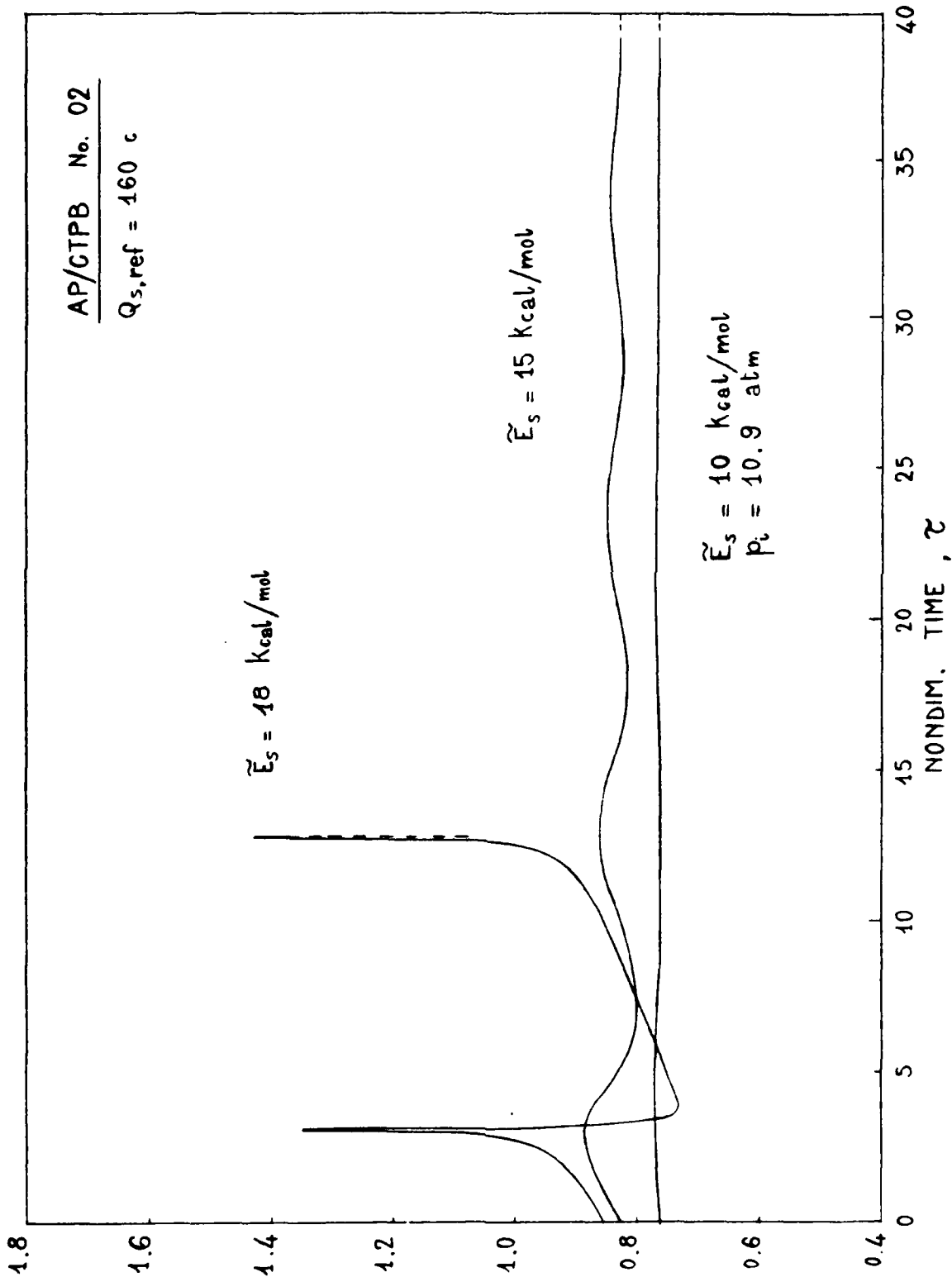


FIG. 56

AP/PBAANo.941

$P = 10$ atm

$T_a = 300$ K

$Q_s = +158.2$ cal/g

MTS FLAME

$Br = 200$

$Z_b = 0.006$

$C_g = 1$

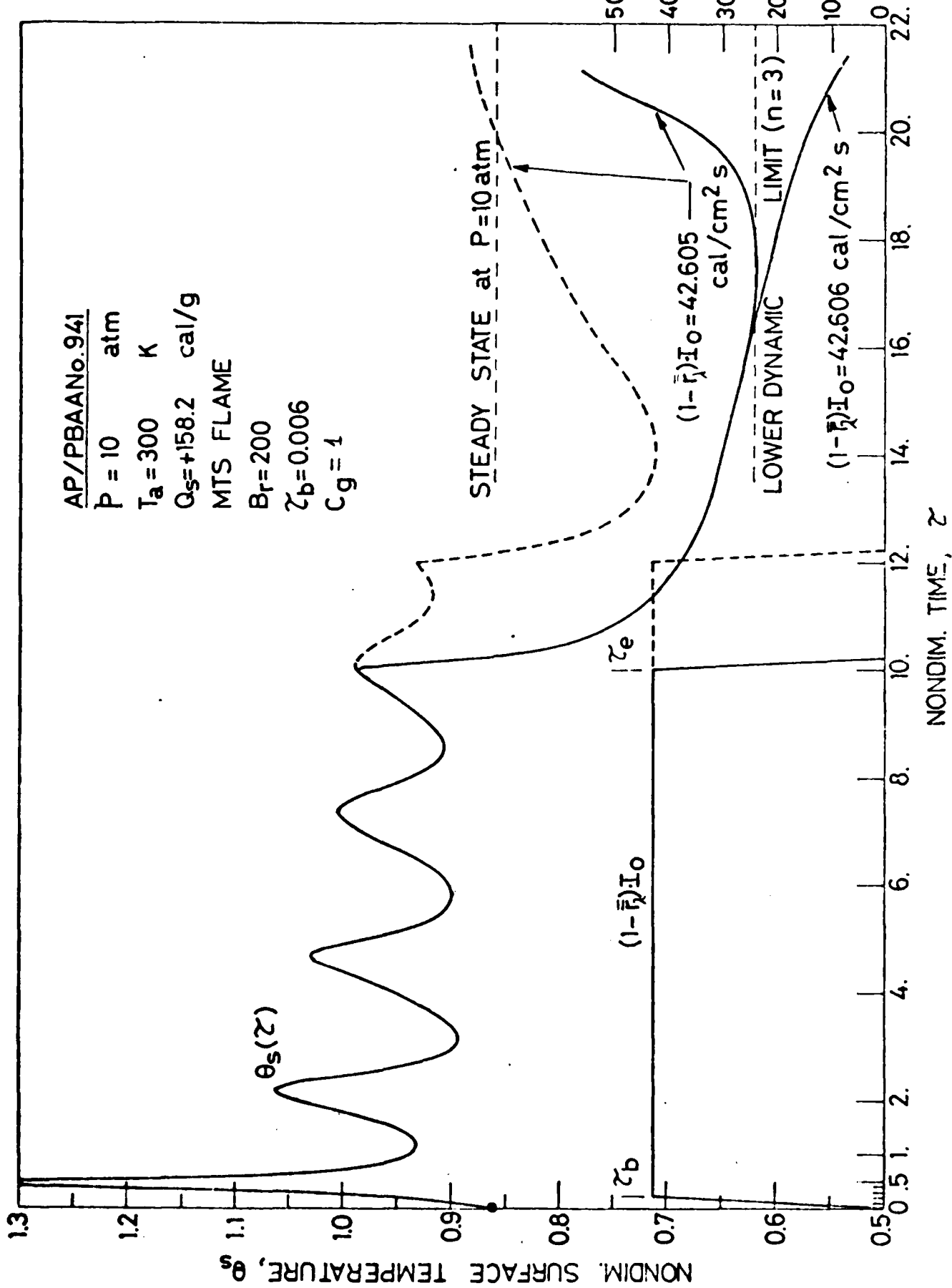


FIG. 57

AP/PBAA-941
 T_0 (K) = 300.0
 P (atm) = 10.0
 Q_0 (Cal/cm²) = 158.20
 OPAQUE
 L_0 = 90.010
 B_0 = 200.00
 r = 0.00
 RADIATION: DIRAC
 KISE NON LINEAR
 IMSEC. RICHMYER 3 STEPS
 $\tau_0 = 0.9$

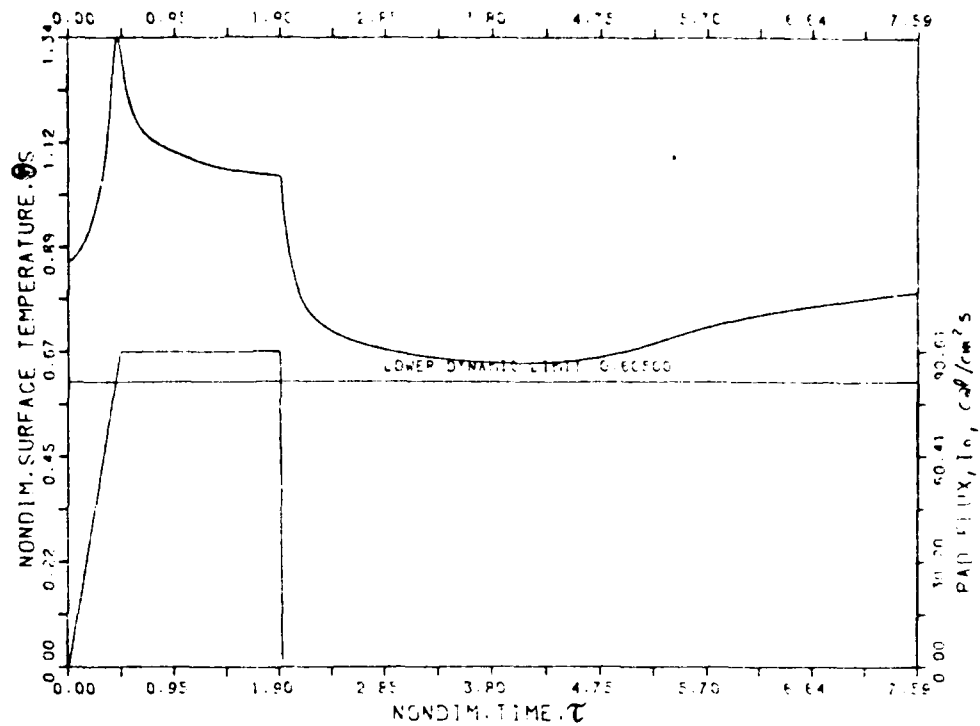


FIG. 58a

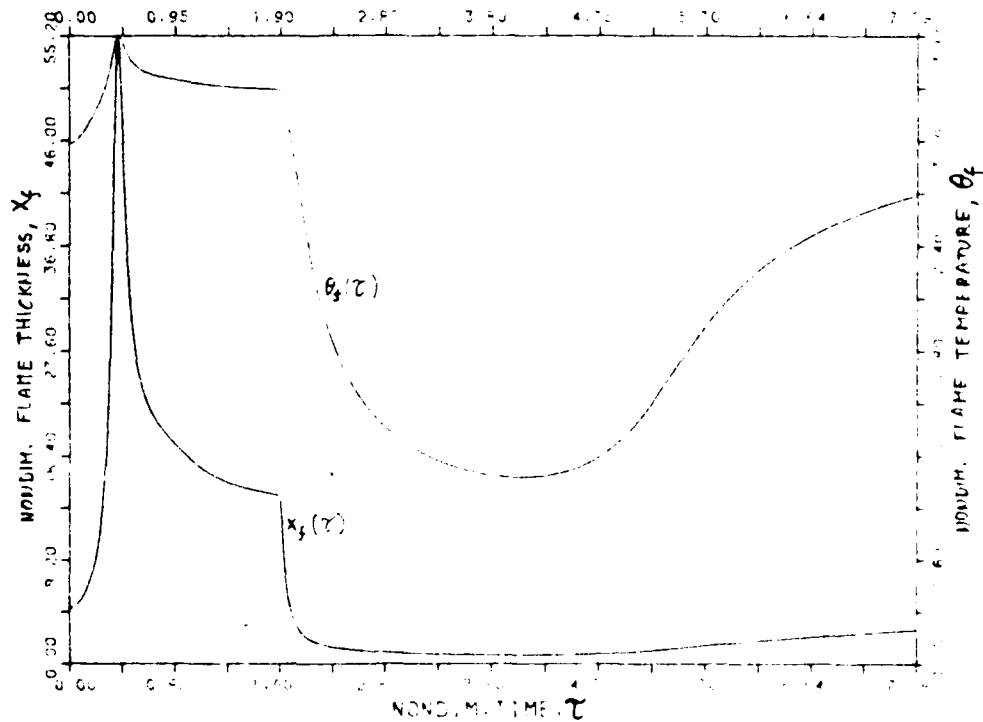


FIG. 58L

AP/PSAA-941

γ_0 (K) = 300.0

P (atm) = 10.0

D_0 (cm²/s) = 158.20

OPAQUE

l_0 = 90.610

B_0 = 200.00

ν = 0.00

RADIATION: DIRAC

KISS NON LINEAR

INTEG. RICHTMYER 3 STEP

$\gamma_0 = 2$

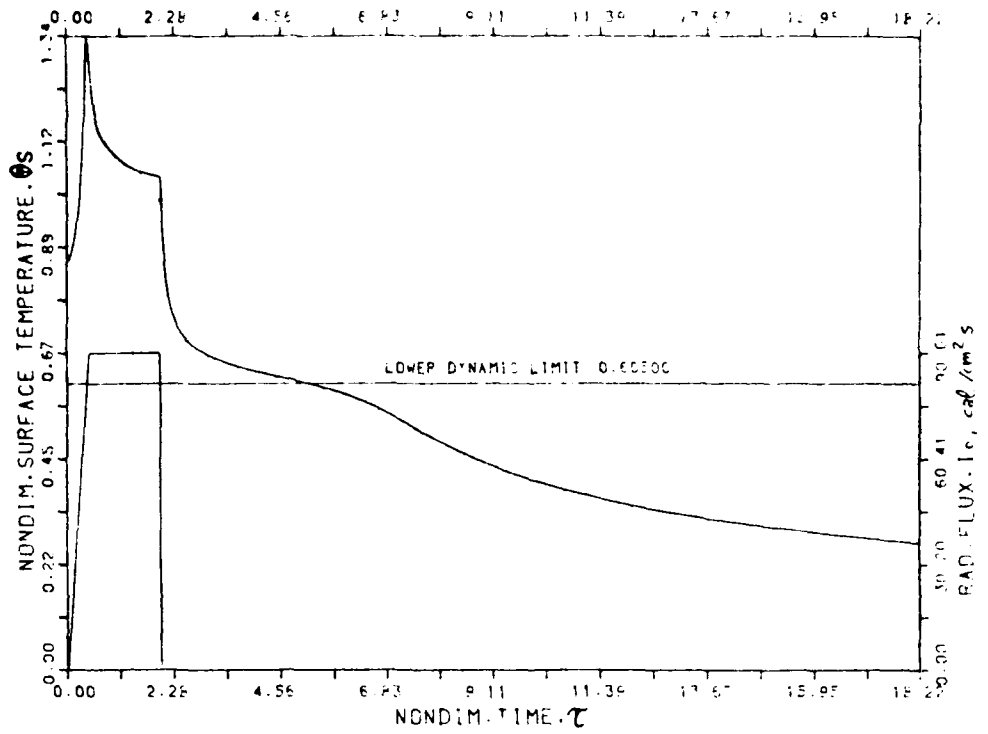


FIG. 59a

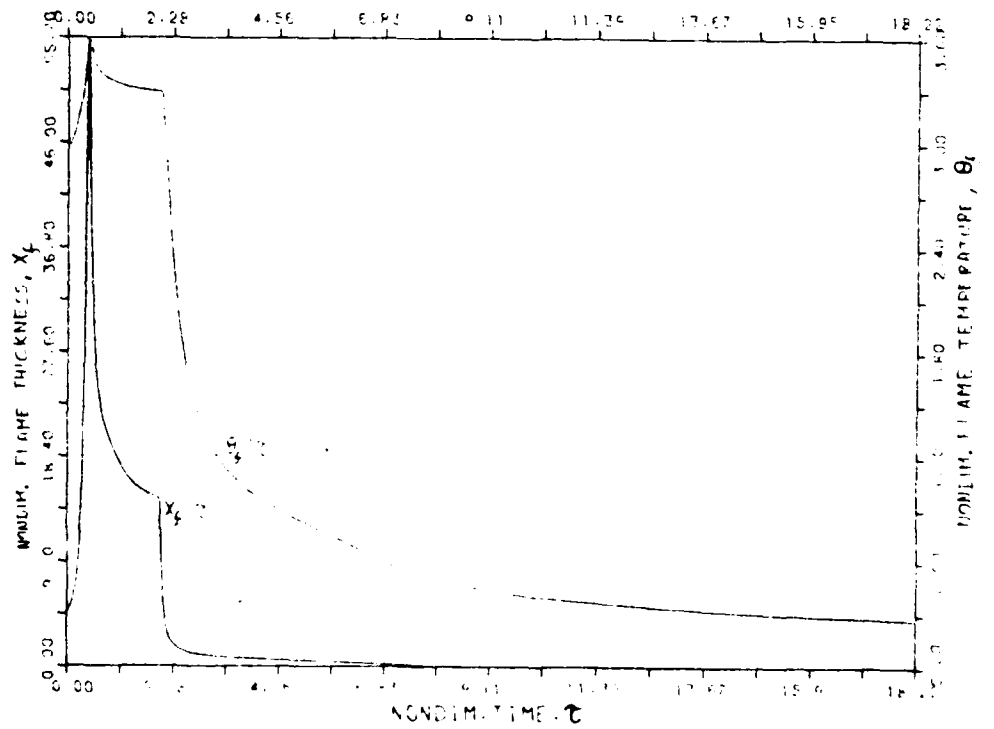


FIG. 59b

*P/PBFA-441
 *K1 = 300.0
 *K2 = 10.0
 *D = 158.20
 *DPRDF
 *D = 40.001
 *B = 200.00
 *C = 0.00
 *DEGRADATION: DIRAC
 *K1: NON-LINEAR
 *INTRO: RICHMYER 2 STEP

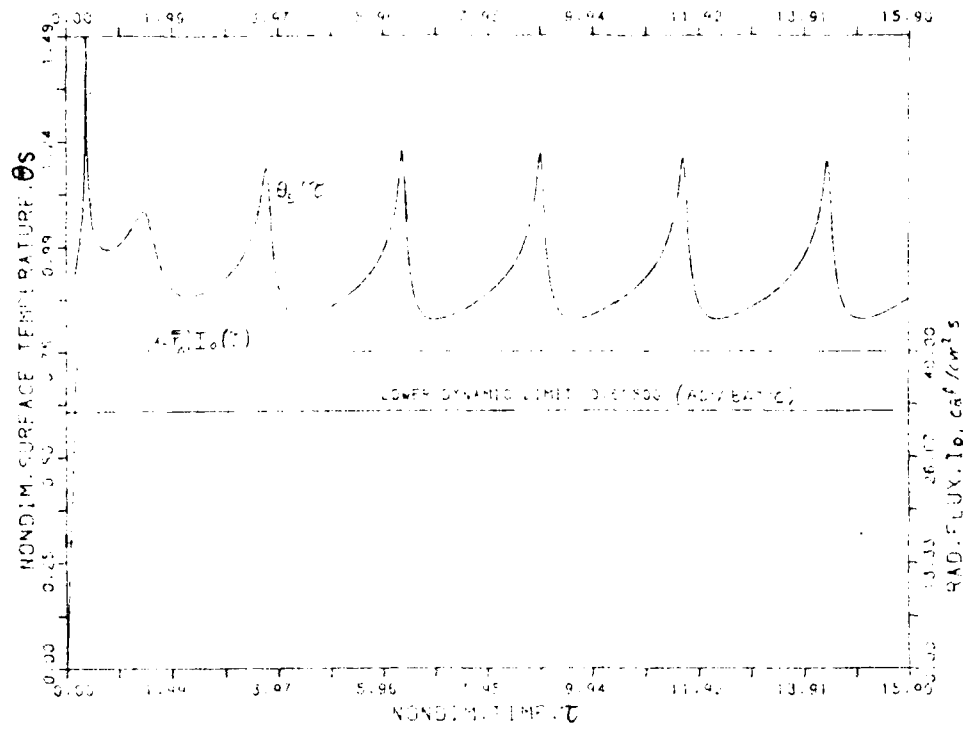


FIG. 40

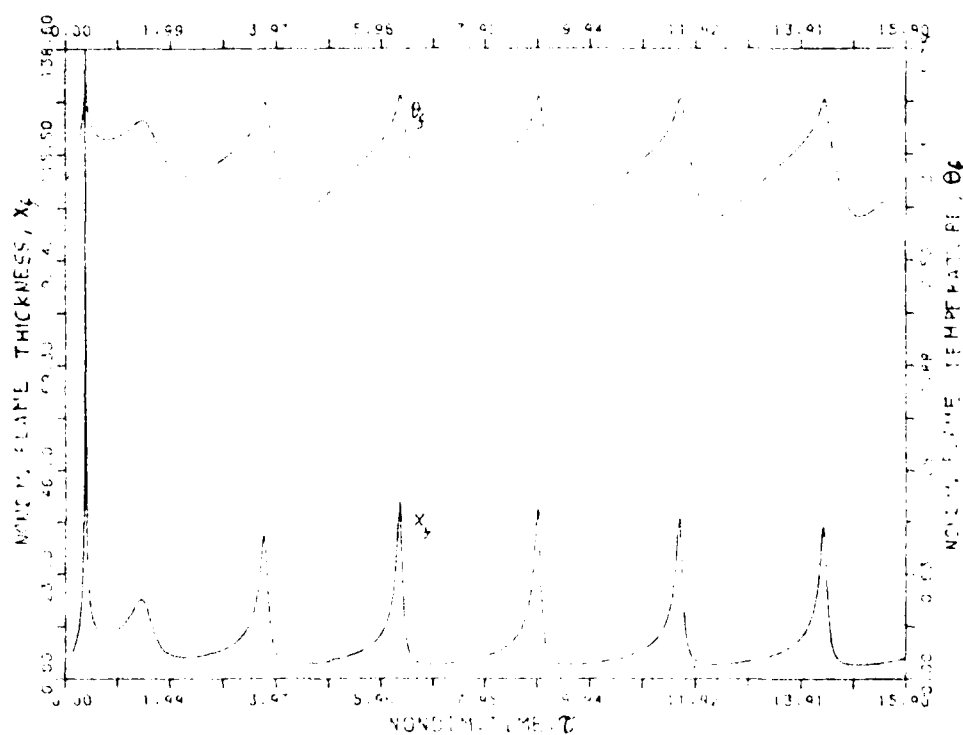
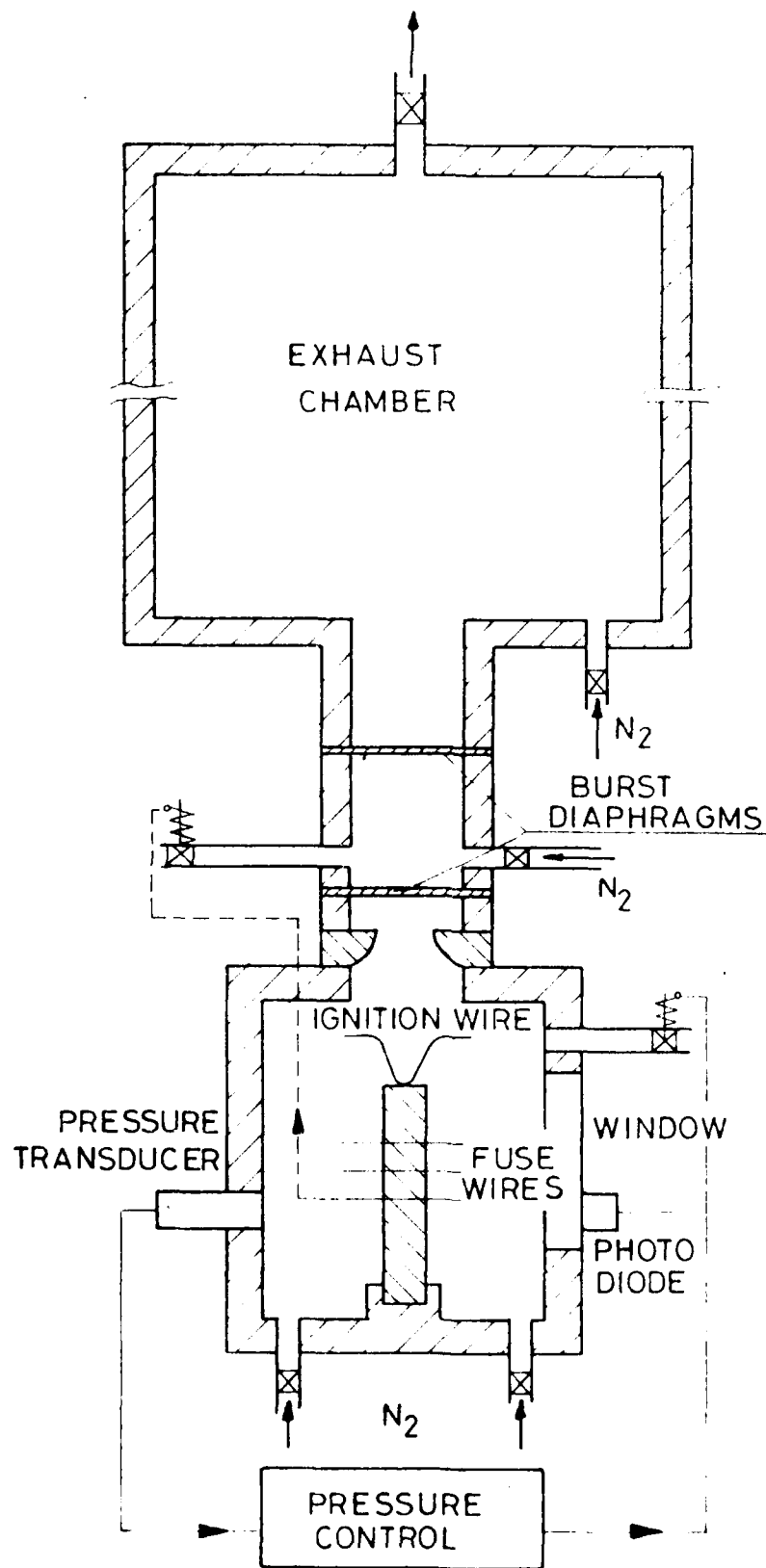


FIG. 60



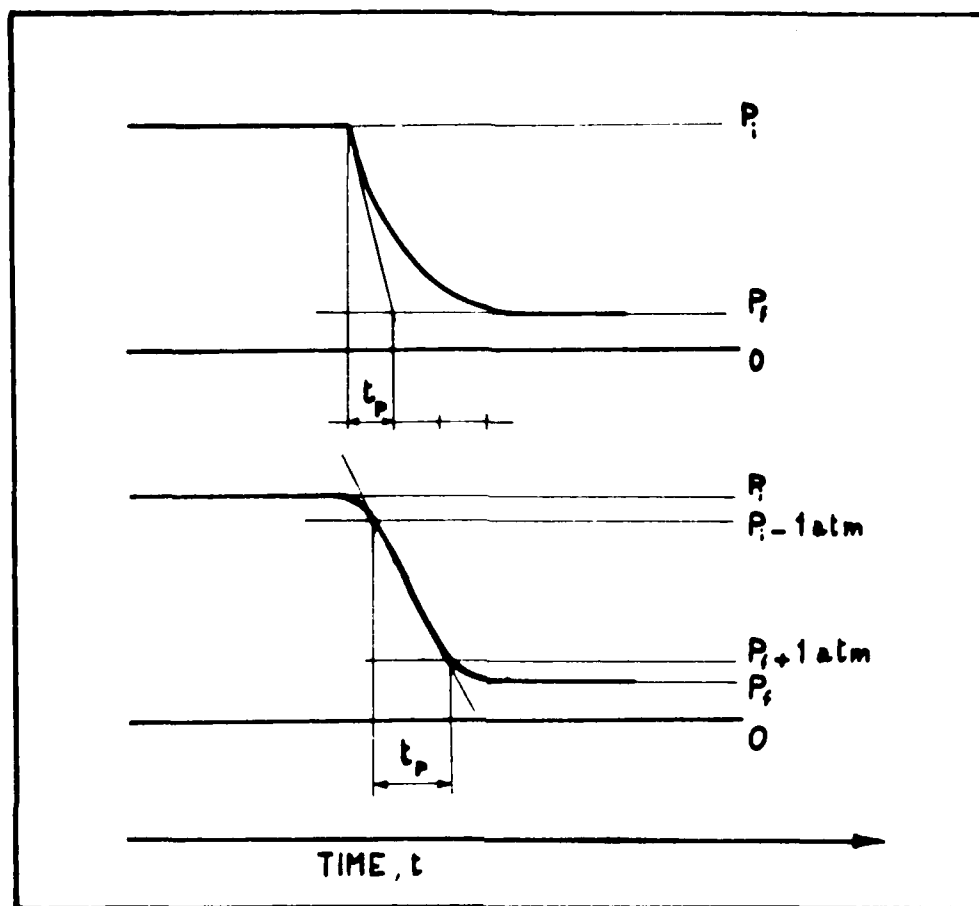


FIG. 62

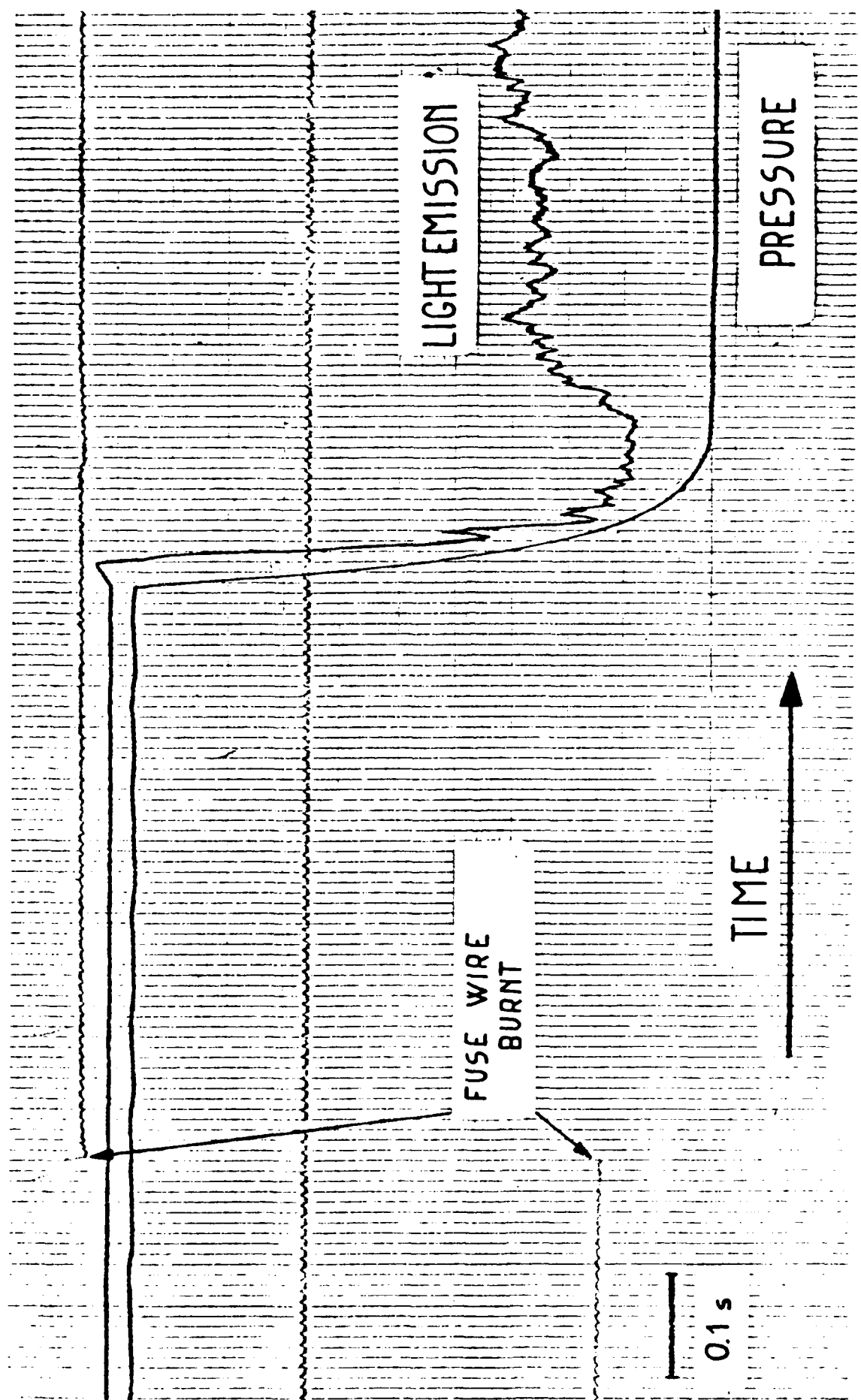


FIG. 63

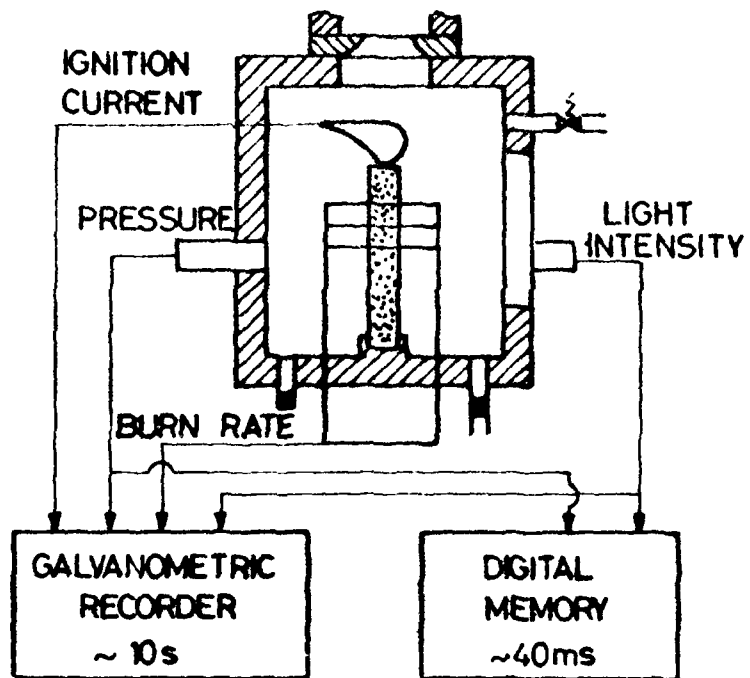


FIG. 64

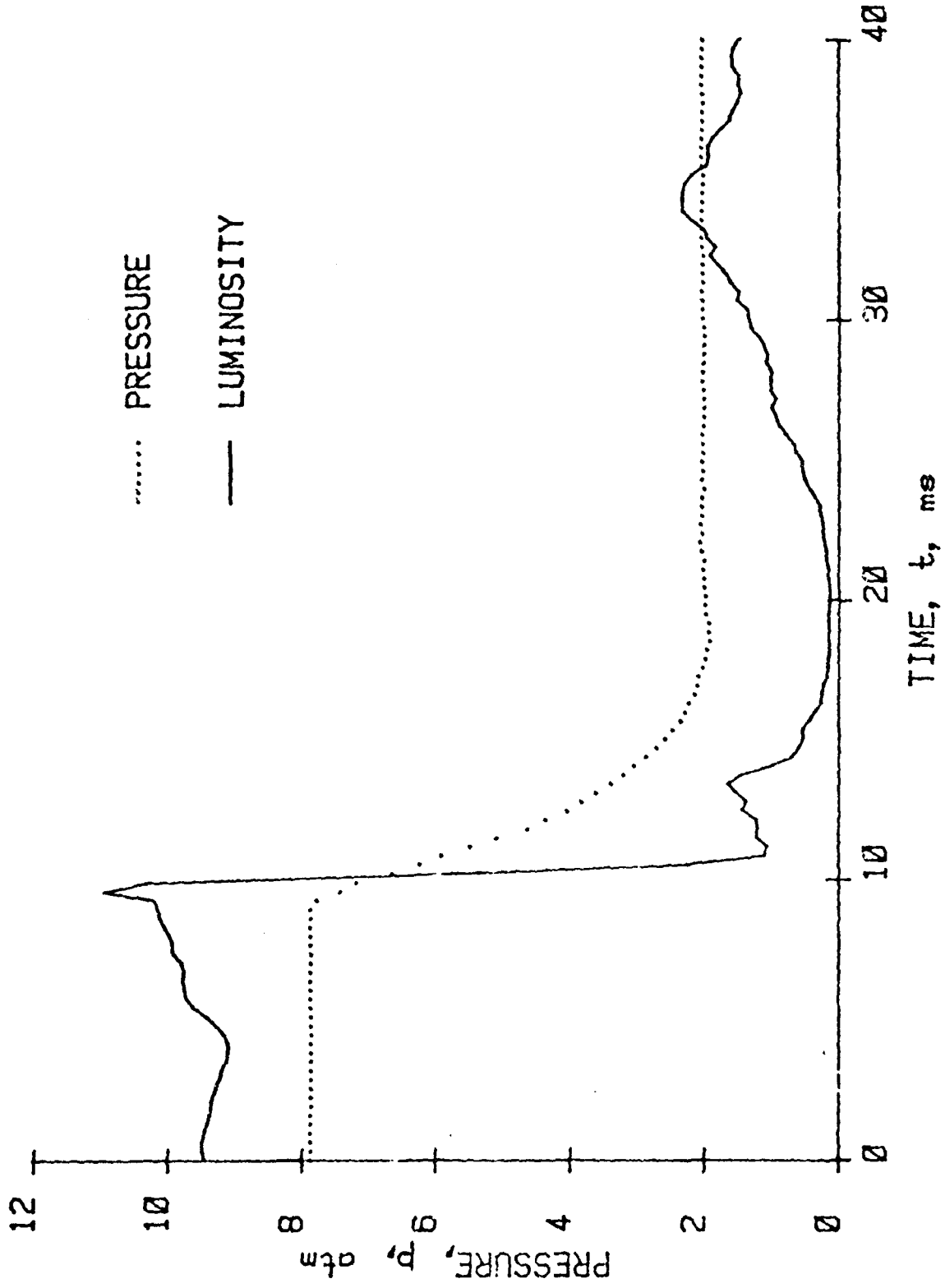


FIG. 65

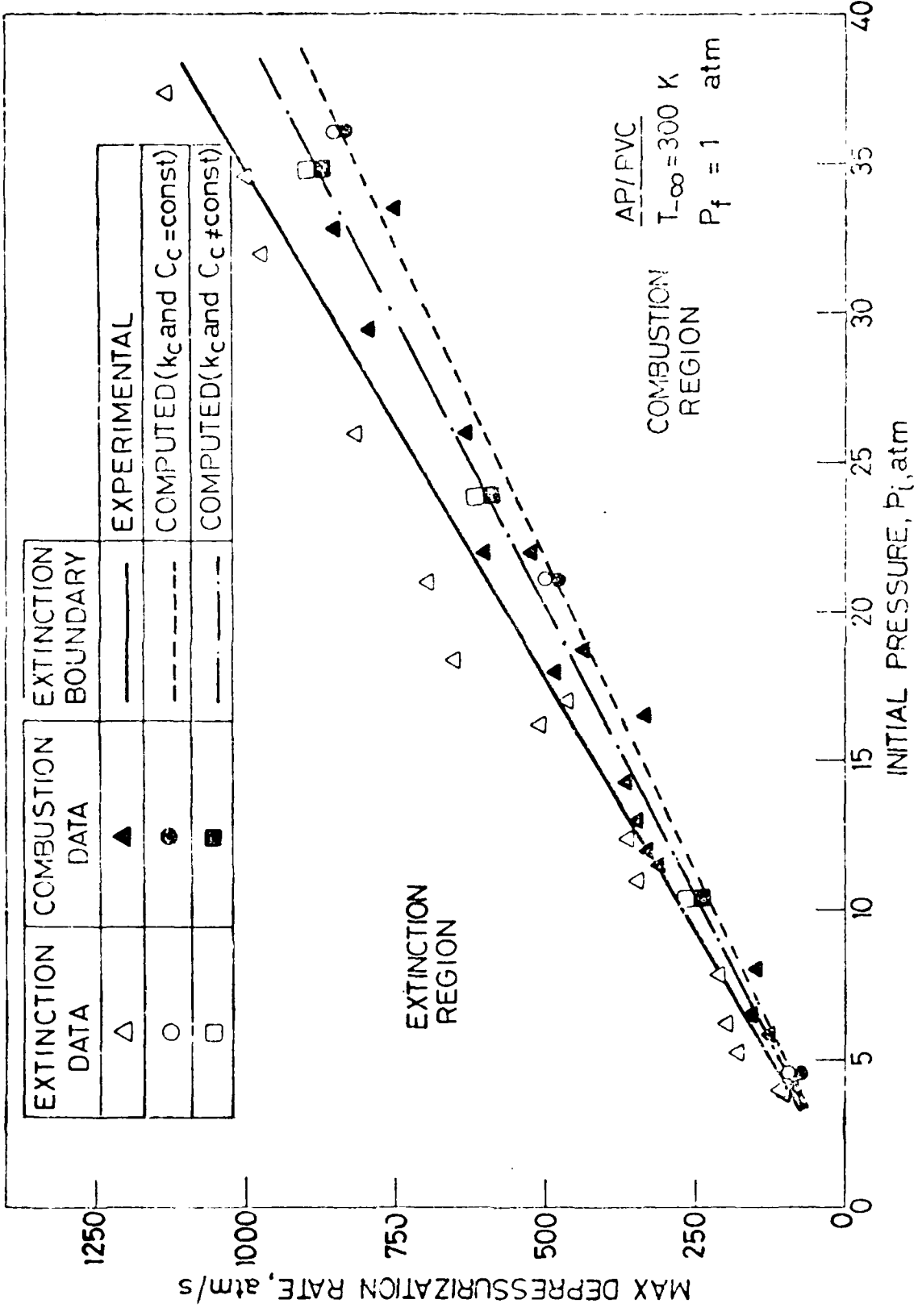


FIG. 66

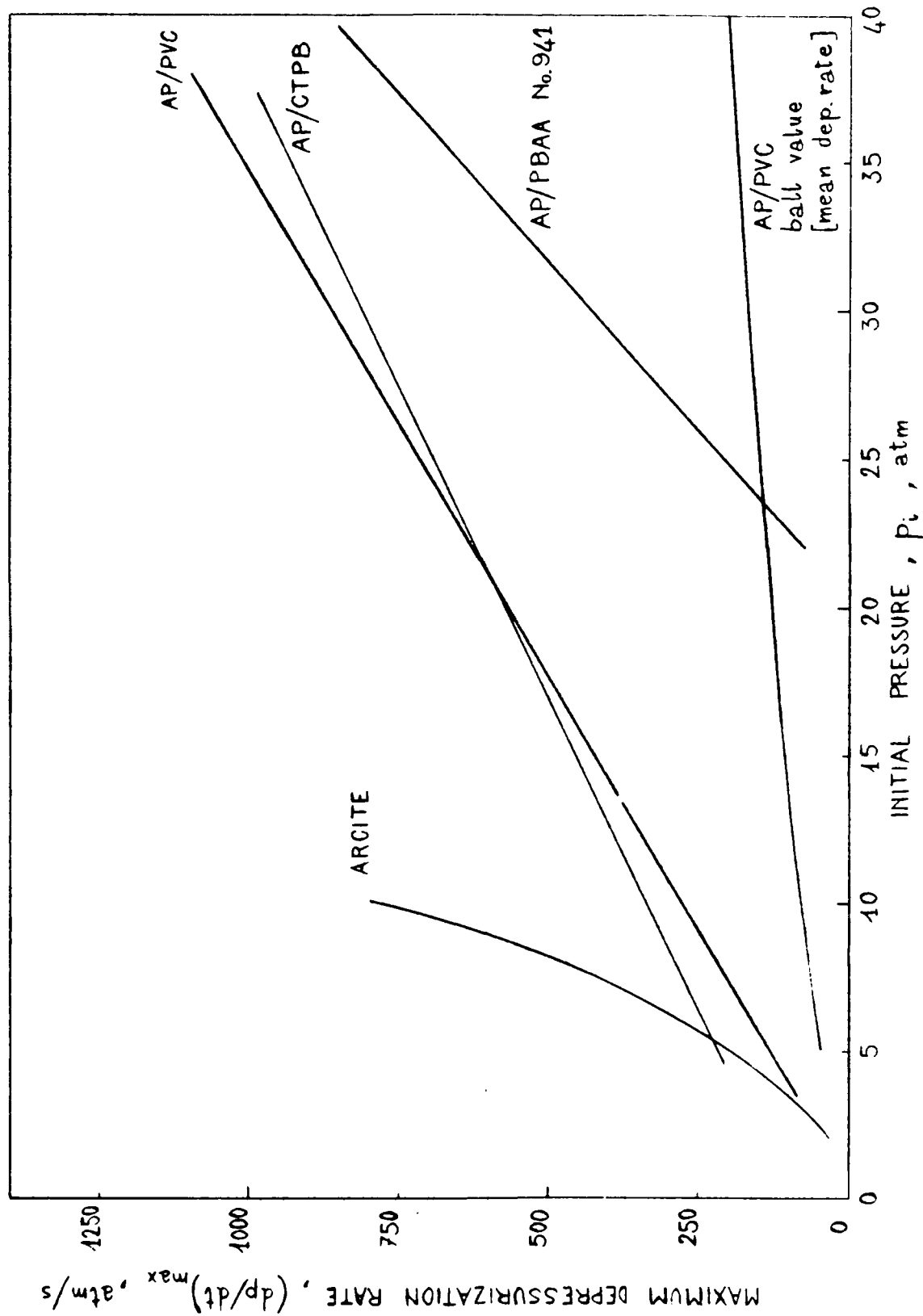


FIG. 67

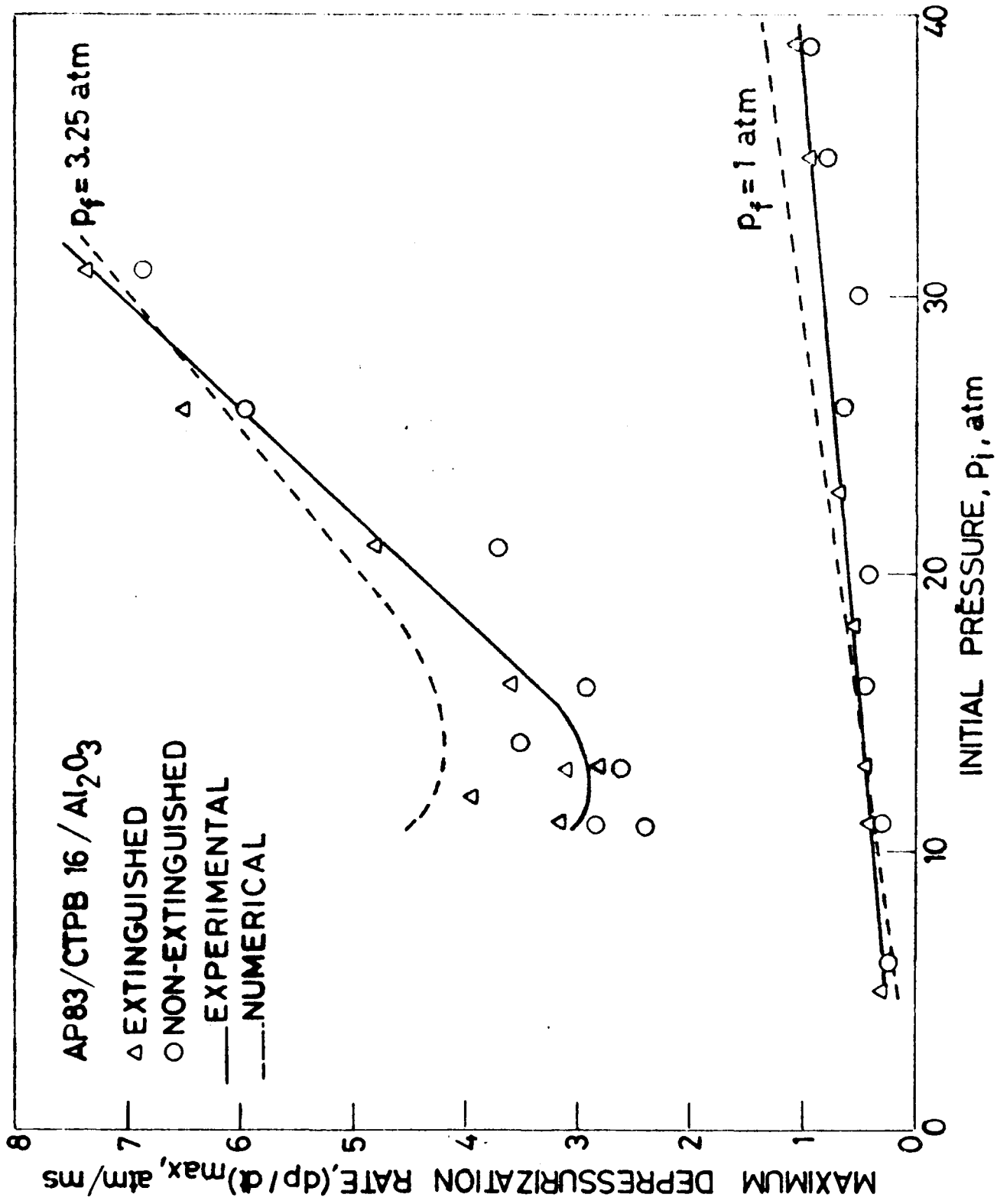


Fig. 5a

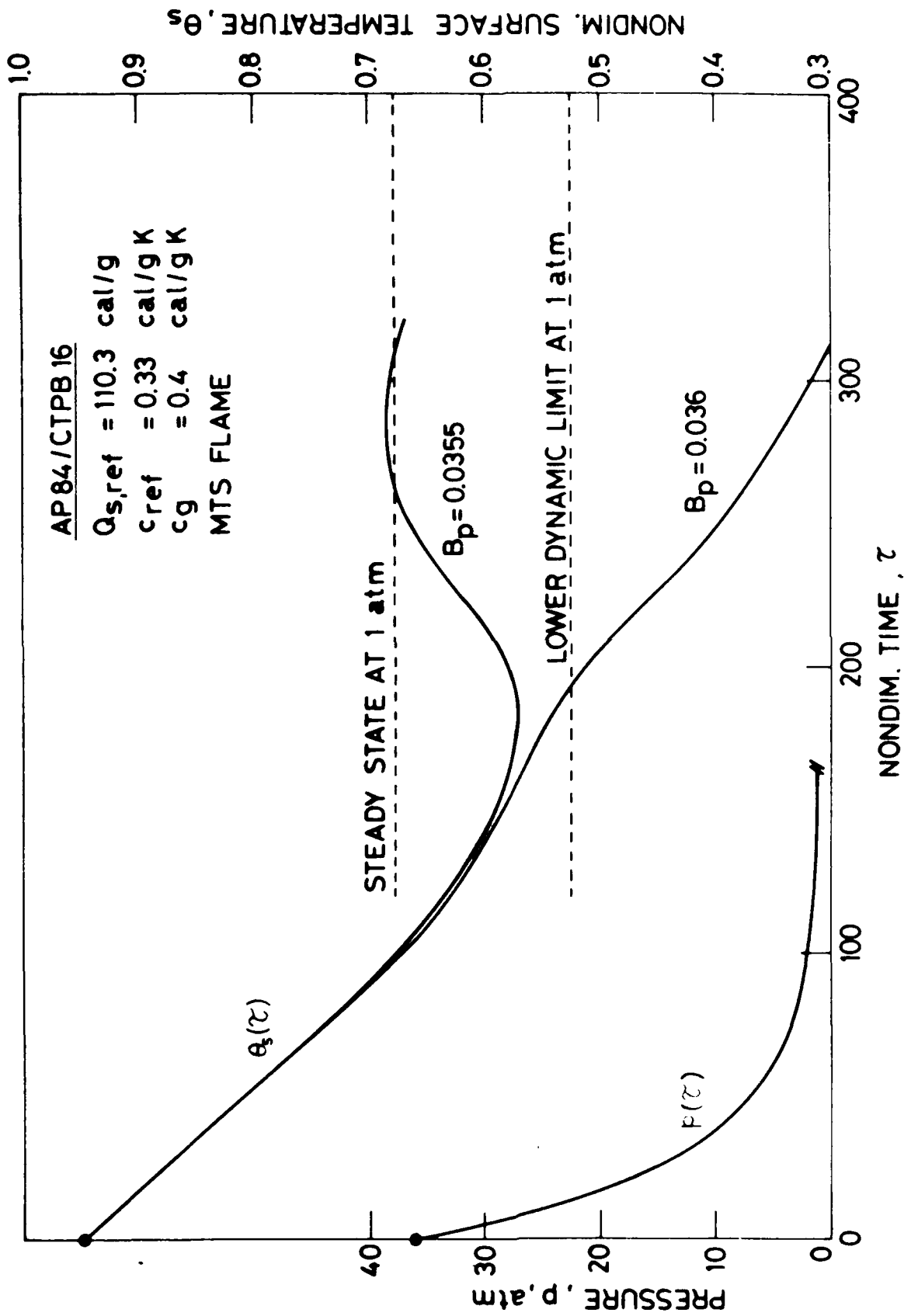


FIG. 69

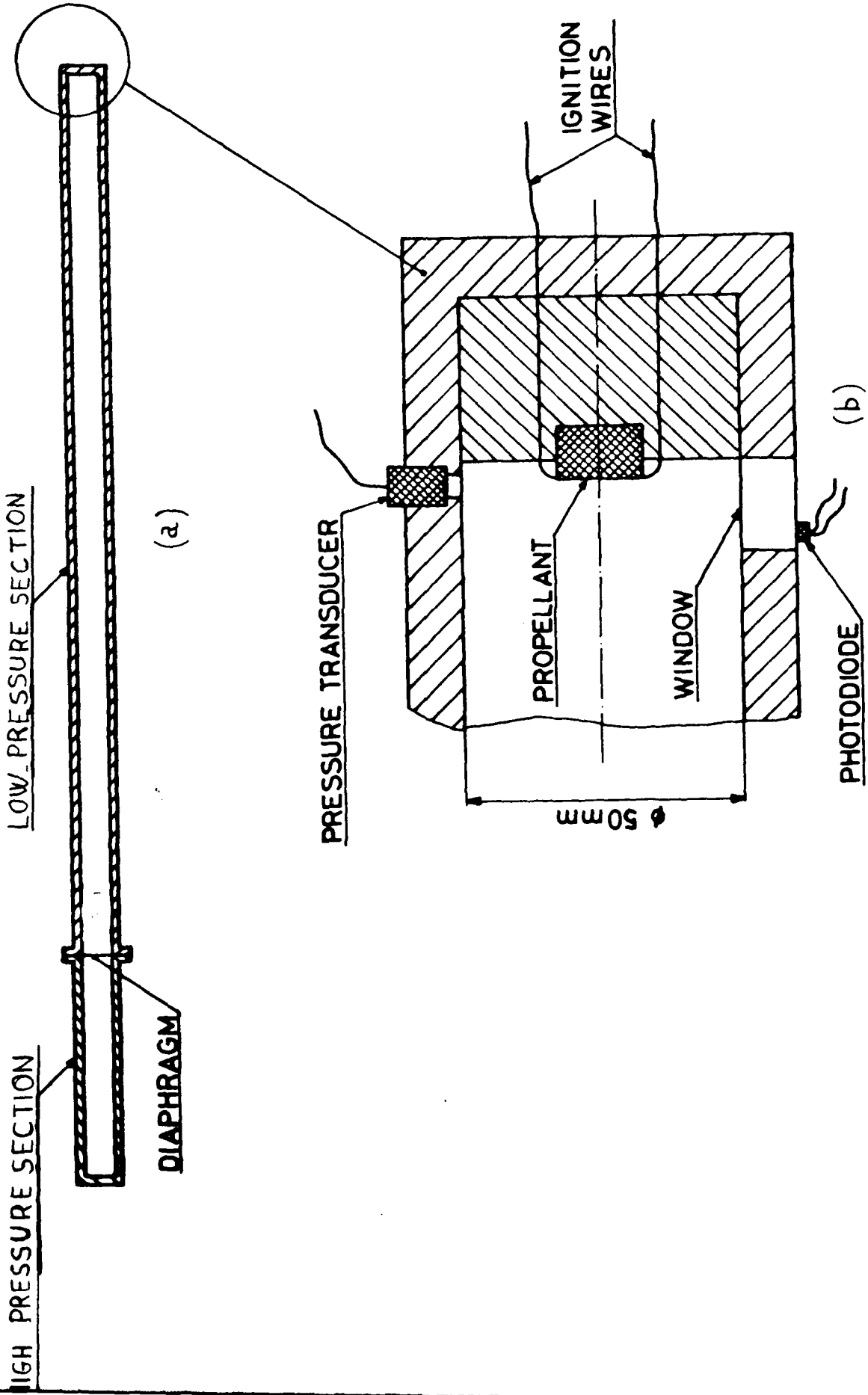


FIG. 70

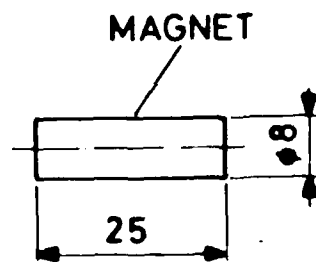
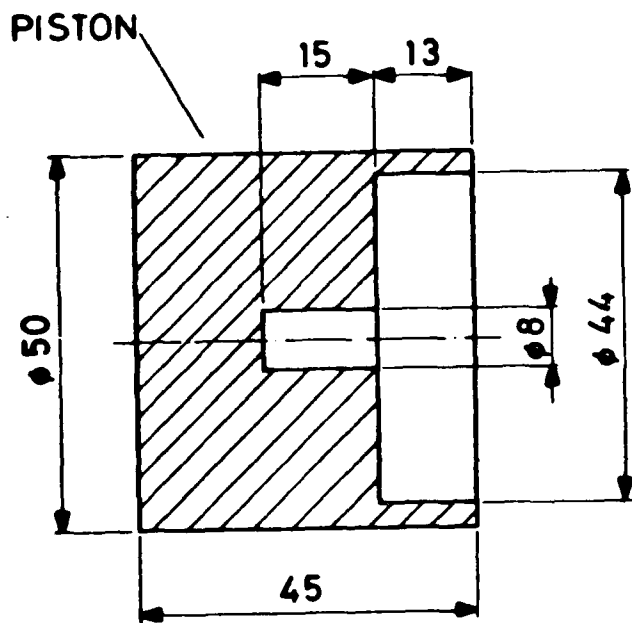


FIG. 71

PISTON TUBE SCHEME

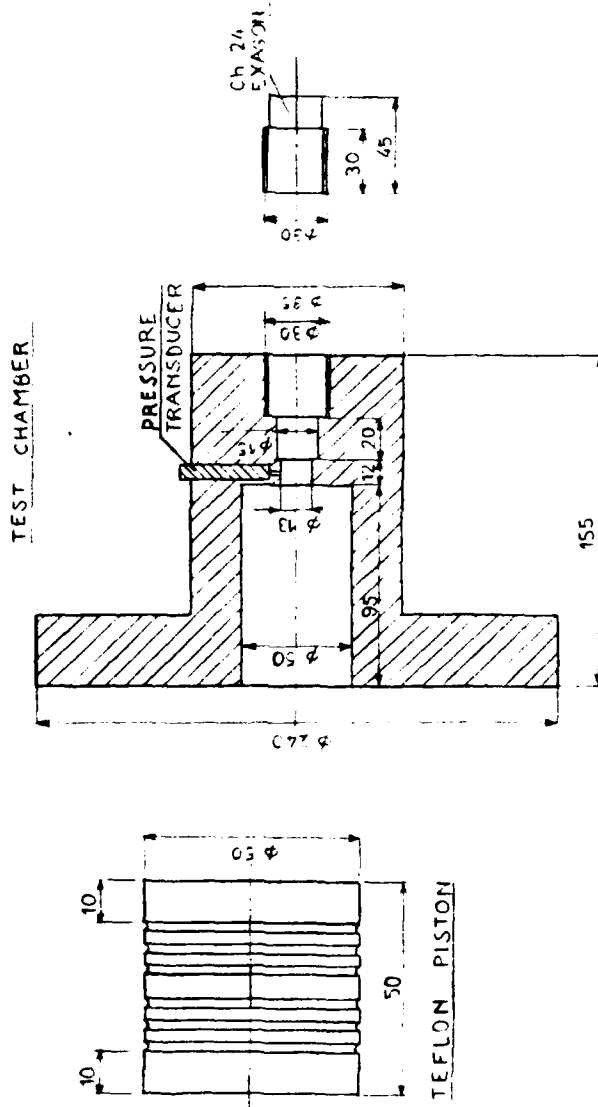
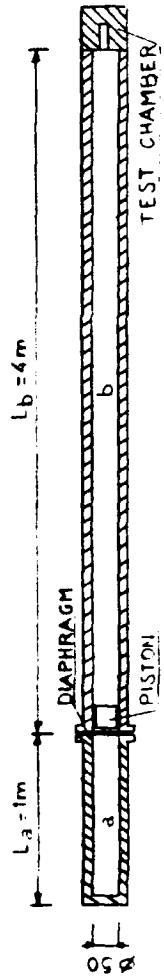


FIG. 72

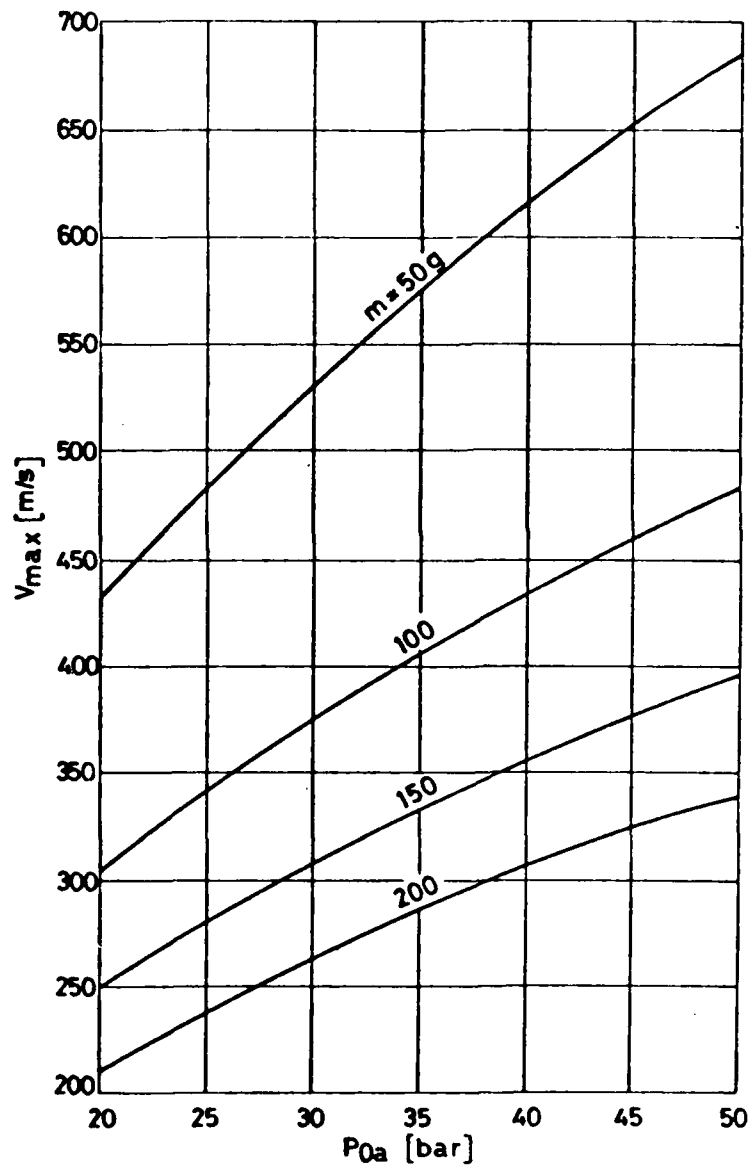


FIG. 73

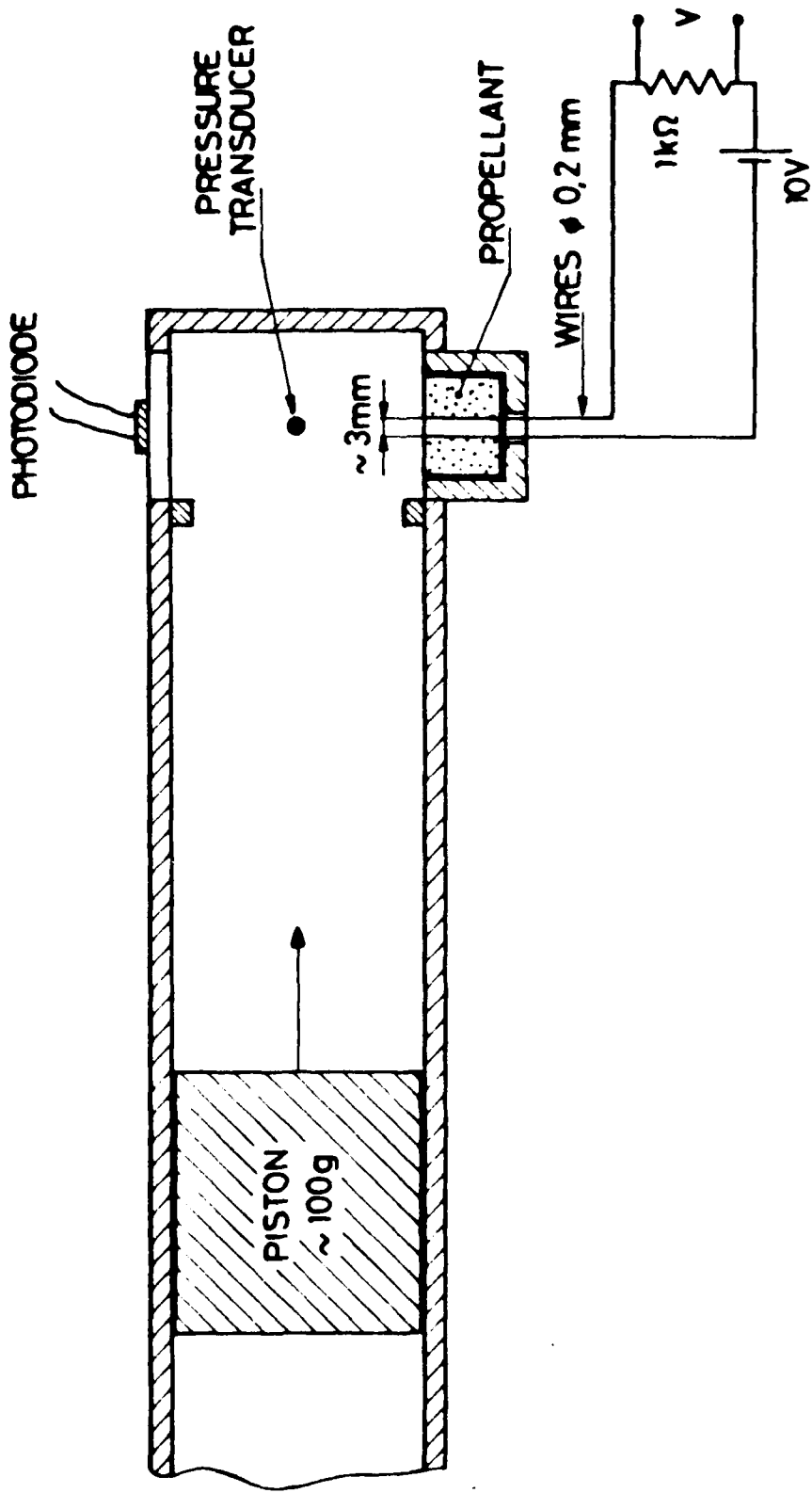


FIG. 74

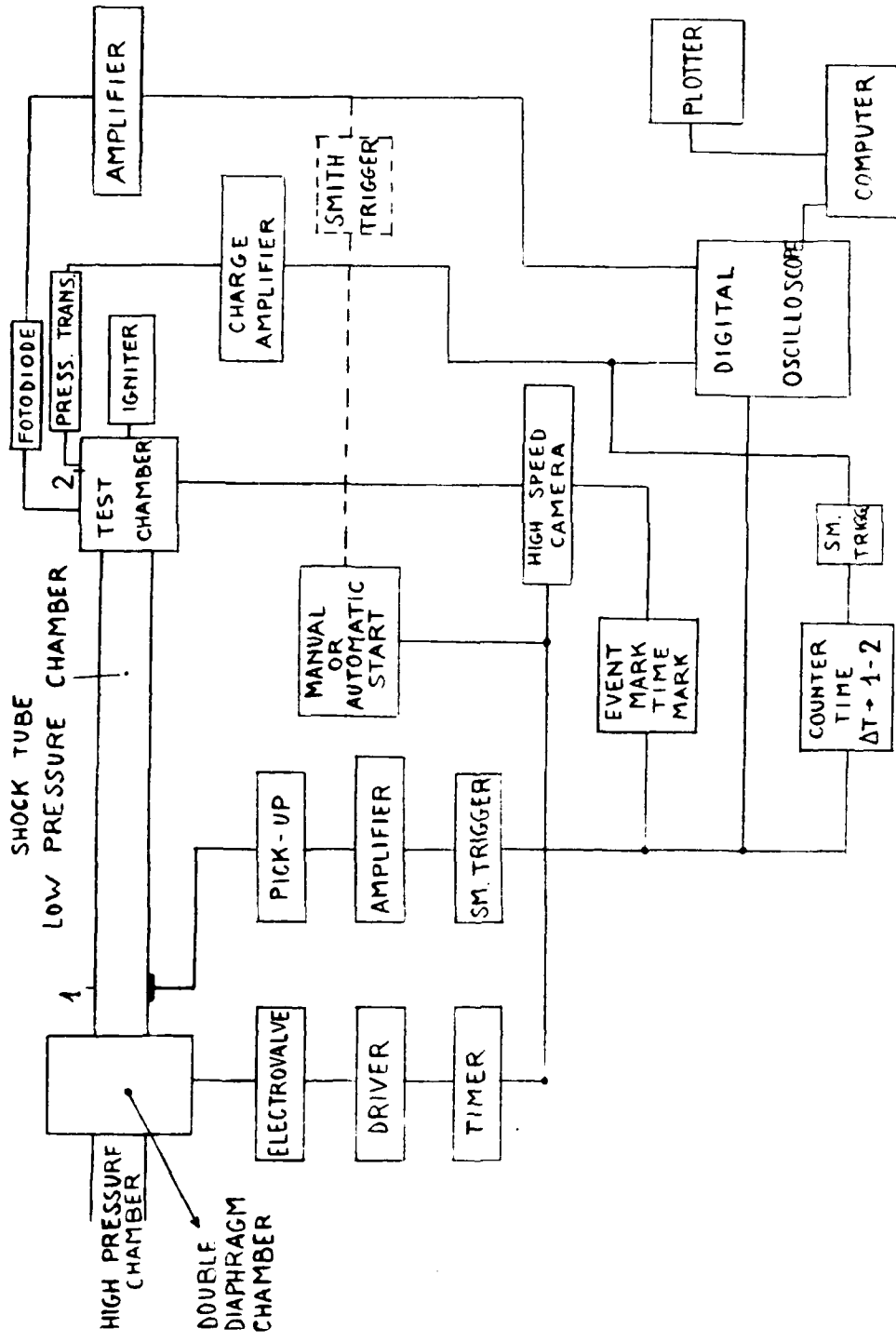


FIG. 75

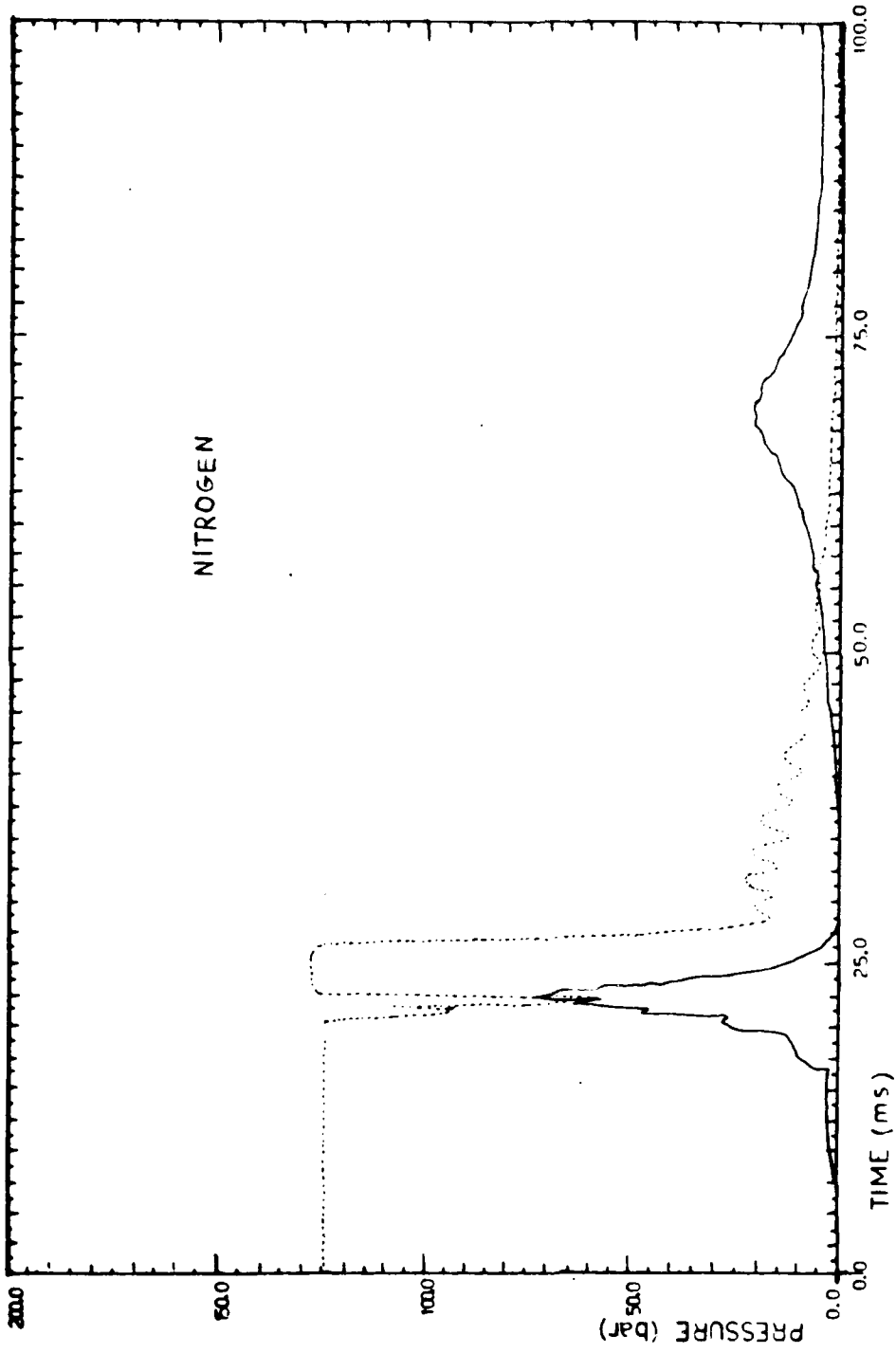


FIG. 76

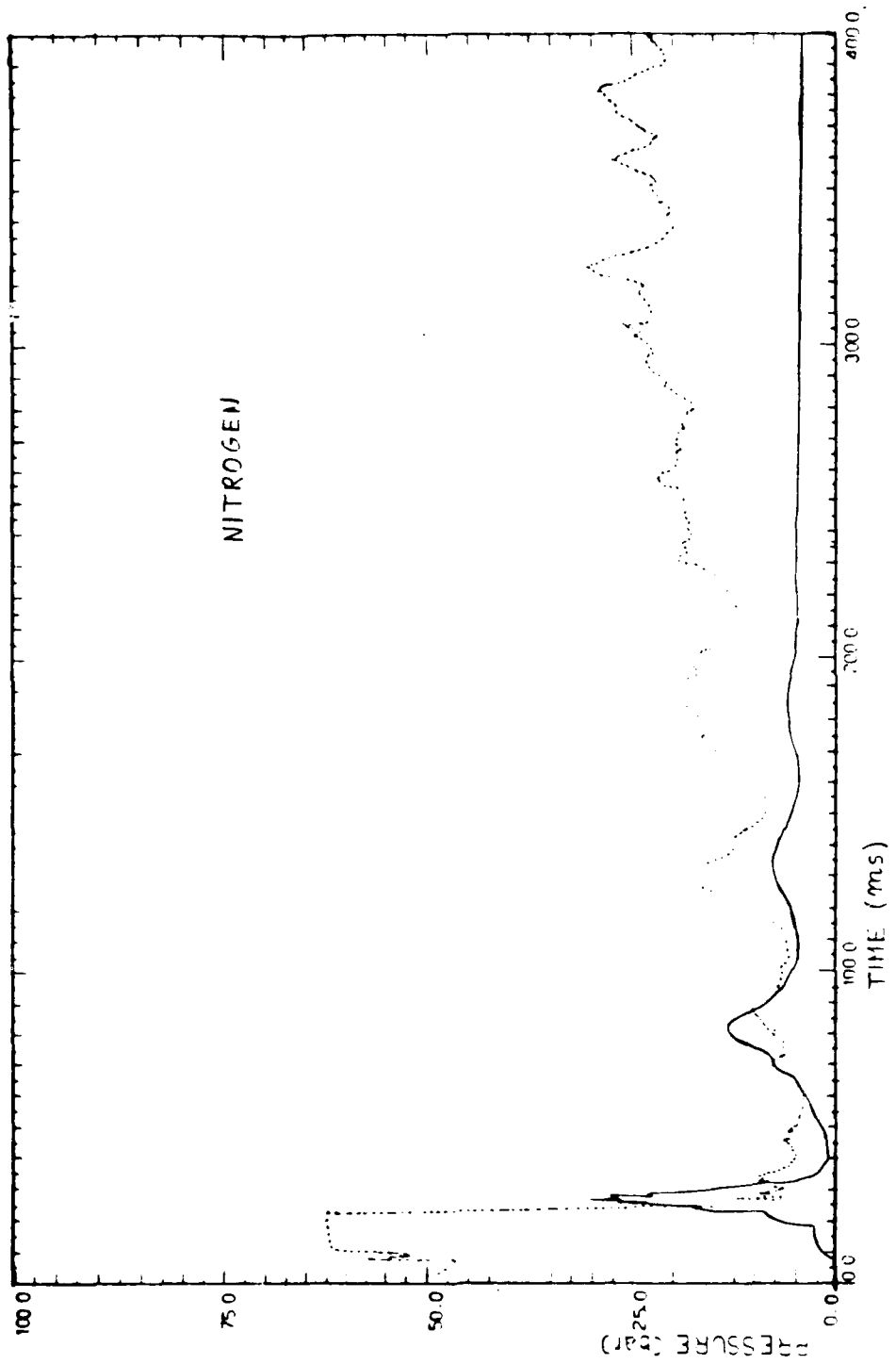


FIG. 77

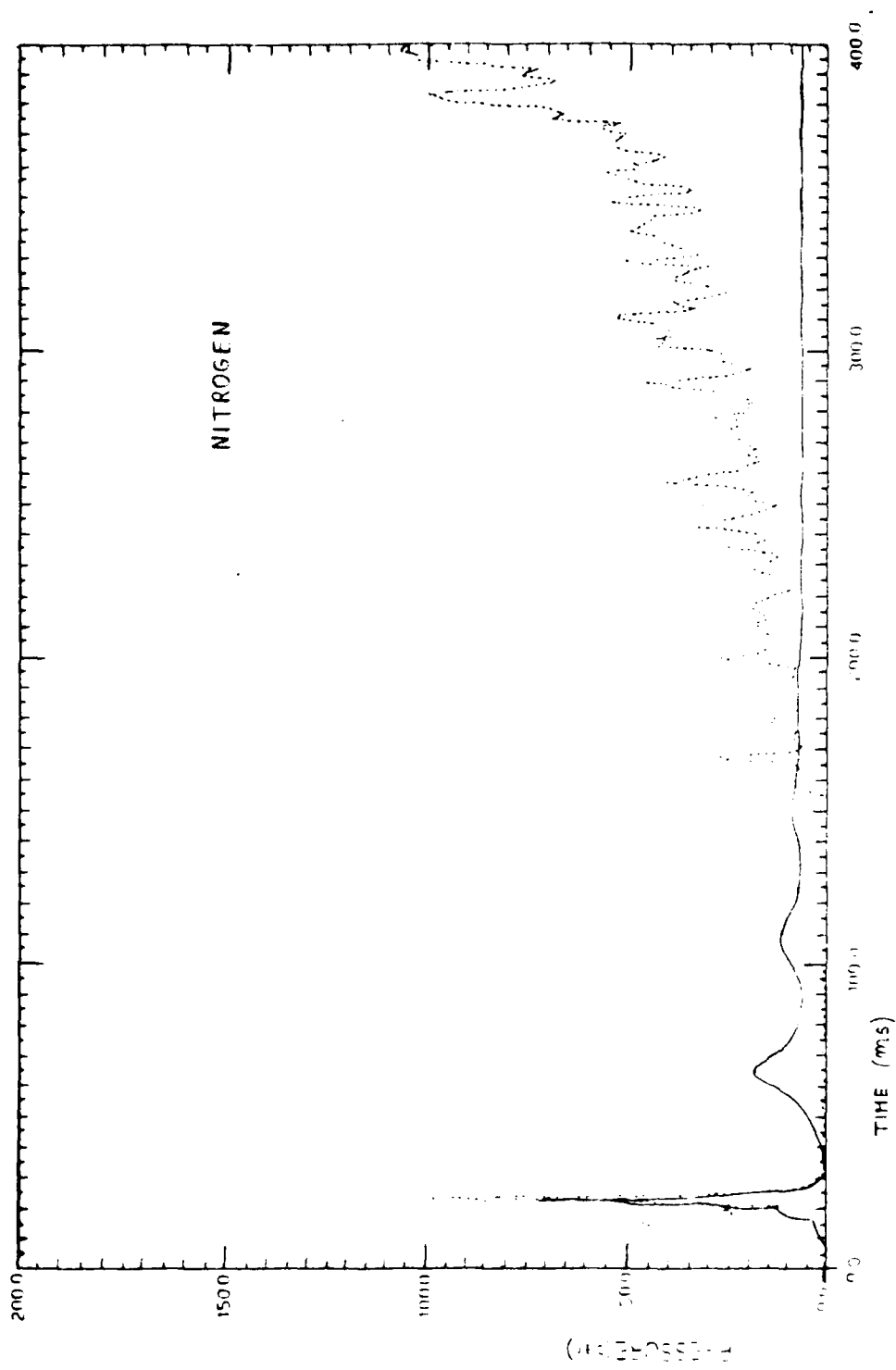


FIG. 78

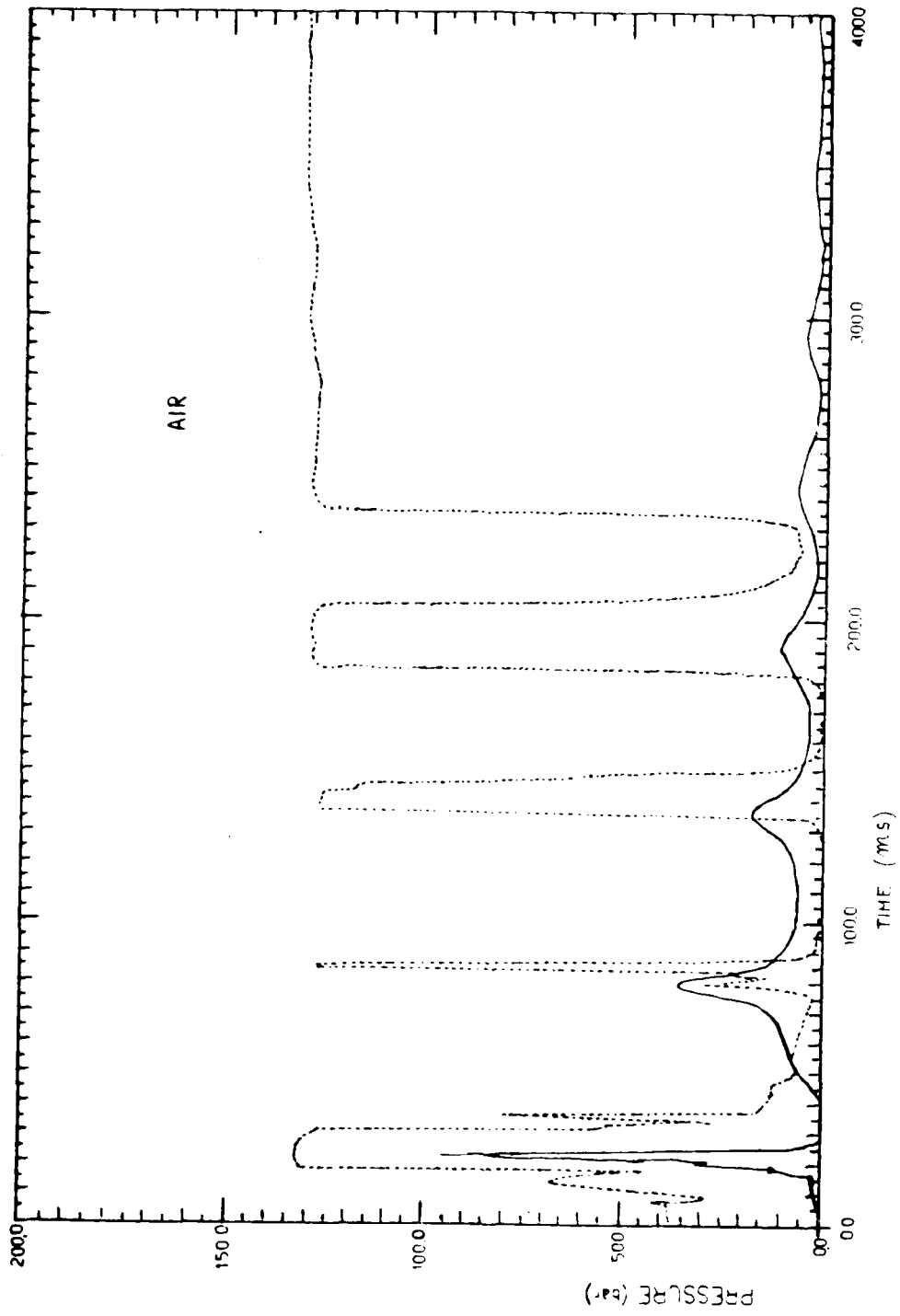


FIG. 79

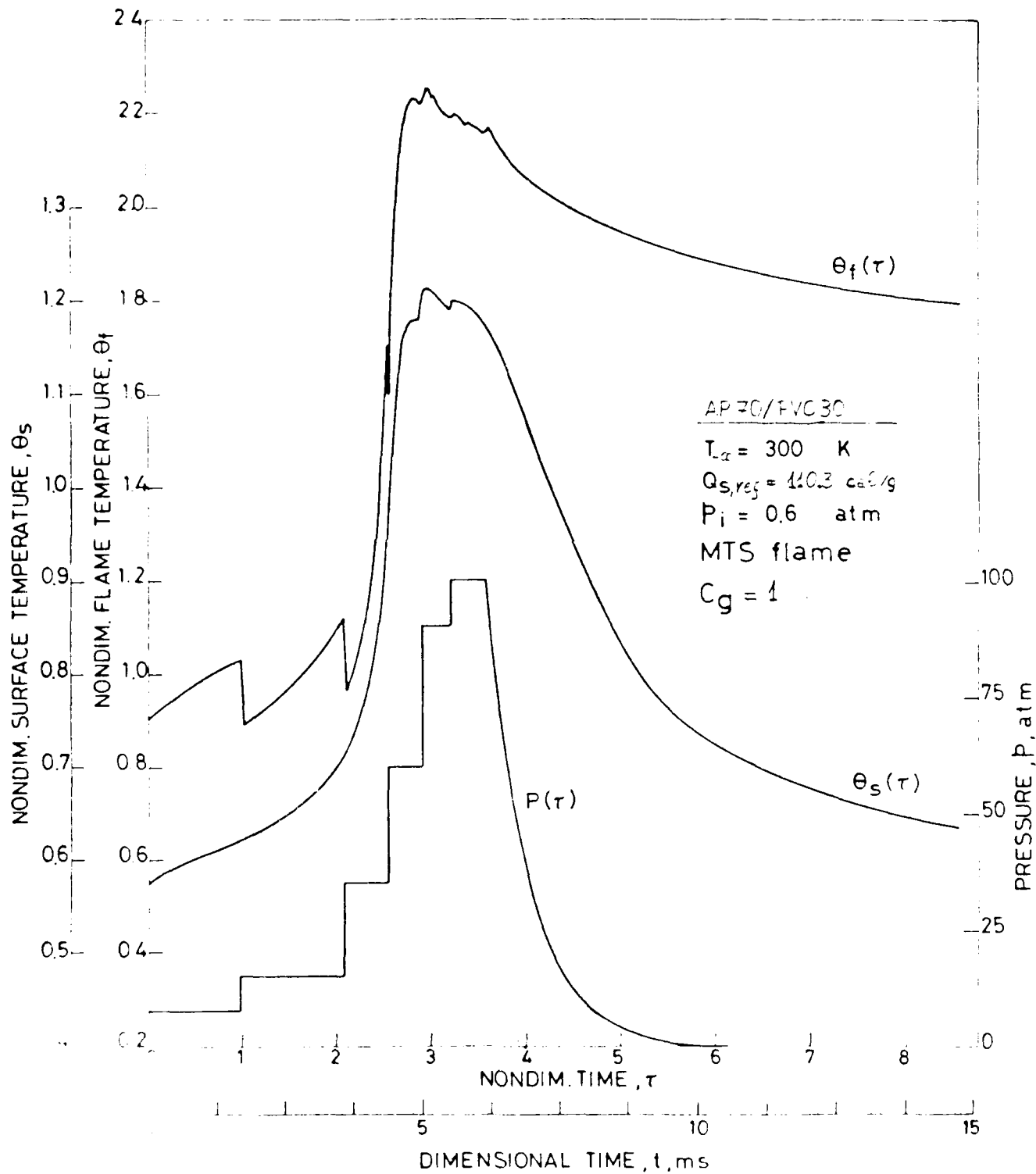


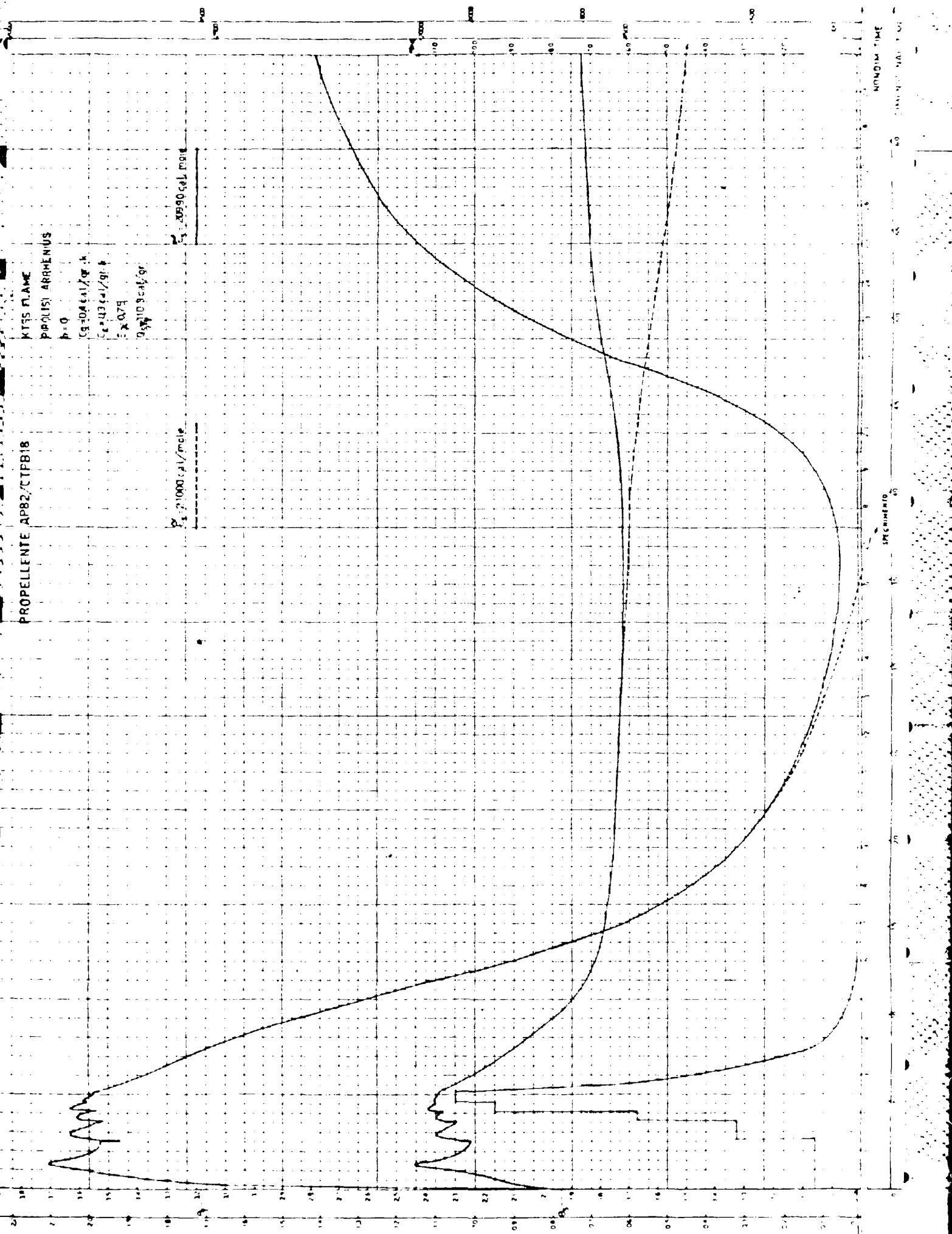
FIG. 80

PROPELLENT AP82/CTPB18

KITTS FLAME
POLYMER ARRHENIUS
 $p = 0$
 $E_a = 104 \text{ cal/gr} \cdot \text{K}$
 $E_a = 103 \text{ cal/gr} \cdot \text{K}$
 $E_a = 107 \text{ cal/gr} \cdot \text{K}$
 $E_a = 109 \text{ cal/gr} \cdot \text{K}$

$Q_p = 1000 \text{ cal/mole}$

$Q_p = 1090 \text{ cal/mole}$



NONDIM TIME

SPECIMEN TIME

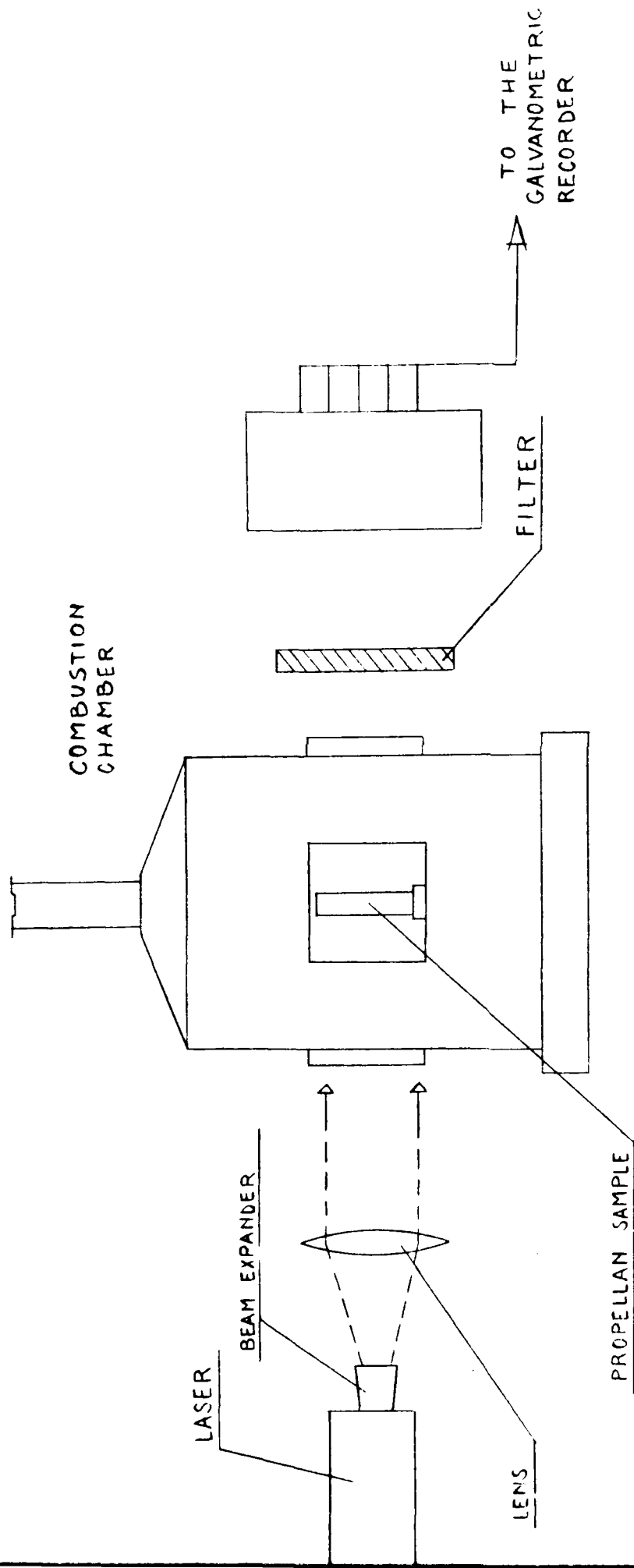


FIG. 82

doppia base non catalizzata
POLI-DONDE' 7-3-82

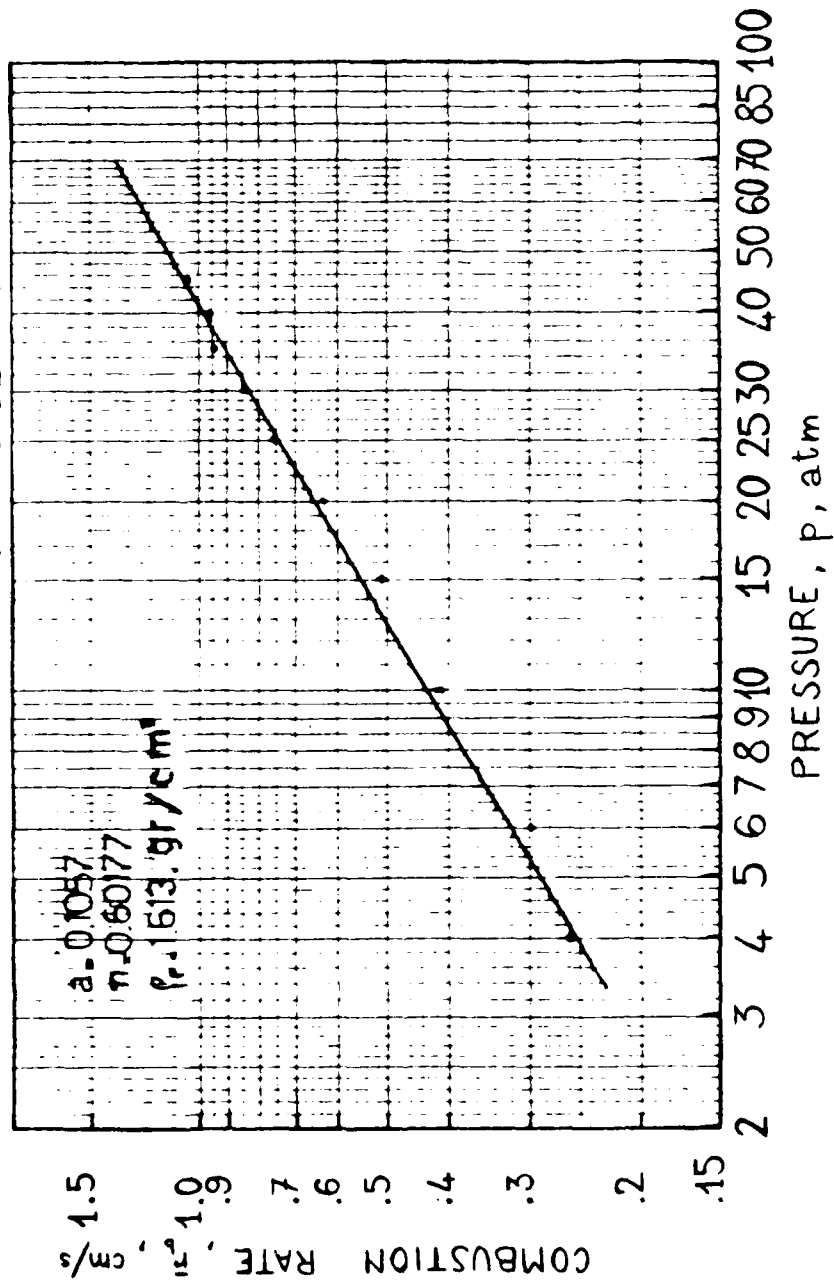


FIG. 83

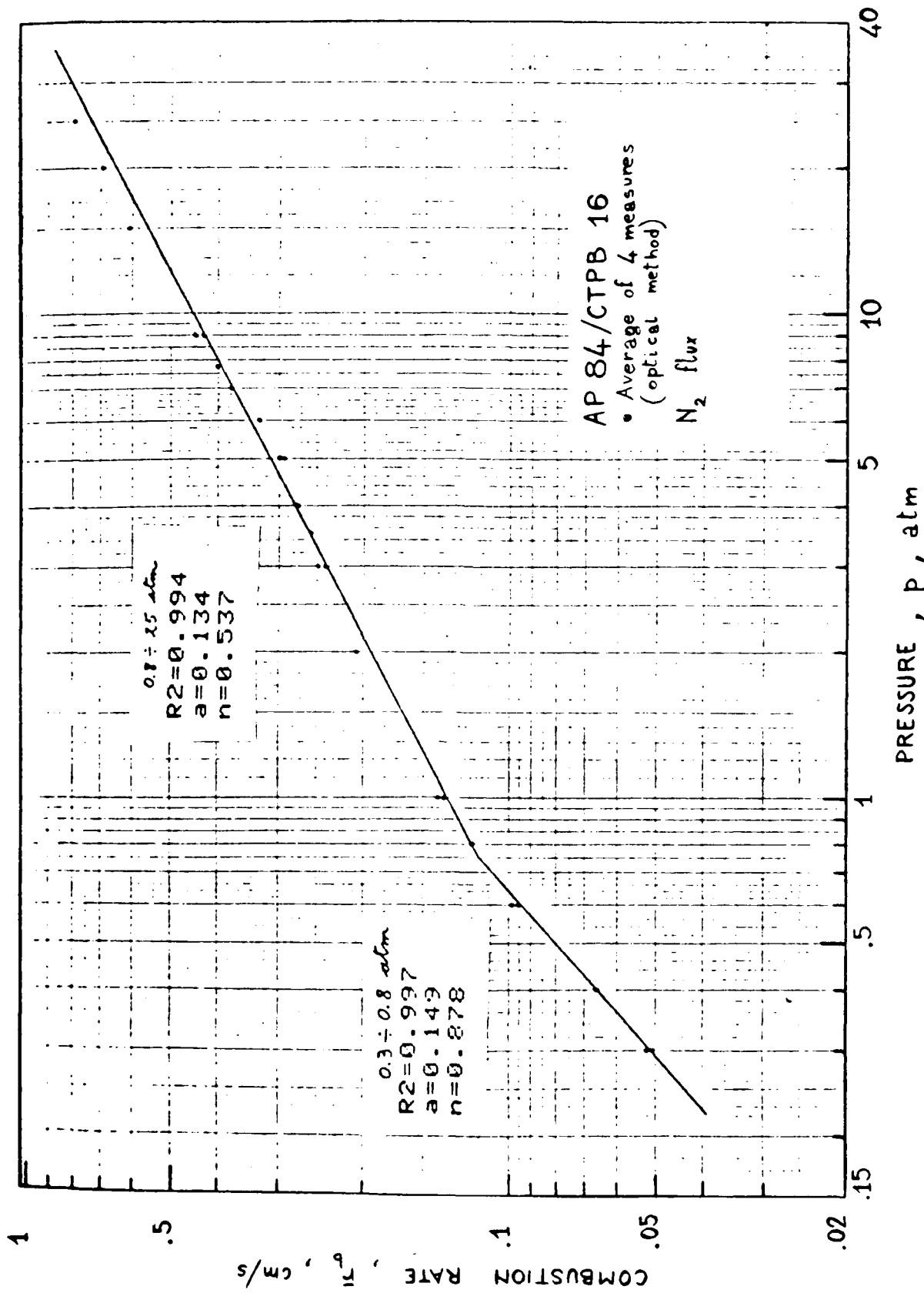


FIG. 84

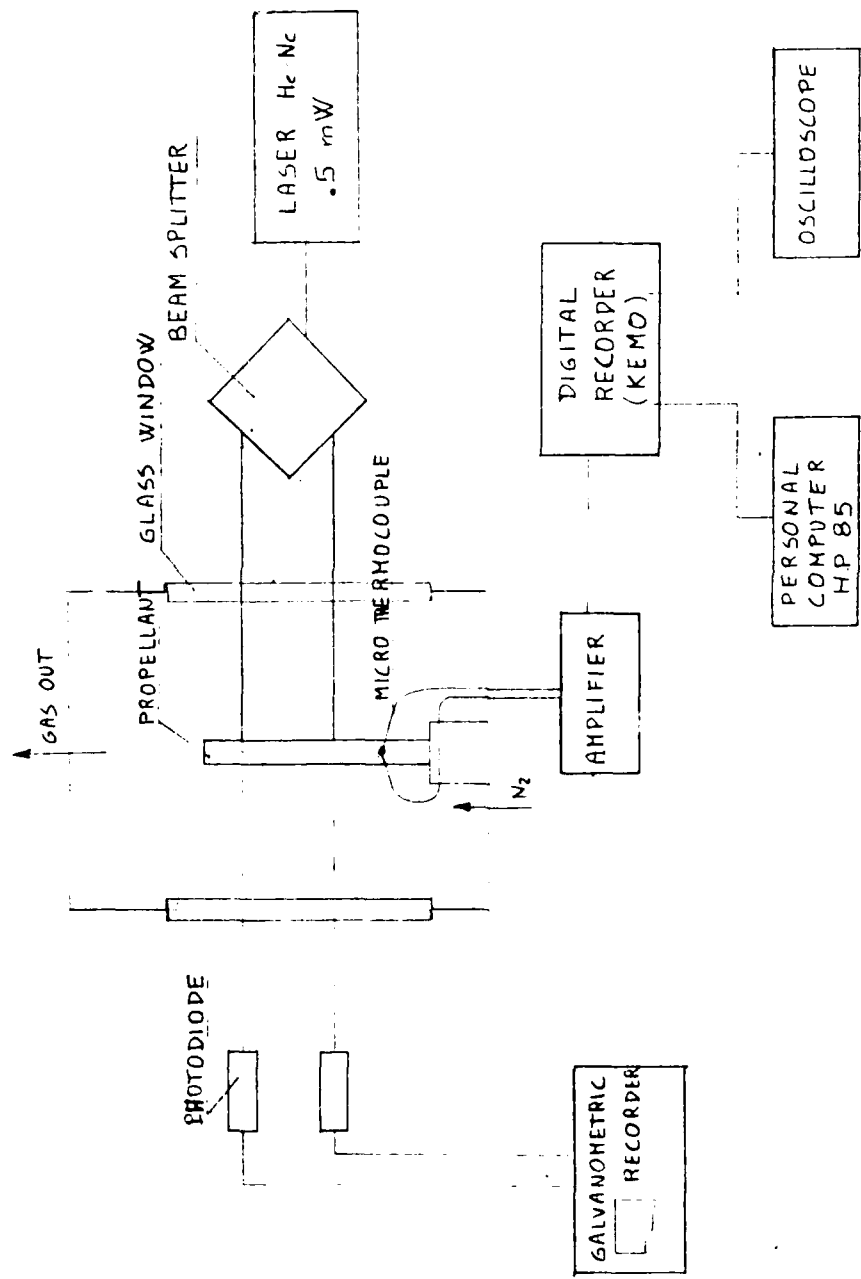


FIG. 85

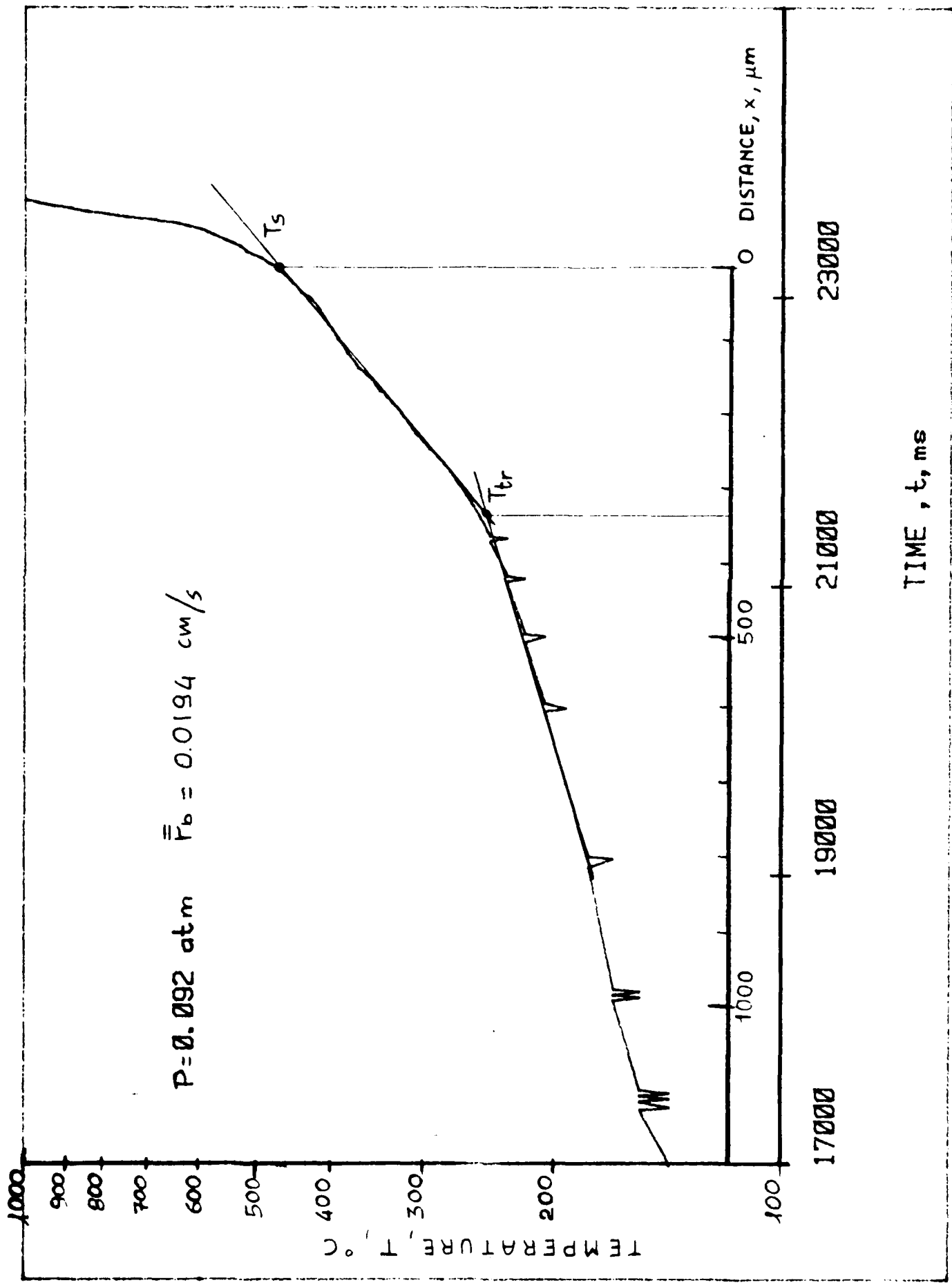


FIG. 86

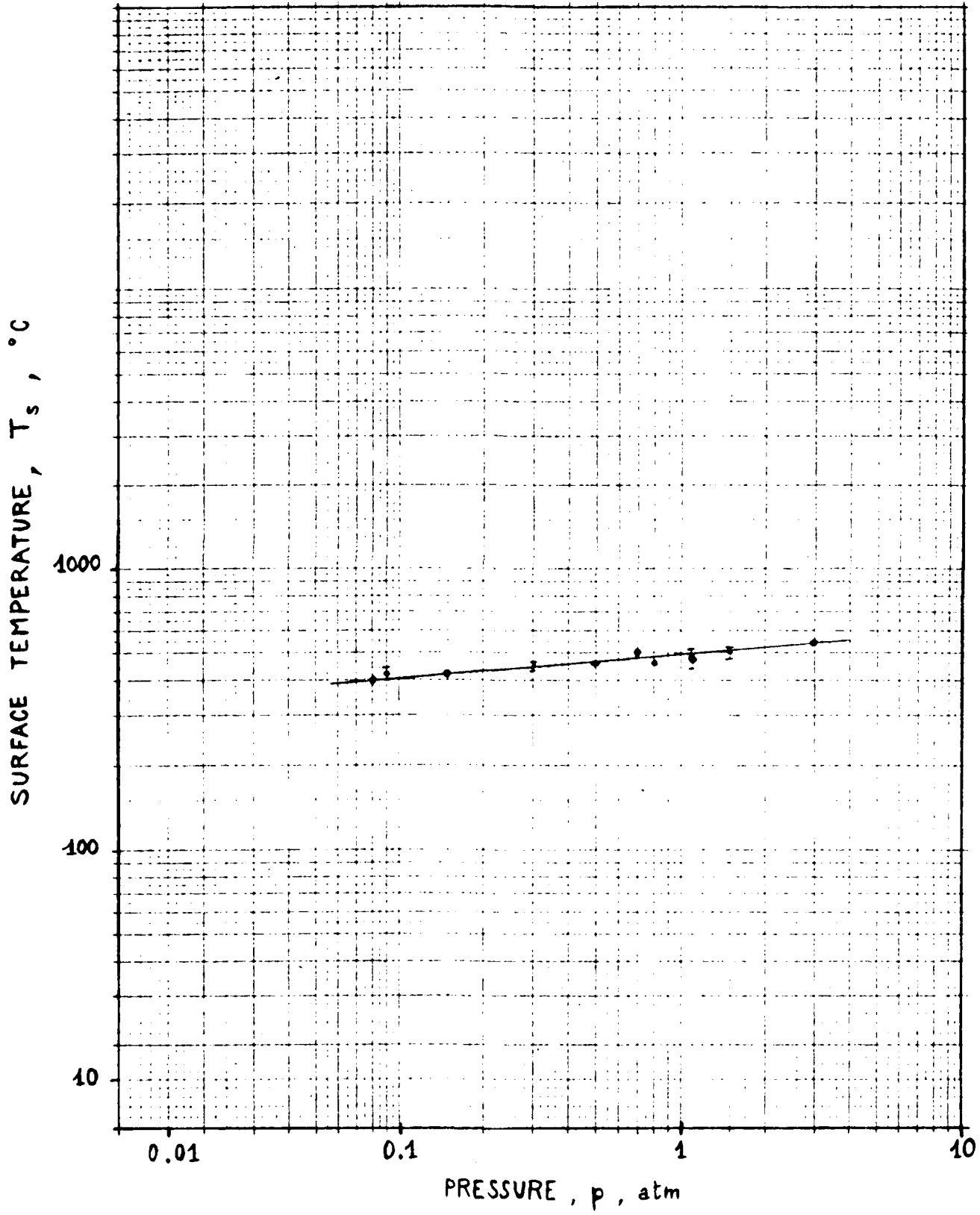


FIG. 87

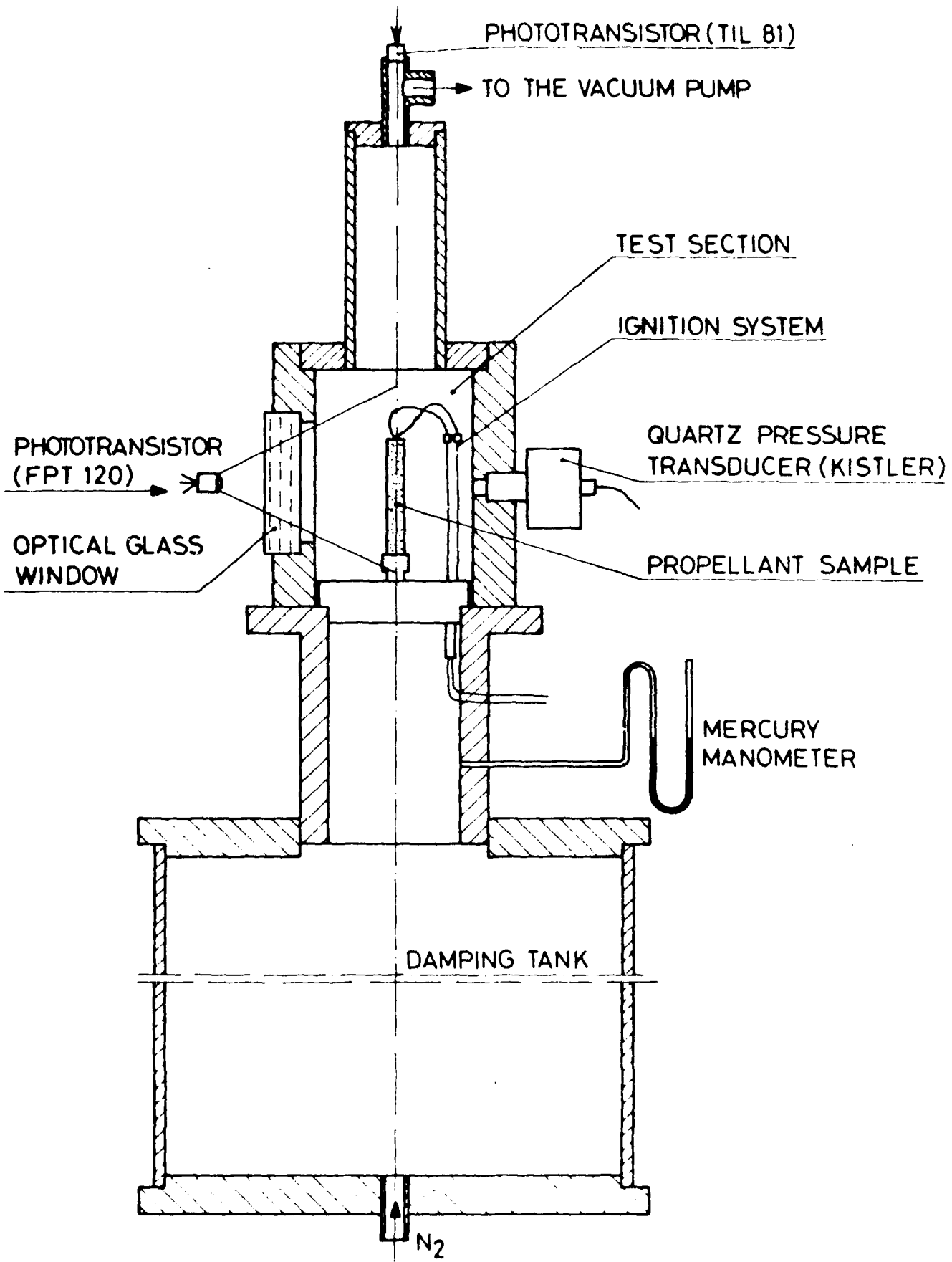


FIG. 88

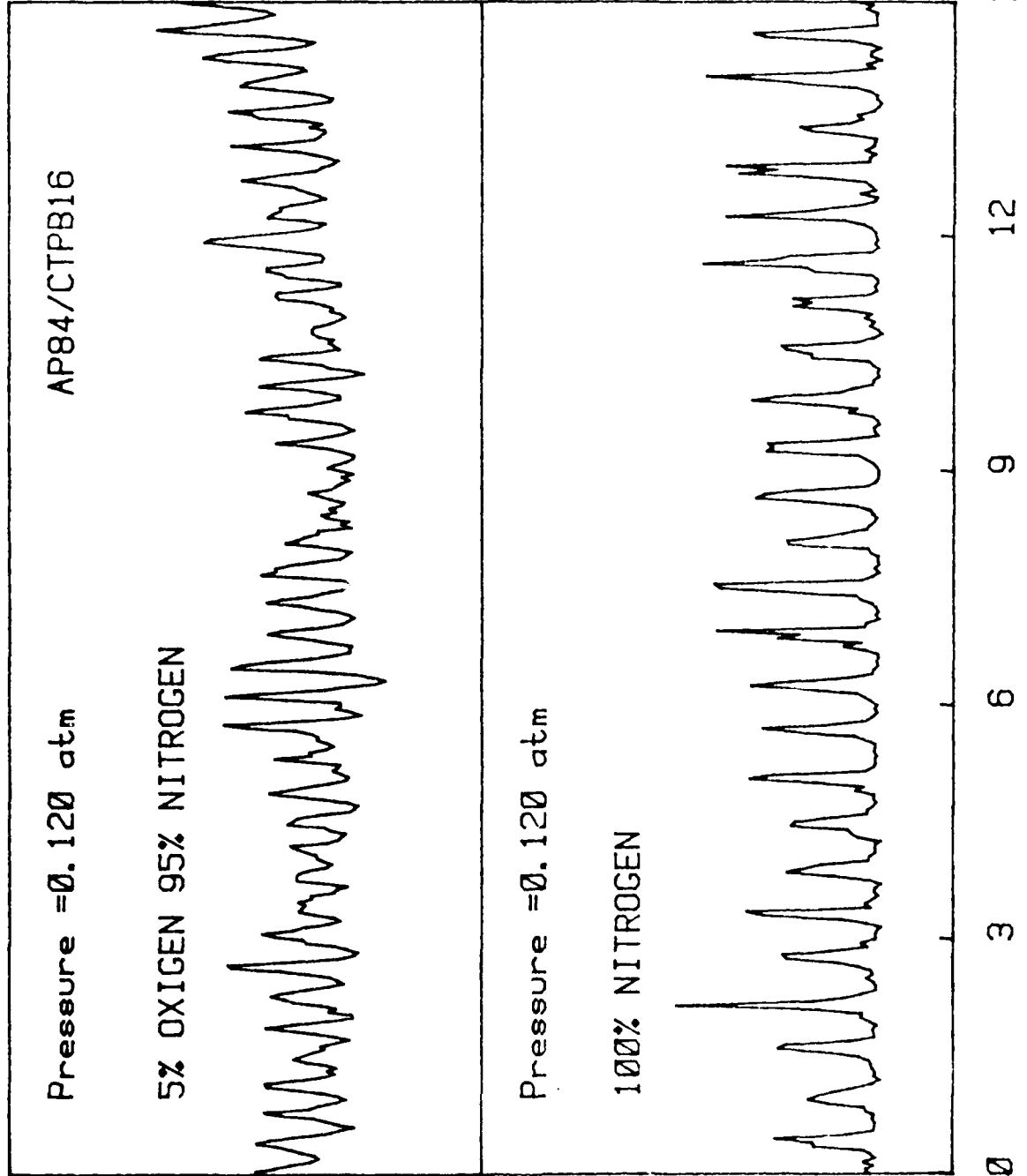


FIG. 83

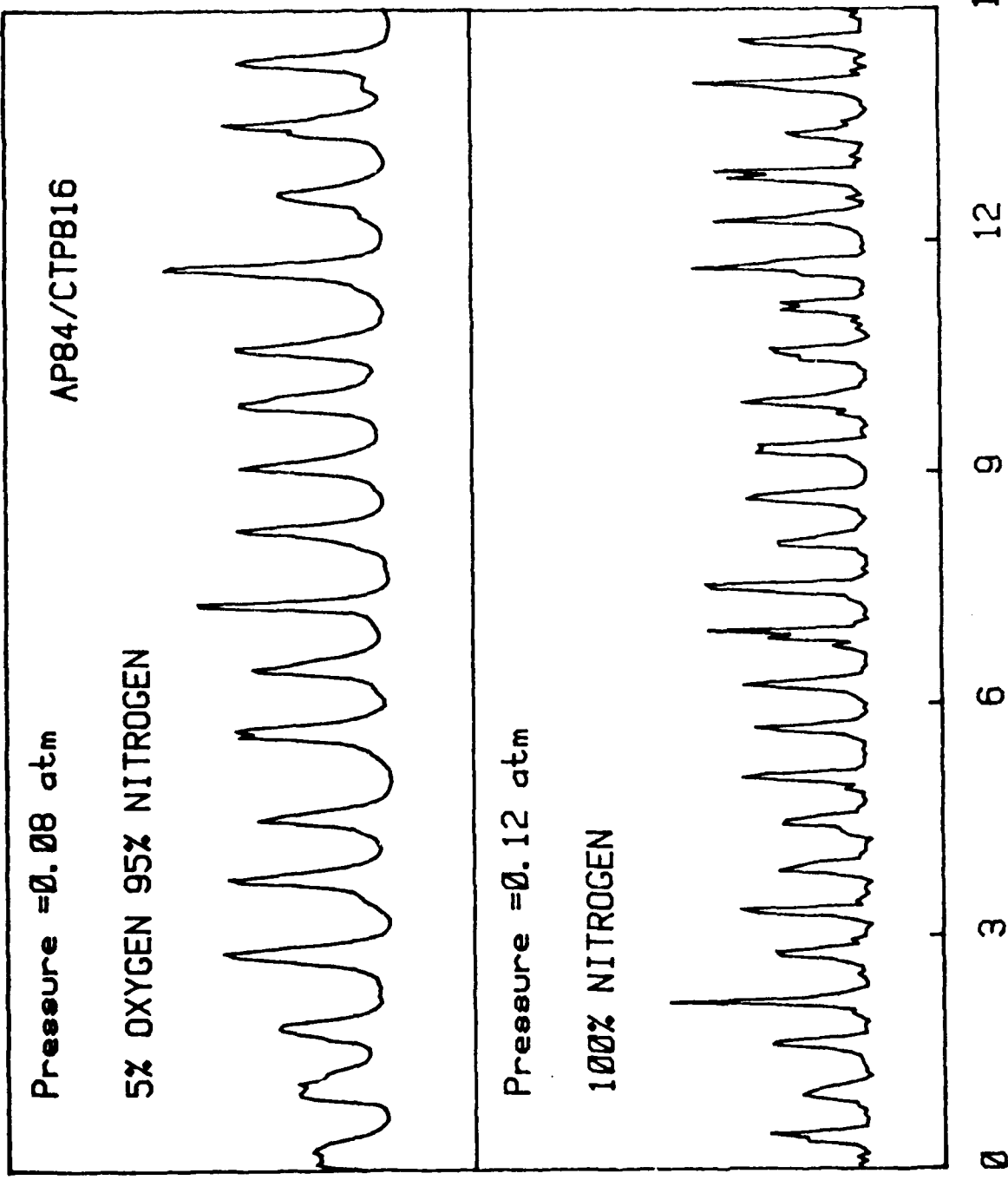


FIG. 20

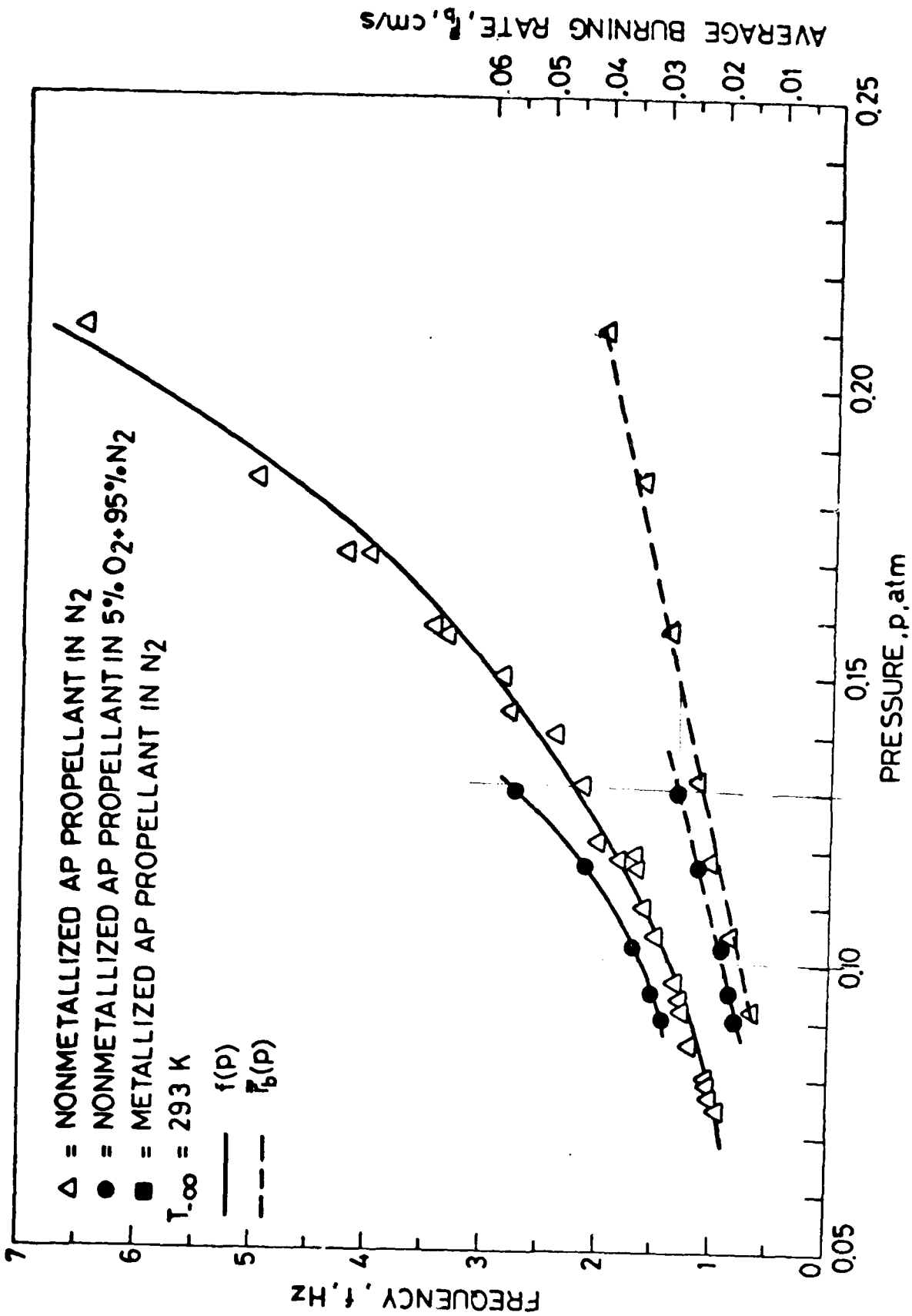


FIG. 91

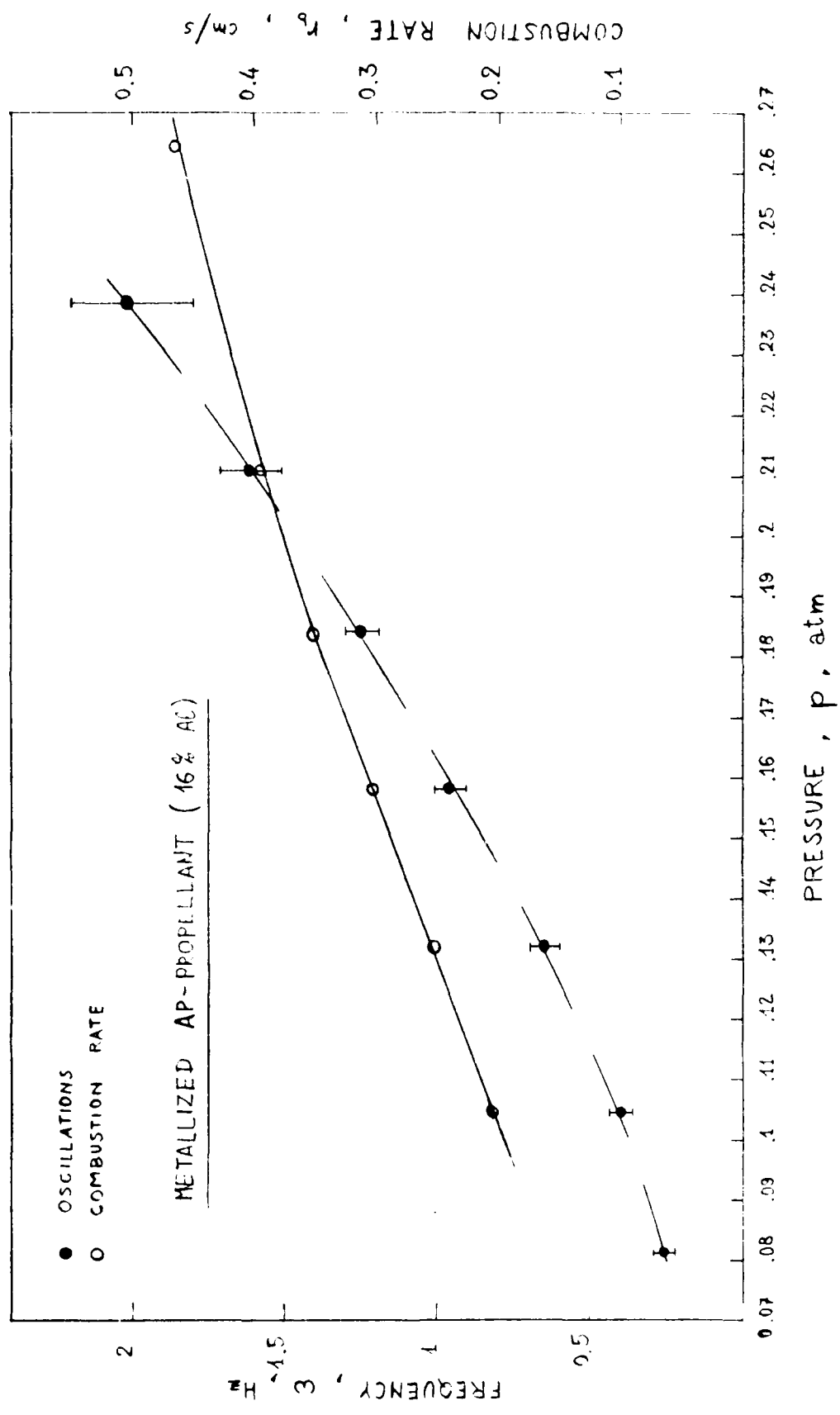


FIG. 92

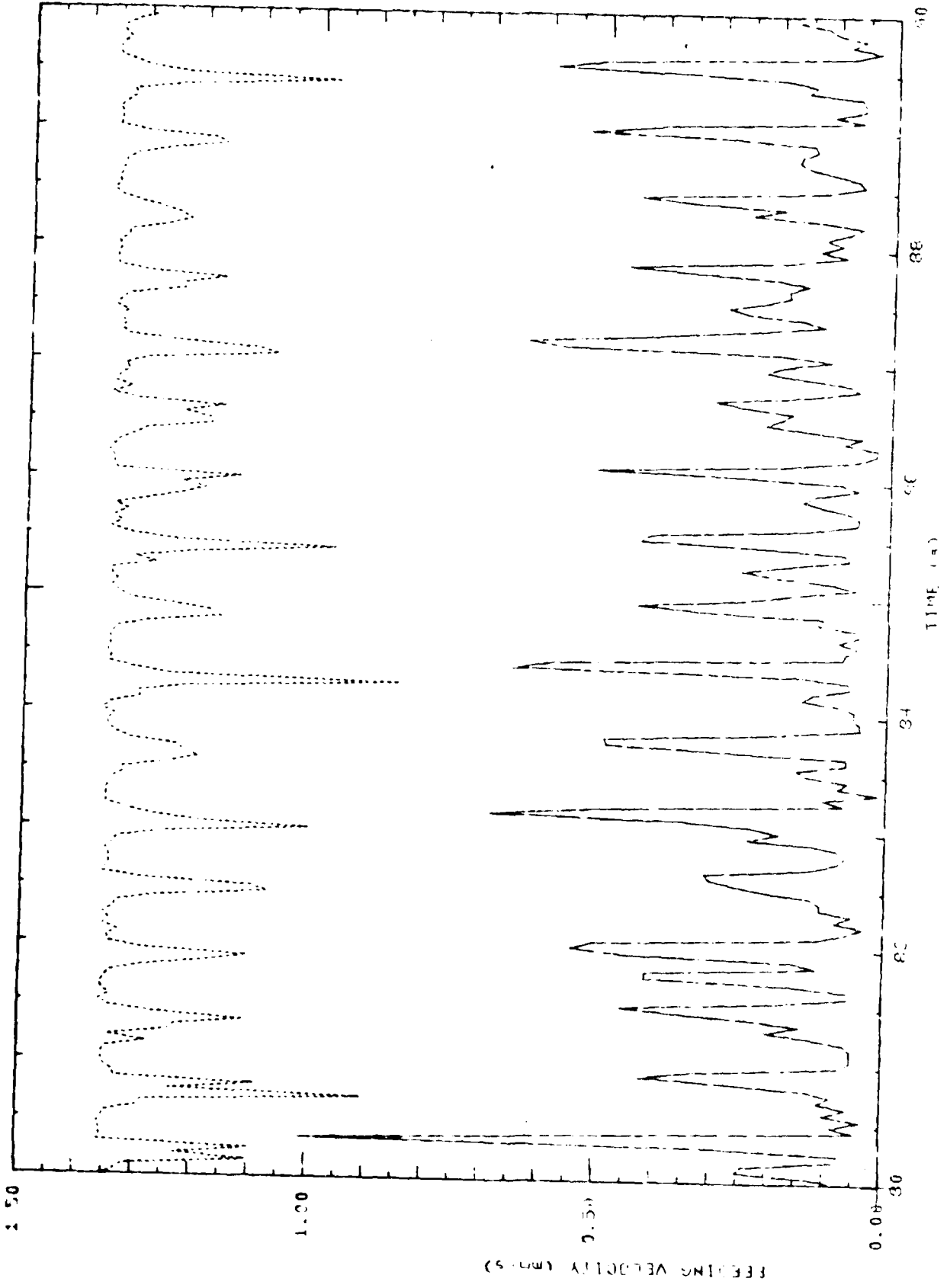


FIG. 33

AD-A143 573

NONLINEAR BURNING STABILITY OF SOLID PROPELLANTS(U)
POLITECNICO DI MILANO (ITALY) IST DI MACCHINE
L DE LUCA ET AL. 31 DEC 83 DAJA37-81-C-0215

4/8

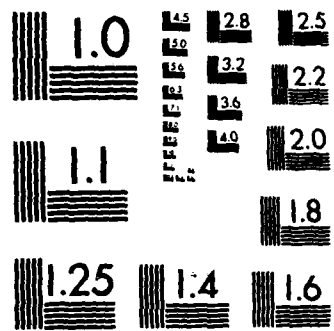
UNCLASSIFIED

F/G 21/9.2 NL

END

FORMED

DTIC



MICROCOPY RESOLUTION TEST CHART
NATIONAL BUREAU OF STANDARDS-1963-A

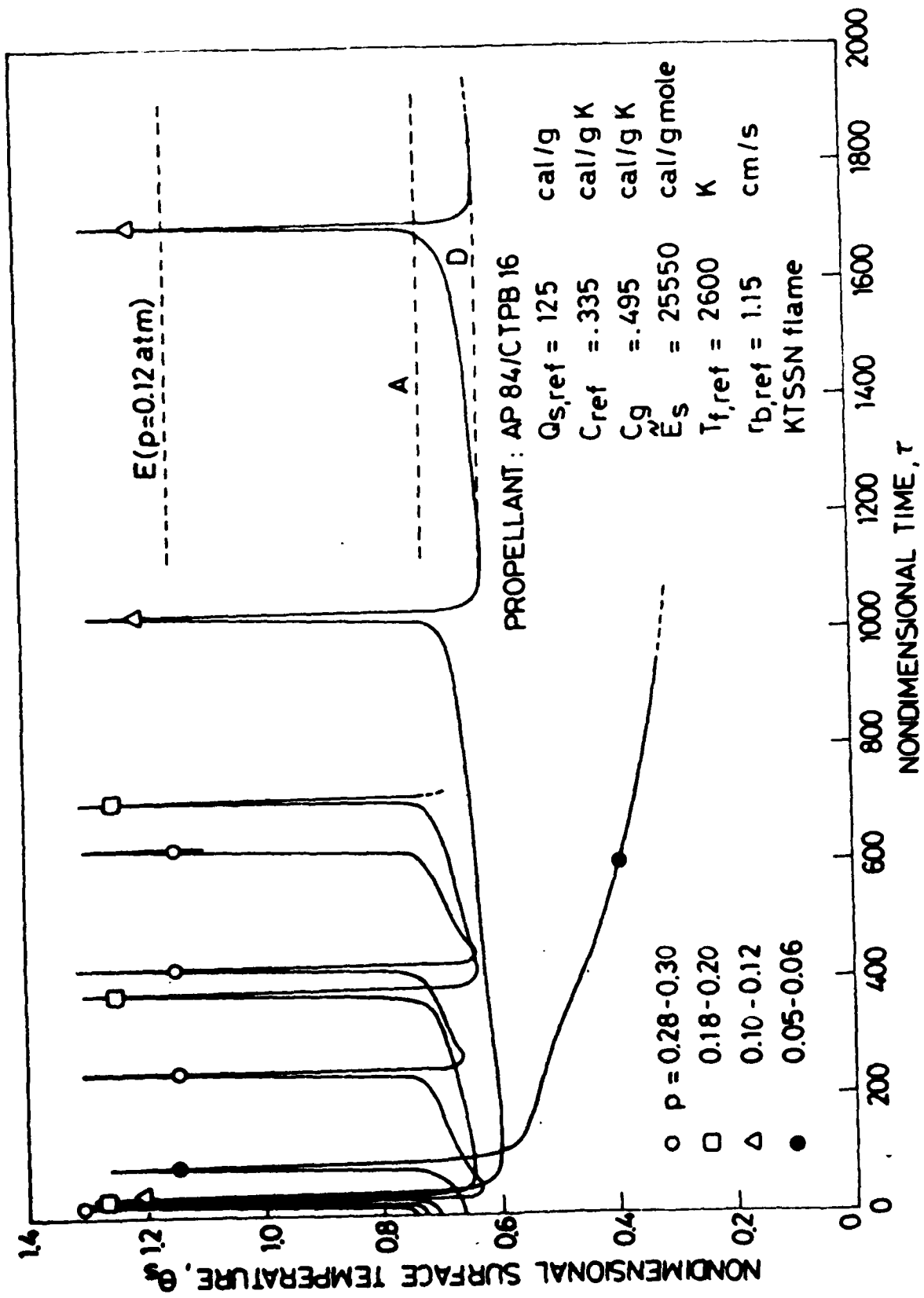


FIG. 34